Hydrodynamic and Water Quality Simulations in the Perdido and Wolf Bay System

by

Xueqian Li

A thesis submitted to the Graduate Faculty of

Auburn University

in partial fulfillment of the requirements for the Degree of

Master of Science

Auburn, Alabama

May 4, 2019

Keywords:

Water Temperature, Salinity, Dissolved Oxygen, Simulations, Estuary

Approved by

Dr. Xing Fang, Chair, Arthur H. Feagin Chair Professor of Civil Engineering

Dr. Joel S. Hayworth, Associate Professor of Environmental Engineering

Dr. Luke Marzen, Professor of Geosciences

ABSTRACT

The widespread fish kills of Gulf menhaden (*Brevoortia patronus*) were reported beginning on 7/31/2015 in the Cotton Bayou, Orange Beach City, Alabama. Although some possible reasons for the fish kill event were provided (e.g., high water temperature, low wind speed, low dissolved oxygen, and so on), there were no existing water quality models to show when the assumed low dissolved oxygen condition could happen and what environmental factors affect/control the water quality condition. Therefore, a quantitative analysis was done to simulate salinity, water temperature, dissolved oxygen temporal and spatial distributions and their internal reciprocal linking by developing a three dimensional hydrodynamic and water quality model using EFDC (Environmental Fluid Dynamics Code) for the Perdido and Wolf Bay system including the Cotton Bayou. The external driving forces include the freshwater inflows into the study area, atmospheric variables, and the astronomical tides contributing/affecting hydrodynamic and the heat exchange. The model was validated using statistical parameters to assess the accuracy against observed data. The simulated hydrodynamic and water quality parameters (water temperature, salinity and dissolved oxygen) had reasonable agreements with the observed data. Simulation results in the Cotton Bayou were analyzed to diagnose the fish kill that could happen in 2015. Through the sensitivity analysis, it was found that the chemical oxygen demand, sediment oxygen demand, and wind speed could have a large effect on the vertical distribution of the dissolved oxygen, especially for the shallow water region. The model was also further used to examine how the system responds to the future climate change (sea level rise and air temperature increase under the global warming projection). Future air temperature increase is projected to reduce dissolved oxygen but the sea level rise can increase the mixing and then the dissolved oxygen.

ACKNOWLEDGEMENT

I would first like to share my sincere gratitude to my advisor Dr. Xing Fang for his continuous support of my research, for his enormous patience, immense knowledge, and encouragement during my Master program. His guidance helped me in all the time of research and writing of this thesis. I would also like to express my most heartfelt appreciation to Dr. Xing Fang for providing me an opportunity to come to the United States to purse my Master degree and for his tremendous support for my future career plan. His self-cultivation also sets a good example for me to follow throughout my life. I could not have imaged having a better advisor and mentor.

This study is partially supported by the funding from the OUC-Auburn Joint Center of Aquaculture and Environmental Sciences for the project "Forecasting the Ecological Health of Coastal Waters in Alabama and China. The investigators in Auburn were Drs. Alan E. Wilson (PI), Xing Fang, and Joel S. Hayworth and in OUC (Ocean University of China) were Prof. Sun Dajiang (PI), Dr. Yangen Zhou, Dr. Kai You, and Dr. Hongwei Shan. The study is also partially supported by the grant from the City of Orange Beach. Both supports are acknowledged.

I also would like to thank the rest of my thesis committee member, Dr. Joel S. Hayworth and Dr. Luke Marzen for their encouragement and insight suggestions. I would like to thank Dr. Luke Marzen for assisting with ArcGIS; Dr. Janesh Devkota for providing me the original data for EFDC model and valuable suggestions; Dr. Gang Chen for assistance with the EFDC model and Delft3D grid modification software; and Caleb Wilson for providing the measured data.

I would also like to thank my friends Jalil Ahmad Jamily, Xiaoning Li, Liping Jiang, Sagar Kumar Tamang, Kyle Dorian Lusk, Sudan Pokharel, Yasemin Eldayih, Jie Pu and Wenjun Song during my research. Finally, yet importantly, I would like to thank my family for their support throughout my study period.

Table of Contents

List of Figures

List of Tables

CHAPTER 1 INTRODUCTION

1.1 Background

The rapid development of science and technology greatly promote people's living standards. For example, the wide usage of fertilizer significantly improved the quantity and quality of food for the world. However, it also brought obvious effect to the environment such as cultural eutrophication. Eutrophication can greatly deplete the dissolved oxygen (DO) in the river, which further bring completely catastrophe to the aquatic animals. The fish kill is a phenomenon referring to a localized die-off of the fish population. It is primarily caused by the reduced oxygen in the water, which is the combining results of a variety of causes such as the algae bloom, overpopulation, increased water temperature, spill or release of toxic chemicals and pollutants, and so on (https://en.wikipedia.org/wiki/Fish_kill). It often occurs in the summer because the warm water holds less DO than cold water does. Since many fish species require a specific living environment with the low variations of aquatic conditions, fish kills are often a clear sign indicating the local environment is under the stress. If situations continue to turn out badly, they will have a negative effect on the other aquatic animals and plants because the dead and decaying fish will remove more dissolved oxygen in the waterbody. Besides, the pathogenic microorganisms attached to the fish carcasses probably affect the drinking water sources and the foul smell from the dead fishes can also strike at the local tourism.

Tourism is gradually playing a more and more important role in the economic development, especially for the coastal community far from the local economic center. One significant benefit of this industry is that it can quickly increase the local household average income because the primary

recreational providers are micro-operators such as restaurants, bars, short-term lodging rental through Airbnb, equipment rental, and so on. However, like a double-edged sword, it can also bring issues if it is the primary revenue of local governments. The negative factors such as an unexpected fish kill event (Figure 1-1, https://www.al.com/news/index.ssf/2018/01/gulf_shores_fish_kill_leaves_l.html) would leave the local economy vulnerable to ruin.

Figure 1-1 Fish kill in Gulf Shores, Alabama on January 11, 2018.

The City of Orange Beach, located in the Baldwin County, Alabama, faces such worries. It is a small city locating between the Mobile Bay and Perdido Key along the Gulf of Mexico. As of the 2010 census, the population was 5441 and the total area was 15.9 square miles. Due to its exclusive location, tourism is an important pillar industry. Pleasure islands, canoe and kayak trails, fishing pier, and so on are the vital elements to local tourism. However, widespread fish kills were reported around Perdido Pass and other areas of Orange Beach on August 3, 2015 (Figure 1-2). The large fish kills were first noticed in Cotton Bayou by boaters on July 31, 2015, and the tragedy continued throughout the weekend from Robinson Island, north of Perdido Pass, to Bayou Saint John, between Ono Island and Bear Point (https://www.al.com/news/mobile/index.ssf/2015/08/fish_kills_reported_in_orange.html). The massive fish kill significantly harmed local economic development. From the financial statement of the City of Orange Beach, the revenue from the service charging decreased by nearly 5% in 2016, from $10,427,642 in 2015 to $9,832,448 in 2016

(https://www.orangebeachal.gov/departments/finance-department/financial-reports) because the fish kill occurred in a particular year could affect tourism in the next year.

Dr. Bob Shipp, professor emeritus and past Chair of the Department of Marine Sciences at the University of South Alabama, developed a "Guide to Fishes of the Gulf of Mexico". It says "… during summer months, menhaden often congregate in shallow, poorly flushed estuaries. They are intolerant of low dissolved oxygen levels such as those found in hot, still waters. Thus, 'fish kills' may occur in a chain reaction of spreading area ensues…" (Shipp 1986). The dead and decaying fish remove even more oxygen from the water column, resulting in more kills.

Figure 1-2 Fish kill in Cotton Bayou area, Alabama on August 3, 2015.

Cotton Bayou, where the above fish kills were observed, is a shallow semi-closed water body that is in the Perdido and Wolf Bay system (Figure 1-3). The surface area and the average depth of it are around 0.73 km^2 and 1.36 m, respectively. The Cotton Bayou is connected eastward

to the Terry Cove and Perdido Pass (Figure 1-4), which is also the only open connection for the Cotton Bayou. The hydrodynamic characteristics, water level, and salinity in the Cotton Bayou show periodical variation patterns due to the water exchange with the Gulf of Mexico through the Perdido Pass. Compared with the west portion of the Cotton Bayou, the tidal effect to the east side from the Gulf of Mexico is more pronounced.

Figure 1-3 Southern Alabama coastal areas showing Mobile Bay, Wolf Bay, Perdido Bay and the location of Cotton Bayou, which are connected to the Gulf of Mexico

1.2 Environmental Requirements of Gulf Menhaden

Gulf menhaden (*Brevoortia patronus*) is an important commercial fish species supporting the largest single fishery (by weight) and popular fishing goals, in consideration of its high omega-3 fat content and medium size. This fish is found only in the Gulf of Mexico and a tremendously

abundant species (Shipp 1986). The living environmental requirements and habitats (depth, temperature, salinity and DO) change with the age of Gulf menhaden. The life of Gulf menhaden

Figure 1-4 Lower portion of Perdido Bay that connects with the Gulf of Mexico and the zoned view of Cotton Bayou with surrounding areas

can be categorized four stages, larvae, postlarvae, juveniles, and adults based on the age and fork length. The larvae usually refer to the 3–5 weeks menhaden with 10–30 mm fork length (Wilkens and Lewis 1971). Postlarvae were observed in the estuaries from November to June in the low salinity and shallow region (0 to 2 m) (Fore and Baxter 1972). In the estuary, postlarvae, 30–50 mm, in April appeared to transform to juveniles with size of 91 to 120 mm by August based on the field experiment in 1971 in the Pensacola Bay with the salinity 6.5–13.1 ppt in July and 12.2–19.6 ppt in August (Tagatz and Wilkens 1973). After transformation, juveniles remain in these low salinity, nearshore areas, often near the surface (Lassuy 1983). Most juveniles move out of the estuary after August (Tagatz and Wilkens 1973). The dead fish in Cotton Bayou primarily were Gulf menhaden with length from 101.6 to 177.8 mm (4 to 7 inches), which were primarily juveniles and some adult menhaden.

The Gulf menhaden are sensitive to the marine environment. Many factors such as water temperature and DO concentration can significantly affect them. In 1983 Dennis R. Lassuy at U.S. Fish and Wildlife Service developed a report to summarize the comprehensive information on life histories and environmental requirements of Gulf menhaden. In estuaries, juvenile menhaden have been captured over a salinity range of 0 to 35 ppt and a temperature range of 5 to 35 °C (Benson 1982; Christmas and Waller 1973). Lassuy (1983) reported the water temperature is better not higher than 30° for menhaden. Definitive data on the optimum temperature, upper and lower lethal limits are lacking (Lassuy 1983). While Gulf menhaden have been reported to occur in waters from fresh to hypersaline (0–67 ppt) (Etzold and Christmas 1979), there may be somewhat narrow salinity ranges with various life stages. Simmons reported juveniles of Gulf menhaden commonly occurred in waters from 20 to 66 ppt (Simmons 1957).

Gulf menhaden are often among the species hardest hit by low DO “fish kills” in estuaries (Christmas and Waller 1973; Etzold and Christmas 1979). Postlarvae and juveniles in restricted

bays and backwaters (e.g., Cotton Bayou) are particularly susceptible to low-DO kills because they have low mobility and capacity to avoid low DO areas (Lassuy 1983). A minimum DO level of 3 mg/L was suggested although the empirical basis for it was not given (Christmas and Waller 1973). Since there are no published accounts of controlled experimental testing of Gulf menhaden response to temperature and/or salinity (or any other environmental parameters such as DO) at any life stage, it is difficult to define causal mechanisms and have defined limits (thresholds) to determine exact habitat or mortality conditions for Gulf menhaden.

The living depth for menhaden changes with the season that generally reflects the annual inshore-offshore migration pattern (Lassuy 1983). From June to September, Gulf menhaden were taken from 2 to 15 m in the northern Gulf of Mexico (Roithmayr and Waller 1963), most likely for adult menhaden.

In addition to low DO kill to Gulf menhaden, larval menhaden may suffer mass mortalities when water temperatures are below 3°C for several days or fall rapidly to 4.5°C in winter months (Reintjes and Pacheco 1966), and juvenile and adult menhaden could suffer cold-kills during periods of freezing winter conditions, especially in narrow or shallow tidal areas (GSMFC 2015). The largest cold-kill of Gulf menhaden occurred in the Texas Gulf coast in December 1983 (GSMFC 2015). The fish kill in Gulf Shores (Figure 1-1) on January 11, 2018 could be a cold-kill because recorded air temperatures at Bon Secour (very close to Gulf Shores) decreased from 14.1 ^{o}C on December 30 of 2017 to -5.7 ^{o}C on January 2 of 2018 and had an average air temperature of 1.2 ^{o}C from January 1 to 5 of 2018; most likely water in the certain shallow bayou was frozen to possibly kill Gulf menhaden.

Due to obvious economic loss caused by the dead fish phenomenon, it is necessary to understand and figure out its causes, then we would know whether the fish kill is a natural disaster due to certain weather conditions or a preventable event if certain environmental management

practices are implemented. The preliminary assumed reason for the fish kill was the low dissolved oxygen in this region, a common reason for fish kill. Stefan et al. (1996) and Fang et al. (2004) studied fish habitat in small lakes under the past (1960–1979) and future climate scenarios in Minnesota and over the contiguous USA using daily time-step lake water quality model simulations. When a freshwater lake becomes shallow (e.g., < 4 m), the lake could be a polymictic lake, which can be well mixed many times in a year. When a waterbody is well mixed, all water quality variables are uniform along with the depth, then dissolved oxygen would be the same from the water surface to the lake bottom. Saturated DO concentration is about 7.5–6.9 mg/L in freshwater when the water temperature is 30–35 °C. When the salinity is 25 ppt and temperature is 30–35 °C in an estuary, saturated DO concentration is still 6.6–6.1 mg/L, which could be high enough to support normal fish habitat. When the stratification occurs in a waterbody, water temperatures and DO concentrations would be different in the surface and near the bottom. DO concentration in the hypolimnion could be low enough (< 3 mg/L) or anoxic condition (DO = 0 mg/L) that would not support various fish species. A recent study (Jamily 2018) shows that for shallow lakes, even the daily time-step model predicts the well-mixed condition in most of the days, the hourly time-step model predicts much more stratification, e.g., predicted stratification in several hours during the day and well-mixed condition in several hours during the night. Therefore, plus the impact of salinity (density difference), the strong temperature and DO stratification in a shallow waterbody such as Cotton Bayou is highly possible, especially due to low wind speed and low tidal. Additional studies are definitely needed to understand and predict the stratification or well-mixed conditions in shallow waterbodies before we can qualify the possibility of a fish kill in shallow lakes or estuaries. In general, to figure out how eutrophication or pollutant discharge or nutrient load affects the water quality, numerical model to quantify such effect needs to be developed.

When Stefan et al. (1996) and Fang et al. (2004) studied fish habitat in small lakes, constant oxythermal limits (thresholds) were used. Based on available US Environmental Protection Agency

data (Chapman 1986; EPA 1976), the DO limit used for warm-water fish was 2.5 mg/l (Fang et al., 1998), slightly lower than the limit for cold-water and cool-water fish (3 mg/l). The temperature criteria for the 12 fish species included in the warm-water guild (Hokanson et al. 1977) were available for their study and agreed closely with one given by Eaton et al. (1995). The lethal temperature (LT) for 12 warm-water fish species was the average value of 34.5 °C obtained from two different sources (Fang et al. 2004). Both DO limit of 2.5 mg/L and LT of 34.5 °C were kept as constant to determine whether a fish kill or a suitable fish habitat exists in small lakes under the past and future climate scenarios (Fang et al. 2004).

In 2008, a fish habitat model for cold-water fish species "cisco" was developed by Jacobson et al. (2008) and is a fitted regression equation as the lethal-niche boundary of adult cisco.

$$DO_{lethal} = 0.4 + 0.000006e^{0.59T_{lethal}} \quad (1.1)$$

where DO_{lethal} and T_{lethal} are the DO concentrations (in mg/L) and the water temperatures (in °C), respectively, which define the lethal niche boundary (Jacobson et al. 2008). The computed DO_{lethal} is the required minimum DO concentration at a given water temperature T_{lethal} for cisco to survive. The equation is plotted on Figure 1-5 and mapped the DO concentrations and water temperatures from the profiles measured in 16 Minnesota lakes that experienced cisco mortality in 2006. Equation (1.1) indicates the DO survival limit for adult cisco is not constant but depends on water temperature. From the regression equation (1.1), when the water temperature is less than 15 °C, the DO survival limit is about 0.4 mg/L; the lethal temperature is 22.0°C when DO = 3.0 mg/L is used as the DO survival limit for cisco. When DO is greater than 22.0°C, the required DO concentration increases rapidly to 4–6 mg/L. When observed or simulated DO is higher than calculated lethal DO based on water temperature, cisco can live there, otherwise, it does not have a fish habitat or fish needs to swim away and search for the habitat condition in other places.

Based on the literature search, currently, it lacks in-depth research studies (both in the laboratory and in the field) to quantify water temperature and DO survival or lethal limits for Gulf menhaden. Does Gulf menhaden require more dissolved oxygen to survive when water temperature is higher such as > 30 °C that menhaden typically avoids? It is highly possible, based on the lethal-niche boundary of adult cisco; and Figure 1-5 shows a hypothetical lethal-niche boundary of Gulf menhaden. It assumes when water temperature is less than 25 °C, the DO survival limit is 3.0 mg/L for Gulf menhaden, which is slightly larger than 2.5 mg/L lethal DO for warm-water fish used by Fang et al. (2004); when temperature is 28 °C, the lethal DO = 3.5 mg/L. When water temperature is 34 °C, the DO survival limit is about 8.7 mg/L. Even the lethal-niche boundary of Gulf menhaden in Figure 1-5 is purely hypothetical, we will analyze later whether the hypothetical lethal-niche boundary is somewhat reasonable or not.

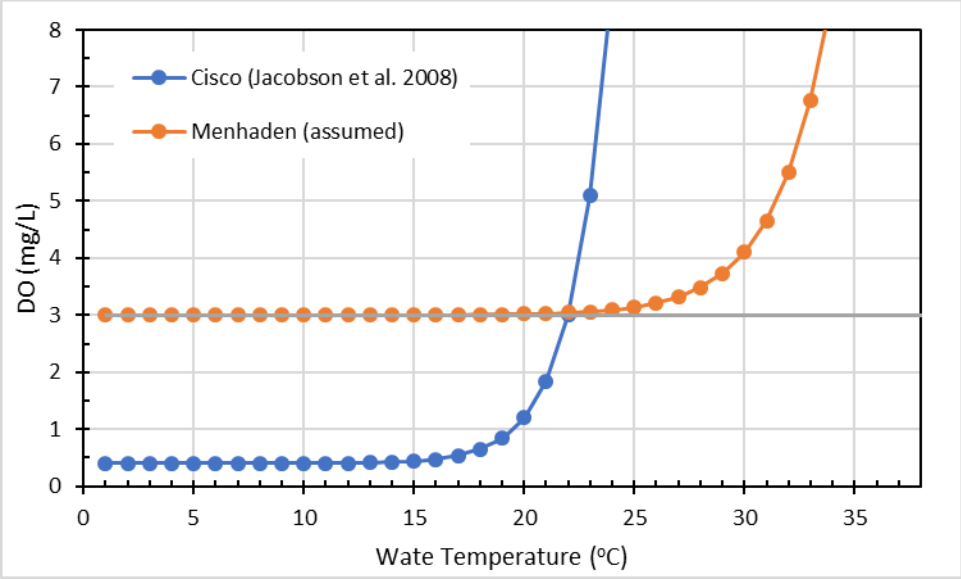

Figure 1-5 The lethal-niche boundary of adult cisco from Jacobson et al. (2008) and a hypothetical lethal-niche boundary of Gulf menhaden.

1.3 Scope and Objectives

The primary objective of this study is to set up an effective hydrodynamic and water quality simulation model for the Perdido and Wolf Bay system. After calibrating the numerical model, a quantitative analysis can be made to potentially figure out the reasons behind the massive fish kills occurred in 2015 and identify the most influential driven forcing parameters affecting the stratification, water temperature, and DO characteristics by performing necessary sensitivity analyses. Besides, the study also examines the impact of future climate warming and the sea level rise on water quality conditions in Cotton Bayou.

Although the Cotton Bayou is the most interesting area where the fish kills occurred, it is hard to only model the Cotton Bayou since it is lack of available input data to set appropriate boundary conditions, e.g., water level, temperature, salinity, and velocities at the east boundary of Cotton Bayou connecting to Terry Cove, Perdido Pass, and Bayou Saint John are very dynamic and no available data for them. Therefore, the selected study area was expanded to the whole Perdido and Wolf Bay because there exist many monitoring stations providing necessary model input data.

There are numerous kinds of water data in connection with the aquatic life such as the water temperature, pH, DO, toxics and so on. However, it is impossible to simulate all of them in one surface water quality model. In consideration of the availability and correlation about the research objective, only the following parameters are simulated: water level, water temperature, salinity, the concentration of nitrogen, phosphorus, carbon, chlorophyll-a, and DO using the environmental fluid dynamics code (EFDC)–multi-dimensional multi-purpose unsteady water quality model (Ji 2017; Tech 2007).

In order to reach the expected objective, the following programs were used: Google Earth – used to delineate the study area by placing marks along the shoreline; CORPSCON – used to convert the coordinate data to UTM coordinate system; ArcMap – for listing locations of the

monitoring stations and editing the bathymetry; EXCEL – for data sorting, calculation, and developing graphs; EFDC – for hydrodynamic and water quality parameter simulations.

1.4 Thesis Organization

Chapter 1 is the introduction that describes the fish kill phenomenon in the study area and its possible causes, analyze the environmental requirements for the Gulf menhaden (dead fish) and gives some basic geographic information about the study area and the objective of this study.

Chapter 2 is the literature review that briefly describes five current popular water quality models such as their respective advantages and drawbacks from the aspect of the model dimension, applied water body structures, the required input parameters; and primarily introduced/reviewed EFDC model in details because it is applied in this study to the Perdido and Wolf Bay system.

Chapter 3 deals with the process to develop the EFDC model for the study area including the selection of the simulation region, modification of the existing available simulation model, preparations and derivations for different input parameters and internal coefficients.

Chapter 4 presents the simulation/validation results of salinity (2015–2017), water temperature (2015–2017), and DO (2015–2016). The simulation results such as hydrodynamics, water temperature, DO, and habitat of Gulf menhaden in the Cotton Bayou were further analyzed based on the validated model from 7/27 to 8/5 in 2015. The sensitive analysis is included to detail how DO in Cotton Bayou are affected by different selections of chemical oxygen demand (COD), sediment oxygen demand (SOD), wind speed, and wind direction. Then DO in Cotton Bayou are analyzed using the projected air temperature increase and sea level rises in response to the future global warming.

Chapter 5 summarizes this study briefly and contains conclusions of the study and some suggestions for future study.

CHAPTER 2 Review of Hydrodynamic and Water Quality Models

2.1 Brief Review of Hydrodynamic and Water Quality Models for Waterbodies

Water quality modeling is an effective and economical tool to simulate and predict the changes in surface water quality, through saving the cost of labors and materials for a large number of chemical experiments (Wang et al. 2013). In addition, it is necessary to make a prediction to the pollutant transport through water quality model in some cases due to special environmental pollution issues. Water quality modeling has a long history, which dates back to the work of Streeter and Phelps in the 1920s (Ambrose Jr et al. 2009). Its first modern version, however, was not developed until in the 1960s with the availability of mainframe computers. Since a water quality modeling is essentially a process of the calculation of a collection of mass, energy, and momentum conservation equations, the development of water quality model is consistent with the development of the computer technology.

With the improvement of computing speed and storage capacity of the computers, the water quality models also make a progress from steady-state to a dynamic model, from zero-dimensional mode to one-dimensional, two-dimensional, and three-dimensional models (Zu-xin and Shi-qiang 2003). Generally, the development of water models can be divided into three stages, the primary stage (1925-1965), the improving stage (1965-1975) and the deepening stage after 1975 (Wang et al. 2013). At the beginning stage, the simple BOD-DO bilinear system was developed and the one-dimensional model was applied to solve pollution issues in rivers and estuaries (Burn and McBean 1985). During the improving stage, the one-dimensional model was updated into a two-dimensional model which was applied to water quality simulation of reservoirs and estuaries/gulfs and the

nonlinear system models including the N and P cycling systems were also developed (Gough 1969). In the deepening stage, the three-dimensional models were developed with an increase in the number of state variables. In addition, watershed models were also included to deal with the nonpoint source pollution together with the water quality model. Several typical one-dimensional, two-dimensional, and three-dimensional models are discussed in the following sections.

2.1.1 MINLAKE (one-dimensional lake water quality model)

The Minnesota Lake Water Quality Management Model (MINLAKE) is a one-dimensional (vertical) unsteady lake water quality model developed in the 1980s (Riley and Stefan 1988) for lake management studies; and it simulates water temperature, suspended solids, nutrient solids, nutrient dynamics (NH_4, NO_2/NO_3, and reactive P), chlorophyll-a, BOD, and DO. MINLAKE divides the lake into several well-mixed horizontal layers along with the depth. To understand the impacts of climate warming on lake water quality and fish habitat, the model was revised to a regional water quality model that only simulates water temperature and dissolved oxygen in lakes in response to ambient weather condition in the 1990s. The main input data are air temperature, dew point temperature, wind speed, wind direction, solar radiation, sunshine percentage, and precipitation (snowfall and rainfall). MINLAKE96 does not include the inflow and outflow so that it is more suitable for lakes where the water level is more or less constant over the simulation period and inflow or outflow has limited or no effect on overall lake water quality. MINLAKE96 includes the simulation of winter ice cover period and the heat transfer into and from the sediment at the bottom of the lake. Since the observed water quality data are scarcely available at different locations and at different depths in a single lake, the one-dimensionality of MINLAKE makes it easier to calibrate, validate, and apply to different lakes whenever nearby weather data and limited observed data are available. MINLAKE96 can simulate long-term water quality conditions in lakes over many years continually.

2.1.2 CE-QUAL-R1 (one-dimensional reservoir water quality model)

CE-QUAL-R1 is a one-dimensional reservoir model (vertical direction) developed by the USACE Waterways Experiment Station. It was designed to solve water quality problems associated with reservoir eutrophication under anaerobic conditions through simulating the major physical, chemical, and biological processes (total 27 water quality variables) within an impounded body of water. In addition, one characteristic feature is that it can use Monte Carlo methods to give probabilistic estimates for some key output variables. In this model, the vertical water column is divided into several horizontal layers where thermal energy and materials are uniformly distributed in each layer. The horizontal layers thickness is determined by the balance of the inflowing and outflowing waters. Due to its own one-dimensional limitation, it cannot model the water bodies with high variability in the horizontal plane (Wlosinski and Collins 1985). These drawbacks can be overcome by the following two or three-dimensional models.

2.1.3 CE-QUAL-W2 (two-dimensional water quality model)

CE-QUAL-W2 (W2) is a free two dimensional (vertical-longitudinal) hydrodynamic and water quality model developed by the USACE Waterways Experiment Station. It has been used for the environmental assessment and management in rivers, estuaries, lakes, reservoirs and river basin system through computing water levels, horizontal and vertical velocities, temperature, and 21 other water quality parameters such as DO, pH, dissolved/suspended solids and so on (http://www.ce.pdx.edu/w2/download_model_information.html). Comparing with the above models, the significant advantage of W2 is that it can accurately compute the two-dimensional velocities for stratified narrow-reservoir systems. However, stuck with its essential two-dimensional simulation limitation, it can be only used for water systems with little lateral variation in the water quality constituents due to its default lateral homogeneity assumption (Gao and Li 2014). In addition, it also cannot model sloping riverine waterbodies.

2.1.4 WASP (three-dimensional water quality model)

The water quality analysis simulation program (WASP) is a general dynamic surface water quality model developed by the US Environmental Protection Agency. It has three simulation modes, one, two and three dimensions with advection and dispersion transport. In addition, it also provides an optional model to simulate the toxicants. The WASP can be used to simulate the hydrodynamic and water quality parameters in pond, stream, and estuarine. To some extent, WASP seems like Lego because it can be easily linked with other models. It can receive the calculated hydrodynamic results such as flow, temperature, salinity from SWMM, HSPF, LSPC, NPSM and so on. Once receiving hydrodynamic information, users can choose one or more sub-models from Eutrophication, Conservative Toxicants, Organic Toxicants, and Mercury options to activate corresponding functions.

2.1.5 EFDC (three-dimensional water quality model)

The environmental fluid dynamics code (EFDC) is a versatile surface water modeling system developed by the Virginia Institute of Marine Science. It can be used to simulate the process of hydrodynamics, sediment transport, and toxic contaminant transport and water quality eutrophication in one, two, and three dimensions. It also has already been used to simulate aquatic systems in nearly all kind of waterbodies, rivers, lakes, reservoirs, estuaries and coastal waters. The availability of the orthogonal curvilinear horizontal and sigma vertical coordinate systems make it better to represent the complex physical characteristics of the estuaries through making grid sizes to vary and fit the estuary coastline. EFDC works through solving the internal vertically hydrostatic, free surface, turbulent averaged equations of motion for the variable-density fluid (Ambrose Jr et al. 2009). Many computational schemes of the EFDC are similar to the widely used Blumberg-Mellor model, POM (Princeton Ocean Model) and USACE's Chesapeake Bay Model, CH3D (Ambrose Jr et al. 2009; Blumberg and Mellor 1987; Chapman et al. 1996).

2.2 Description of EFDC Hydrodynamic and Water Quality Models

2.2.1 EFDC Sub-models and State Variables

As an advanced hydrodynamic and water quality simulation model, EFDC includes six internal correlative sub-models: wind wave model, hydrodynamic model, sediment transport model, eutrophication model, toxic model, and sediment bed model/sediment diagenesis model (Figure 2-1). The hydrodynamic model is the most fundamental part of the EFDC simulation model (Figure 2-1). It works as the energy source to motivate the remaining models. Once receiving the information from the hydrodynamic model such as water level, water velocity, water temperature, salinity and so on, the eutrophication model can further simulate the water quality parameters distribution. Meanwhile, the concentrations of water quality parameters are also affected by the sediment transport model and sediment bed model. Theses sub-models work together to generate the simulation results as accurate as possible. In this model study, however, the simplified constant benthic flux rate and sediment oxygen demand were used to represent the sediment bed model. The reason to take this simplification form instead of the full sediment simulation sub-model is because the full model requires many unavailable inputs such as bed spatially varying condition, cohesive/non-cohesive sediment settings and so on. Therefore, a simplified but relatively reliable representative form was used in this modeling study. Besides, the model for Perdido and Wolf Bay system also did not activate the sediment transport and toxic sub-models, which is considered to have slightly influence on the DO simulation.

Table 2-1 lists all the 21 EFDC state variables and corresponding abbreviation symbols in the water quality (eutrophication) model. The 21 state variables are divided into 6 groups: algae group, organic carbon group, phosphorus group, nitrogen group, silica group, and other water quality variables. Figure 2-2 is a schematic diagram showing their relationship and that the algae group is placed as the base because they are primary producers that are the originator and receiver

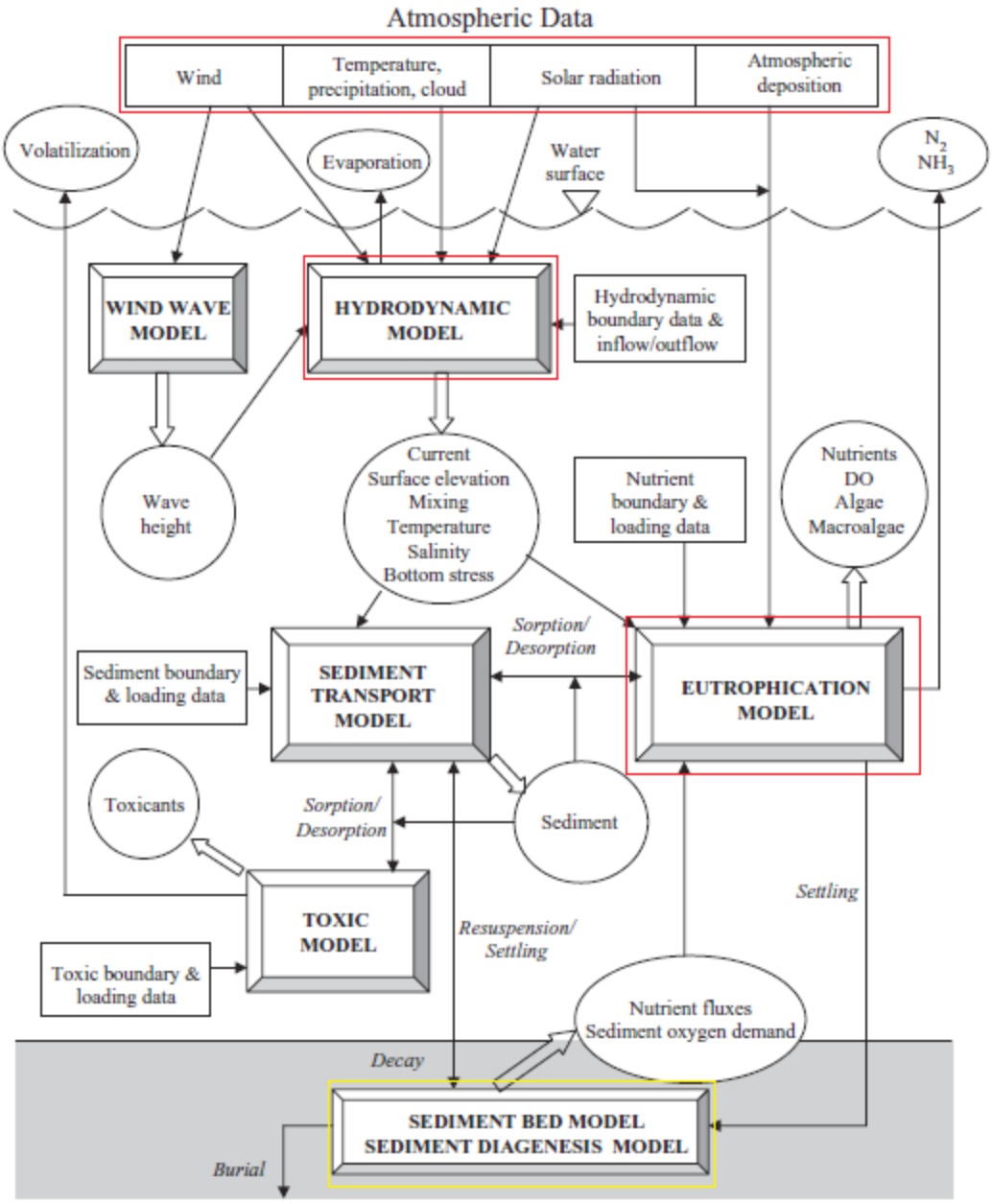

Figure 2-1 Major components (sub-models) of the EFDC model

of change of water quality. For the four kinds of nutrients (carbon, nitrogen, phosphorus, and silica), they have the direct relationship in their respective group(s), but there is a little direct relationship between the elements in the different nutrient groups although all of them link to the DO

concentration. Given that the actual situation in the study area after reviewing measured water quality, several state variables (silica, cyanobacteria, diatom algae, total active metal, and fecal coliform bacteria were not simulated because they either are the negligible elements such as silica, diatom algae, and cyanobacteria or have a weak influence on the DO simulation. Based on the calculated state variables everywhere in the study area, EFDC can also derive the concentration of total nitrogen, total phosphorus, and chlorophyll-a.

Table 2-1 The EFDC water quality model state variables

Water Quality Variable Group	Variable Number and Name
Algae	(1) Cyanobacteria (blue-green algae) (B_c)
	(2) Diatom algae (B_d)
	(3) Green algae (B_g)
	(22) Macroalgae (B_m)[b]
Organic carbon	(4) Refractory particulate organic carbon (RPOC)
	(5) labile particulate organic carbon (LPOC)
	(6) dissolved organic carbon (DOC)
Phosphorus	(7) refractory particulate organic phosphorus (RPOP)
	(8) labile particulate organic phosphorus (LPOP)
	(9) dissolved organic phosphorus (DOP)
	(10) total phosphate (PO4t)
Nitrogen	(11) refractory particulate organic nitrogen (RPON)
	(12) labile particulate organic nitrogen (LPON)
	(13) dissolved organic nitrogen (DON)
	(14) ammonia nitrogen (NH4)
	(15) nitrate nitrogen (NO3)
Silica	(16) particulate biogenic silica (SU)
	(17) available silica (SA)
Other	(18) chemical oxygen demand (COD)
	(19) dissolved oxygen (DO)
	(20) total active metal (TAM)[c]
	(21) fecal coliform bacteria (Feb)[d]

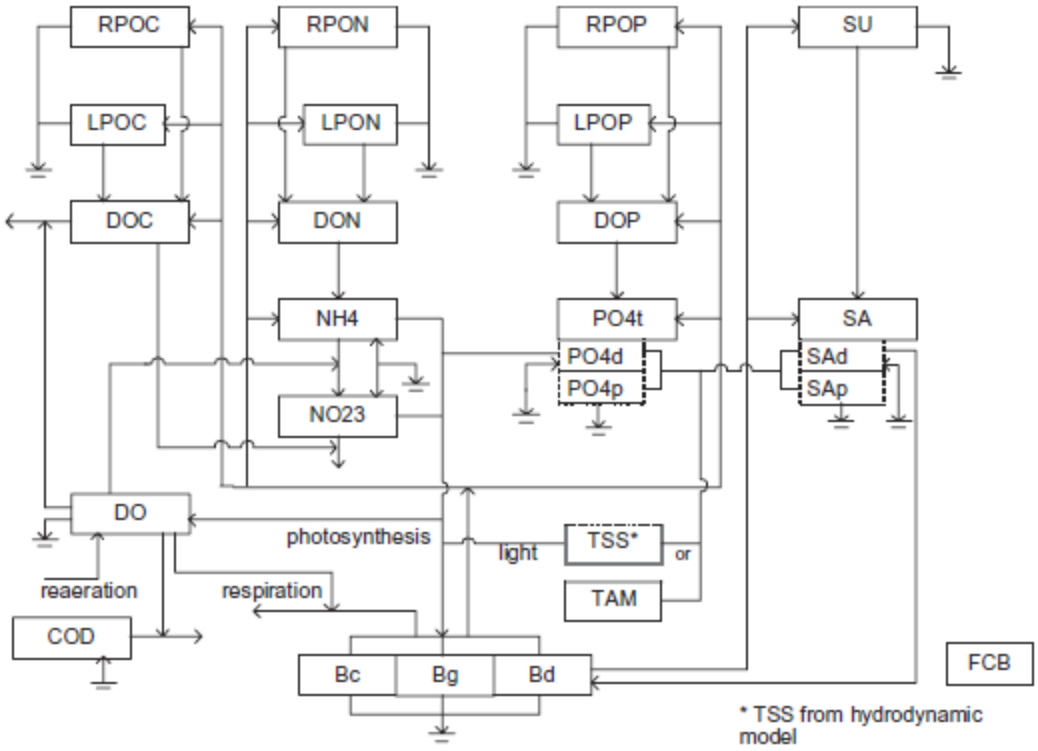

Figure 2-2 Schematic diagram showing the dynamics and interconnections of the state variables simulated in the water quality model

2.2.2 Hydrodynamic Model

Hydrodynamic is a study focusing on the motion of water featured the transportation of sediments, toxics, and nutrients in the water body. The solution of the hydrodynamic model is a complex process which often involves atmospheric forcing, Coriolis force and geostrophic flow, upstream inflows and downstream outflows. Their effect can be expressed as the flow velocity, pressure, density, and temperature functions of space and time under the governing of conservation laws. The precipitation, relative humidity, cloud cover, and atmospheric pressure can affect the water capacity holding by the study area showing by the change of water level. The wind speed and direction form the forces acting on the water column, together with the gravitational force, the viscous force, and the force from water pressure gradients. For a relatively large study area, Coriolis

force can also be significant to circulations in the water body, which is caused by the Earth rotation. Under the influence of the Coriolis force, the objects in the water body tend to deflect a few degrees to the right in the Northern Hemisphere to some extent. In addition, the dispersion also plays an important role in the transportation of dissolved substance such as the salinity, DO and so on, through the horizontal spreading and mixing of water mass caused by turbulent mixing and molecular diffusion. Besides, the turbulence model developed by Mellor and Yamada is used to represent the vertical mixing process in EFDC. The detail functions linking with the hydrodynamic model under the curvilinear horizontal and sigma vertical coordinate system are listed as the following:

$$\partial_t(m_x m_y Hu) + \partial_x(m_y Huu) + \partial_y(m_x Hvu) + \partial_z(m_x m_y wu) - m_x m_y f_e Hv = -m_y H\partial_x(p + g\eta) - m_y(\partial_x h - z\partial_x H)\partial_z p + \partial_z(m_x m_y H^{-1} A_v \partial_z u) + Q_u \quad (2.1)$$

$$\partial_t(m_x m_y Hv) + \partial_x(m_y Huv) + \partial_y(m_x Hvv) + \partial_z(m_x m_y wv) + m_x m_y f_e Hu = -m_y H\partial_y(p + g\eta) - m_x(\partial_y h - z\partial_y H)\partial_z p + \partial_z(m_x m_y H^{-1} A_v \partial_z v) + Q_v \quad (2.2)$$

$$\partial_z p = -gHb = -gH(\rho - \rho_0)\rho_0^{-1} \quad (2.3)$$

$$\partial_t(m_x m_y H) + \partial_x(m_y Hu) + \partial_y(m_x Hv) + \partial_z(m_x m_y w) = Q_H \quad (2.4)$$

$$\partial_t(m_x m_y H) + \partial_x(m_y H\int_0^1 u dz) + \partial_y(m_x H\int_0^1 v dz) = \int_0^1 Q_H dz \quad (2.5)$$

$$m_x m_y f_e = m_x m_y f - u\partial_y m_x + v\partial_x m_y \quad (2.6)$$

$$\rho = \rho(S,T) \quad (2.7)$$

$$\partial_t(m_x m_y HS) + \partial_x(m_y HuS) + \partial_y(m_x HvS) + \partial_z(m_x m_y wS) = m_x m_y \partial_z(H^{-1} A_b \partial_z S) + Q_S \quad (2.8)$$

$$\partial_t(m_x m_y HT) + \partial_x(m_y HuT) + \partial_y(m_x HvT) + \partial_z(m_x m_y wT) = m_x m_y \partial_z(H^{-1} A_b \partial_z T) + Q_T \quad (2.9)$$

where x and y = the curvilinear-orthogonal coordinates, z = vertical sigma coordinate, u and v = the horizontal velocities in the curvilinear-orthogonal horizontal coordinates (x, y); w = the vertical velocity in the stretched vertical coordinate, p = the excess pressure above the reference density hydrostatic pressure divided by the reference density ρ_0, z_s^* = the free surface elevation, z_b^* = the bottom or topography elevation, $H(=z_s^* - z_b^*)$ is the total water column depth in a grid, A_v = the horizontal eddy or turbulent viscosity, f_e = the Coriolis parameter; Q_u and Q_v represent additional forces or momentum sources and sinks, including horizontal turbulent momentum diffusion, vegetation resistance, and wave Reynolds stress due to high frequency gravity waves, Q_H = the source/sink term used to represent direct rainfall, evaporation, groundwater interaction, water withdrawals, and point and nonpoint source discharge, Q_T = the horizontal turbulent diffusion and external sources-sinks, m_x and m_y = the metric coefficients obtained by the model when curvilinear grids were transformed into Cartesian girds.

2.2.3 Temperature Model

Water temperature is almost the most important parameter in water quality modeling. All the other parameters of the hydrodynamic and water quality models are nearly in connection with the water temperature more or less. In addition, the water stratification is also affected by the vertical temperature profile because the water density changes with the temperature. The combining results from surface heat exchange and the water temperature of inflow and outflow in the study area determine the temperature of the water body (Eq. 2.10).

The surface heat exchange can be regarded as a combination of five processes, net solar shortwave radiation net atmospheric longwave radiation, longwave back radiation from the water, conduction, and evaporation (Figure 2-3) (Eq. 2.11). The net solar shortwave radiation is the

recorded radiation from the monitoring station (W/m^2). Solar radiation at the most weather stations is not recorded but estimated/predicted by the numerical models. Among the five processes, solar radiation is the most important in terms of magnitude. It primarily depends on the altitude of the sun and also reduces by cloud cover. It contributes to the surface heat exchange only in the daytime because there is no sunshine at night. The net atmospheric longwave radiation refers to the downward radiation from the atmosphere, which represents the mechanism of how the air temperature affects the heat flux penetrating into the water column. In contrast to the solar radiation, atmospheric radiation is a significant component for heat balance during the night because the air temperature will never reach absolute zero on the Kelvin scale.

For the longwave back radiation from the water, it means the upward radiation emitted by the water surface. This value is in connect with the surface water temperature. Conduction is a process that heat spontaneously transfers from a hotter to a colder body. It will occur when substance with different temperature come into contact. In the surface heat exchange model, conduction occurs only in the thin layer where the air touches the surface water. The evaporation is a process that the liquid surface water converts to the vapor state. In this process, latent heat flux is removed from the water body as the energy to break down the hydrogen bonds among the liquid water molecules to convert them to the vapor state. Equation 12 is the detailed temperature transport function in sigma coordinate,

$$Accumulation = inflow - outflow \pm surface\ heat\ exchange \tag{2.10}$$

$$H_{net} = H_s + H_L + H_E + H_C \tag{2.11}$$

where H_{net} = net heat flux across the air/water interface, H_s = shortwave solar radiation flux, H_L = net longwave radiation flux from the atmosphere and the waterbody, H_E = latent heat flux due to evaporation, and H_C = sensible heat flux due to conduction.

$$\frac{\partial(HT)}{\partial t}+\frac{\partial(HuT)}{\partial x}+\frac{\partial(HvT)}{\partial y}+\frac{\partial(wT)}{\partial z}=\frac{\partial}{\partial z}(\frac{A_b}{H}\frac{\partial T}{\partial z})+\frac{\partial I}{\partial z}+Q_T \tag{2.12}$$

where x and y = Cartesian coordinates in the horizontal direction, z = sigma coordinate in the vertical direction, H = water depth, A_b = vertical turbulent mass mixing coefficient, I = solar radiation, and Q_T = horizontal turbulent diffusion and external source/sinks.

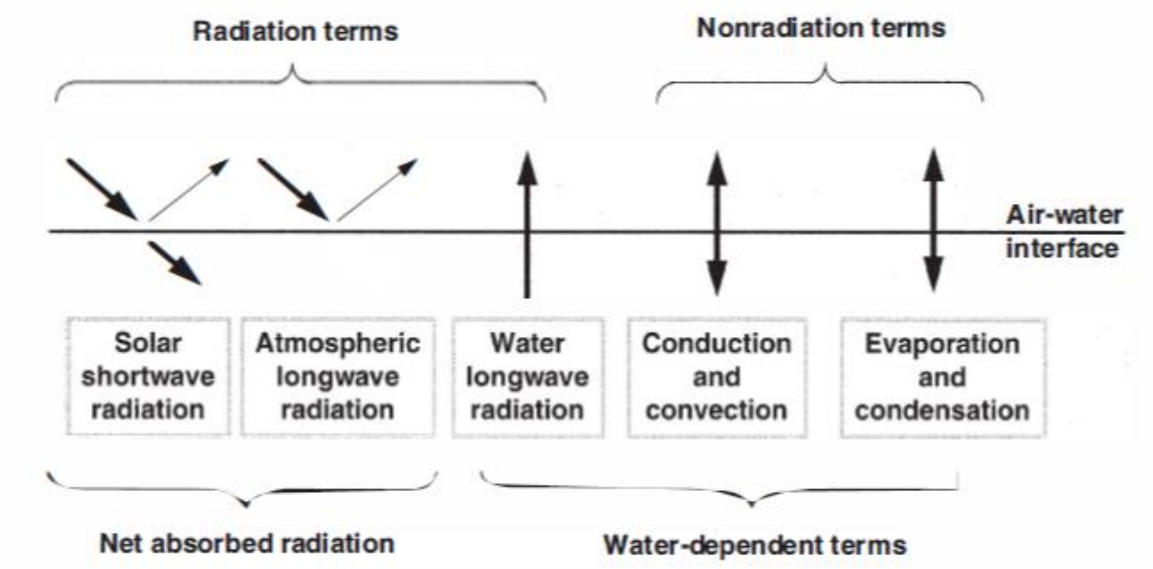

Figure 2-3 The components of surface heat exchange

2.2.4 Water Quality Model

Comparing with the above hydrodynamic processes that control the transport of pollutants, the water quality or eutrophication model focuses on the DO change that is linked with algae and nutrients as a function of space and time. Nutrients such as nitrogen, carbon, and phosphorus, provide the food for the algae growth that produces the oxygen through photosynthesis. In turn, the decomposition of the debris of the dead phytoplankton contributes to the source of the nutrients.

Nitrogen has two forms, inorganic and organic form (Eq. 13). Organic nitrogen is from the waste and the death of animals. The organic nitrogen can also be divided into three forms, refractory, labile and dissolved form based on the time scale for decomposition. The labile form often has a rapid decomposing period (weeks to months) while the refractory form needs years to decompose. Ammonia, nitrate, and nitrogen gas are the inorganic forms of Nitrogen. Although there is sufficient nitrogen gas in the atmosphere, it can only be absorbed and utilized by one special kind of algae, blue-green algae, which is the rare algae in the study area. Ammonia and nitrate are only two forms of Nitrogen suitable for algal growth. Although algae prefer to uptake nitrogen as the form of ammonia, nitrate can also be directly utilized by them for growth. Organic nitrogen can convert to ammonium through the mineralization or decomposition. Then nitrate can be generated through the nitrification process, ammonia oxidization in the presence of nitrifying bacteria and oxygen. When the DO is limited, nitrogen gas will be produced from nitrate through the denitrification process. Algae then utilize the inorganic nitrogen to synthesize the protein and the organic nitrogen is released with the death of them. The conceptual equations for the change of all forms of nitrogen are listed from Eq. 14 to Eq. 17 including total Nitrogen (TN), particulate organic Nitrogen (PON), dissolved organic Nitrogen (DON), ammonia (NH_4) and nitrate (NO_3).

$$TN = NO_2 + \frac{NH_3}{NH_4} + ON \tag{2.13}$$

$$\begin{aligned} &\textit{The change of } PON = \textit{Algal basal metabolism} + \textit{algal predation} - \\ &\textit{PON hydrolysis} - \textit{settling} + \textit{external source} \end{aligned} \tag{2.14}$$

$$\begin{aligned} &\textit{The change of } DON = \textit{Algal basal metabolism} + \textit{algal predation} + \\ &\textit{PON hydrolysis} - \textit{mineralization} + \textit{external loads} \end{aligned} \tag{2.15}$$

$$\begin{aligned} &\textit{The change of } NH_4 = \textit{Algal contributions} + \textit{DON mineralization} - \\ &\textit{nitrification} + \textit{bottom flux of } NH_4 + \textit{external source} \end{aligned} \tag{2.16}$$

$$\text{The change of } NO_3 = -\text{Algal uptake} + \text{nitrification} - \text{denitrification} + \text{bottom flux of } NO_3 + \text{external source} \quad (2.17)$$

where TN = total nitrogen, ON = organic nitrogen, NO_2 = nitrite, NO_3 = nitrate, NH_3 = ammonia gas, NH_4 = ammonium ion, PON= particulate organic nitrogen (the sum of the refractory organic nitrogen and labile organic nitrogen), DON = dissolved organic nitrogen.

Like the nitrogen, phosphorus also has an organic and inorganic form. It is a key nutrient for algal growth because it can convert sunlight into usable energy forms. Compared with nitrogen, phosphorus is regarded as a common limiting nutrient in the water body for algal growth. One reason is that the source of phosphorus is very limited, unlike the organic nitrogen which can be obtained from the nitrogen gas in the atmosphere through the fixation process. The second reason is that phosphorus is a very active element. The quick reactions with other cations reduce the amount of the inorganic phosphorus which is the suitable form for algal growth. Like the nitrogen cycle, the organic phosphorus is also from the death of algae (decomposition). Then the available form for algal growth, inorganic phosphorus can be converted from the organic form through the mineralization or decomposition process. Unlike the two forms of inorganic nitrogen (ammonia and nitrate), there is only one inorganic phosphorus form, orthophosphate that is suitable for algal growth. In addition, phosphorus does not exist in the gas phase. The conceptual equations for the change of all forms of phosphorus are listed from Eq.2.18 to Eq.2.20.

$$\text{The change of } TP = \text{Algal metabolism} + \text{algal predation} + \text{miniralization} - \text{settling of } PO4_p \pm \text{exchange of } PO4d \text{ at the sediment interface} + \text{external source} \quad (2.18)$$

$$\text{The change of } POP = \text{Algal basal metabolism} + \text{algal predation} - \text{POP hydrolysis} - \text{settling} + \text{external source} \quad (2.19)$$

$$\text{The change of } DOP = \text{Algal basal metabolism} + \text{algal predation} + \text{POP hydrolysis} - \text{mineralization} + \text{external source} \quad (2.20)$$

Algae is the primary producer in surface water when photosynthesis uses light to convert carbon dioxide and nutrients to the new organic material and release the oxygen. There are three kinds of algae, blue-green algae, diatom algae, and green algae, respectively. Blue-green algae is a special kind of algae which can fix the nitrogen gas in the atmosphere. This character makes it extremely tolerant in the environmentally stressed situation. With this attribute, nitrogen is not a limiting nutrient for blue-green algae growth. Diatom algae is a unique species due to its silica cell wall structure. This kind of algae requires silica in their metabolism activity. Therefore, they can only survive in the aquatic environment full of silica. Green algae are the most common algae. Their growth is limited to all the nutrients. The conceptual representation of the change of algae is showing in Eq.2.21.

$$\begin{aligned} &\textit{Net algal production} = \textit{algal growth} - \textit{metabolism} - \textit{predation} - \\ &-\textit{settling} + \textit{external source} \end{aligned} \tag{2.21}$$

DO is the core terms in water quality analysis. Especially in the estuary, the stratification may inhabit the surface DO passing to the bottom. The DO calculations involve in lots of the physical and chemical factors such as the solubility, transport, production, and consumption of DO. The factors affecting the change of DO can generally be divided into two groups: sink and source, as shown in Eq. 2.22. Eq.2.23 details the accurate sub items involving the change of DO.

$$\begin{aligned} \textit{Net change of DO} = {} & \textit{photosynthesis} - \textit{respiration} - \textit{nitrification} - \\ & \textit{DOC decomposition} - \textit{COD} + \textit{Reaeration} - \\ & \textit{SOD} + \textit{external loads} \end{aligned} \tag{2.22}$$

$$\frac{\partial DO}{\partial t} = \sum_{x=c,d,g} \left((1.3 - 0.3 \cdot PN_x) P_x - (1 - FCD_x) \frac{DO}{KHR_x + DO} BM_x \right)$$
$$AOCR \cdot B_x - AONT \cdot Nit \cdot NH4 - AOCR \cdot K_{HR} \cdot DOC - \frac{DO}{KH_{COD} + DO} \quad (2.23)$$
$$KCOD \cdot COD + K_r (DO_s - DO) + \frac{SOD}{\Delta z} + \frac{WDO}{V}$$

Where PN_x = preference for ammonium uptake by algal group x ($0 \le PN_x \le 1$); *AONT* = mass of DO consumed per unit mass of ammonium nitrogen nitrified; *AOCR* = dissolved oxygen/carbon ratio in respiration; K_r = reaeration coefficient (day-1); DO_s = saturation concentration of dissolved oxygen (g O_2/m^3); *SOD* = sediment oxygen demand (g O_2/m^2/day); *WDO* = external loads of dissolved oxygen (g O_2/day)

2.2.5 Previous Applications of EFDC

EFDC is a relatively new-developed versatile water quality model comparing with other water quality models but a lot of applications were applied due to its high accuracy of simulation results in the hydrodynamic and water quality simulation as the following.

A hydrodynamic and water quality model was developed using EFDC to simulate the fate and transport of nutrients, along with eutrophication dynamics in the estuarine system of Mispillion Creek and Cedar Creek, Delaware (Zou et al. 2008). Their model also included the surrounding tidal marsh areas in addition to the Mispillion Creek and Cedar Creek. The topography in this study is kind of like the Perdido and Wolf Bay system. Both of them focused on the hydrodynamic and water quality parameters simulation for the estuary. Seven variables (salinity, temperature, chlorophyll-a, PO_4, NH_4, NH_3, and DO) were calibrated using monitoring data at 9 stations in 2002, and it was applied to a subsequent year, 2003 to validate the model performance. The results show that the model was able to reasonably reproduce the observed spatial-temporal pattern of physical and biological features in the Mispillion Creek and Cedar Creek.

A similar study was also conducted to predict the algal blooming using EFDC model in Daoxiang Lake, China (Wu and Xu 2011). Daoxiang Lake is a typical city lake in China, that the main inflow of the lake comes from domestic and outflows mainly include evaporation, seepage, and irrigation for plants. With the water quality deterioration, two water bloom events happened in summer and autumn in 2005 and 2006, respectively. As a result, the landscape functions of the lake decreased rapidly because water body became feculent and smelly and many fish were killed. The field data from March to July 2008 were selected for the calibration of the eutrophication model and the data from August to October 2008 for the validation. The final modeled results showed that the EFDC model can successfully be used to predict the trend of chlorophyll-a on the whole. For the water quality simulation, sever other studies were applied to the different places around the world based on the similar methods, such as (Wang et al. 2008), eutrophication of the Danjiangkou Reservoir, China (Chen et al. 2016), eutrophication of the Yilong Lake, China (Zhao et al. 2013), water quality model of the Yonddam Lake, Korea (Seo and Kim 2011).

EFDC also has high accuracy when simulating the sediment in a shallow river. A study was conducted to investigate the transport processes of sediment and metals and the impacts of various contaminant sources in the river through modeling the sediment and metals in Blackstone River, Massachusetts (Ji et al. 2002). The Blackstone River is a shallow river with 77 km in length. Six variables (TSS, Ca, Cr, Cu, Ni, and Pb) were collected through September 22- September 24, 1992, November 2–November 6, 1992, and October 12–October 14, 1993, respectively to set up the model. Finally, the sediment transport and resuspension processes are depicted satisfactorily in the model by validating the model in 1994.

In addition, to simulate the hydrodynamic and water quality variables corresponding to the natural change, EFDC also can be used to study the waterbody hydrodynamic change due to the introduction of the man-made facility such as power plant. Hamrick et al. conducted an analysis

of water temperature in Conowingo Pond as influenced by the Peach Bottom atomic power plant thermal discharge which is located in York County, Pennsylvania ((Hamrick and Mills 2000)). Conowingo Pond serves as a cooling reservoir for the power plant that is approximately 23 km long and widths range from 800 m to 2.4 km with an average depth 7 m. The final water temperature comparison results between model results and field observations in the summer of 1997 indicate that this model is very capable of predictive thermal simulation on seasonal and annual time scales. Besides, several other studies focusing on the hydrodynamic variables simulation using EFDC model also reached a satisfactory agreement between the observed data and simulated results, such as Hydrodynamic modeling of the James River (Hamrick 1995), water temperature simulation of the Conowingo Pond (Hamrick and Mills 2000), salinity intrusion characteristics analysis of the Geum River, Korea (Jeong et al. 2010), hydrodynamic modeling of the Yongdam Lake, Korea (Seo et al. 2010), tidal currents simulation of the Jiaozhou Bay, China hydrodynamic analysis of the Nakdong River, Korea (Hur and Park 2009).

CHAPTER 3 EFDC Model Development for the Perdido and Wolf Bay System

3.1 Study Area

The Perdido and Wolf Bay system (the study area) is a shallow to moderately deep inshore water body in southeast Alabama and southwest Florida (Figure 3-1). It is an inter-connective estuarine system that isolates itself from the surrounding water bodies (Figure 3-1): The Gulf of Mexico (south), Mobile Bay (west) and Big Lagoon (east). The Wolf Bay is a relatively small and shallow inland estuary with the surface 14.7 km^2 and an average depth of 1.9 m in Baldwin County, Alabama (Devkota et al. 2013). The Wolf Bay is connected eastward to Perdido Bay and its west connects to the Mobile Bay through a very long and narrow navigational channel, the Gulf Intercoastal Waterway (GIWW). Five tributaries, Wolf Creek, Mifflin Creek, Owens Bayou, Graham Bayou, and Hammock Creek are the freshwater sources flowing into the Wolf Bay from the north. The Wolf Creek is the primary inflow source flowing into the Wolf Bay (Lusk 2017).

The Perdido Bay is located at the border between the Baldwin County, Alabama, and the Escambia County, Florida. The surface area and average depth of the Perdido Bay are approximately 130 km^2 and 2.6 m, respectively. It is connected eastward to the Big Lagoon through the Dolphin Pass and southward to the Gulf of Mexico through a fan-shaped outlet named Perdido Pass (Figure 3-1). Four rivers are the freshwater sources to the Perdido Bay in the north: the Perdido River, Styx River, Elevenmile Creek, and Bayou Marcus. Among them, the Perdido River is the primary source of freshwater input to the estuary, which flows southward about 96.5 km long (Livingston 2000). Although there are 9 freshwater rivers and three open boundaries flowing into

the study area, the hydrodynamics and water quality distribution in the lower Perdido Bay are primarily influenced by the tidal fluctuations from the Gulf of Mexico through the Perdido Pass due to its high salinity and water level variation. Despite the ocean water from the Mobile Bay, Big Lagoon also exerts certain influences on the study area in a similar way like the Gulf of Mexico, the magnitudes of their influences are significantly decreased by the long and narrow connecting channel to the Perdido and Wolf Bay.

The Perdido Bay can be divided into three regions based on their geographic uniqueness: the upper Perdido Bay (north of the route 98 bridge), lower Perdido Bay (bounded to the south by a line between Ross Point and Innerarity Point), and the Perdido Pass Complex (Livingston 2000) (Figure 3-1). For the upper Perdido Bay, it could be significantly affected by its upstream rivers during the wet season. During the rest of the year, it is affected by the combining forces from the upstream inflow and the tidal current from the south. For the lower Perdido Pass complex, it is primarily under the control of the Gulf of Mexico. The lower Perdido Bay is in the region which is affected by the above both forces (freshwater inflows and tides) all the time.

The Perdido Pass is the mouth of the Perdido Bay with the surface 0.37 km^2 (Figure 3-2). It forms a water passage that connects Perdido Bay with the Gulf of Mexico to the south, 2 miles west of the Alabama/Florida state line. The water passage is wrapped by the lands on the east and west with the open ends along the north-south direction, where the tides from the Gulf of Mexico exchange with the Perdido Bay. At the entrance into the Gulf, the two rock barriers are the west jetty and east jetty (https://en.wikipedia.org/wiki/Perdido_Pass). Comparing with the east boundary, a nearly straight coastal line, the west boundary of the Perdido Pass has a triangular shape layout. The widths of the north and south ends, and the widest part are 257 m, 200 m, and 570 m, respectively. This wedge-shaped entrance can reduce the flow speed from the ocean due to the buffer effect of the expansion part in the middle of the Perdido Pass.

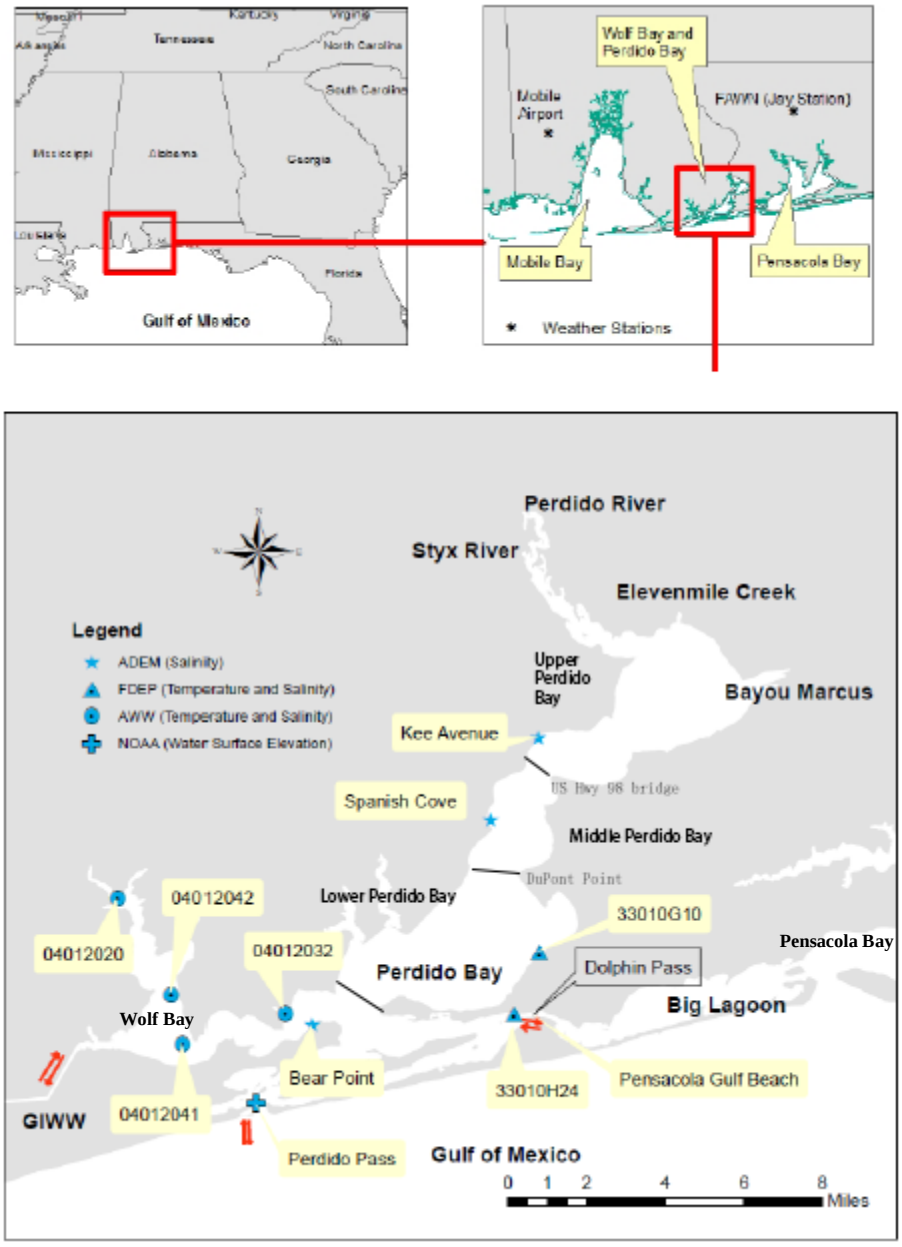

Figure 3-1 Location of the Perdido and Wolf Bay

The Perdido Pass is the mouth of the Perdido Bay with the surface 0.37 km^2 (Figure 3-2). It forms a water passage that connects Perdido Bay with the Gulf of Mexico to the south, 2 miles west of the Alabama/Florida state line. The water passage is wrapped by the lands on the east and west with the open ends along the north-south direction, where the tides from the Gulf of Mexico exchange with the Perdido Bay. At the entrance into the Gulf, the two rock barriers are the west jetty and east jetty (https://en.wikipedia.org/wiki/Perdido_Pass). Comparing with the east boundary, a nearly straight coastal line, the west boundary of the Perdido Pass has a triangular shape layout. The widths of the north and south ends, and the widest part are 257 m, 200 m, and 570 m, respectively. This wedge-shaped entrance can reduce the flow speed from the ocean due to the buffer effect of the expansion part in the middle of the Perdido Pass.

A bridge spanning the Perdido Pass forms the boundary separating the Perdido Pass and the Terry Cove (Figure 3-2). The Terry Cove is a 1.27 km^2 T-shaped water body connecting with three surrounding water bodies: Cotton Bayou (west), Perdido pass (south), and Bayou Saint John (east). Comparing with the Cotton Bayou, Bayou Saint John that has turnings and small islands in the water to weak the tides from the Gulf of Mexico, the Terry Cove is directly exposed to the fire of the oceanic tides. This leads to strong hydrodynamic mixing so that the salinity and water temperature in this region are close to those in the Gulf of Mexico.

The Cotton Bayou (the focus area of the study) and its surrounding areas (Terry Cove and Perdido Pass) are the locations where large fish kills were observed from 7/31/2015 to 8/3/2015 (Figure 3-2). Under normal conditions, the whole region forms a pleasant recreation area featuring plenty of the wharves and beaches. The Cotton Bayou is a semi-closed small-shallow bay that connects Terry Cove and Perdido Pass to the west, and it is in the city of Orange Beach, Alabama. It is a small bay with the surface 0.73 km^2, the average depth of 1.36 m, and a shoreline length of 6.24 km. The shape of the Cotton Bayou is somewhat like the letter V, with the closed end in the

extreme west and the east open end having the widest distance (515 m) from north bank to south bank. There is a relatively large island near the east open end although the land area above the water surface is small. There is a relatively narrow neck connecting the east open end and the open-water (lake likely) region (Figure 3-2). This diminishing caliber shape makes the west side of the region less susceptible to the tides from the Gulf of Mexico compared with its east side because the land surrounding the bay gradually reduces the strength of winds and blocks waves.

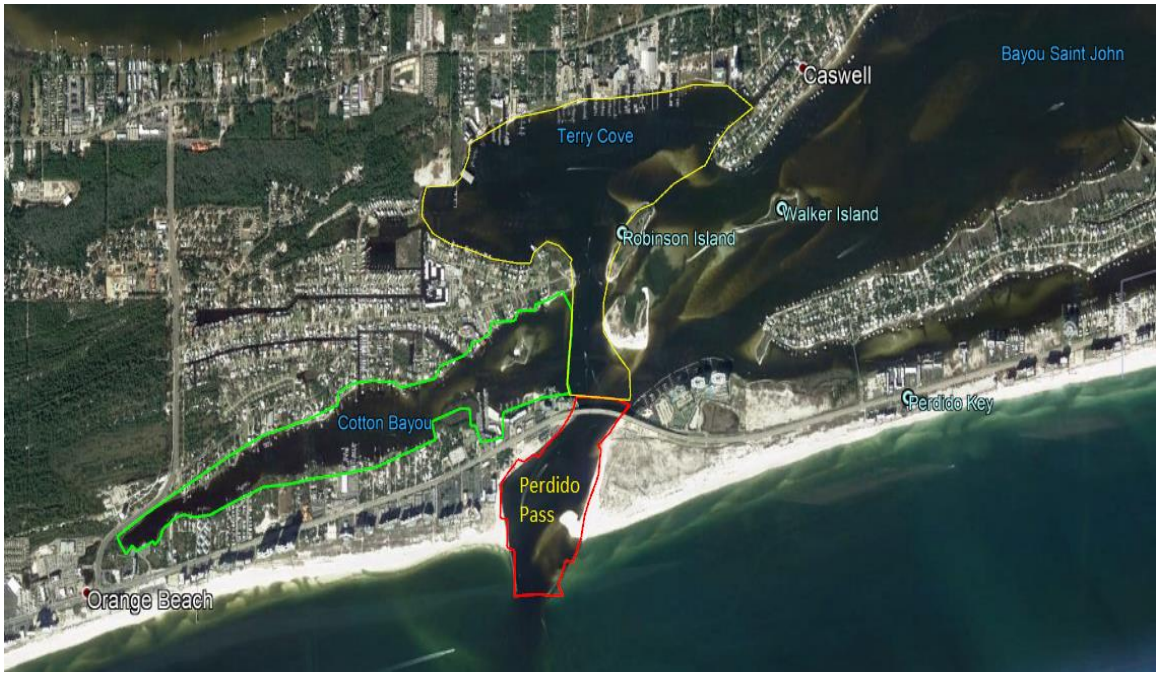

Figure 3-2 Locations and outlines of the Cotton Bayou, Terry Cove, and Perdido Pass

The lower portion of the Perdido and Wolf Bay system has a complex shoreline configuration, varying bathymetry, and complex flow pathways (Figure 3-3). The resulting action of the above geographic characteristics would affect the salinity exchange in this area. Four sub-regions are included in this region, Bayou Saint John, Terry Cove, Perdido Pass, and Cotton Bayou. Contrasting with the other three subregions that would be significantly affected by the Gulf of Mexico, the Bayou Saint John would probably primarily be influenced by the Big Lagoon, the model's east side boundary, instead of the nearby Gulf of Mexico. This is because there are several

small highlands (Robinson Island and Walker Island, Figure 3.2) like the alluvial plain lying in the middle between Perdido Pass and Bayou Saint John. These high lands potentially prevent the water exchange between them in a way.

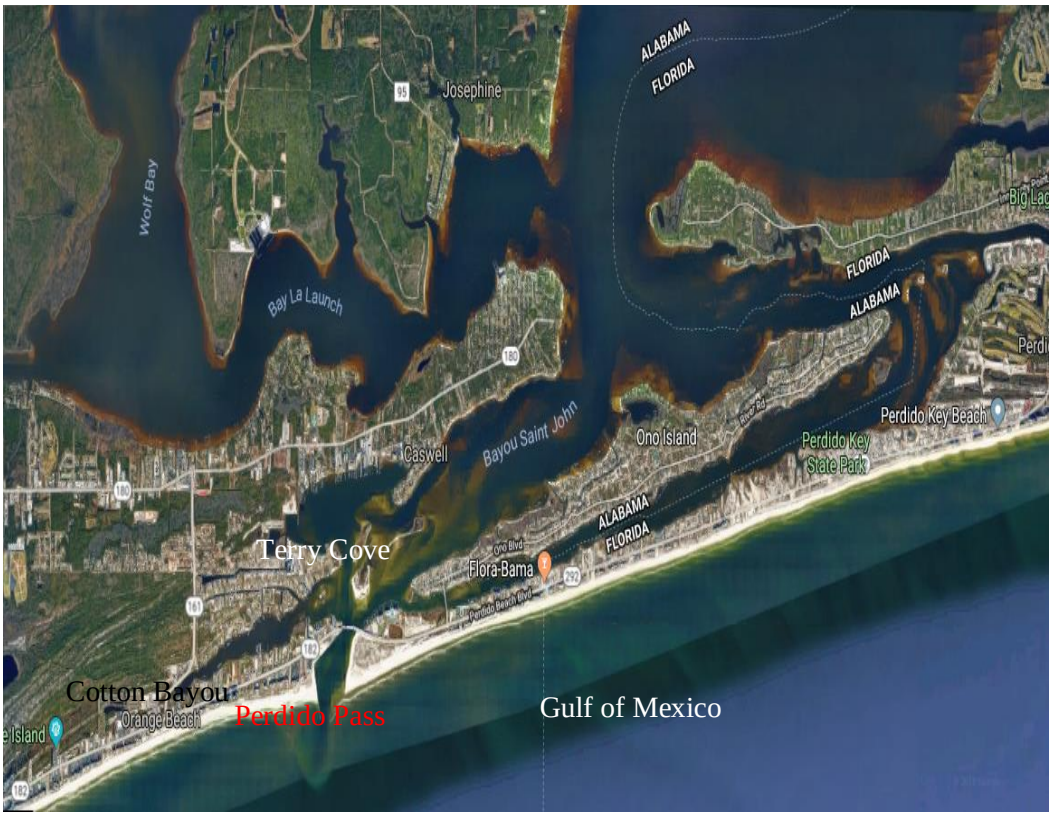

Figure 3-3 Lower portion of the Perdido and Wolf Bay system showing complex flow pathways

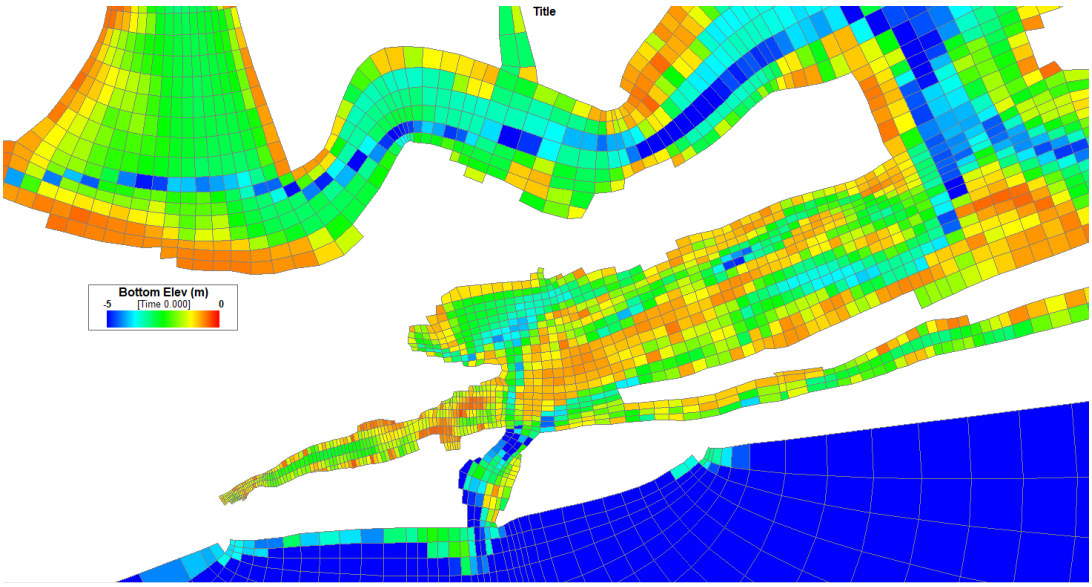

Figure 3-4 Bottom elevation configuration for the lower portion of the Perdido and Wolf Bay system

3.2 Model Grid Modification

3.2.1 Existing Perdido and Wolf Bay Hydrodynamic Model

The grid creation of the study area is the first step to develop a two- or three-dimensional numerical model. A model grid is a network of grid cells (or points) covering the study area (Ji 2017). Although rectangular grids are the simplest configuration representing the study area, curvilinear grids were used in this study due to the highly irregular characteristics of the shorelines and islands in the Perdido and Wolf Bay system. The curvilinear coordinates are better to simulate how the irregular boundaries would affect the water flows because the flows near the borderlines are always parallel to the boundaries instead of colliding with them representing in the Cartesian coordinates.

The water temperature and salinity simulation and analysis in 2008 and 2009 for the same study area, the Perdido and Wolf Bay system, were done by Devkota using the EFDC hydrodynamic model (Devkota et al. 2013). Their model had a reasonably good agreement between

the observed and simulated hydrodynamic variables such as water temperature, salinity and so on. Since there is no significant change of the shorelines, the grid configuration file from their model was directly used in this study after doing some modifications. The detailed steps to create the original grid cells are given in Appendix A.

3.2.2 Modification of Grid Cells

Since the previous study by Devkota et al. (2013) was primarily focused on the Wolf Bay, not Cotton Bayou, the grid network of Cotton Bayou in the original EFDC model is relatively coarse for the current study. Therefore, it is necessary to do some modifications to make the model fully simulate the hydrodynamic and water quality variables in the focus area. The modifications primarily added grid cells in the Perdido Pass and Cotton Bayou.

Figure 3-5 shows the change of grid cells in the Perdido Pass by comparing the grid cells configurations under the original and revised version. The number of grid cells increased by 38.5% from 52 cells to 72 cells. The covered surface area increased by 40% from 0.3 km^2 to 0.42 km^2. The average cell sizes under the original and revised version are 5769 m^2 and 5800 m^2, respectively. It can be seen that there is an obvious change of the model coverage (spatial area) from the original version to the revised version. The effect to the current research from the revised model is not limited to the more coverage and higher resolution with smaller cell size. An important effect is that it obviously changed the shape of the Perdido Pass, from the smooth water passage to a likely diamond-shaped exchange mouth. The revised shape will obviously decrease the flow speed from the Gulf of Mexico due to the buffer function of the expansion part in the middle of the Perdido Pass.

The similar comparison for the model coverage in the Cotton Bayou is shown in Figure 3.6. Visually an extension part was added to the west side of the original map and the size of a single cell is significantly decreased. This change allows the revised model to fully cover the whole

Cotton Bayou with a much higher resolution. There are 70 cells covering 0.67 km^2 surface water in the original model. In contrast to the original model, the revised model contains 443 cells covering 0.93 km^2. The number of cells and covering area are increased by 533% and 39%, respectively. The average cell sizes are decreased by 78% from 9571 to 2100 m^2. The obvious decrease of the cell size would significantly improve the simulation accuracy in the focus area, especially considering the complex bathymetry condition in the shallow and narrow Cotton Bayou. In the process of modifying the grid cells, Delft3D, a three-dimensional modeling suit for hydrodynamic calculation, was used to do the modification.

After the modification, the current model cover $mile^2$ of the simulation domain (43.86 km^2 in the upper Perdido Bay, 50.56 km^2 in the middle Perdido Bay, 0.37 km^2 in the Perdido Pass, 0.73 km^2 in the Cotton Bayou, 20.6 km^2 in the Wolf Bay, 184.7 km^2 in the Gulf of Mexico) with 5303 curvilinear horizontal grids and 4 layers in the vertical direction, a total of 21,212 3D cells.

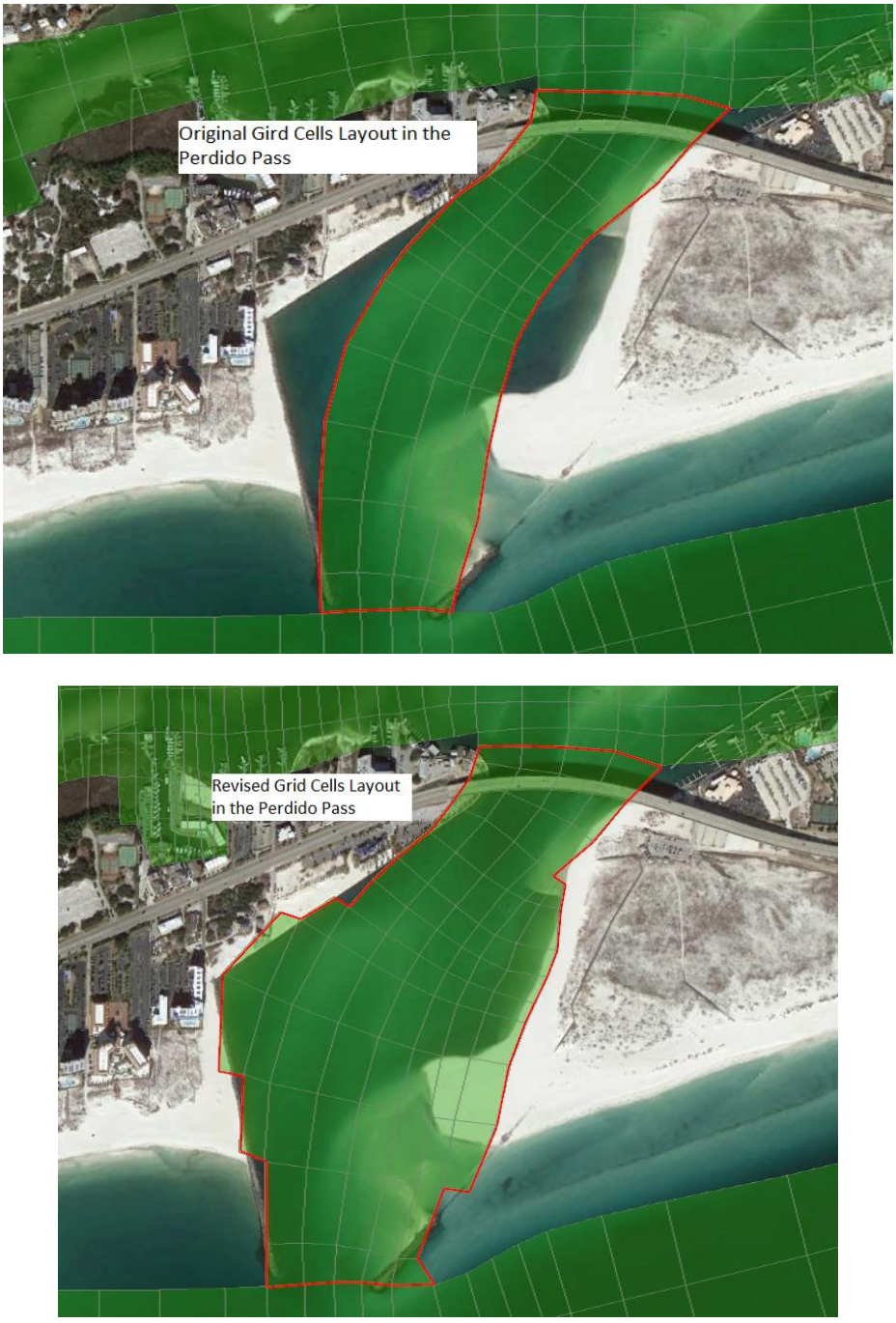

Figure 3-5 Grid cells layout comparison between original and revised scenarios in the Perdido Pass

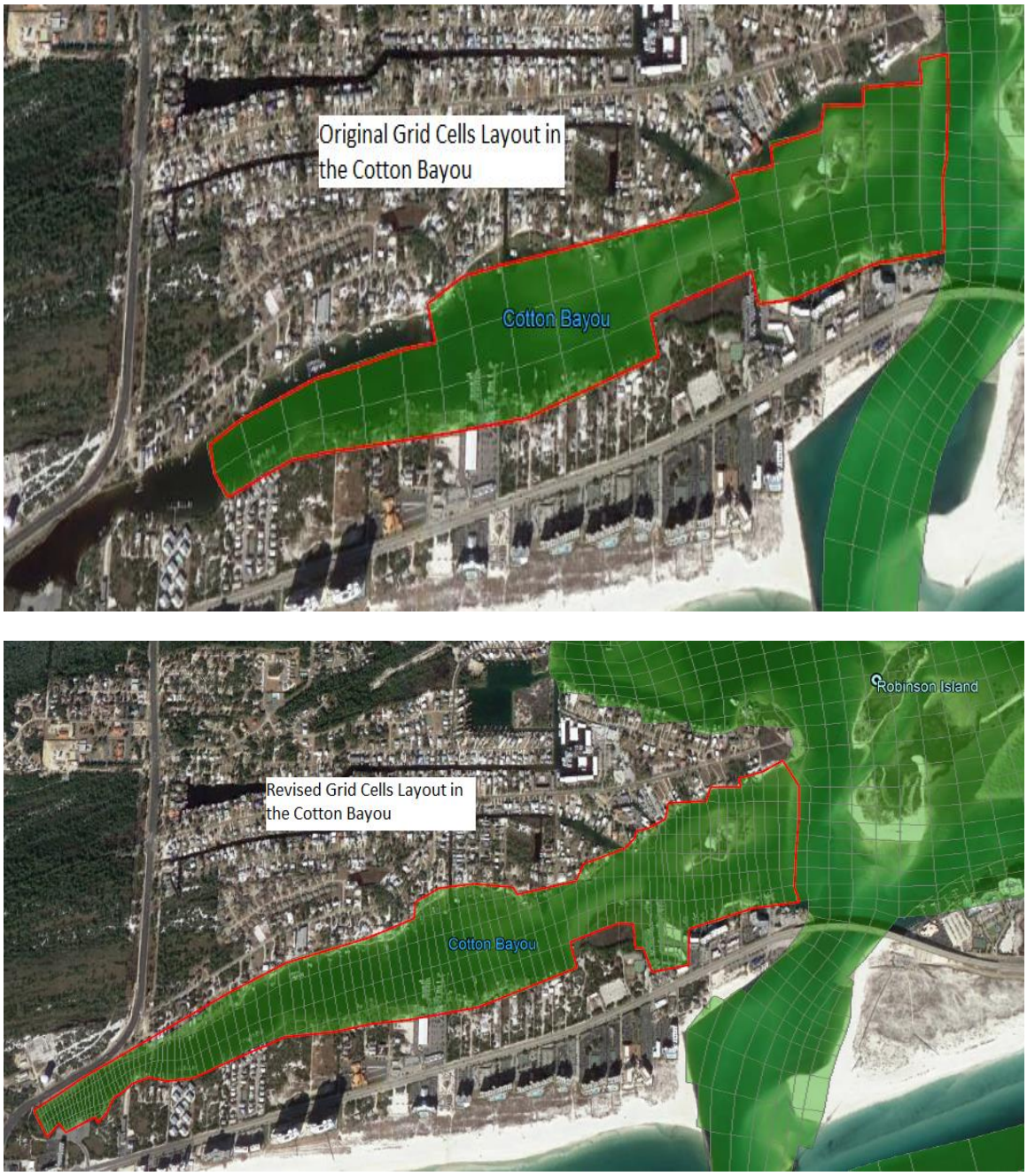

Figure 3-6 Grid cells layout comparison between original and revised scenarios in the Cotton Bayou

3.2.3 Bathymetry Data

The term bathymetry in this study means the ocean's depth relative to sea level. It is a key input for a three-dimensional surface-water model. The bathymetry data, which were recorded based on the Mean Lower Low Water (MLLW), were obtained from the NOAA website (https://maps.ngdc.noaa.gov/viewers/bathymetry/). The limitation of the downloaded bathymetry data is that the data were not collected in recent years and not all the bathymetry data were measured in the same year. This is because the study area (Figure 3-1) is a relatively wide area and NOAA only provides the water depth data for a part of the study area as a unit. Therefore, the final available bathymetry is a combination of the data from several broader overlapped measurement zones. The latest NOAA bathymetry data were measured in 2007 and the oldest ones are from the measurements done in 1985. However, the latest bathymetry data in 2007 are primarily measured in the upper Perdido Bay area.

For the focus area (Cotton Bayou), the bathymetry data were from the measured values in 1994. There were total of 219 measured depth values from NOAA in Cotton Bayou (Figure 3-7). The deepest depth was 2.7 m and the shallowest depth was 0.3 m. Among the 219 observed depth values, 31 depths were between 2.5 m and 2.7 m, 42 depths are between 2 m and 2.5 m (not including 2.5 m), 34 depths were between 1.5 m and 2 m (not including 2 m), 48 depths were between 1 m and 1.5 m (not including 1.5 m), 41 depths were between 0.5 m and 1 m (not including 1 m), and 15 depths were less than 0.5 m. These 219 depth measurement points were not uniformly distributed in Cotton Bayou. Using the surface area (A_s) of 930,000 m^2 (0.93 km^2) and the maximum depth (H_{max}) of 2.7 m, one can find the lake geometry ratio $GR = As^{0.25}/H_{max} = 11.5\ m^{-0.5}$. This large geometry ratio (> 5) indicates Cotton Bayou is a polymictic waterbody that can be mixed many times in a year. It does not mean Cotton Bayou cannot be stratified over a short period of time that is the research topic of the study: under what environmental and weather conditions Cotton Bayou can be stratified. When it was stratified, especially under hot weather condition, if water

temperature became quite high and dissolved oxygen became enough low in Cotton Bayou, then fish kill would happen.

Figure 3-8 shows the bottom elevation distribution of 443 grid cells in the focus area, which is derived from the NOAA bathymetry data in 1994. Through the plot, it can be seen that the focus area was primarily modeled by three rows of simulation cells: north row (labeled cells from 1330 to 1428), middle row (labeled cells from 1177 to 1275), and south row (labeled cells from 1012 to 1110) (Figure 3-8). Visually the bottom elevations in the middle row of the simulation cells are deeper than the ones in the other two rows. The deepest bottom elevations are primarily located in the middle row of cells from 1206 to 1239 with the depth around -2.5 m (Figure 3-8). The distance between the deepest cells labeling 1206 to 1239 is 1.2 km and it takes up around 40% of the total center-line from the west to the east in Cotton Bayou (3.1 km). Figure 3-8 shows that the bottom elevations in the north and south rows are bumpy instead of smooth variation. In reality, the bottom elevation does gradually increase/decrease representing seabed. This is because 0.93 km^2 of Cotton Bayou is represented by 443 computational grid cells, with an average size of one cell 2100 m^2. The bottom elevation of any cell in the EFDC model represents the average depth of all the observed data located in that cell. Some of the model cells along the coastal line also include small parts of lands. The average bottom elevations for those three rows (north, middle, and south) are -1.23 m, -1.75 m and -1.27 m, respectively.

Since the sigma coordinate was used in the vertical direction, the effect from the stale data can be minimized because sigma coordinate allows the smooth representation of the bathymetry and same order of accuracy in shallow and deep waters (Ji 2017). The sigma coordinate system is a common coordinate system used in computational models for oceanography, meteorology and other fields where fluid dynamics are relevant (https://en.wikipedia.org/wiki/Sigma_coordinate_system). The sigma coordinate system applies the same number of vertical layers to the whole

water body regardless of the variation of the water depths. However, the thickness of the vertical layers in one grid is different from one in another grid with different water depths. The sum of the thicknesses of all the horizontal cells (layers) along the vertical direction represents the water depth at that point. Typically, the thicknesses of vertical layers in each grid are the same (thickness = depth/n-layer) but EFDC also allows users to set different thicknesses along with the depth in each grid. Due to this property/character, the sigma coordinate can smoothly delineate the change of the ocean bathymetry.

Figure 3-7 The locations map of the bathymetry data from NOAA

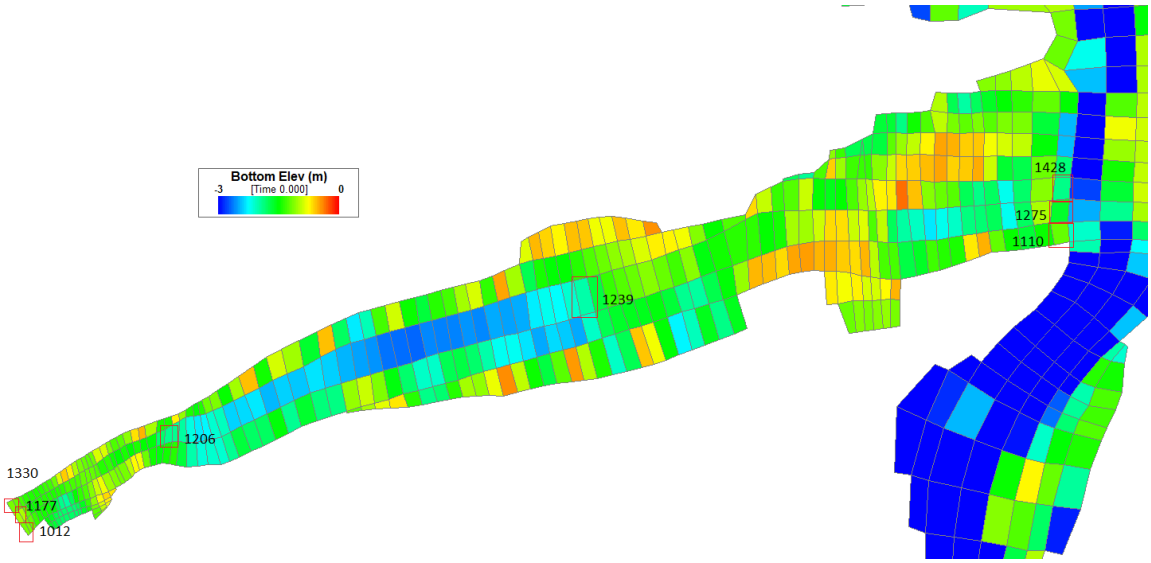

Figure 3-8 The cells labeled with ID and showing the bottom elevations in the Cotton Bayou

3.3 Input Data

3.3.1 Overview of the Input Data

Simulating water temperature and DO conditions in Cotton Bayou is one of the key tasks of the study. At first sight, DO simulation looks like a straightforward and clear process. However, DO modeling is a complex and elaborate process relating to preparing dozens of input data files and selecting many internal model coefficients. In general, the input data can be categorized into two groups: hydrodynamic and water quality modeling (Table 3-1); and two types: initial conditions and boundary conditions (time series data for unsteady simulation). If any state variables (Table 2-1) were activated for EFDC to simulate, corresponding input data of those variables should be provided at all boundaries of the simulation domain and for initial conditions, as shown in Table 3-1. Typically, we do not have/provide velocity input data for flow boundaries instead of flow discharge or water levels.

The hydrodynamic modeling is a process of studying the water motion, e.g., simulate flow velocities *u*, *v*, and *w* in each grid. It works as a power source to transport/spread the sediments and

nutrients in the waterbody. The hydrodynamic EFDC model simulates also water temperature and salinity, which is different from other hydrodynamic models since both affect the density of water. The water temperature and salinity simulated in the hydrodynamic part also provide crucial information for the subsequent water quality modeling since temperature affects all chemical and biochemical reactions/processes and both affect the saturated DO concentration then oxygen reaeration at the water surface. For the water temperature modeling, meteorological input data as atmospheric boundary conditions are needed. The meteorological data for EFDC are organized into two data files: the first one including time series of wind speed and wind direction and the second one including all remaining weather parameters (time series of atmospheric pressure, air temperature, relative humidity, precipitation, solar radiation, cloud cover, and evaporation).

Comparing with the above hydrodynamic input variables, the water quality modeling directly links with the DO calculation through quantifying the interactive effects among the algae, nutrients and DO. The input variables, algae, DO, and nutrients, are used to simulate the biological productivity which is the real source and sink items of the DO. Nutrients, nitrogen, and phosphorus, provide the food for the algae which produce the oxygen. In turn, the debris of the dead phytoplankton contributes to the source of the nutrients (Chapra, 1997).

Table 3-1 Required input data for EFDC hydrodynamic and water quality modeling

EFDC Model Input Variables by Categories (File Groups)	
Hydrodynamic Modeling	1. Inflow discharge or water level 2. Inflow temperature 3. Inflow salinity 4. Meteorological variables (atmospheric boundary conditions): wind speed & direction, atmospheric pressure, air temperature, relative humidity, precipitation, solar radiation, cloud cover, and evaporation[#]
Water Quality Modeling	5. Cyanobacteria (blue-green algae) (B_c)[#], diatom algae (B_d)[#], green algae (B_g), and macro algae (B_m)[#]; 6. Refractory particulate organic carbon (RPOC), labile particulate organic carbon (LPOC), dissolved organic carbon (DOC); 7. Refractory particulate organic phosphorus (RPOP), labile particulate organic phosphorus (LPOP), dissolved organic phosphorus (DOP), total phosphate (TP); 8. Refractory particulate organic nitrogen (RPON), labile particulate organic nitrogen (LPON), dissolved organic nitrogen (DON), ammonia nitrogen (NH4), nitrate nitrogen (NO3); 9. Particulate biogenic silica (SU)[#], available silica (SA)[#]; 10. Chemical oxygen demand (COD), dissolved oxygen (DO); 11. Total active metal (TAM)[#], fecal coliform (Feb)[#]

[#]Variables were not simulated or used for the Perdido-Wolf Bay model.

3.3.2 Boundary Condition Settings and Simulation Periods

Since the study area is a relatively wide water body, several boundaries were set to represent how the adjacent rivers affect the study area (Figure 3-9): four tributaries discharging into the Perdido Bay (Styx River, Perdido River, Elevenmile Creek, and Bayou Marcus), five tributaries flowing into the Wolf Bay (Wolf Creek, Mifflin Creek, Owens Bayou, Graham Bayou, and Hammock Creek), flow exchange from the Gulf of Mexico and through Dolphin Pass and GIWW (Figure 3-1). Among 12 flow boundaries, the last three boundaries are the open boundaries through which the flow exchanges between inside and outside of the water body occur. Other nine boundaries are time series of inflow discharges as input data for the EFDC model.

The EFDC model developed in this study run in different simulation periods for the hydrodynamic and water quality modeling due to the limitation of the available observed data. For the hydrodynamic modeling, water temperature and salinity were simulated over three years from 1/1/2015 to 12/31/2017. The water quality modeling was performed in two years, i.e., from 1/1/2015 to 12/31/2016. The sensitive analysis was done based on the simulation from 5/10 to 9/15 in 2015 and 2016. The simulation time periods for sensitive analysis were reduced to one third of the original running for the following three reasons, 1) the DO concentration change in July and August are most interested since the fish kills occurred in this time period and this time period is also the DO minimization threshold period due to the high temperature in summer, 2) it takes around one and half weeks to run through the two years simulation, 3) the purpose of sensitivity analysis is to find which parameter(s) has/have the significant effect to the DO instead of providing a predictive simulation results. Therefore, 128 days of simulation in one year (5/10 – 9/15) was chosen to do the sensitivity analysis.

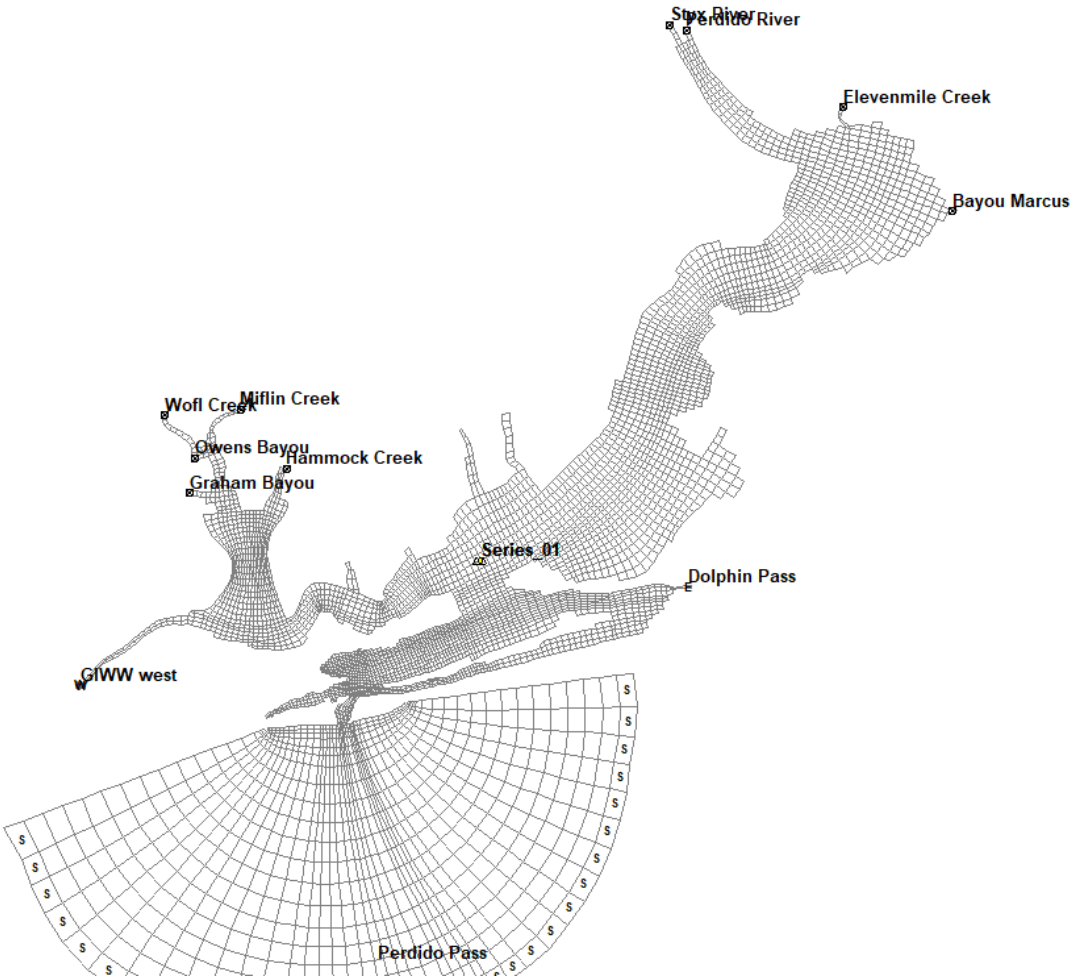

Figure 3-9 Boundary condition configurations

3.3.3 Flow Data and Water Surface Elevation

In the model, there are two kinds of boundaries representing the flow change received by the EFDC model, flow data and water surface elevation. Flow data were assigned to upstream rivers where the freshwater flows into the Perdido and Wolf Bay system. The water elevations represented the flow exchange in the three open boundaries: the Gulf of Mexico, Dolphin Pass, and GIWW.

For the four tributaries discharging into the Perdido Bay (Styx River, Perdido River, Elevenmile Creek, and Bayou Marcus), the flow data in 2015–2017 were obtained from the closest USGS gaging stations (Figure 3-10). Figure 3-11 -

Figure 3-15 plot the flow comparison in 2015 -2017 at each station. Statistical summary of observed USGS discharges in 2015 and 2016 is given in Table 3-2 including maximum, minimum, average discharges and standard deviations (m^3/s).

In the Wolf Bay, only the flow data for the Wolf Creek were available from USGS and ranged from 0.06 to 13.54 m^3/s with an average of 0.27 m^3/s in 2015 (Table 3-2). There were no recorded flow data for the other four smaller tributaries flowing into the Wolf Creek (Miflin Creek, Owens Bayou, Graham Bayou, and Hammock Creek). The previous research conducted by Dr. Devkota for the same study area in 2008–2009 used discharges simulated by SWAT model for those four tributaries. By plotting discharge data in the four tributaries versus discharge in the Wolf Creek, four regression equations were derived with R^2 greater than 0.95. Then discharge in the four rivers were calculated using the regression equations for the current study period (Figure 3-16).

Since the recorded flow data for Wolf Creek, Styx River, Elevenmile Creek, Bayou Marcus, and Perdido River are 15-minute, 30-minute, 30-minute, 30-minute, and 60-minute data, respectively, linear interpolation was used to extend all the flow data to 15-minute data. Figure 3-10 shows observed USGS-gaging discharges of four rivers flowing into the Perdido bay in 2015–2017 and indicates that the Styx and Perdido rivers are the major sources of inflow discharging into the Perdido Bay. Table 3-2 shows that the discharge increased from 2015 to 2017 based on the average water flow. The discharge from Wolf Creek is similar to the discharge from Bayou Marcus (Table 3-2), which provided the smallest flow to the Perdido Bay. Although the maximum discharges from Styx River and Perdido River in 2015 were larger than corresponding maximum discharges in 2016, their average discharge in 2016 was higher than ones in 2015 for both inflows into Perdido Bay and Wolf Bay.

EFDC allows not also discharge but also water level as boundary conditions to model hydrodynamic in a water body. Compared with the discharge input data, water level input as the

boundary can better represent tidal influences. In the current model, the water level was assigned to three boundaries, the Gulf of Mexico, Dolphin Pass, and GIWW. Two monitoring stations: Dauphin Island station and Pensacola Gulf station, offer the available water level data for the open boundaries setting of the Gulf of Mexico and Dolphin Pass. NOAA observed water levels are typically reported above MLLW (mean lower low water). The mean sea level (MSL) at Dauphin Island and Pensacola Gulf stations are 0.17 m and 0.19 m above corresponding MLLWs (Figure 3-20, Figure 3-21). In 2015–2017, water levels at Dauphin Island are 23% less than or equal to MSL and 37% higher than its MHW = 0.37 m (mean high water); water levels at Pensacola Gulf are 23% less than or equal to MSL and 42% higher than its MHW = 0.36 m. Therefore, the water levels at these two stations were very similar, which is also proved in Figure 3-17. When the water level was higher, it could push saline water into Perdido Bay and created density/salinity stratification, which means, the study area would be significantly affected by the tidal influence.

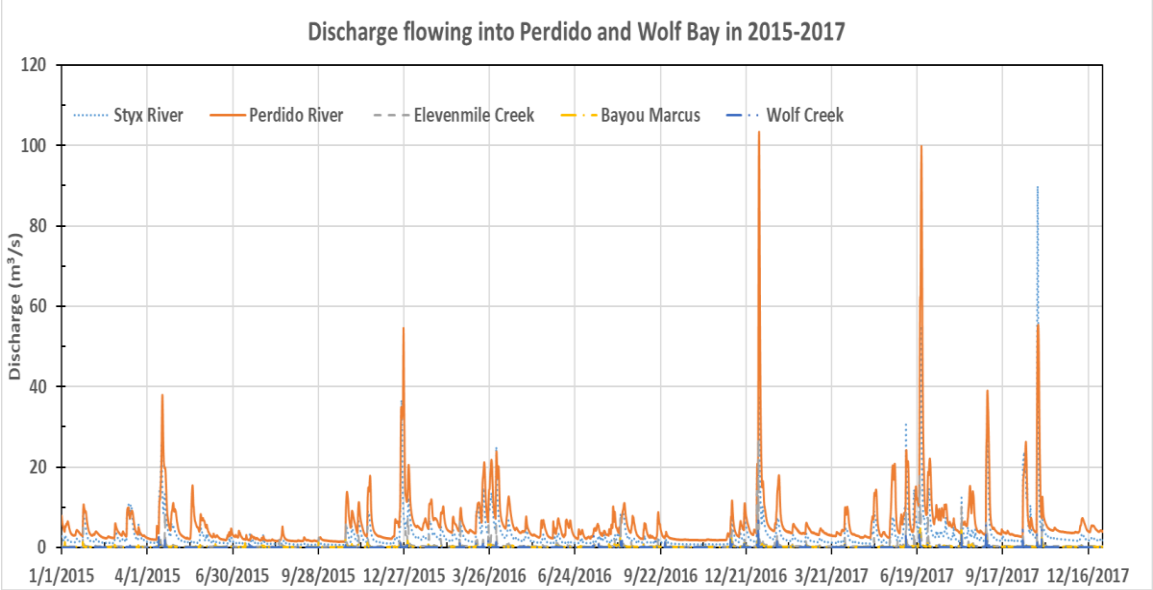

Figure 3-10 Observed USGS discharges of five rivers flowing into the Perdido and Wolf Bay (2015–2017)

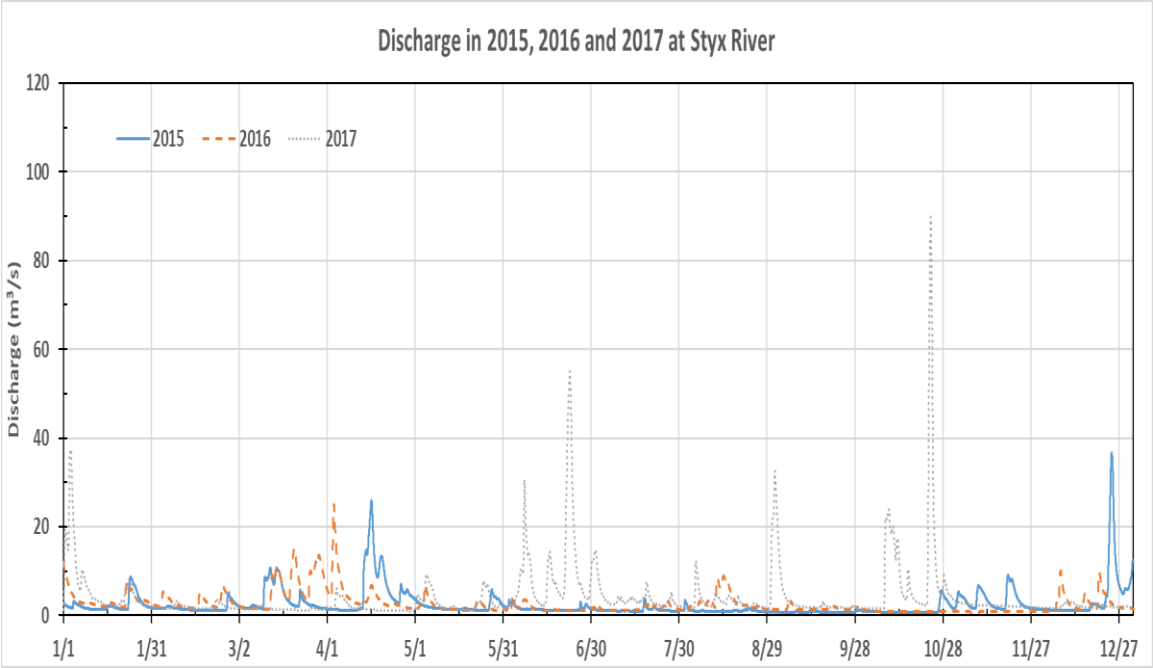

Figure 3-11 Discharge comparison among 2015, 2016 and 2017 for the observed flow from Styx River station

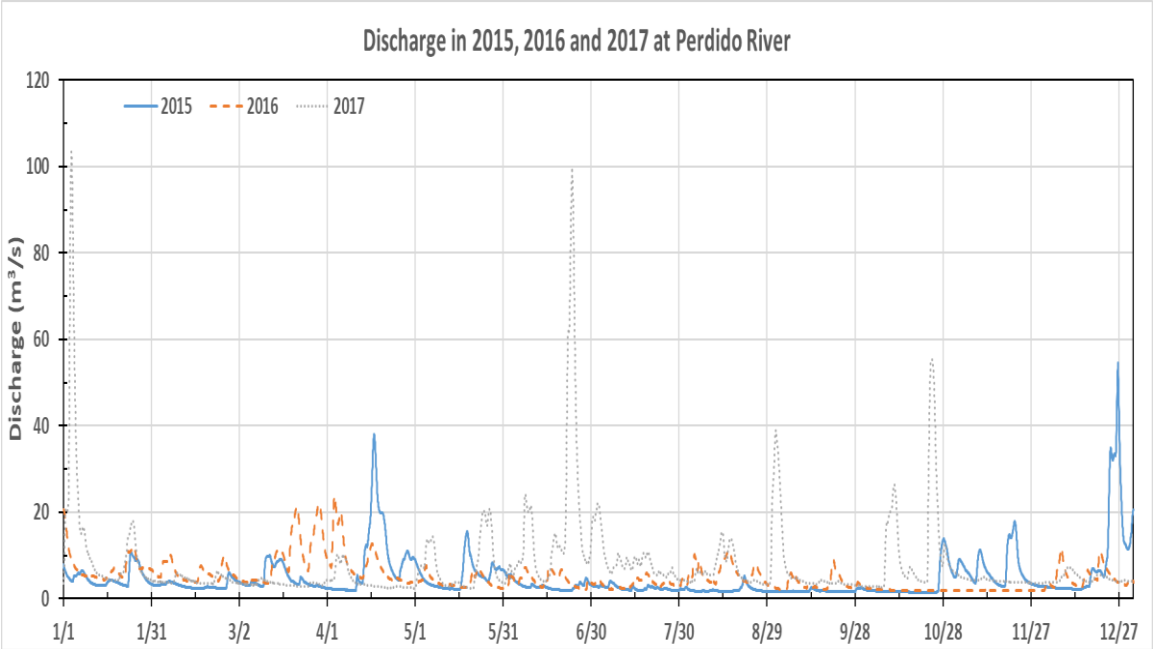

Figure 3-12 Discharge comparison among 2015, 2016 and 2017 for the observed flow from Perdido River station

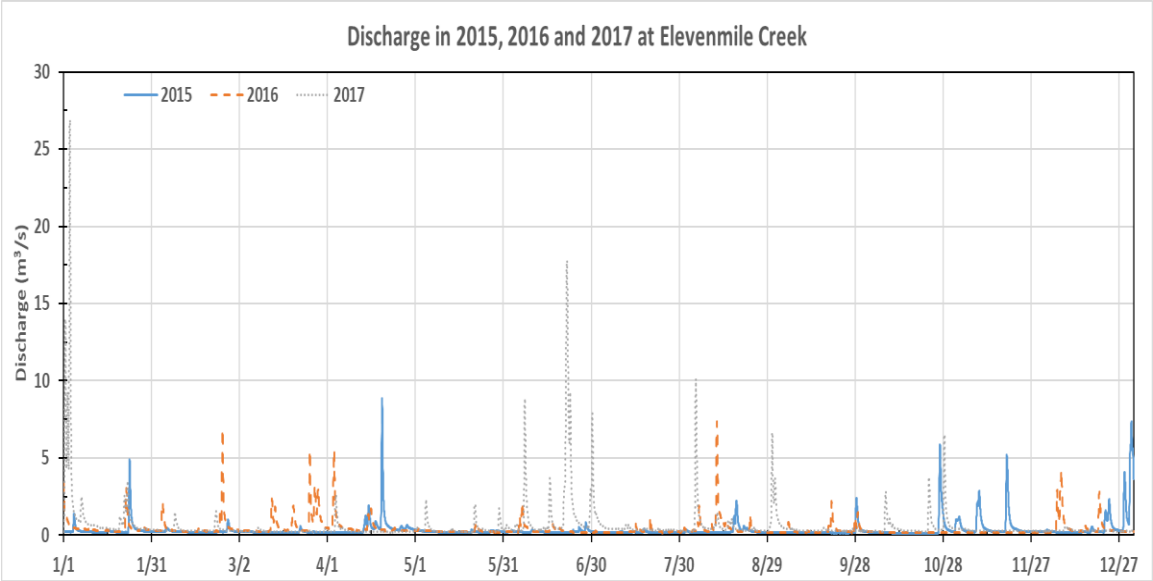

Figure 3-13 Discharge comparison among 2015, 2016 and 2017 for the observed flow from Elevenmile Creek station

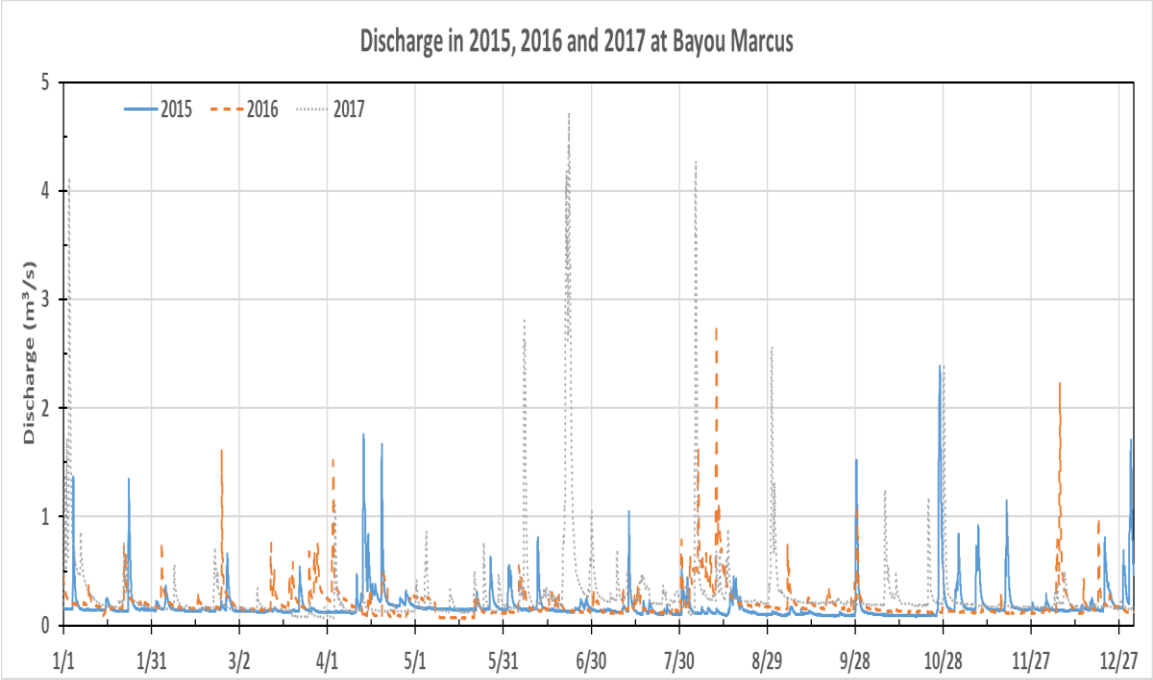

Figure 3-14 Discharge comparison among 2015, 2016 and 2017 for the observed flow from Bayou Marcus station

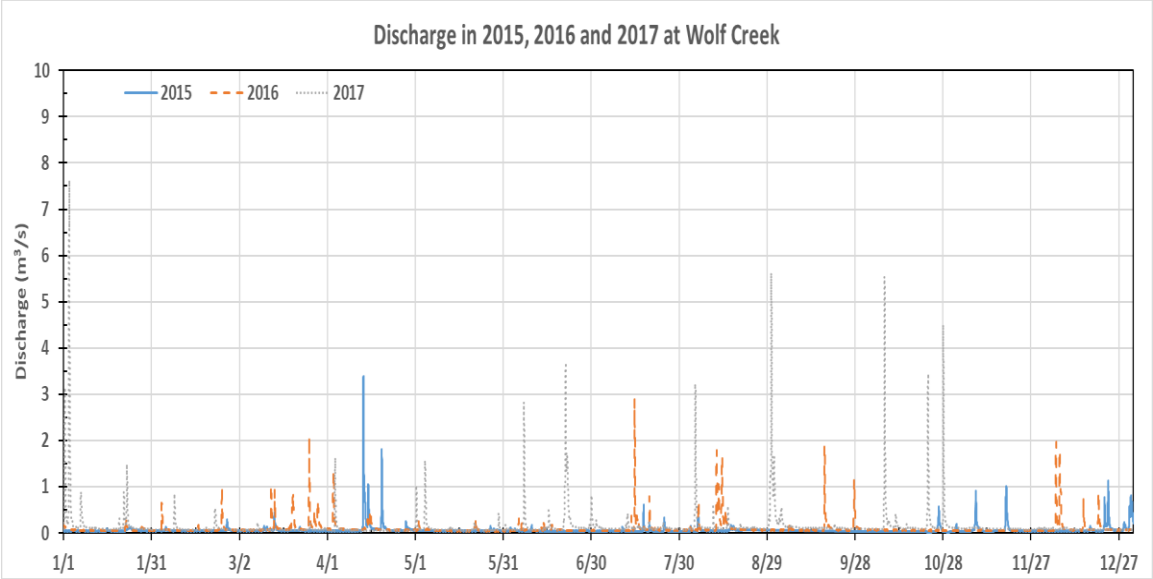

Figure 3-15 Discharge comparison among 2015, 2016 and 2017 for the observed flow from Wolf Creek station

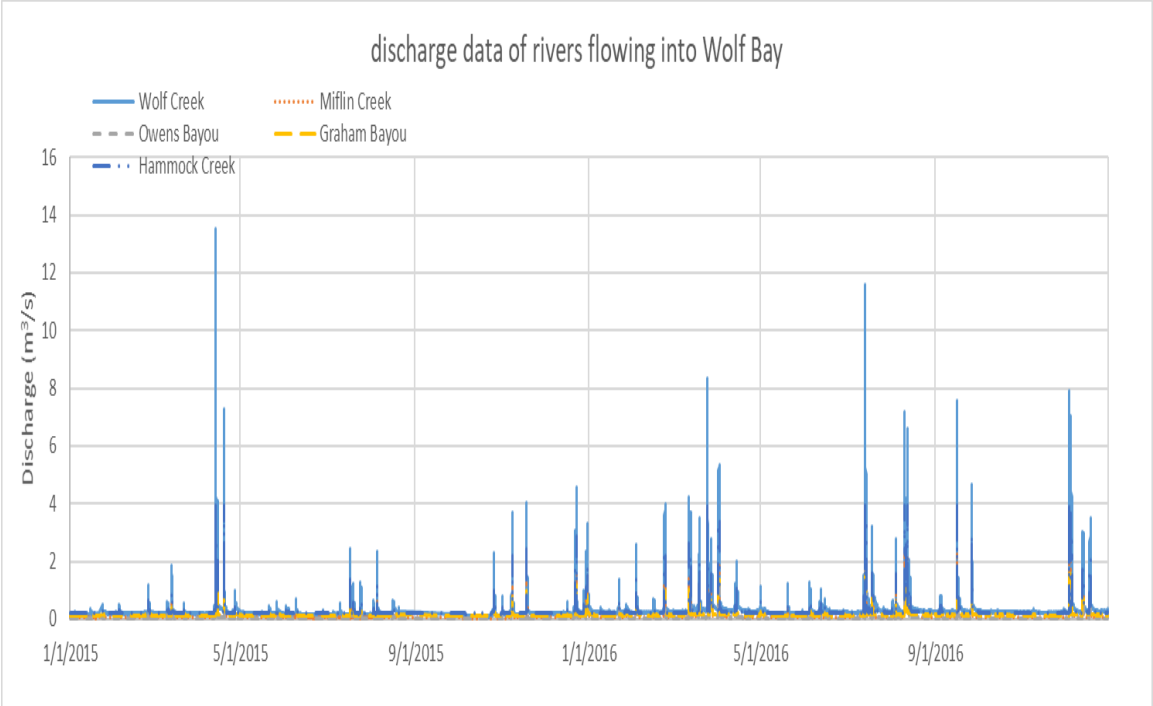

Figure 3-16 Observed (Wolf Creek only) and estimated discharges of five rivers flowing into the Wolf Bay (2015–2017)

Table 3-2 Statistical results of discharge data of rivers flowing into Perdido and Wolf Bay

Items \ Rivers	Styx River	Perdido River	Elevenmile Creek	Bayou Marcus	Wolf Creek
Maxiumum (m^3/s)	37.67|25.06|89.91	54.58|23.86|103.36	8.85|7.36|26.9	2.39|2.79|4.72	3.38|2.9|7.65
Minimum (m^3/s)	0.64|0.76|0.98	1.46|1.8|2.4	0.12|0.16|0.2	0.08|0.06|0.06	0.02|0.04|0.04
Average (m^3/s)	2.44|2.56|4.33	4.63|5.05|7.85	0.35|0.41|0.62	0.18|0.2|0.27	0.07|0.09|0.14
Standard Deviation	3.27|2.48|7.13	5.25|3.52|10.4	0.6|0.53|1.4	0.17|0.16|0.37	0.12|0.14|0.33

Note: Numbers are listed one by one from 2015 to 2017 and separated by the | delimiter

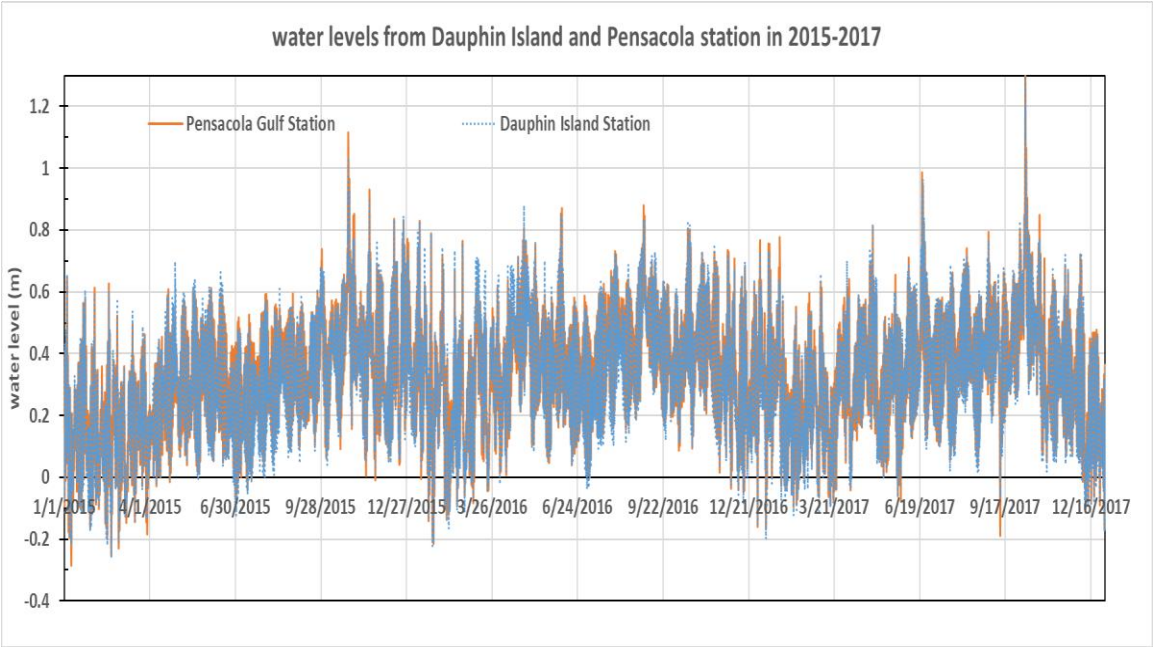

Figure 3-17 Water level comparison between the data from Dauphin Island station and Pensacola Gulf station in 2015-2017

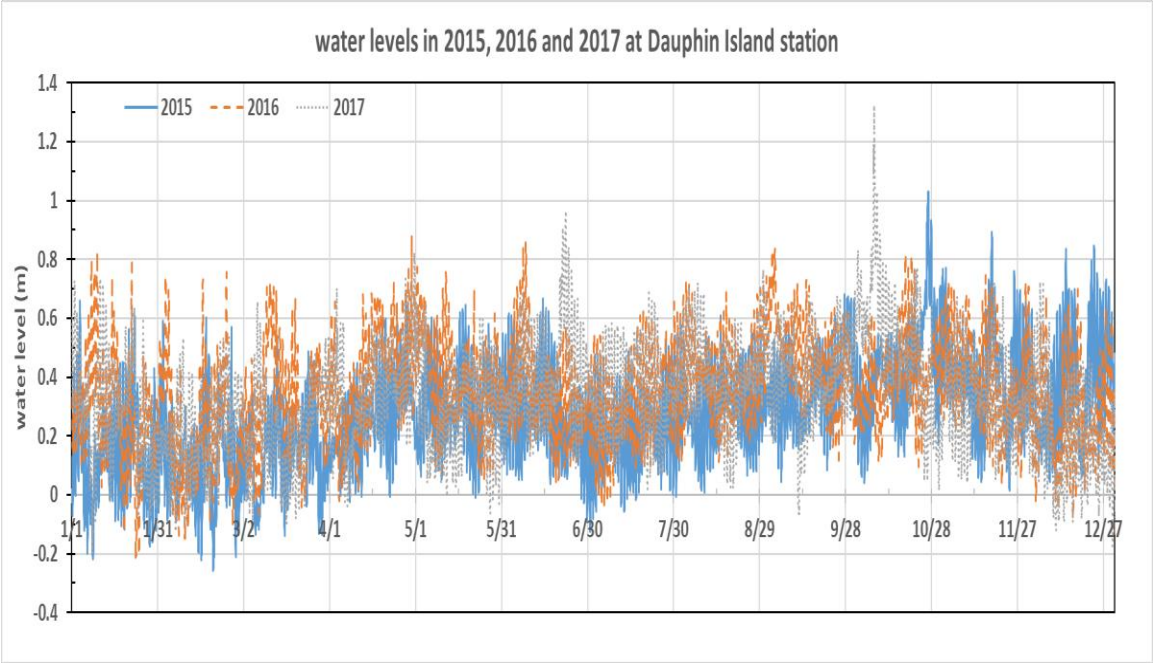

Figure 3-18 water level comparison for the 2015-2017 at Dauphin Island station

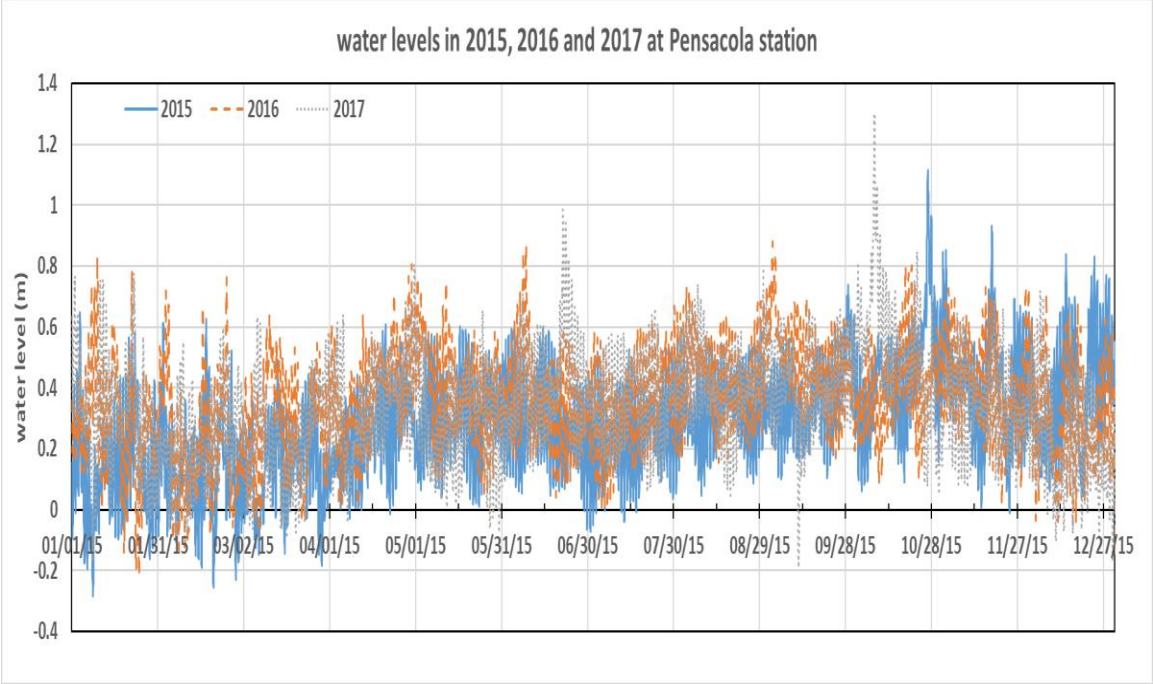

Figure 3-19 water level comparison for the 2015-2017 at Pensacola station

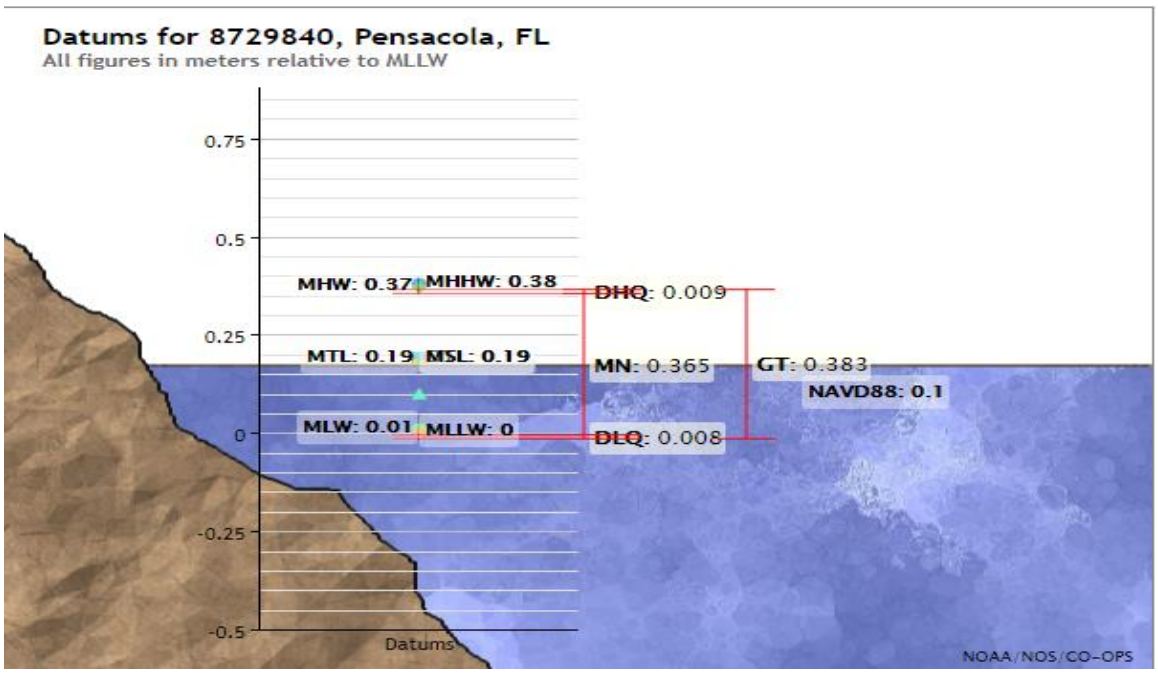

Figure 3-20 Vertical datum used by Pensacola station

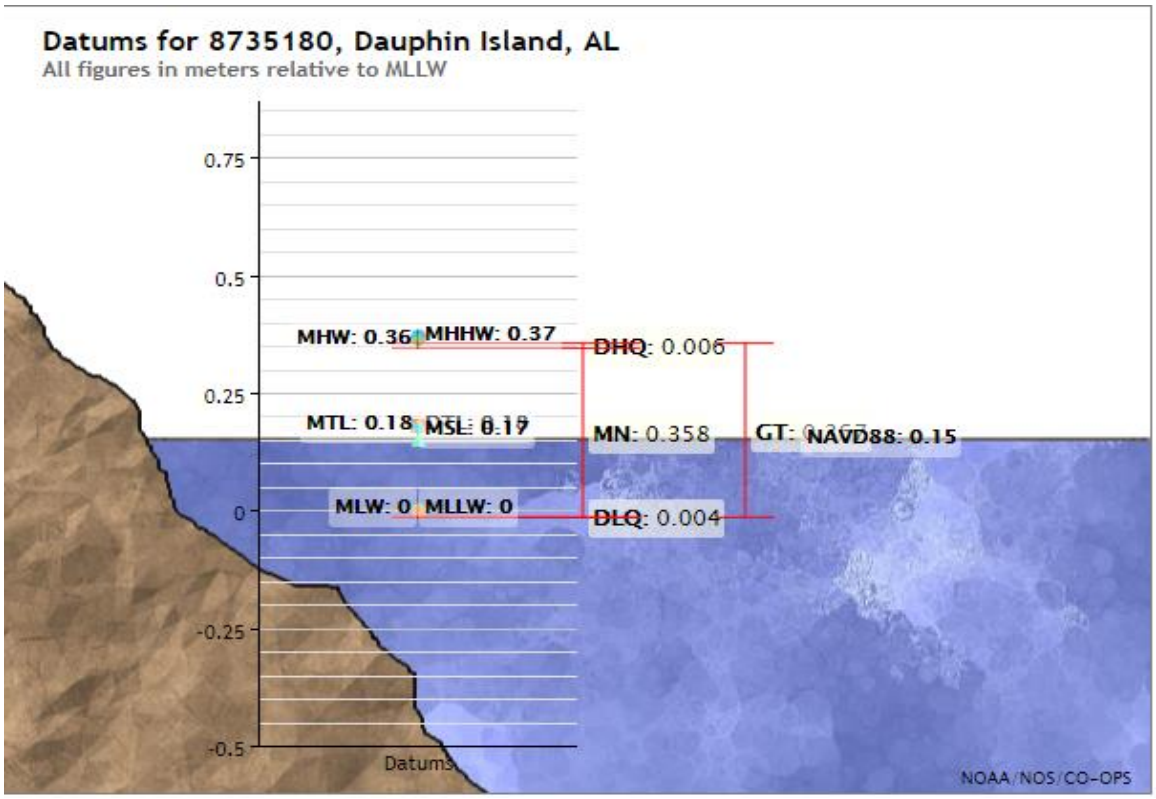

Figure 3-21 Vertical datum used by Dauphin Island station

3.3.4 Atmospheric Forcing

The atmospheric forcing input variables include nine meteorological parameters, atmospheric pressure (millibars), air temperature (Celsius degree, Figure 3-23), relative humidity (fraction), rainfall (m/day, Figure 3-24), evaporation (m/day), solar radiation (W/m^2), cloud cover (fraction), wind speed (m/s, Figure 3-25) and wind direction (degree). The corresponding data were obtained from two monitoring stations, the Mobile Regional Airport (40 miles northwest of the Wolf Bay) and the Jay Station (25 miles northeast of the Wolf Bay) (Figure 3-22). The reason why choosing two monitoring stations as the input data source is that Jay Station did not record the atmospheric pressure and cloud cover data but the Mobile Regional Airport did not have solar radiation data. The combination of them could provide all the required input variables. Hourly data from Mobile Regional Airport were linearly interpolated to develop 15-minute data in order to combine with 15-minute data from Jay station (Figure 3-23 to Figure 3-25). Monthly average wind speeds were calculated and plotted in Figure 3-26. Lower wind speed in the study area typically occurred in summer months (roughly June–September) and on the order of 2 m/s (~4.5 miles/hr or mph), and higher wind speed occurred in winter months (3–3.5 m/s or 6.7–7.8 mph). Figure 3-26 shows daily average wind speed from July 15 to August 15 in 2015 and 2016 for comparison. Figure 3-27 shows the wind rose plot that gives a view (summary) of how wind speed and wind direction (towards to the center of the plot, so "south" is for the wind blowing from south to north) are distributed at Perdido Bay area in 2015–2016. The wind direction was grouped into 16 bands and each band covers a 22.5-degree range of wind direction.

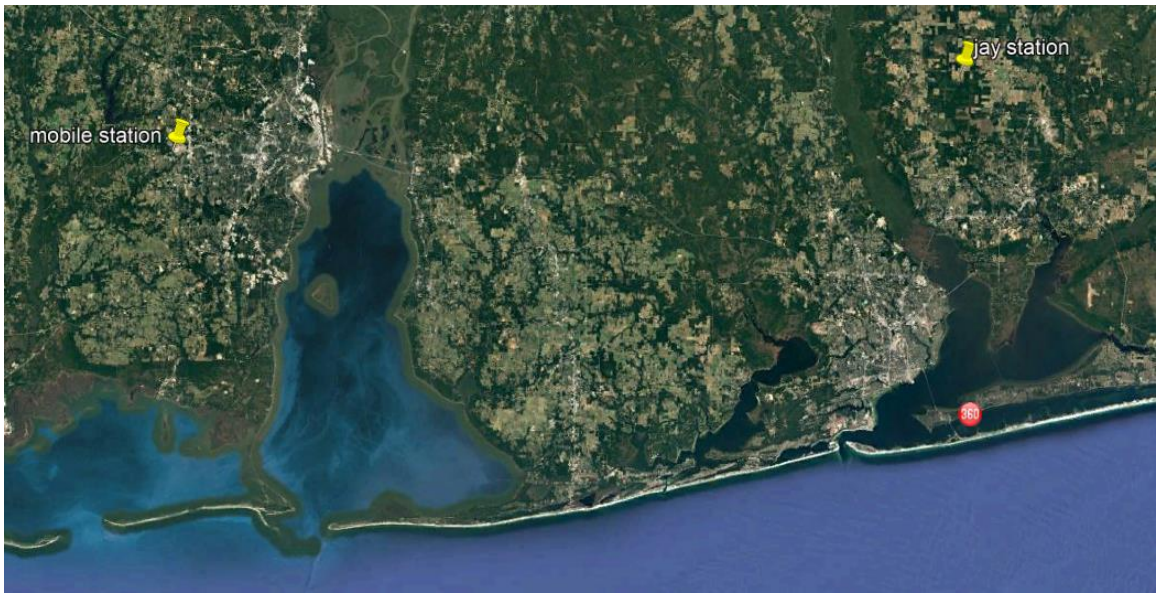

Figure 3-22 Locations of Jay station and Mobile station (change to GIS later)

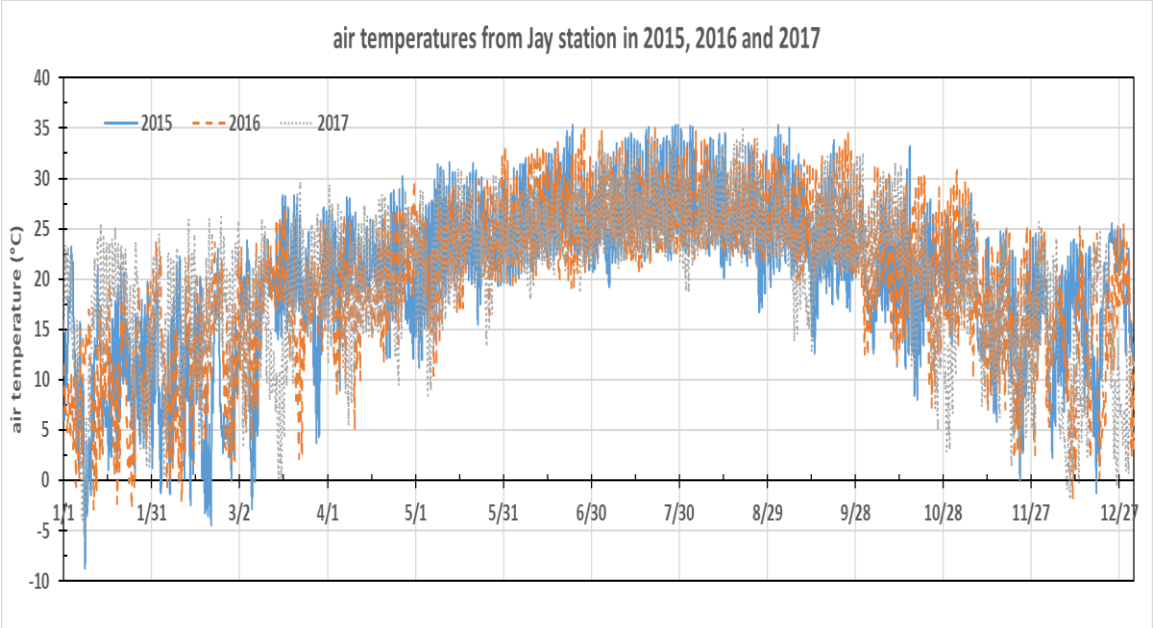

Figure 3-23 Input air temperatures comparison from 2015 to 2017

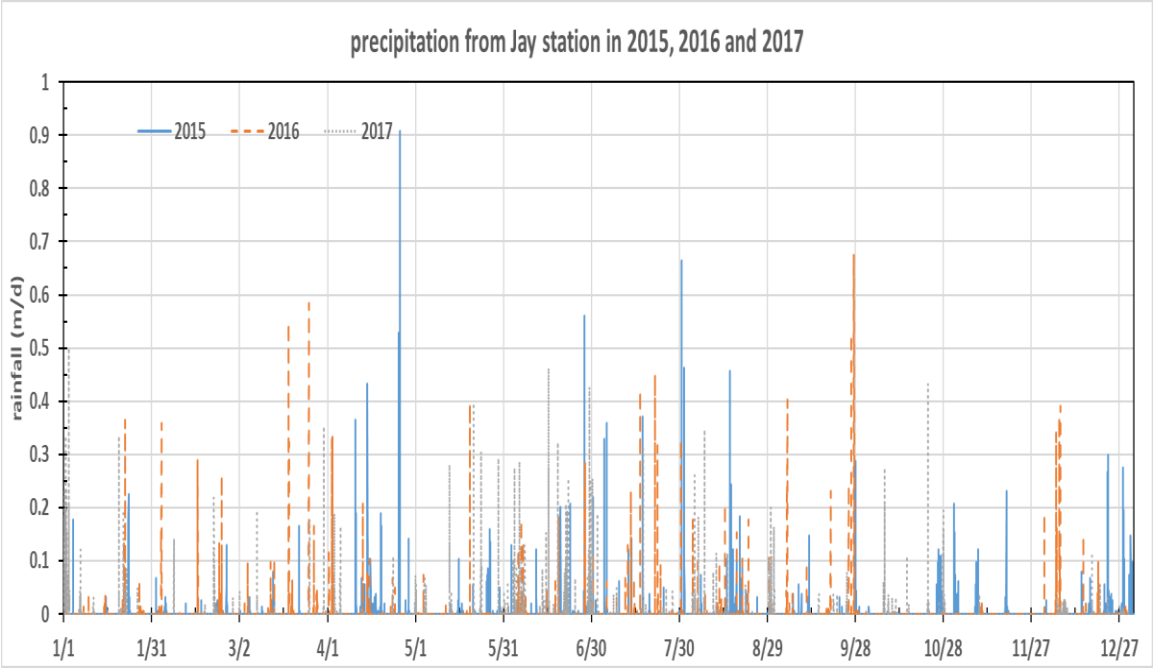

Figure 3-24 Input precipitation from 2015 to 2017

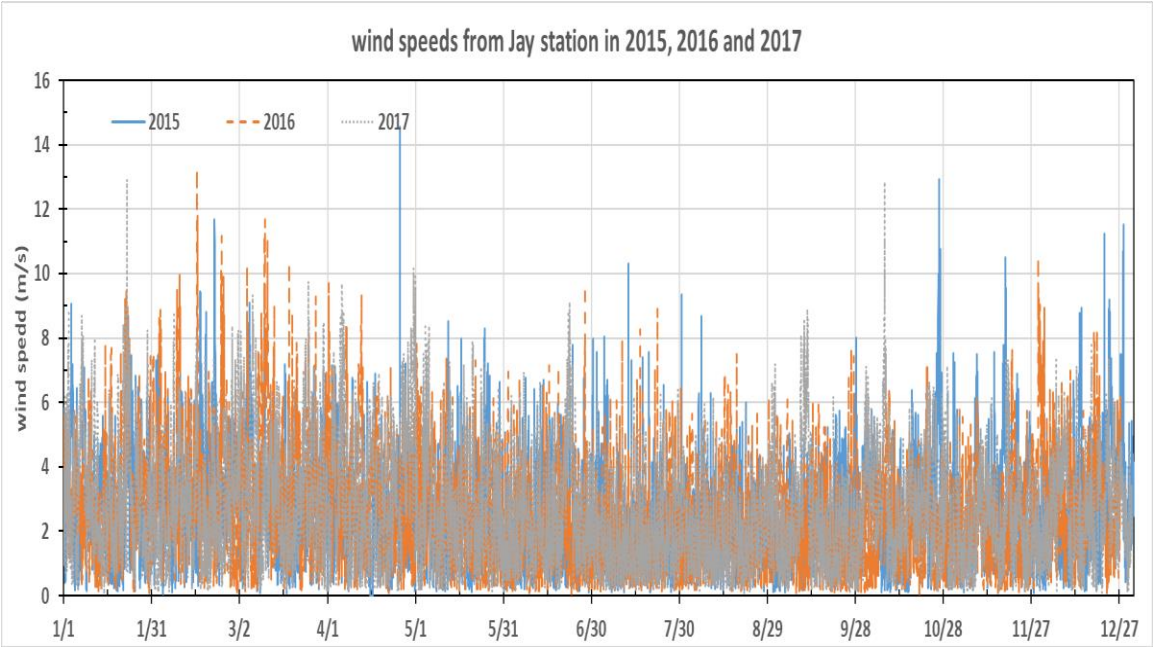

Figure 3-25 Input wind speeds from 2015 to 2017

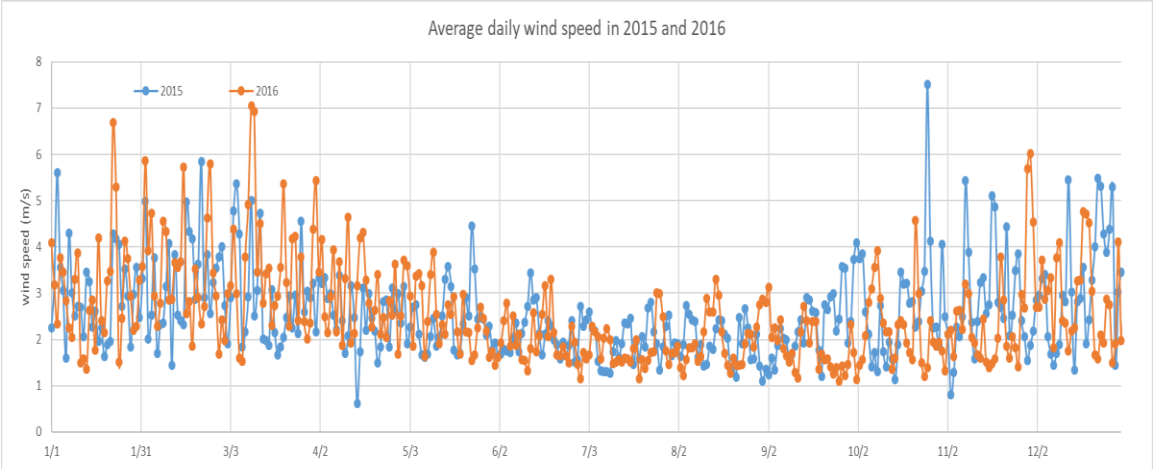

Figure 3-26 Average monthly wind speed (2015–2016)

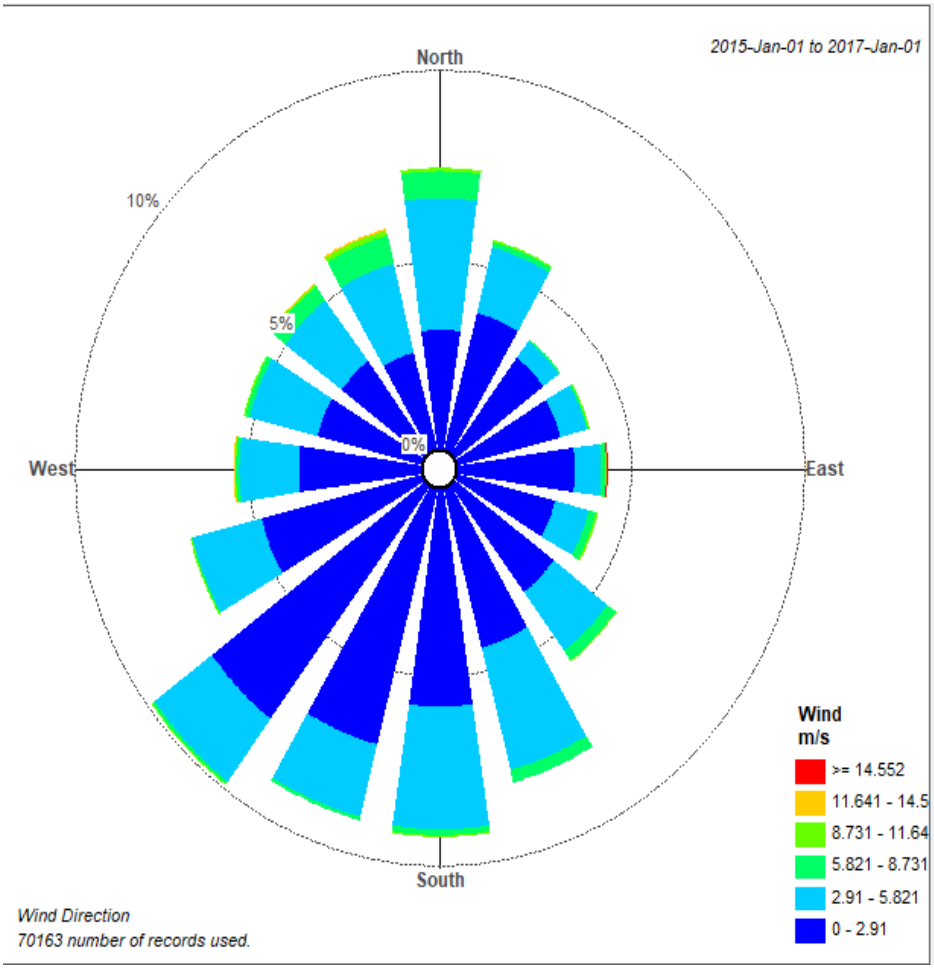

Figure 3-27 Wind rose plot (2015–2016)

3.3.5 Salinity and Water Temperature

Due to the limitation of the available salinity data, constant 0.5 ppt of salinity was assigned to all upstream freshwater rivers and 34 ppt for the Gulf of Mexico. For the Dolphin Pass and GIWW, the salinity data were available from the FDEP 33010H24 monitoring station and the ADEM/ADPH Coastal Alabama Beach monitoring station, respectively, which are the closest monitoring stations (Figure 3-28). Hourly salinity data were interpolated from observations and used for EFDC input data files. Average salinity calculated from observations is 13.01 ppt for GIWW and 21.1 ppt for Dolphin Pass (closer to the Gulf of Mexico, Figure 3-1) in 2015–2017.

The FDEP 33010H24 monitoring station is very close to the model boundary at Dolphin Pass, and its salinity could be affected by the Gulf of Mexico through Perdido Pass and Pensacola (Figure 3-1). ADEM/ADPH monitoring station is located in Wolf Bay near Orange Beach Waterfront Park, which is east of the GIWW open boundary. GIWW or the Portage Creek is a long channel connecting the Wolf Bay and the Mobile Bay (through Oyster Bay). Therefore, its salinity is lower and less affected by the Gulf of Mexico. Although some quantitative differences exist between the salinity from the two monitoring stations, they show a good agreement in the change and trend with the time. The lowest salinity was primarily recorded in April and May, which were the wet season. In addition, a lower salinity on December 2015 also coincided with the higher freshwater discharging into the Perdido and Wolf Bay as shown in Figure 3-10.

Water temperature is almost the most important parameter in water quality modeling. In the study area, only two monitoring stations, Dauphin Island and Pensacola monitoring stations, provided the recorded water temperature in 2015–2017. Since GIWW and Big Lagoon boundary conditions are close to the above two monitoring stations, respectively, the observed water temperatures from the two monitoring stations were used as the input for the two boundaries. **Error!**

Reference source not found. shows that observed water temperatures from the two stations have a good agreement in both magnitude and trend.

Since there are no recorded water temperatures for the other boundaries (freshwater streams), their hourly water temperatures were estimated from observed air temperature in 2015–2016 based on the modified wave function method (Chen and Fang 2015). The first step is to calculate the diurnal maximum and minimum water temperatures (T_{WMIN} and T_{WMAX}) based on the maximum and minimum air temperatures (T_{AMIN} and T_{AMAX}) in the same day using the following equations.

$$T_{WMAX} = 1.00 + \frac{36.50 - 1.00}{1 + e^{0.10(22.33 - T_{AMAX})}} \tag{3.1}$$

$$T_{WMIN} = 0.1 + \frac{33.00 - 0.1}{1 + e^{0.09(11.26 - T_{AMIN})}} \tag{3.2}$$

The hourly water temperatures can then be estimated using the following equations,

$$T_W(H) = T_{WAVE} - AMP(\cos(\pi(\frac{H - RISE - 2}{16 - RISE - 2}))) \quad (RISE + 2) \le H \le 16:00 \tag{3.3}$$

$$T_W(H) = T_{WAVE} + AMP(\cos(\pi(\frac{\pi H'}{10 + RISE}))) \quad H < (RISE + 2) \text{ or } H > 16:00 \tag{3.4}$$

Where $T_{WAVE} = (T_{WMIN} + T_{WMAX})/2$

$AMP = (T_{WMAX} - T_{WMIN})/2$

RISE is the time of sunrise in hours in each day

H' = *H* +8 when *H* < (*RISE*+2), and H is hour from 1:00-24:00

H' = *H*-16 when *H*>16:00

The predicated stream temperatures are less than observed water temperatures in Dauphin Island and Pensacola Bay (Figure 3-29), but their variations with time are similar. Lower predicted

temperatures could be due to slightly lower air temperatures from the Jay station that is 70 miles north of the monitoring stations.

Since there are lots of missing data of observed water temperature from Dauphin Island and Pensacola Bay monitoring stations, they are estimated using the following procedures, which are a variant version of the above calculation. We introduced two correction constants C1 and C2, which can be determined to minimize the error (RMSE) between the observed and estimated temperature at Dauphin Island and Pensacola (called WTDP). Estimated WTDP can be calculated by introducing the C1 and C2 to the above equation 3.3 and 3.4, as shown in the following,

$$T_W(H) = C1 * T_{WAVE} - C2 * AMP(\cos(\pi(\frac{H - RISE - 2}{16 - RISE - 2}))) \quad (RISE + 2) \le H \le 16:00$$

(3.5)

$$T_W(H) = C1 * T_{WAVE} + C2 * AMP(\cos(\pi(\frac{\pi H'}{10 + RISE}))) \qquad H < (RISE + 2) \qquad \text{or}$$

$H > 16:00$ (3.6)

After assigning C1 and C2 to any arbitrary reasonable value, such as 1 and 0.5, respectively, the simulated water temperatures were calculated. By making use of Solver in Excel to minimize the RMSE between simulated and observed water temperature, the optimal C1 and C2 were calculated as 1.21 and 0.399 corresponding to the RMSE 1.68. Figure 3-29 and Figure 3-30 show the original and interpolated water temperatures, which are reasonably calculated.

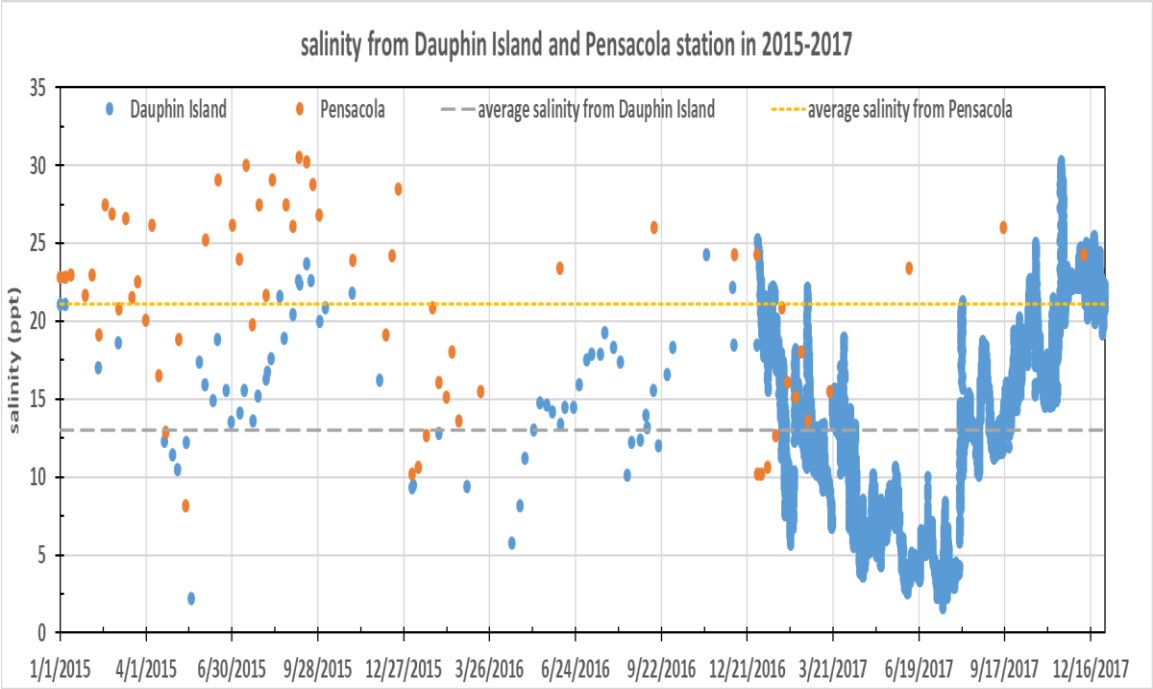

Figure 3-28 Salinity for open boundaries (2015–2017)

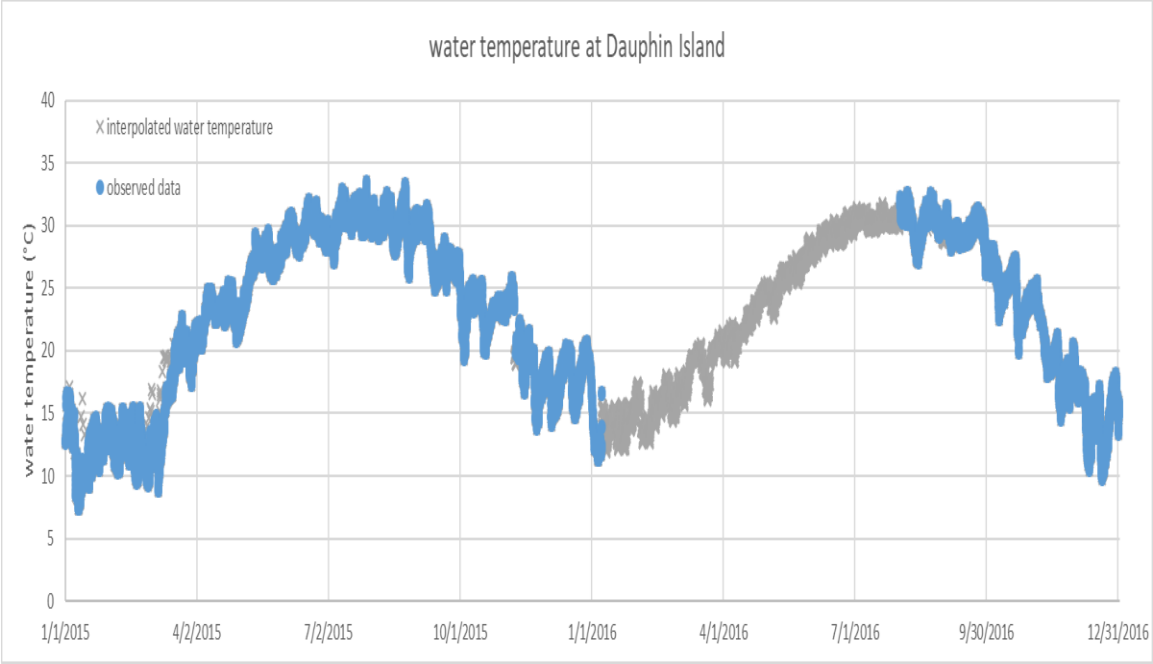

Figure 3-29 The observed and its interpolated water temperature based on data from Dauphin Island

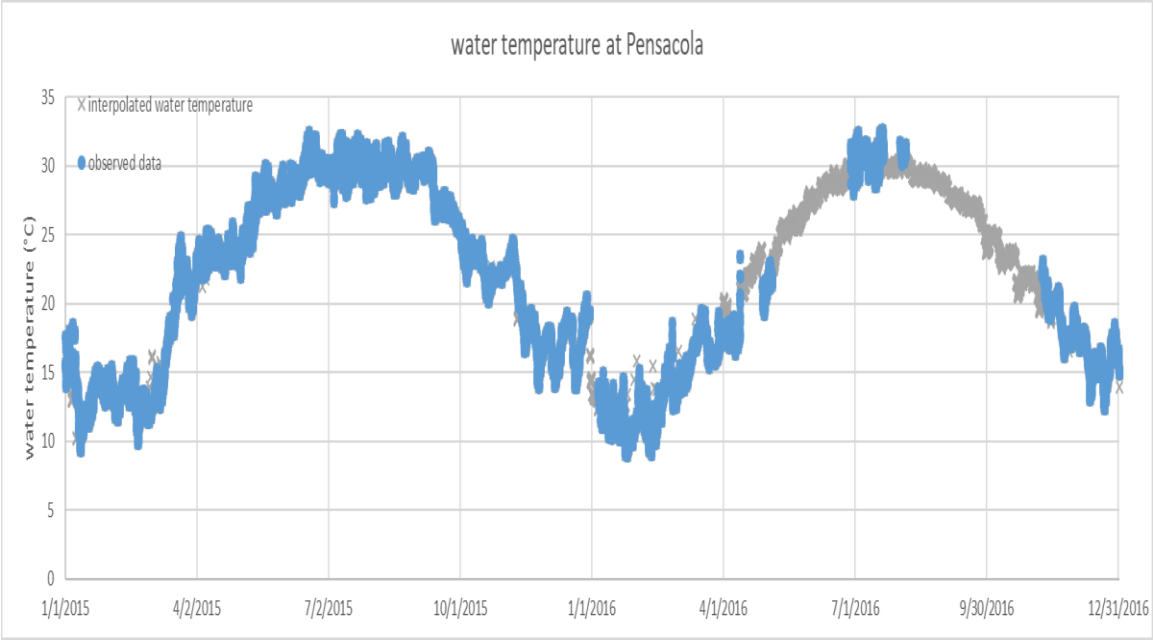

Figure 3-30 The observed and its interpolated water temperature based on data from Pensacola

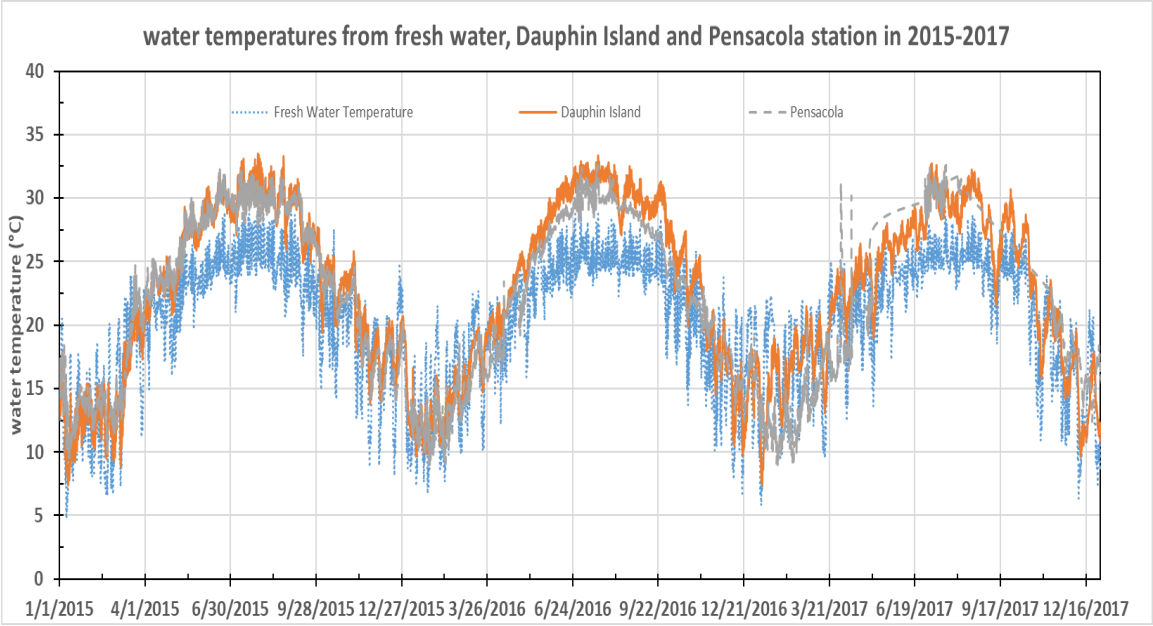

Figure 3-31 water temperature comparison among the data from estimated fresh water, Dauphin, and Pensacola from 2015 to 2017

3.3.6 Nutrients

Nutrients are very important and necessary substance for the growth of phytoplankton. In the EFDC model for Perdido and Wolf Bay, three kinds of nutrients (Nitrogen, Phosphorus, and Carbon) are simulated and their input data are needed at all boundaries. Some observed data of nutrients are available from the Water Quality Portal (STORET) operated by the EPA. Figure 3-32 shows the available locations with a few observed data (e.g., measured from grabbed water samples) provided by the STORET in the study area. None of these locations have monitoring equipment that measures nutrients continuously so that no time series data of nutrients are available at any boundary.

Since one location only can provide at most five records in 2015–2016, observed data from the geographically close locations were grouped as three location groups: Perdido River, Elevenmile Creek, and Big Lagoon (Table 3-3). Then the linear interpolation method was used to expand the observed data to the hourly data in 2015–2016 due to data format requirement of the modeling system (Figure 3-33 to Figure 3-38). The nutrient boundary at the Gulf of Mexico, Dolphin Pass, and GIWW was assumed to use the data from the Big Lagoon group. The Perdido and Styx rivers take the data from the Perdido River group as their nutrients input. All the tributaries in the Wolf Bay utilize the same data from the Elevenmile Creek group due to their flow's similarity. Measured data include chlorophyll-a, organic Carbon, Ammonia, Nitrate & Nitrite, organic Nitrogen, organic Phosphorus, and inorganic Phosphorus (Table 3-3).

Since nutrient inputs or variables for the EFDC water quality have the different forms such as particulate/dissolved or organic/inorganic types, these three types of nutrients finally expand to twelve different substances (variables) in the EFDC, i.e., refractory particulate organic carbon (RPOC), labile particulate organic carbon (LPOC), dissolved organic carbon (DOC), refractory

particulate organic phosphorus (RPOP), labile particulate organic phosphorus (LPOP), dissolved organic phosphorus (DOP), total phosphate (TP, Figure 3-38), refractory particulate organic nitrogen (RPON), labile particulate organic nitrogen (LPON), dissolved organic nitrogen (DON), ammonia nitrogen (Figure 3-33), nitrate nitrogen (Figure 3-34). Since only organic form of nutrients were observed, the ratios, 1:1:8 for Carbon, 3:3.5:3.5 for Nitrogen, 1:3.7:5.3 for Phosphorus were used to divide the organic form into the refractory, labile, and dissolved organic forms, respectively, based on a previous study in the same area done by Xia et al. (2011).

Table 3-3 Number of observed values for three location groups from STORET

number of available data in each group			
	Perdido	*Elevenmile*	*Big Lagoon*
Chlorophyll-a	19	18	11
Organic Carbon	25	21	4
Ammonia	32	22	8
Nitrate & Nitrite	32	23	5
Organic Nitrogen	32	22	8
Organic Phosphorus	31	23	14
Inorganic Phosphorus	7	0	0

Figure 3-32 Locations with observed data near the model boundaries

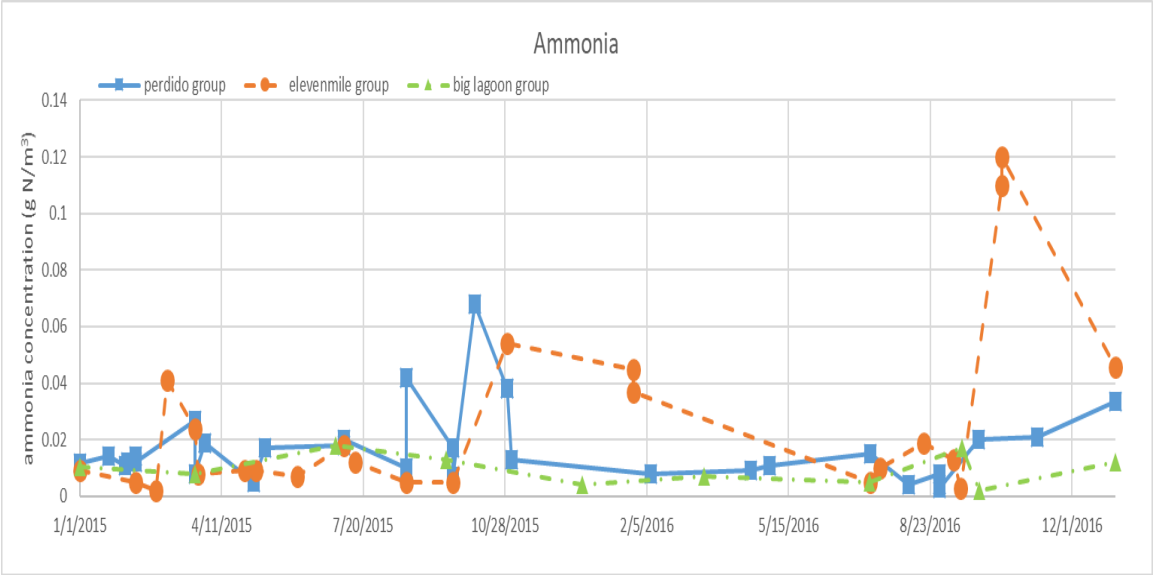

Figure 3-33 Recorded (points) and interpolated (lines) ammonia for three location groups

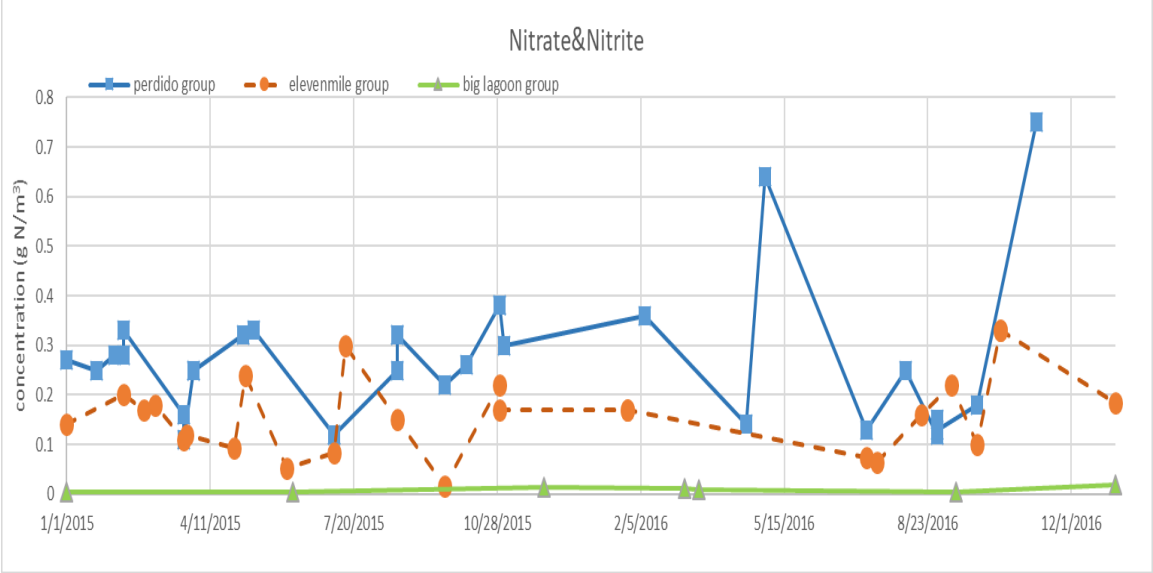

Figure 3-34 Recorded (points) and interpolated (lines) nitrate & nitrite for three location groups

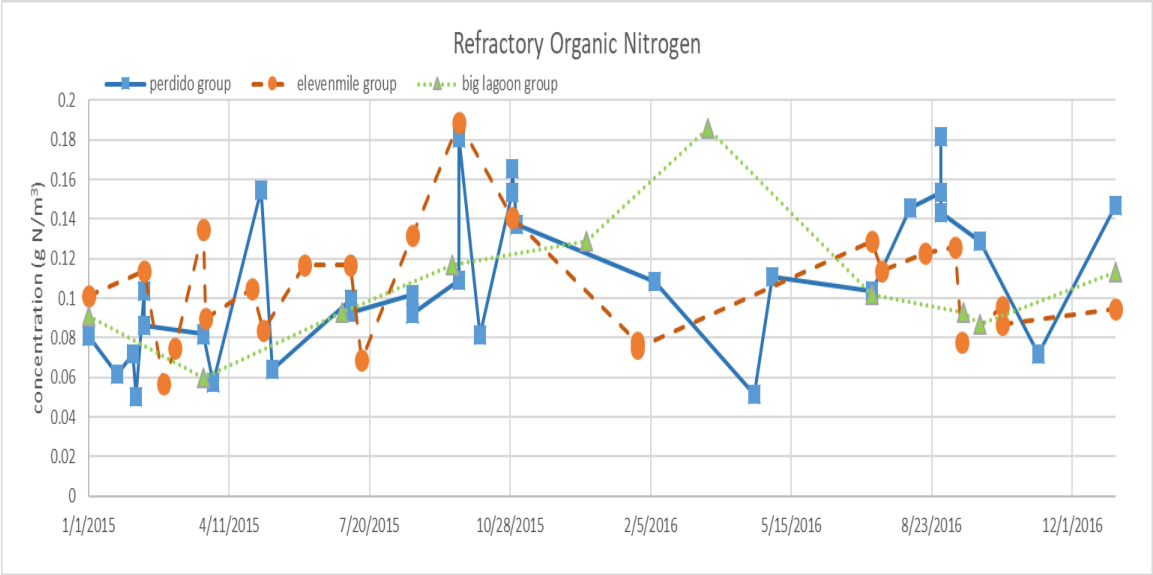

Figure 3-35 Recorded (points) and interpolated (lines) refractory organic nitrogen (RON) for three location groups

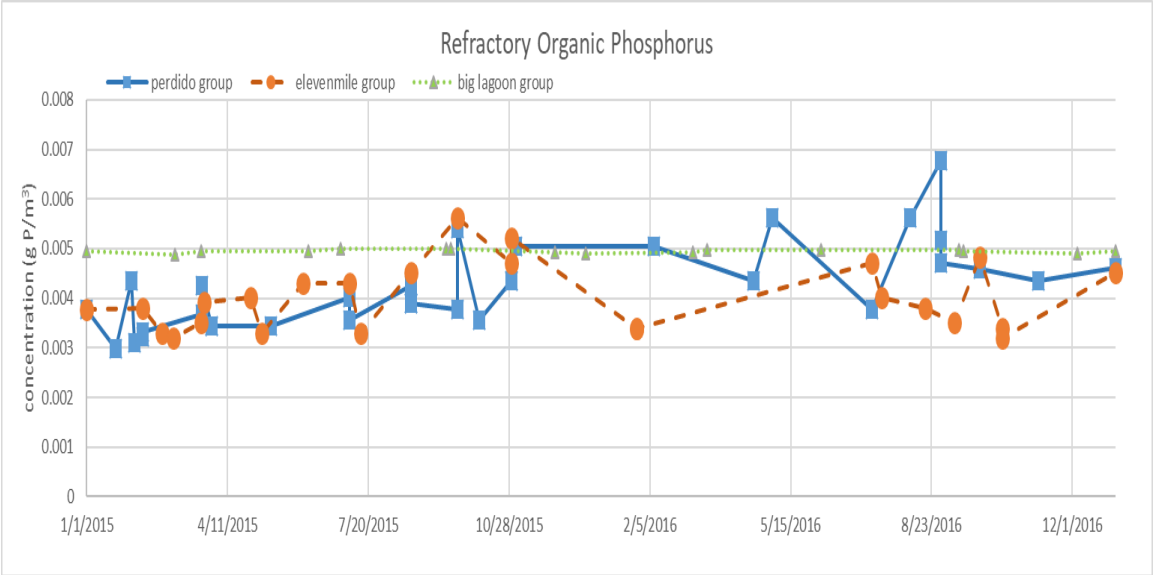

Figure 3-36 Recorded (points) and interpolated (lines) refractory organic phosphorus (ROP) for three location groups

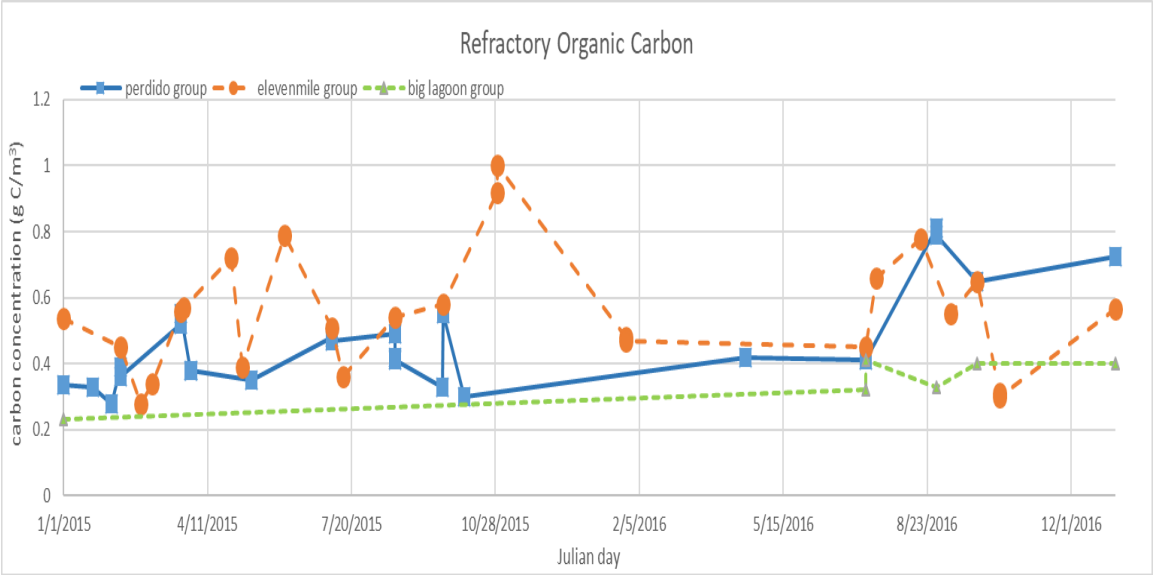

Figure 3-37 Recorded (points) and interpolated (lines) refractory organic carbon (ROC) for three location groups

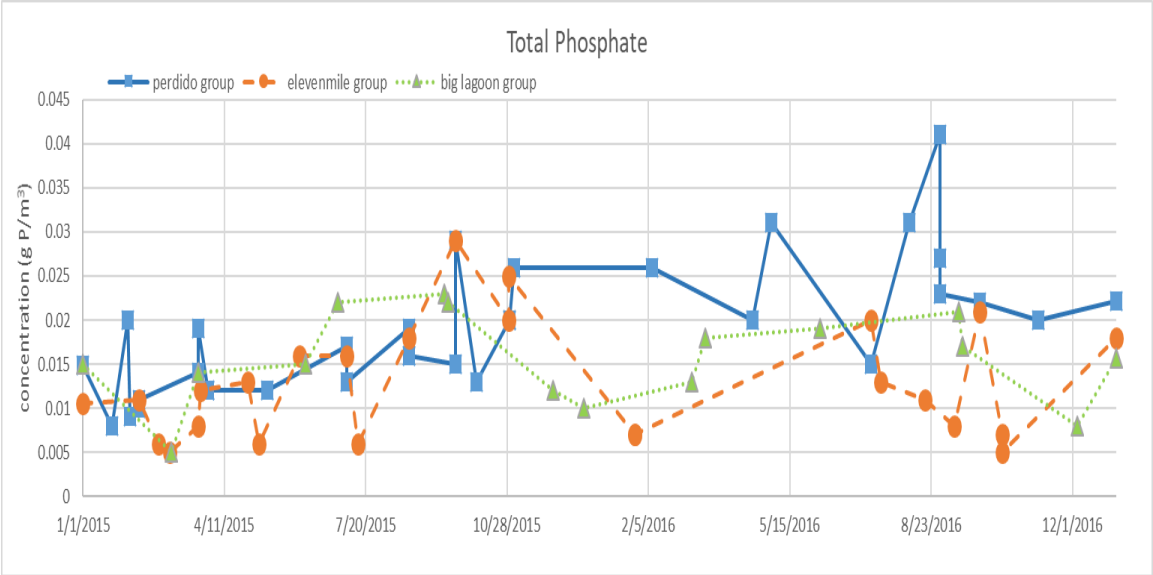

Figure 3-38 Recorded (points) and interpolated (lines) total phosphate (TP) for three location groups

3.3.7 Algae

The algae play a key role in the aquatic environment as the primary producer. They are healthy to the aquatic environment when the biomass is under the stress line because the oxygen they produce is an important source of the DO. When there exist too many algae in the water body, they are harmful because the algal bloom will decrease the DO in the lower layer of the water body through two mechanisms: 1) It inhibits the algal growth under the water surface because the algal bloom in the water surface prevents the light penetrating into the water column, and 2) The decay of dead algae increases further the consumption of DO.

For the required input of green algae biomass, the following conversion equation was used because only the chlorophyll concentration instead of algae biomass were available.

$$B = \alpha Chl \tag{3.5}$$

where B = algal biomass concentration as carbon (C) (*mg C/L*)

Chl = chlorophyll a concentration (*mg Chl/L*)

α = carbon to chlorophyll ratio (*mg C/mg Chl*). This model took a recommended value, 50, for α from the reference range of 25–150 (Cole and Wells 1995).

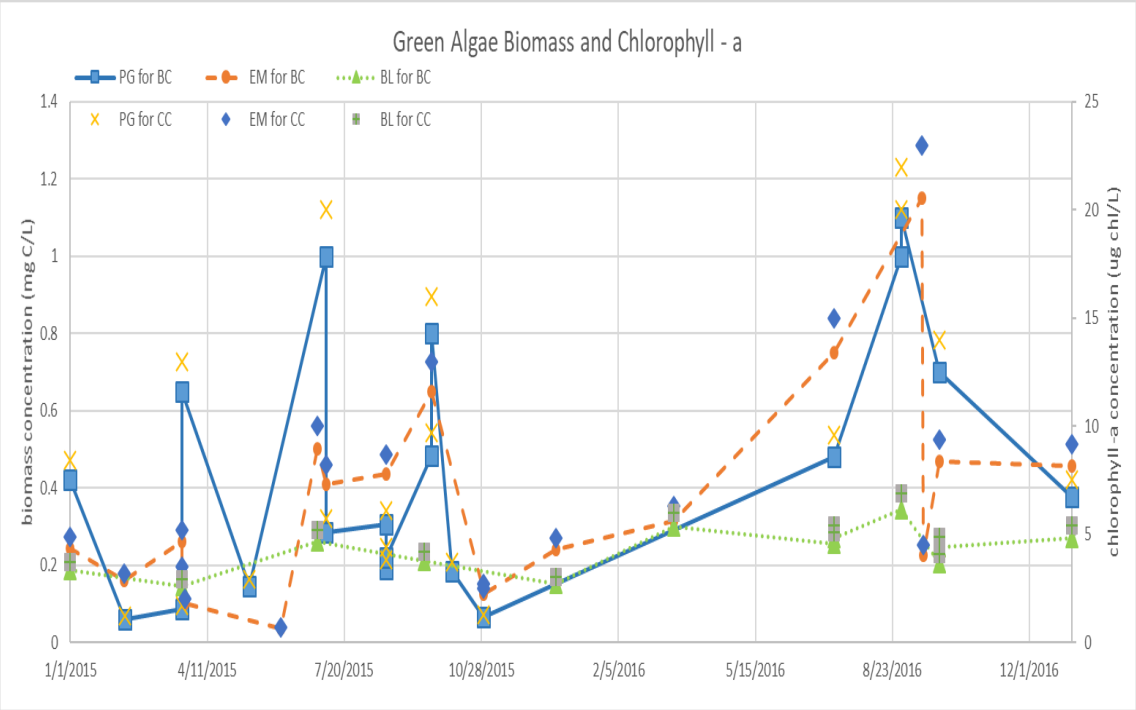

Figure 3-39 Estimated green algae biomass (scatter with straight lines, left y-axis) and observed chlorophyll-a (points, right y-axis) for three location groups. In the legends, PG stands for Perdido group, EM stands for Elevenmile Group, BL stands for Big Lagoon Group, BC stands for green algae biomass concentration, and CC stands for chlorophyll-a concentration.

3.3.8 DO

DO concentration is the center of the water quality modeling since it is a direct standard for judging whether the aquatic animals can survive or not. In strictly, the dissolved oxygen linked with eight factors: surface oxygen exchange, photosynthesis activities, external loads, oxidation of the organic carbon, nitrification, respiration, sedimentary oxygen demand (SOD), and COD in the mathematical representation of the mass balance of DO in a water body. Among them, the first three are the source terms and the last five are the sink terms of DO. The available DO data for boundary conditions were also obtained from the STORET. Figure 3-40 plots the measured DO from the STORET for the boundary conditions.

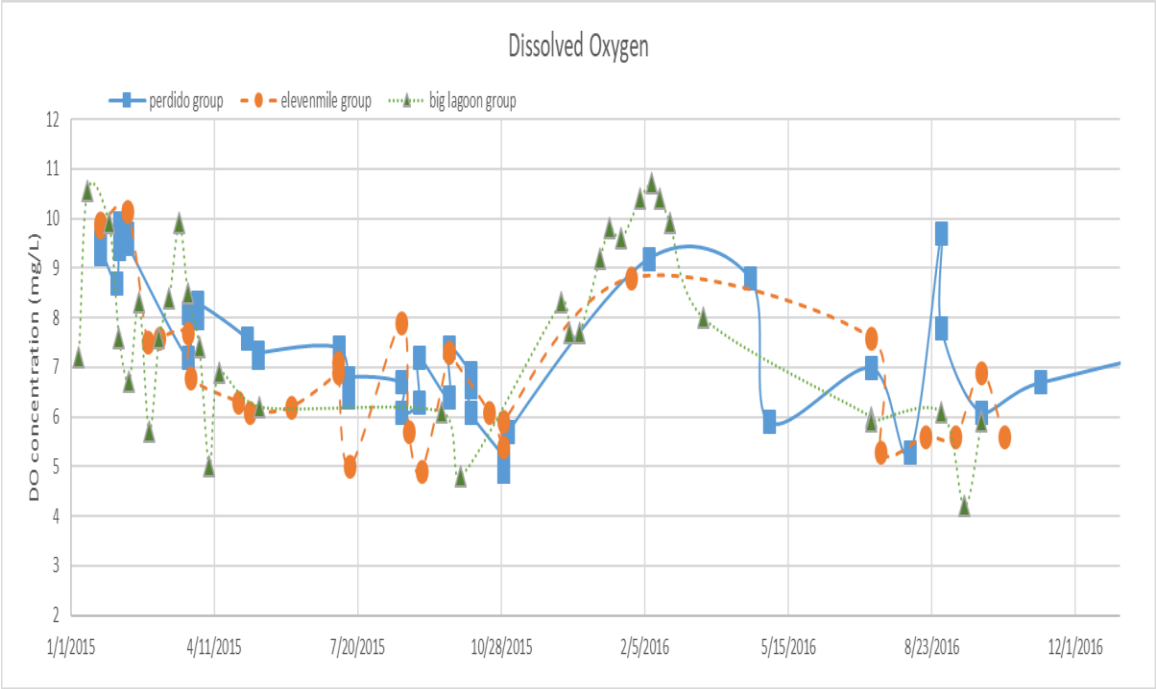

Figure 3-40 DO input at the boundary (2015–2016)

3.4 Internal Model Coefficients

3.4.1 Vertical Eddy Viscosity

Vertical eddy viscosity is a parameter representing the treatment of vertical mixing in mathematical water quality models. The turbulent diffusion plays an important role in vertical mixing of dissolved and suspended materials. In the water body, the blown wind to the water surface contributes to the vertical mixing through the mechanism that the eddy turbulence is transmitted to the lower portion of the water columns by shear stresses (Ji 2017). For the vertical eddy diffusivity generated by the vertical shear, it is stronger than the molecular diffusion to mix dissolved materials. In the estuary, it is often driven by the tidal flows and surface wind effects. The larger the vertical eddy viscosity is, the smaller the vertical DO difference or stratification is. In this study, the vertical eddy viscosity was set to 0.01 m^2/s or 100 cm^2/s (Xia and Jiang 2016).

3.4.2 Oxygen Reaeration Formulas

The reaeration is a process that the atmospheric oxygen will continuously dissolve into the water until it reaches the saturation condition. It is an important source of the DO in a water body. For the different systems (rivers, lakes, and estuaries), the rate of this process is different. The reaeration rate (day^{-1}), which is calculated by the oxygen reaeration formula, is the quantitative parameter to describe this process. Among the numerous reaeration formulas, O'Connor-Dobbins (1956) and Owens-Gibbs (1964) formulas are available in EFDC; they are suitable for the different river systems (Table 3-4) as a function of flow velocity and water depth. Since the average depth of the study area is 2.5 m and it is low-velocity waterbody, O'Connor-Dobbins was used to calculate the reaeration rate. Thomann and Fitzpatrick (1982) have combined the two approaches: O'Connor-Dobbins (1956) and Banks (1975) formulas, for estuaries affected by both tidal velocities and wind. Since the water velocity simulated by EFDC is directly affected by wind, using O'Connor-Dobbins formula has indirectly accounted for the wind effect on recreation.

Table 3-4 Reaeration formulations for ranges of water depth and velocity

Parameter	O'Connor-Dobbins	Churchill (1962)	Owens-Gibbs
Depth (*m*)	0.30–9.14	0.61–3.35	0.12–0.73
Velocity (*m/s*)	0.15–0.49	0.55–1.52	0.03–0.55

3.4.3 Light Extinction Coefficient

Light plays a key role in the biological cycle in the water body through affecting the photosynthesis which is a process of converting the inorganic materials (CO_2 and H_2O) to the organic substance and oxygen in the daytime. The maximum depth that algae can survive is directly determined by the depth that the light can reach. The clearer the water is, the deeper the light can reach. It further results in more production of oxygen due to more algae. The light extinction

coefficient is a parameter representing how far the light can reach. Since the EFDC model for Perdido and Wolf Bay didn't simulate suspended solids, only the background light extinction coefficient was used in the Perdido-Wolf EFDC model. There is a relationship between the light extinction and Secchi depth (light extinction = 1.8/Secchi depth) (Chapra, 1997). Some observed Secchi depths in the study area are available from STORET. Since the average Secchi depth from all the locations in 2015–2016 was 1.6 m (ranged from 0.2 to 3.3 m), 1.1 m^{-1} was used by model calibration as the background light extinction coefficient. The effect of Chlorophyll-a further increases the light extinction (Chapra, 1997).

3.4.4 Other Model Parameters

There are nearly one hundred internal model coefficients linked to the hydrodynamic and water quality variables in EFDC. These coefficients, together with the input boundary conditions, determine the DO balance and concentration. Most of the coefficients required by the EFDC model were initialized with the defaulted values. These default values are primarily from the calibrated results for the Chesapeake Bay model, which is also an estuarine water body, the same as the study area. In general, these coefficients can be categorized into several groups, algae, light, nitrogen, phosphorus and carbon groups, which are listed and summarized using Table 3-5 to Table 3-9. Several coefficients linking to the algae growth were adjusted in light of the reported ranges from the literature (**Error! Reference source not found. - Error! Reference source not found.**).

Table 3-5 Internal model coefficients linking with the algae

Parameter	***Values***
Maximum growth rate for green algae (1/day)	2.5
Basal metabolism rate for green algae (1/day)	0.01
Predation rate on green algae (1/day)	0.215
C : chlorophyll ration for green algae (mg C/μg Chl)	0.065
Stoichiometric algae O_2 : C ratio (g O_2/g C)	2.67
Stoichiometric algae O_2 : NO_3-N ratio (g O_2/g N)	4.33

Nitrogen half-saturation for green algae (mg/L)	0.01
Phosphorus half-saturation for green algae (mg/L)	0.001
Lower optimal temperature for growth, green algae (°C)	22
Upper optimal temperature for growth, green algae (°C)	28
Suboptimal temperature effect coeff for growth, green algae (°C)	0.01
Superoptimal temperature effect coeff for growth, green algae (°C)	0.02
Reference temperature for basal metabolism, green algae (°C)	20
Temperature effect coeff for basal metabolism, green algae	0.069
Optimal depth for growth, green algae (m)	1

Table 3-6 Coefficients linking with the light

Parameters	***Values***
Background light extinction coefficient (1/m)	1.1
Light extinction due to TSS (1/m per mg/L)	0.052
Light extinction due to Chlorophyll (1/m per mg/L)	0.031
Light extinction due to POC (1/m per mg/L)	0.078
Light extinction due to DOC (1/m per mg/L)	0.2

Table 3-7 Coefficients linking with the carbon

Parameters	***Values***
Algal predation, carbon fraction to RPOC	0.35
Algal predation, carbon fraction to LPOC	0.55
Algal predation, carbon fraction to DOC	0.1
Minimum dissolution rate of RPOC (1/day)	0.005
Minimum dissolution rate of LPOC (1/day)	0.075
Minimum dissolution rate of DOC (1/day)	0.01
Reference temperature for dissolution (°C)	20
Reference temperature for mineralization (°C)	20
Temperature effect coefficient for dissolution	0.069
Temperature effect coefficient for mineralization	0.069
Half-saturation constant for denitrification (g N/m^3)	0.1
Ratio of denitrification rate to DOC respiration rate	0.5

Table 3-8 Coefficients linking with the Nitrogen

Parameters	***Values***
Algal predation, nitrogen fraction to RPON	0.35
Algal predation, nitrogen fraction to LPON	0.55
Algal predation, nitrogen fraction to DON	0.1
N:C ration for green algae (g N/g C)	0.167
Mass NO_3 reduces per DOC oxidized (g N/g C)	0.933
Maximum nitrification rate (1/day)	0.07
Oxygen half-saturation constant for nitrification (g O_2/m^3)	1
NH4 half-saturation constant for nitrification (g N/m^3)	1
Reference temperature coeff for nitrification (°C)	27
Suboptimal temperature effect coeff for nitrification (°C)	0.0045
Superoptimal temperature effect coeff for nitrification (°C)	0.0045
Minimum hydrolysis rate of RPON (1/day)	0.005
Minimum hydrolysis rate of LPON (1/day)	0.075
Minimum hydrolysis rate of DON (1/day)	0.015

Table 3-9 Coefficients linking with the Phosphorus

Parameter	***Values***
Algal predation, phosphorus fraction to RPOP	0.1
Algal predation, phosphorus fraction to LPOP	0.2
Algal predation, phosphorus fraction to DOP	0.5
Algal predation, phosphorus fraction to InP	0.2
Partition coeff for sorb/dissolved PO4	0.04
Minimum hydrolysis rate of RPOP (1/day)	0.005
Minimum hydrolysis rate of LPOP (1/day)	0.075
Minimum mineralization rate of DOP (1/day)	0.1

Table 3-10 Maximum growth rate and corresponding reference temperatures (Burn and McBean 1985)

Algal Type	Maximum Growth Rate (1/day)	Reference Temperature (^{o}C)	References
	1.75**	27^{o}C**	Di Toro et al. (1971)
	0.55 3.4**	20^{o}C**	Collins & Wlosinski (1983)
	1.1 5.0**	20^{o}C**	Jorgensen (1979)
Green Algae	1.9	25^{o}C	Bierman (1976)
	1.4	20^{o}C	Bierman et al. (1980)
	2.0 - 2.5	T_{opt}	Tetra Tech (1980) Bowie et al. (1980) Porcella et al. (1983)
	1.9	20^{o}C	Canale et al. (1976)
	1.8 - 2.5	T_{opt}	Scavia et al. (1976) Scavia (1980)
	1.6	25^{o}C	DePinto et al. (1976)
	3.0	T_{opt}	Lehman et al. (1975)
	1.5 3.9**	25^{o}C**	Di Toro et al. (1971)
	0.7 - 2.1**	20^{o}C	Collins & Wlosinski (1983)
	0.9 4.1**	25^{o}C**	
	9.0 9.2**	39^{o}C**	
	1.4 2.4**	20^{o}C**	Jorgensen (1979)
	1.5 3.9**	25^{o}C**	
	1.3 4.3**	35^{o}C**	
	5.65**	40^{o}C**	

Table 3-11 Half-saturation constants (Burn and McBean 1985)

Algal Type	Half-Saturation Constant: Nitrogen (mg/l)	Phosphorus (mg/l)	Carbon (mg/l)	Silicon (mg/l)	References
Green Algae	0.03 0.035	0.004	0.03		Tetra Tech (1980) Bowie et al. (1980) Porcella et al. (1983)
	0.15	0.01			Di Toro et al. (1971)
	0.001 0.035	0.005 0.024			Scavia et al. (1976) Scavia & Park (1976) Scavia (1980)
	0.15	0.0025			Canale et al. (1976)
	0.03*	0.03*	0.03*		Tetra Tech (1979)
	0.005 0.15**	0.01**			Jorgensen (1979)
	0.006 1.236**	0.002 0.475**	0.068 - 1.5**		Collins & Wlosinski (1983)

Table 3-12 Algae respiration rates and reference temperatures (Burn and McBean 1985)

Algal Type	Respiration Rate (1/day)	Reference Temperature (^{o}C)	References
Green Algae	0.05 0.07	$20^{o}C$	Tetra Tech (1980) Porcella et al. (1983)
	0.05 0.25	T_{opt}	Scavia et al. (1976) Scavia (1980) Bowie et al. (1980)
	0.03 0.05	$20^{o}C$	Bierman (1976) Bierman et al. (1980)
	0.01 0.46**	$20^{o}C$	Collins & Wlosinski (1983)

Table 3-13 Algae settling rates (Burn and McBean 1985)

Algal Type	Settling Velocity (m/day)	References
Green Algae	0.05 - 0.19	Jorgensen et al. (1978)
	0.05 0.4	Bierman (1976) Bierman et al. (1980)
	0.02	Canale et al. (1976)
	0.8	Lehman et al. (1975)
	0.1 0.25	Tetra Tech (1980) Porcella et al. (1983)
	0.3	DePinto et al. (1976)
	0.08 0.18**	Collins & Wlosinski (1983)
	0.27 - 0.89**	Jorgensen (1979)

CHAPTER 4 Results, Discussions and Sensitivity Analysis

4.1 Validation of the Model

The model validation is aimed at assessing the reliability of the model by comparing the simulated and observed results. For the current project, it includes validation for three variables: salinity, water temperature, and DO concentration, respectively. Salinity is an important factor to affect water density. Given that the research area is an estuary, the interaction between the freshwater and tide with high salt concentration further causes vertical transport or mixing of water columns and pollutants. The denser salt water flows under the upper less dense water. Water temperature not only affects the density but also determines the DO concentration in the water body. The warmer the water is, the less the DO will be. DO is the key water quality parameter. Low DO directly threatens the survival of the plankton.

Although the model was run 3 years, 2015–2017, the validation was categorized into two groups, 2015–2016, and 2017, due to the different locations of observed data and the activation of different sub-models. The DO was simulated only from 2015–2016 but not in 2017 due to not enough required input data related to the DO simulation in 2017. Since the dissolved oxygen simulation is a subsequent process based on the hydrodynamic model, the salinity and water temperature were firstly validated to test the accuracy of the model. Then the calibrated hydrodynamic model was used for the DO simulation. Therefore, the validation part was organized as the following sequence, salinity and water temperature validation in 2015–2016, salinity and water temperature validation in 2017, and DO validation in 2015–2016.

4.1.1 Statistical Model

The choice of statistical error parameters for a simulation model is a critical process of judging whether a model can be regarded as a sound and robust model in addition to the visual comparison by plotting the observed data and simulated results. No commonly accepted statistical criteria were established since each statistical evaluation method has its own advantages and disadvantages. Many statistical guidelines were developed for the different hydrological and water quality models. These quantitative statistics generally can be categorized into three groups, standard regression, dimensionless, and error index. The slope and y-intercept, Pearson's correlation coefficient (r), and coefficient of determination (R^2) are quantitative statistics in the standard regression group. The dimensionless group contains the index of agreement (d), Nash-Sutcliffe efficiency (*NSE*), Persistence model efficiency (*PME*), prediction efficiency (*Pe*), performance virtue statistic (PV_k), and logarithmic transformation variable (e). The mean absolute error (*MAE*), mean square error (*MSE*), and root mean square error (*RMSE*) are included in the error index group (Moriasi et al. 2007).

Given that the characteristics of the study area (a shallow estuary) and limited observed data, only *NSE*, R^2, and *RMSE* calculated from the observed data and simulated values were used to evaluate the accuracy and performance of the hydrodynamic and water quality EFDC model. The *NSE* is a normalized statistic that determines the relative magnitude of the residual variance compared to the measured or observed data variance, which is computed using the following equation (Nash and Sutcliffe 1970),

$$NSE = 1 - [\frac{\sum_{i=1}^{n}(Y_i^{obs} - Y_i^{sim})^2}{\sum_{i=1}^{n}(Y_i^{obs} - Y_i^{mean})^2}] \quad (4.1)$$

where Y_i^{obs} is the i^{th} observation for the constituent (such as water temperature, salinity, and DO) being evaluated, Y_i^{sim} is the i^{th} simulated value for the constituent being evaluated, Y_i^{mean} is the mean of observed data for the constituent being evaluated, and n in the total number of observations.

The value of NSE ranges between -∞ and 1.0 (1 inclusive). The higher the *NSE* value, the more accurate the model's simulation is. The *NSE* value with 1.0 represents the optimal value (the simulation matches perfectly with observation). The models are generally regarded as acceptable levels of performance with *NSE* values between 0.6 and 1. If the value is less than 0.0, it indicates the simulation is worse than the mean of observed values. In another word, the model performs unacceptably.

The coefficient of determination (R^2) is a statistical parameter to evaluate how close the data are to the fitted linear regression line, e.g., between observed and simulated data. Since it shows the strength of a linear relationship between two variables (observed data and simulated values), it is also often called goodness of fit, which is computed as the following equation,

$$R^2 = [\frac{\sum_{i=1}^{n}(x_i - \bar{x})(y_i - \bar{y})}{\sqrt{\sum_{i=1}^{n}(x_i - \bar{x})^2 \sum_{i=1}^{n}(y_i - \bar{y})^2}}]^2 \quad (4.2)$$

where x_i is the ith observed data (such as water temperature, salinity and DO), y_i is the ith simulated value, $\bar{x}$ and $\bar{y}$ are the mean values of observed data and simulated values for the constituent being evaluated, respectively, and n in the total number of observations.

The R^2 changes between 0 and 1. As with *NSE*, the higher R^2 is, the more accurate the model is. Typically the model with evaluation results of R^2 greater than 0.5 can be regarded as an acceptable model (Moriasi et al. 2007). Although R^2 has been widely used for model evaluation, it is over sensitive to high extreme values and insensitive to additive and proportional differences between model predictions and measured data (Legates and McCabe Jr 1999).

RMSE is another popular metrics to measure accuracy for continuous variables by indicating an error in squared units (Moriasi, Arnold et al. 2007). In contrast to the MAE that gives the same weight to all errors, the RMSE penalizes variances as it gives errors with larger absolute values more weight than errors with smaller absolute values. RMSE is calculated as the following equation,

$$RMSE = \sqrt{\frac{\sum_{i=1}^{n}(P_i - O_i)^2}{n}} \tag{4.3}$$

where n is the number of observed data; P_i is the ith predicated value; O_i is the corresponding ith observed data.

RMSE is greater than 0 ranging from 0 to ∞. The lower the RMSE, the more accurate the model is. Since RMSE has the same units as the parameters to be evaluated, it is easier to be understood in comparison to the other measures of goodness of fit.

4.1.2 Salinity Validation in 2015 and 2016

Salinity is a measure of the concentration of salts dissolved in the water. It is an important hydrodynamic parameter due to its effect on the vertical stratification. The heavier water with higher salinity sinks/flows underneath the less saline water or freshwater, which forms the saltwater intrusion phenomenon. In addition, it can also influence the solubility of DO (Chapra, 1997). The solubility of DO decreases as salinity increases. The vertical stratification prevents the mixing of the water body. Therefore, the higher DO concentration in the surface layers cannot adequately diffuse/transfer to the bottom layer so that DO in the bottom layers could be even lower. For the coastal region, salinity levels usually vary seasonally due to variations of tides and the freshwater inflows, which significantly increase during the wet season.

Observed salinity data from 2015–2016 for model validation were available at eleven monitoring stations which are operated by three agencies (Figure 4-1). Two stations are located in

the Cotton Bayou (Figure 4-2). The Perdido Pass monitoring station is run by Mobile Bay National Estuary Program (http://www.mymobilebay.com/). Three monitoring stations at Bear Point, Kee Avenue, and Spanish Cove are operated by the Alabama Department of Environmental Management (ADEM) and accessed from http://aldem.maps.arcgis.com/apps/webappviewer/index.html?id=e5b6ee63a2df45f187832d492bdb2298, and all the other six stations are from the Alabama Water Watch (AWW) (http://www.alabamawaterwatch.org/) that are monitored by citizen volunteers. The Bear Point monitoring station is located at the north of Bear Point (part of the City of Orange Beach) and in the connection channel between Perdido Bay and Wolf Bay. The Kee Avenue and Spanish Cove monitoring stations are located at the middle portion of Perdido Bay (near Highway 98 Bridge). For the salinity data form ADEM, they were only labeled the sample collection date instead of the actual date, hour and minute, so that they were assumed/regarded as measurement at noon in the corresponding date in the subsequent statistical analysis. Since all the data were recorded near the water surface, the statistical error parameters *NSE* and R^2 were derived by comparing the recorded data and the simulated salinity values of the top water layer from the EFDC model.

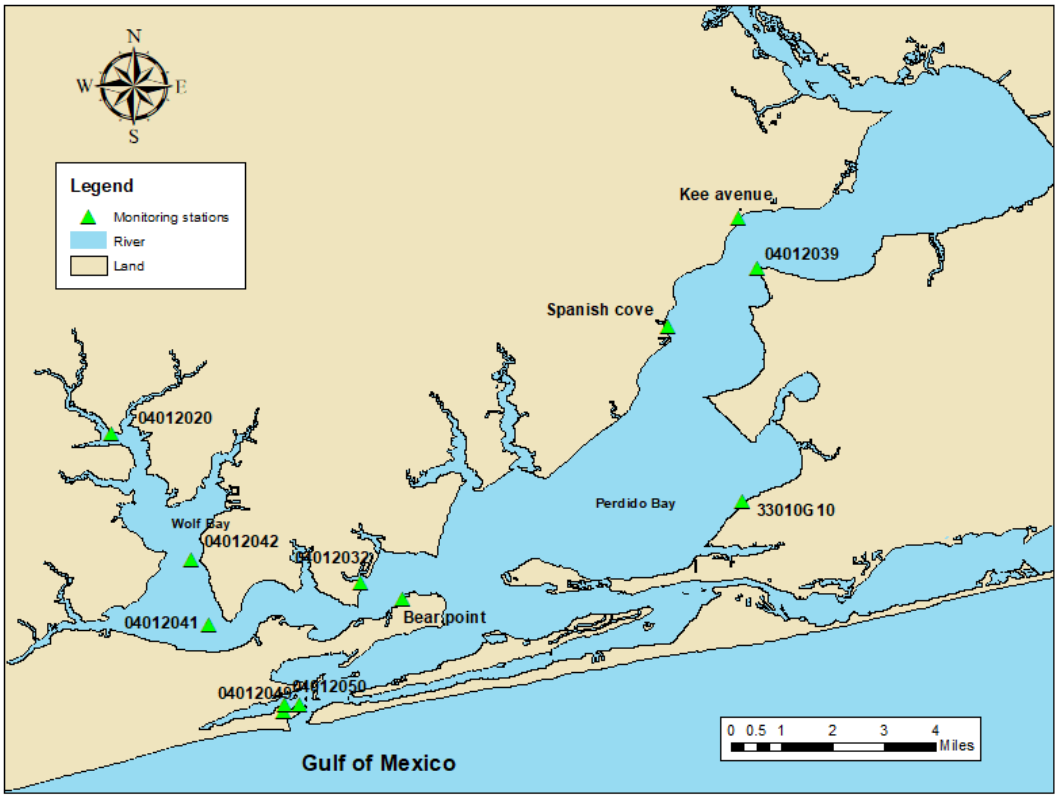

Figure 4-1 Locations and station numbers of monitoring stations for the salinity validation in 2015–2016

Given the locations of eleven monitoring stations, they can be simply grouped into three geographic parts (Table 4-1). The Bear Point and station 04012032 are located at the connecting channel or waterway between Perdido Bay and Wolf Bay but are grouped as Wolf Bay. Table 4-2 shows the validation statistical results and Figure 4-3–Figure 4-13 plot the simulated salinity at four layers versus the observed data. In the Wolf Bay region, the simulated values of salinity were generally in reasonable agreement with the observed data. The smaller *NSE* was derived at station 04012020 located at the most upstream part of Wolf Bay. Figure 4-7 shows the simulated salinity is generally higher than the observed data. This is possibly due to the flow data from the upstream creeks of Wolf Bay. Since there were only available flow data for the Wolf Creek boundary condition, the derived flows for the other four boundaries may be smaller than the actual values

since their estimated flows were derived based on a study conducted in 2008. The lower flow led to higher salinity. For station 04012032, the observed salinity is higher than the simulated results from 1/1/2015 to 8/1/2015, especially from 4/1/2015 to 8/1/2015. This could be due to the complex bathymetry and shoreline variation near station 04012032, which is also connected with a not-modeled small tributary in the north (Figure 4-14). However, its neighbor two stations 04012041 (Figure 4.9) and Bear Point (Figure 4.11) show acceptable simulated results. Vertical stratification of salinity for five stations in Wolf Bay was typically small. All *NSE* values for five stations associated with Wolf Bay are positive (0.28–0.83) with R^2 ranging from 0.31 to 0.87, which indicate these salinity validation results are acceptable. Freshwater inflow from upstream streams/creeks is small and the impact of dynamic oceanic waves from the Gulf of Mexico is attenuated so that the spatial and temporal salinity variations at all locations in Wolf Bay are smaller and more gradual; therefore, the model does a better job to predict/simulate salinity variations in Wolf Bay.

Figure 4-3 – Figure 4-6 show the salinity validation for four stations in the Perdido Bay region. The simulated salinity was in good agreement with the observed data from Spanish Cove and Kee Avenue in 2015 and 04012039 in 2016. The simulated values look like higher than the observed data in 2016, especially from 5/30/2016 to 8/1/2016 at Spanish Cove and Kee Avenue, which could be due to various possible reasons, such as not representative upstream freshwater inflows. Observed salinity at three nearby stations (Kee Avenue, Spanish Cove and 04012039, Figure 4-1) in some days were similar but in some other days were quite different. This could be caused by their different bathymetry and shoreline variations to result in complex hydrodynamic patterns. Simulated salinity at Kee Avenue and 04012039 shows certain vertical stratification but Spanish Cove has much large vertical stratification and almost no stratification at 33010G10. Both *NSE* and R^2 are acceptable at Kee Avenue and Spanish Cove stations but *NSE* values are negative for other two stations in Perdido Bay.

For Perdido Pass and 04012050 stations, R^2 and *NSE* values were low (Table 4-2) because they are so close to the shoreline (Figure 4-2) and have large variations in salinity over time (much more dynamic, Figure 4-12, Figure 4-13). Small time shifting of water level at the open boundary (Dolphin Island), which may not be representative of actual water level variations at Perdido Pass, could significantly affect the model performance on predicting the salinity in lower Perdido Bay region.

Table 4-1 List of the monitoring stations by locations

Perdido Bay	Kee Avenue	04012039	Spanish Cove	33010G10	
Wolf Bay	04012020	04012042	04012041	04012032	Bear Point
Cotton Bayou	04012050	Perdido Pass			

Table 4-2 Statistical results of surface salinity validation in 2015–2016 in different stations

Perdido Bay	Station	Kee Avenue	04012039	Spanish Cove	33010G10	
	# of observed data	65	19	64	48	
	R^2	0.56	0.22	0.44	0.4	
	NSE	0.53	-0.06	0.39	-0.24	
	RMSE	3.46	6.26	3.67	4.96	
Wolf Bay	Station	04012020	04012042	04012041	04012032	Bear Point
	# of observed data	23	13	15	21	38
	R^2	0.31	0.87	0.85	0.69	0.64
	NSE	0.28	0.83	0.8	0.33	0.43
	RMSE	5.16	2.03	2.65	4.41	3.17
Cotton Bayou	Station	04012050	Perdido Pass			
	# of observed data	9	16927			
	R^2	0.3	0.22 [1]			
	NSE	-1.27	-0.29 [1]			
	RMSE	7.63	6.43 [1]			

Note: [1] — these were developed between simulated at the lower layer and observed water temperatures

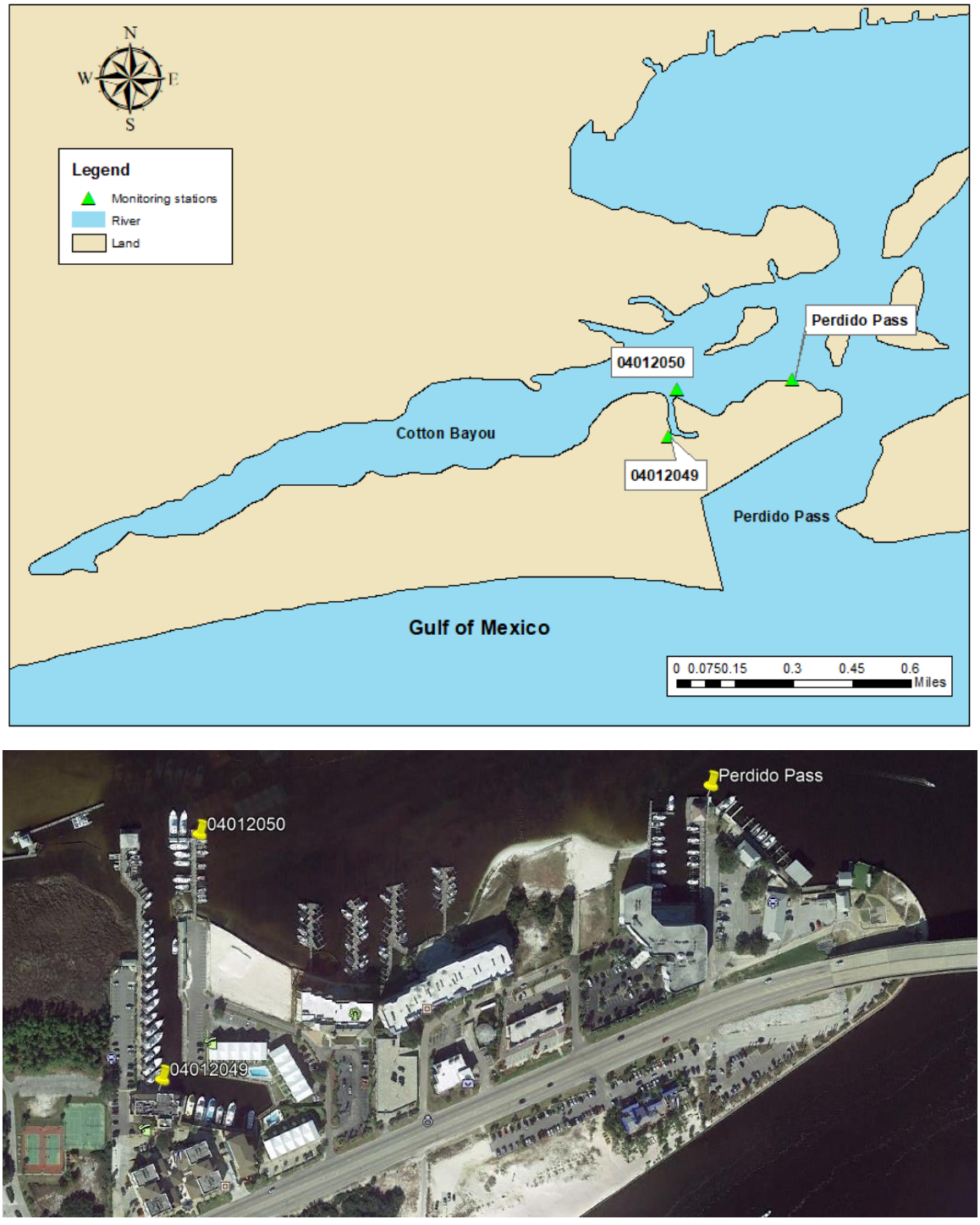

Figure 4-2 Locations of three monitoring stations (04012049, 04012050 and Perdido Pass) in the mouth of Cotton Bayou

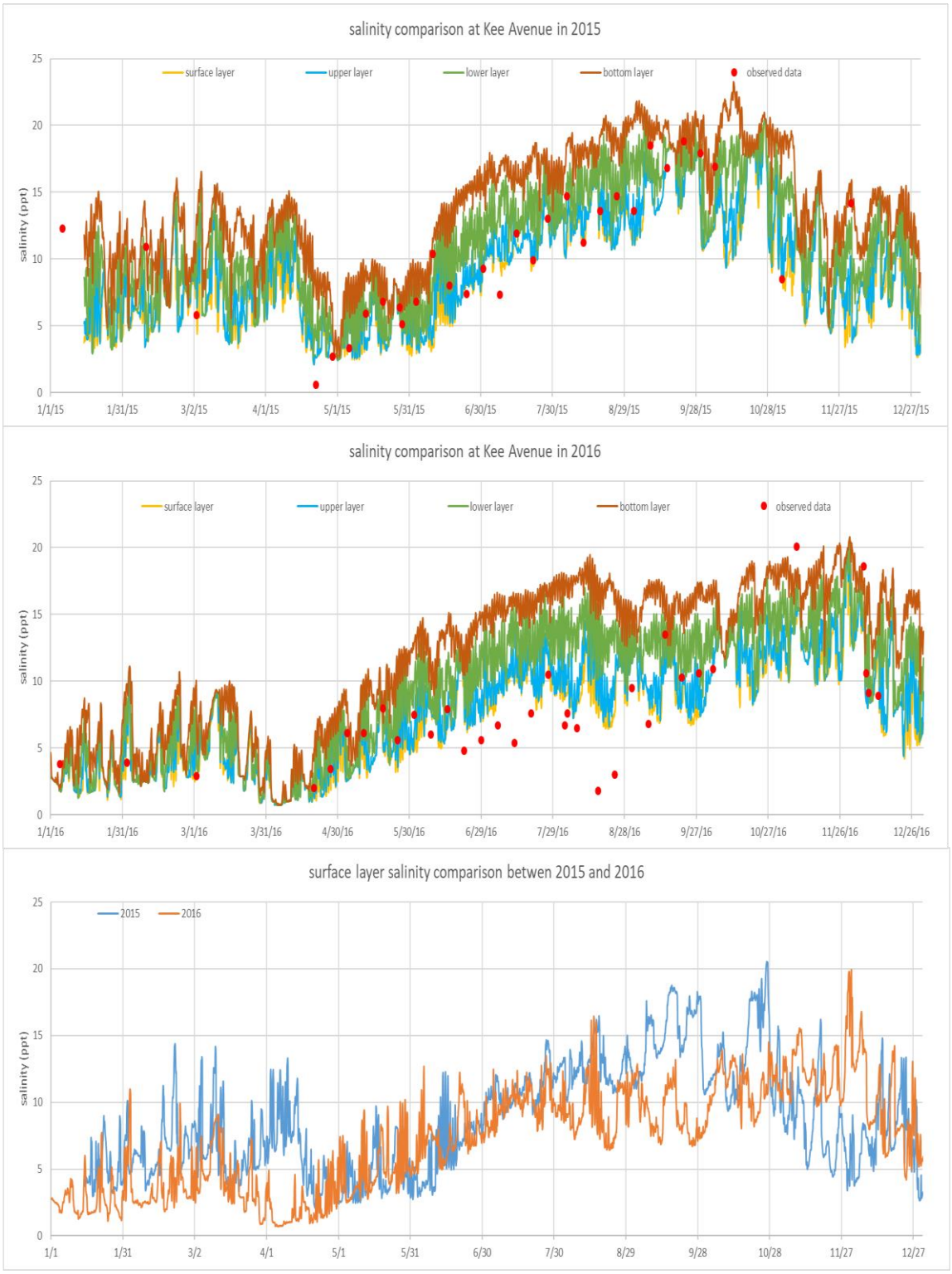

Figure 4-3 Salinity comparison among 2015–2016 simulated results at four layers and observed data at Kee Avenue in Perdido Bay

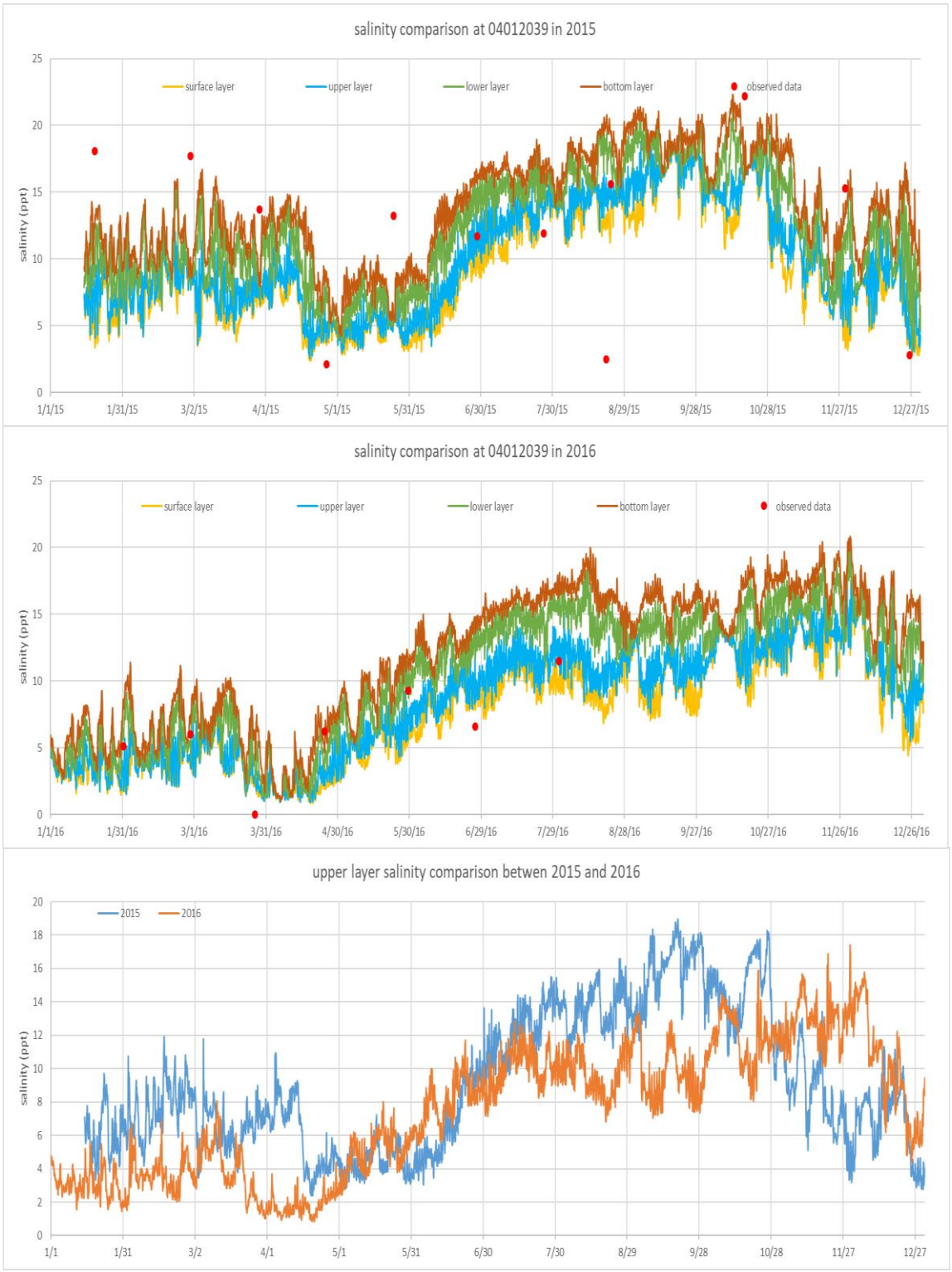

Figure 4-4 Salinity comparison among 2015–2016 simulated results at four layers and observed data at 04012039 in Perdido Bay

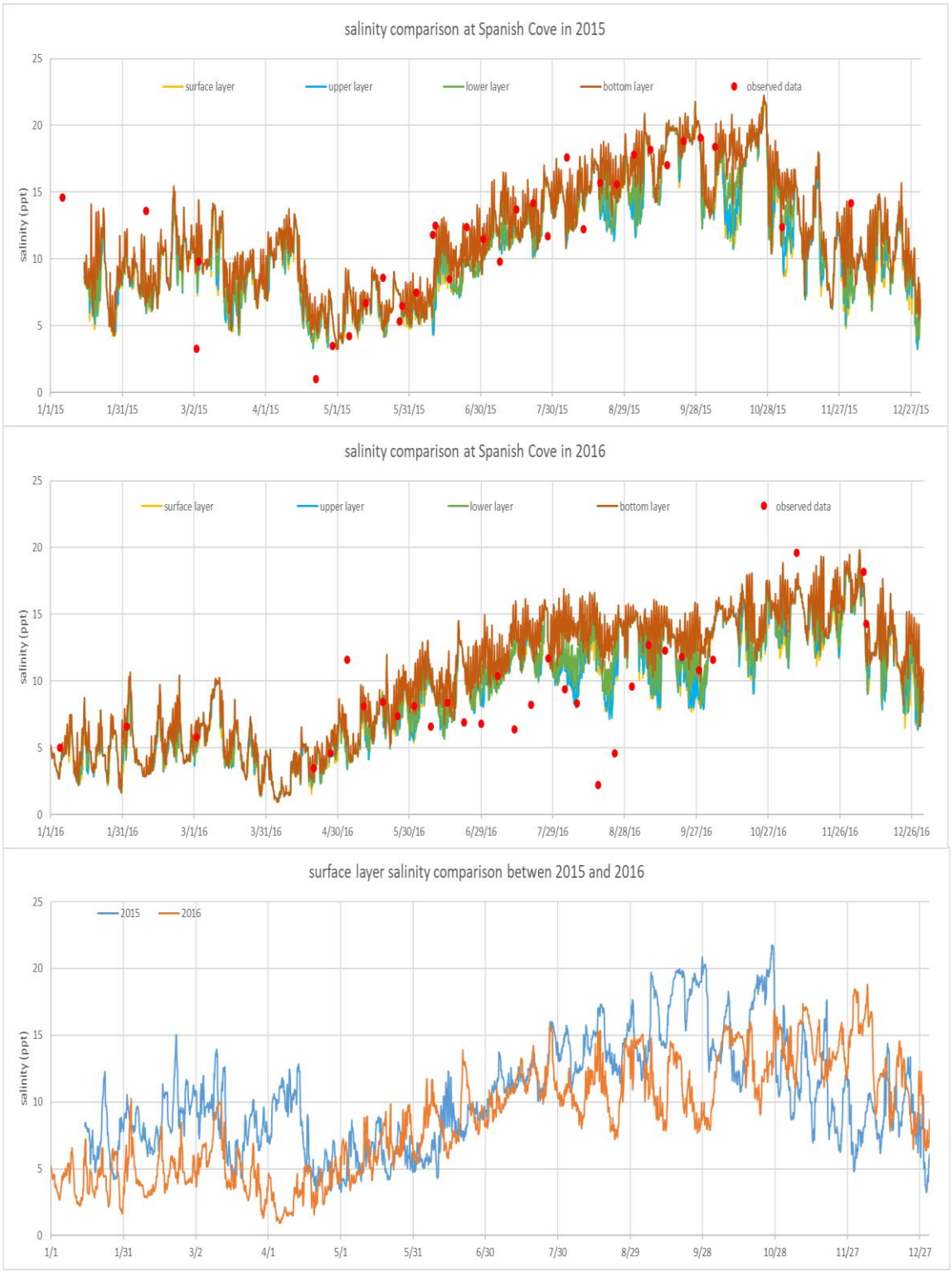

Figure 4-5 Salinity comparison among 2015–2016 simulated results at four layers and observed data at Spanish Cove in Perdido Bay

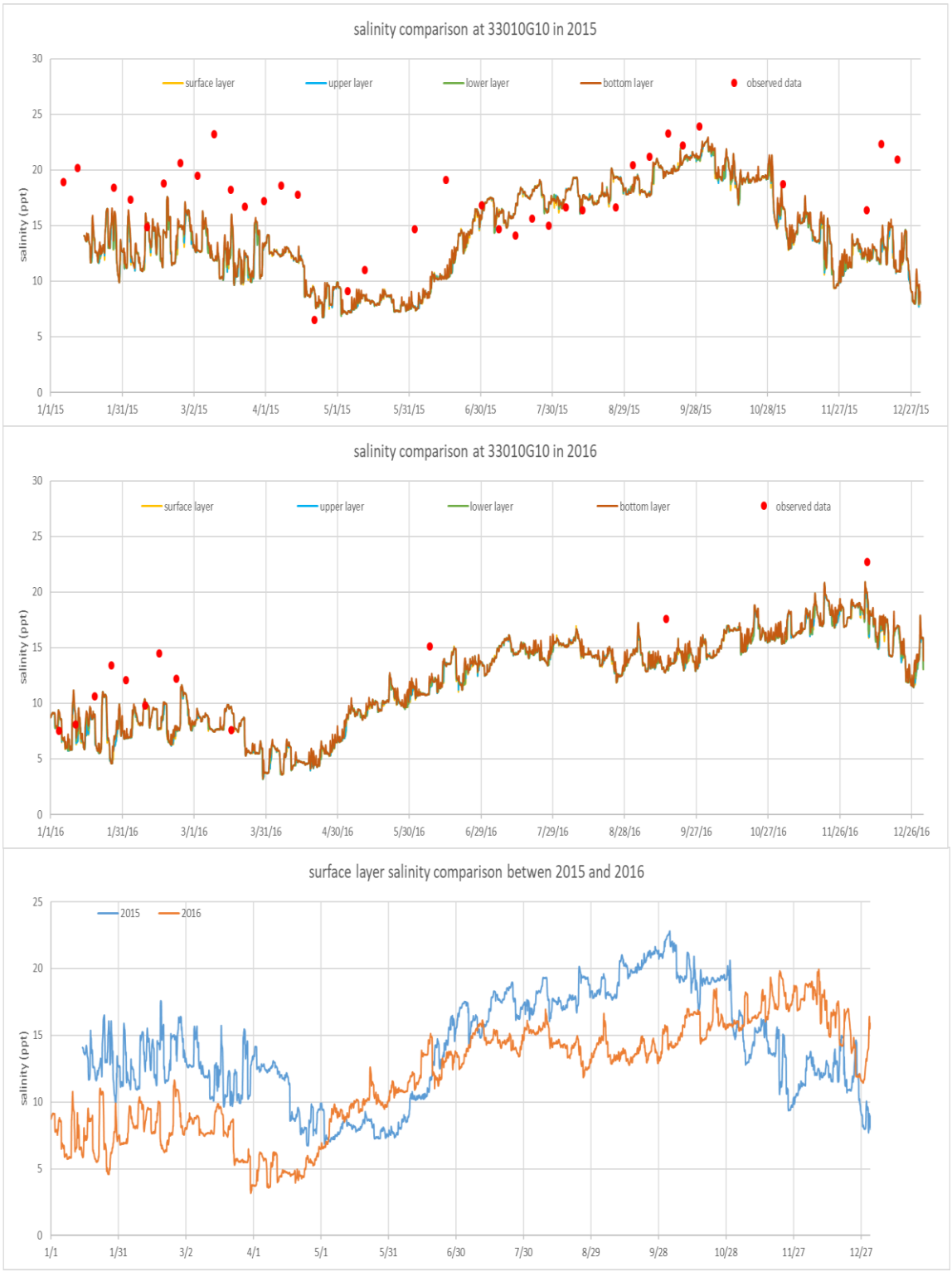

Figure 4-6 Salinity comparison among 2015–2016 simulated results at four layers and observed data at 33010G10 in Perdido Bay

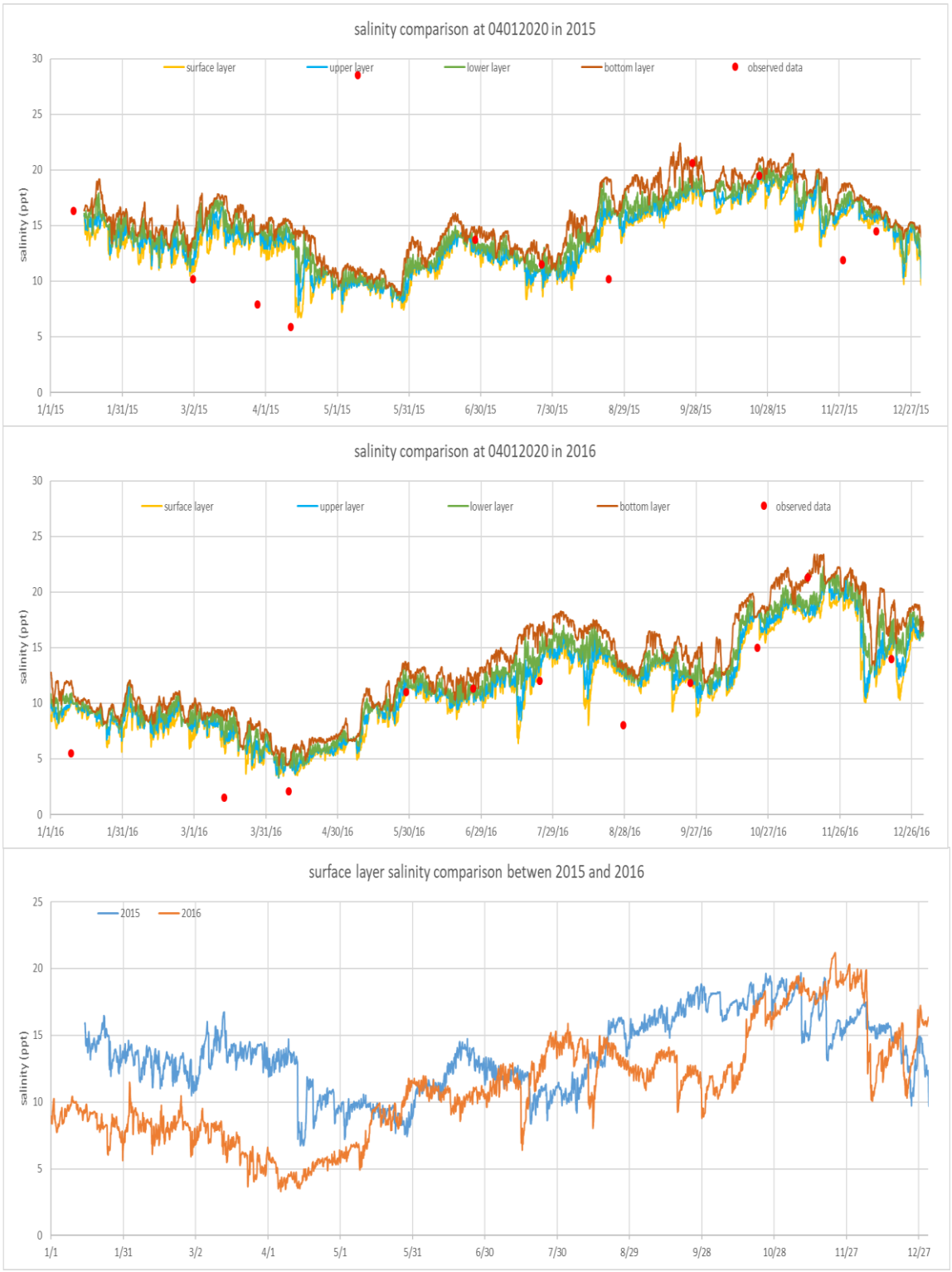

Figure 4-7 Salinity comparison among 2015–2016 simulated results at four layers and observed data at 04012020 in Wolf Bay

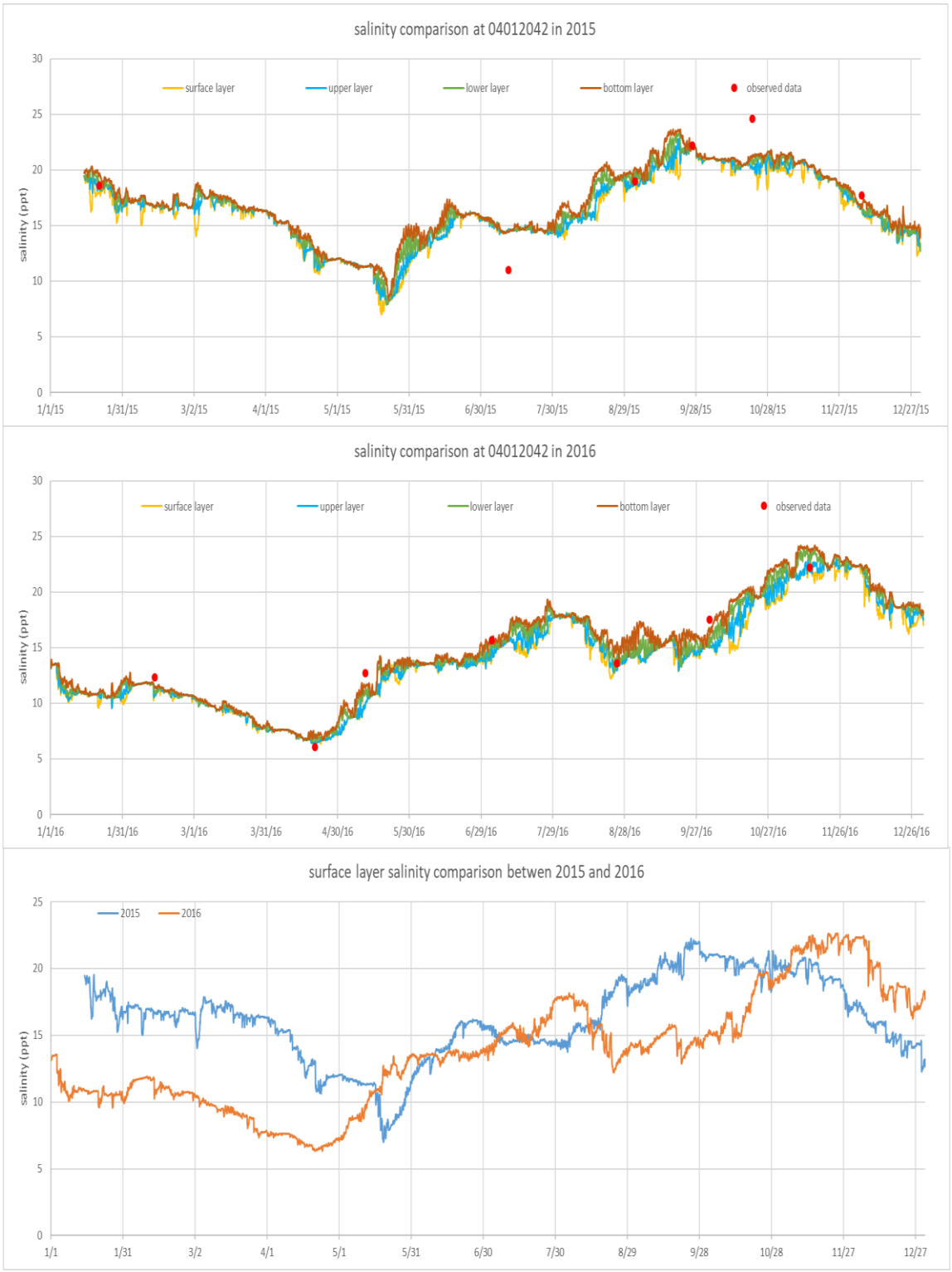

Figure 4-8 Salinity comparison among 2015–2016 simulated results at four layers and observed data at 04012042 in Wolf Bay

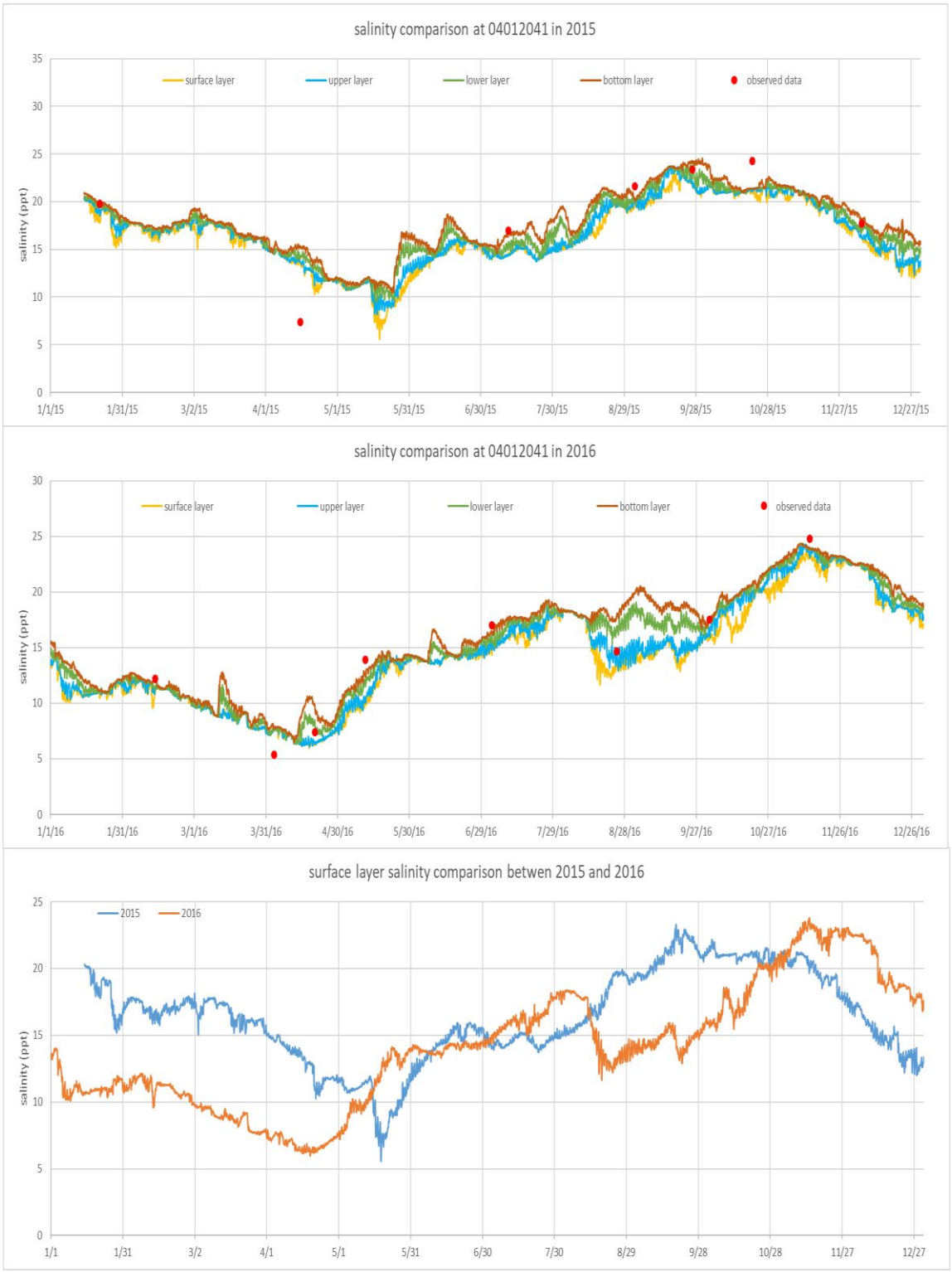

Figure 4-9 Salinity comparison among 2015–2016 simulated results at four layers and observed data at 04012041in Wolf Bay

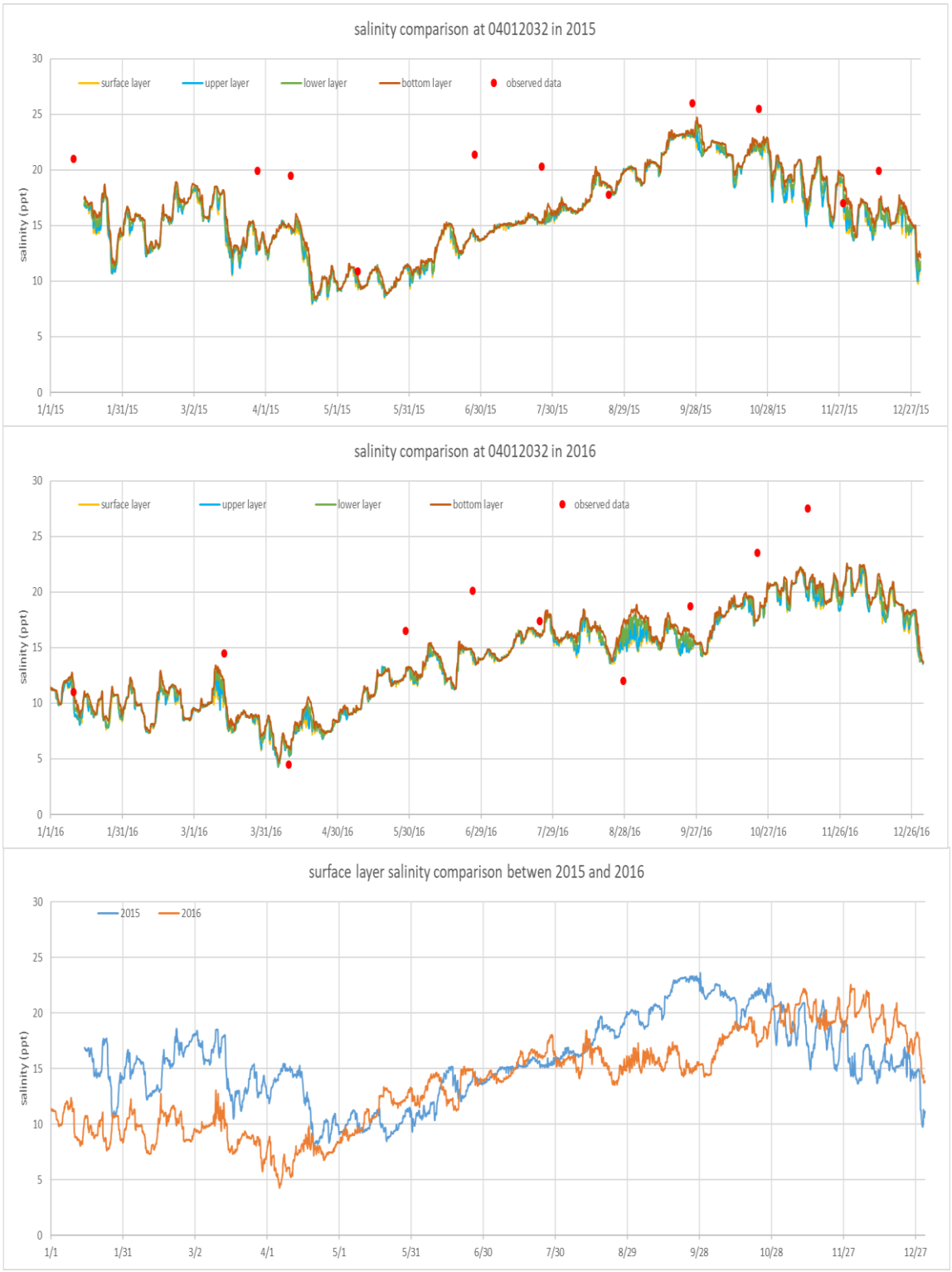

Figure 4-10 Salinity comparison among 2015–2016 simulated results at four layers and observed data at 04012032 in Wolf Bay

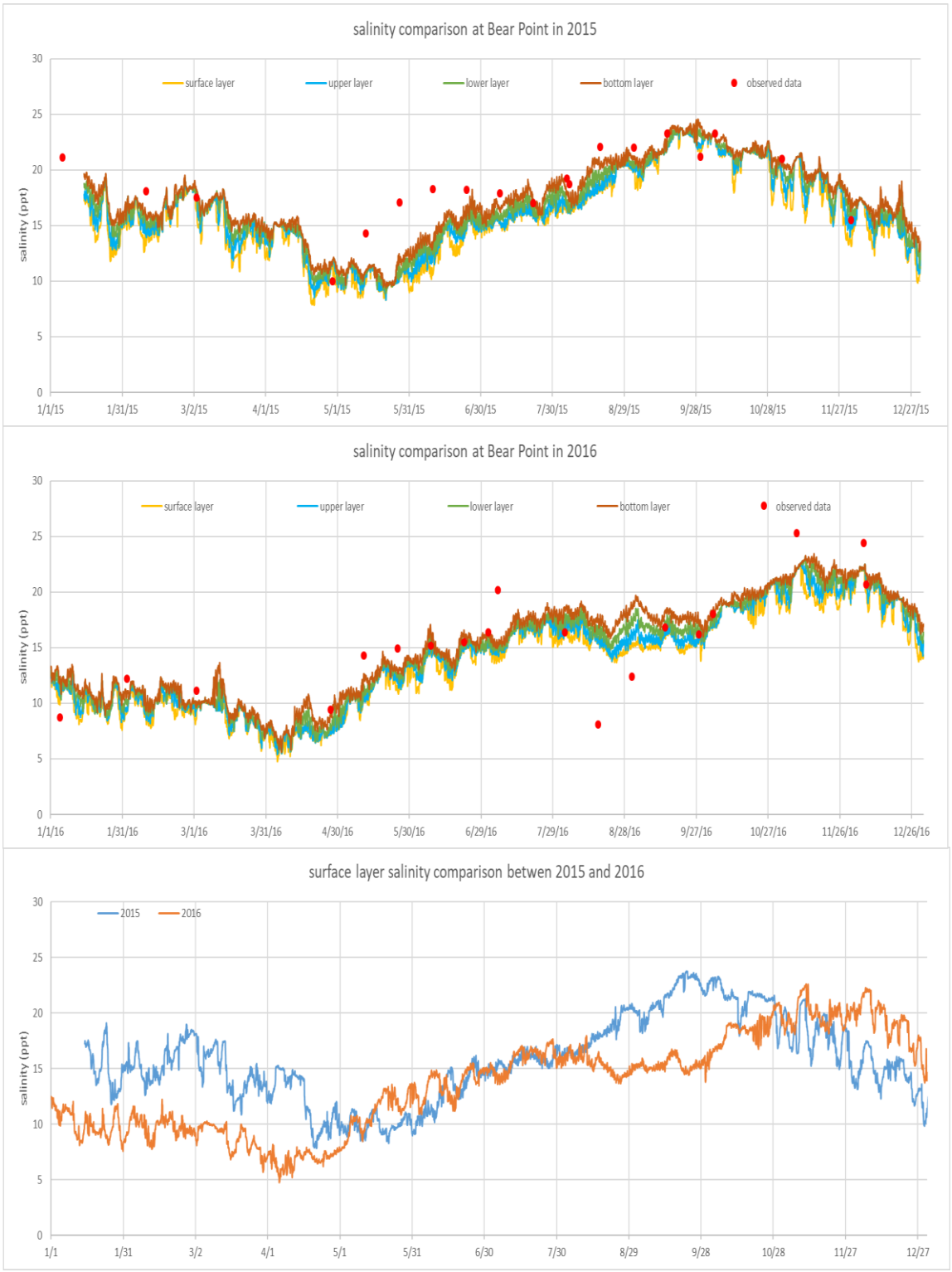

Figure 4-11 Salinity comparison among 2015–2016 simulated results at four layers and observed data at Bear Point in Wolf Bay

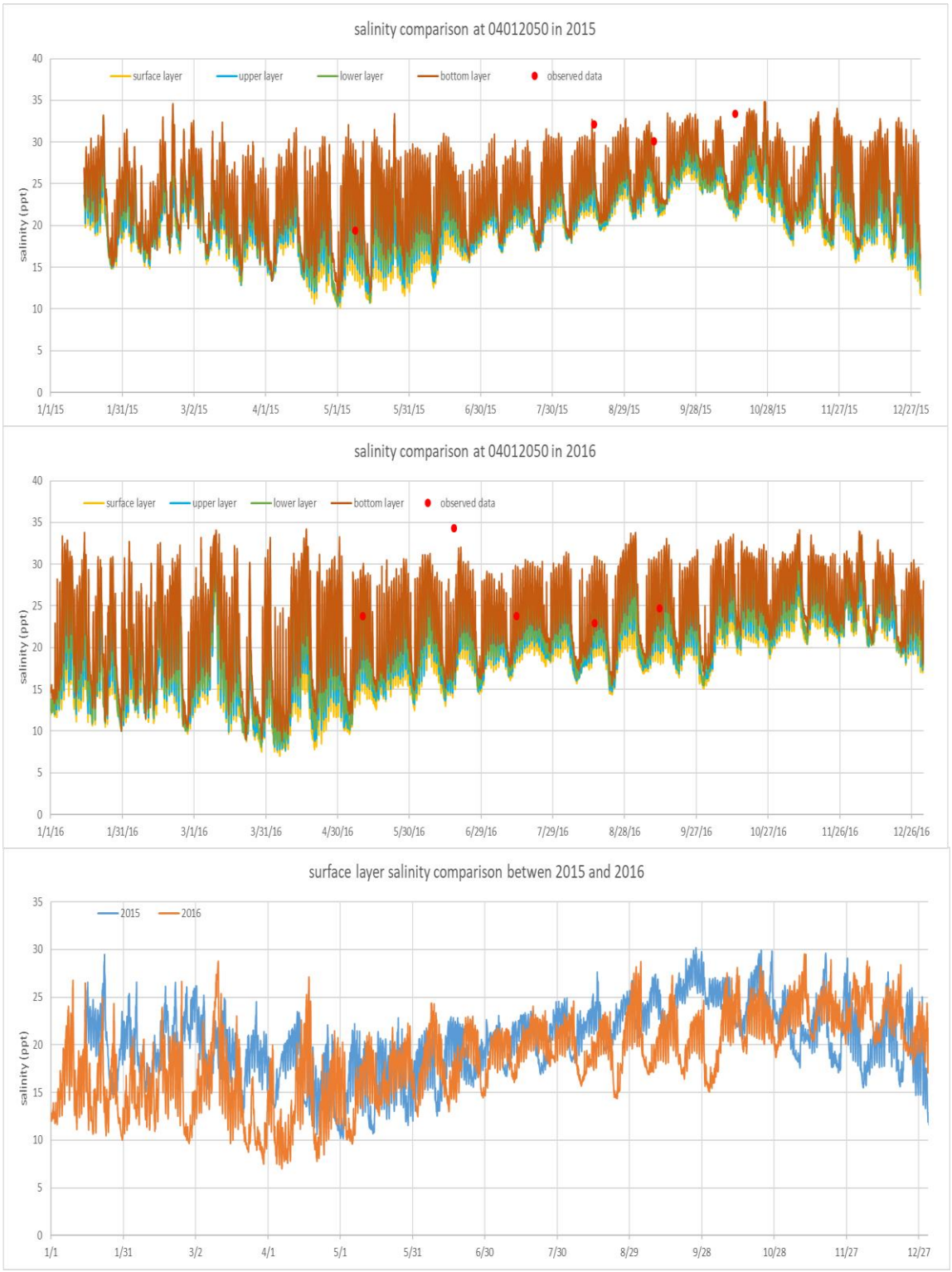

Figure 4-12 Salinity comparison among 2015–2016 simulated results at four layers and observed data at 04012050 in Cotton Bayou

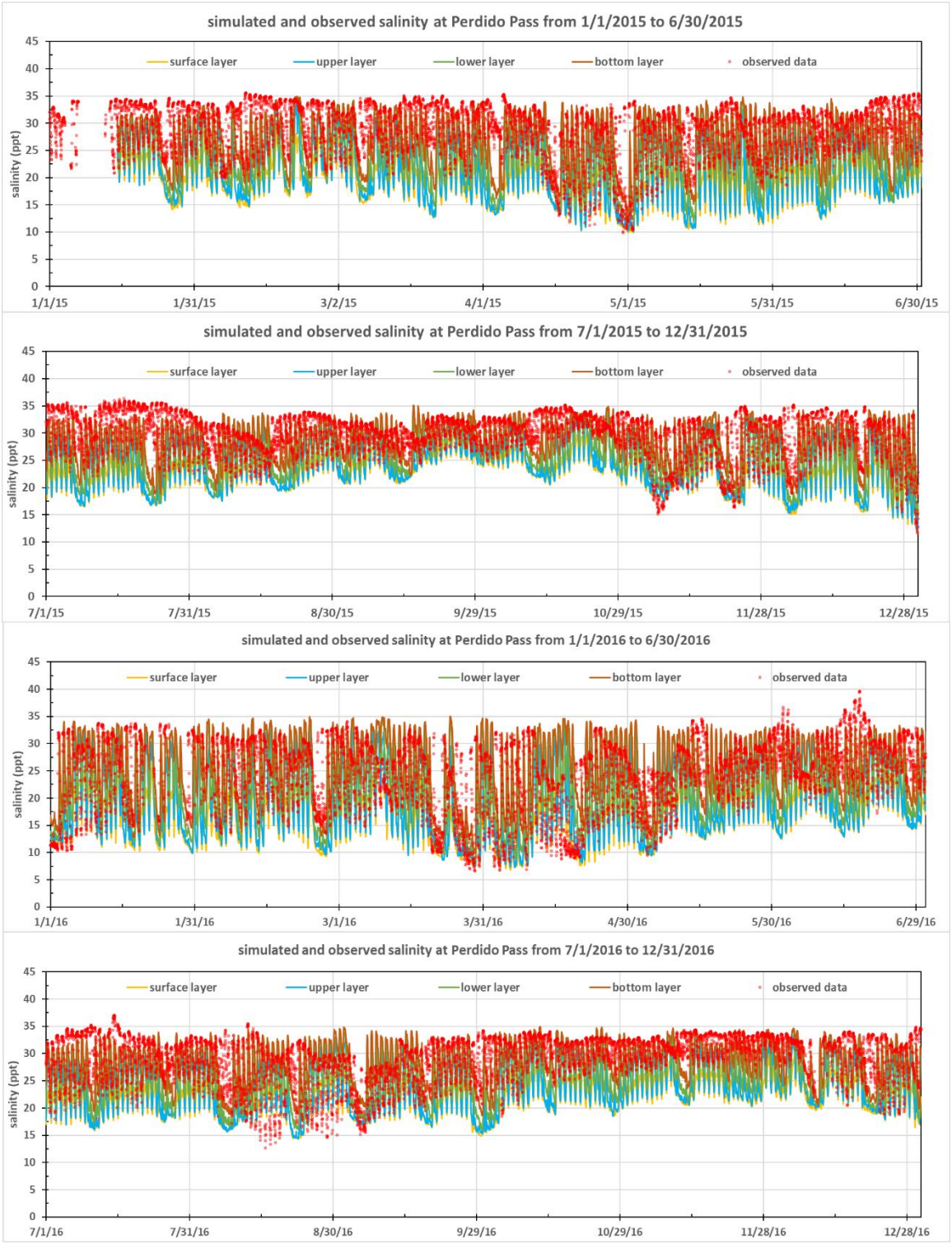

Figure 4-13 Salinity comparison among 2015–2016 simulated results at four layers and observed data at Perdido Pass in Cotton Bayou

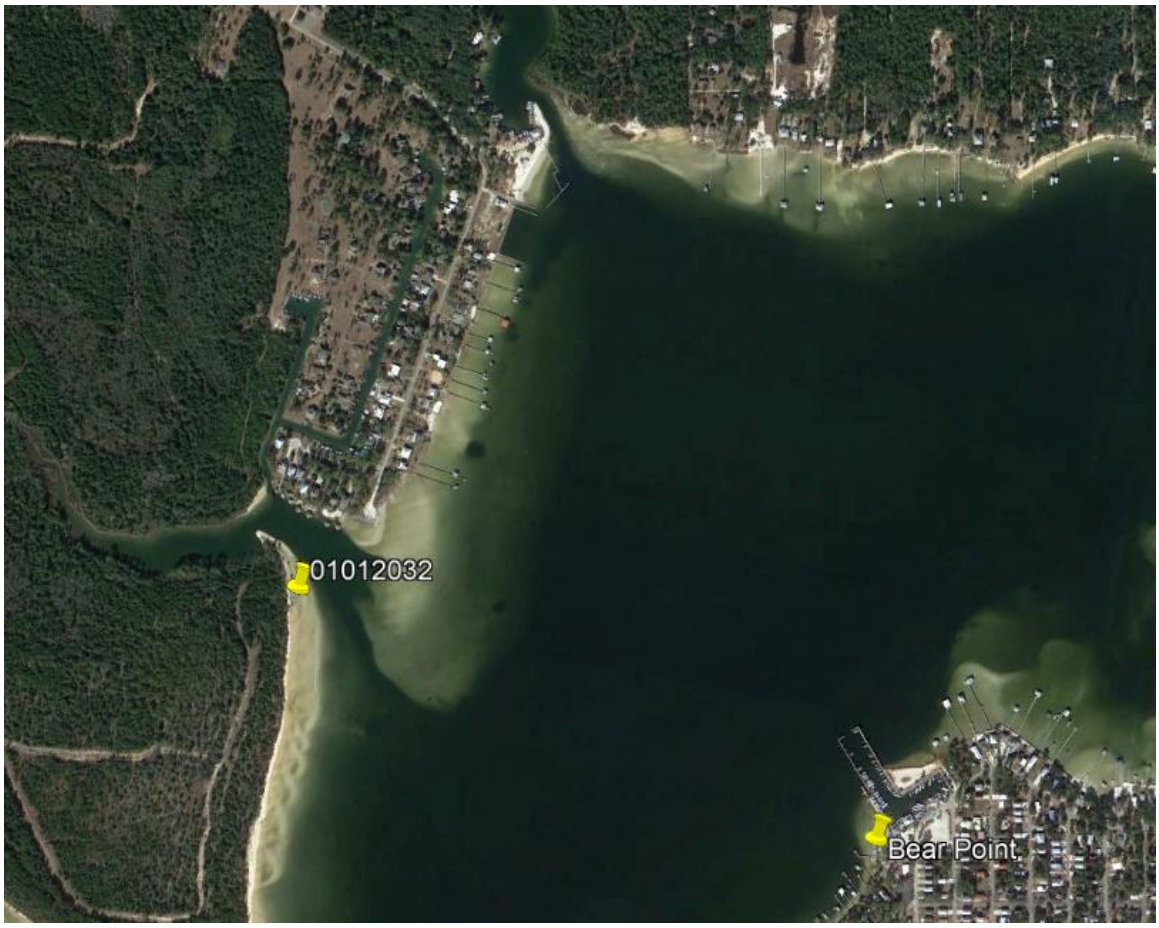

Figure 4-14 Location of station 04012032 and its surrounding landscape

4.1.3 Salinity Validation in 2017

The salinity validation in 2017 was separately listed from 2015–2016 for two reasons, 1) the water sample collection locations in 2017 were different from in 2015–2016, 2) DO was not simulated in 2017 due to the lack of necessary water quality input parameters. Therefore, the salinity validation in 2017 was listed alone as a supplement to test the model effectiveness. Figure 4-15 shows the locations of the 14 monitoring stations: stations 1–5 in Perdido Bay, 6–13 in Wolf Bay and 14 in Cotton Bayou. These 14 water-sample collection locations were designed and selected for the study funded by the OUC-AU grant and they were inside of the water body (not too close to the shoreline as the monitoring stations in 2015–2016). All these water samples were collected by Caleb Wilson and analyzed by graduate students in Dr. Alan Wilson's research lab.

Since averagely there were only 3 available observed data in 2017 at each station (associated with 3–4 field trips of data collection on March 2, May 10, July 26, and October 31), simulated salinity was extracted from all the stations and grouped together to do the statistical analysis with the observed data. Figures 4-16 to 4-19 show that the simulated salinity are generally in good agreement with the observed data with R^2 = 0.68 and *NSE* = 0.6 for the surface layer but statistical results were also derived from other three layers (Table 4-3).

Figure 4-16 plots the salinity comparison between simulated and observed values in the Wolf Bay region. By comparing the validation plots of station 1 in 2017 and station 04012020 (Figure 4-7) in 2015–2016, one can find that the simulated salinity at station 1 matched reasonably well with observed data but the station 04012020 did not. The same result also applies to the other stations. Another possible reason could be because the number of available input salinity data for the GIWW boundary in 2017 were much more than in 2015–2016 (Figure 3-28). Therefore the accuracy of the simulated salinity is closely connected to the input.

Figure 4-17 and Figure 4-18 show the salinity validation in the upper and middle Perdido Bay. For stations 6, 7, 8, and 9 in the upper Perdido Bay, salinity is strongly affected by upstream inflows. For example, in many days in June–August of 2017, simulated salinity at all four layers were the same (well mixed) and less than 1 ppt. The low salinity periods in station 9 inside the upper Perdido Bay were less than low-salinity durations for other three stations (6, 7, and 8) near the mouth of freshwater rivers. The low salinity during the high upstream flow period is also directly verified by the water sample collection on October 31, 2017. Low salinity was shown in a short period at station 10 but not in other stations in the middle Perdido Bay. They show the EFDC model can accurately simulate the salinity at stations or locations inside the water body (less accurate near the shoreline). At station 6, the large difference between the surface and the other

three layers is because the water depth was relatively deep (~5.6 m). The deeper the water depth, the more significant the vertical stratification is.

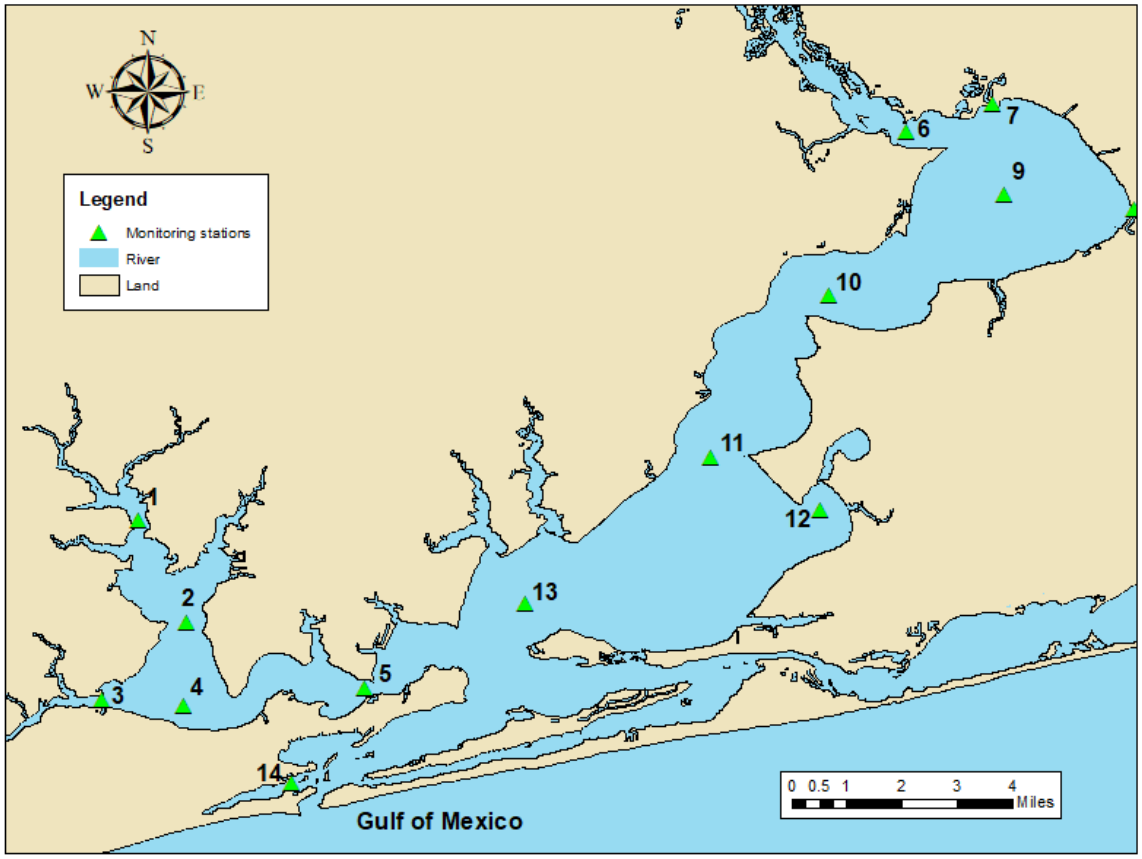

Figure 4-15 Locations of monitoring stations providing observed data for 2017

Table 4-3 Statistical results of salinity validation in 2015-2016 in different stations

	R^2	*NSE*	*RMSE*
Bottom Layer	0.74	0.66	3.81
Lower Layer	0.76	0.75	3.26
Upper Layer	0.75	0.73	3.42
Surface Layer	0.68	0.6	4.14

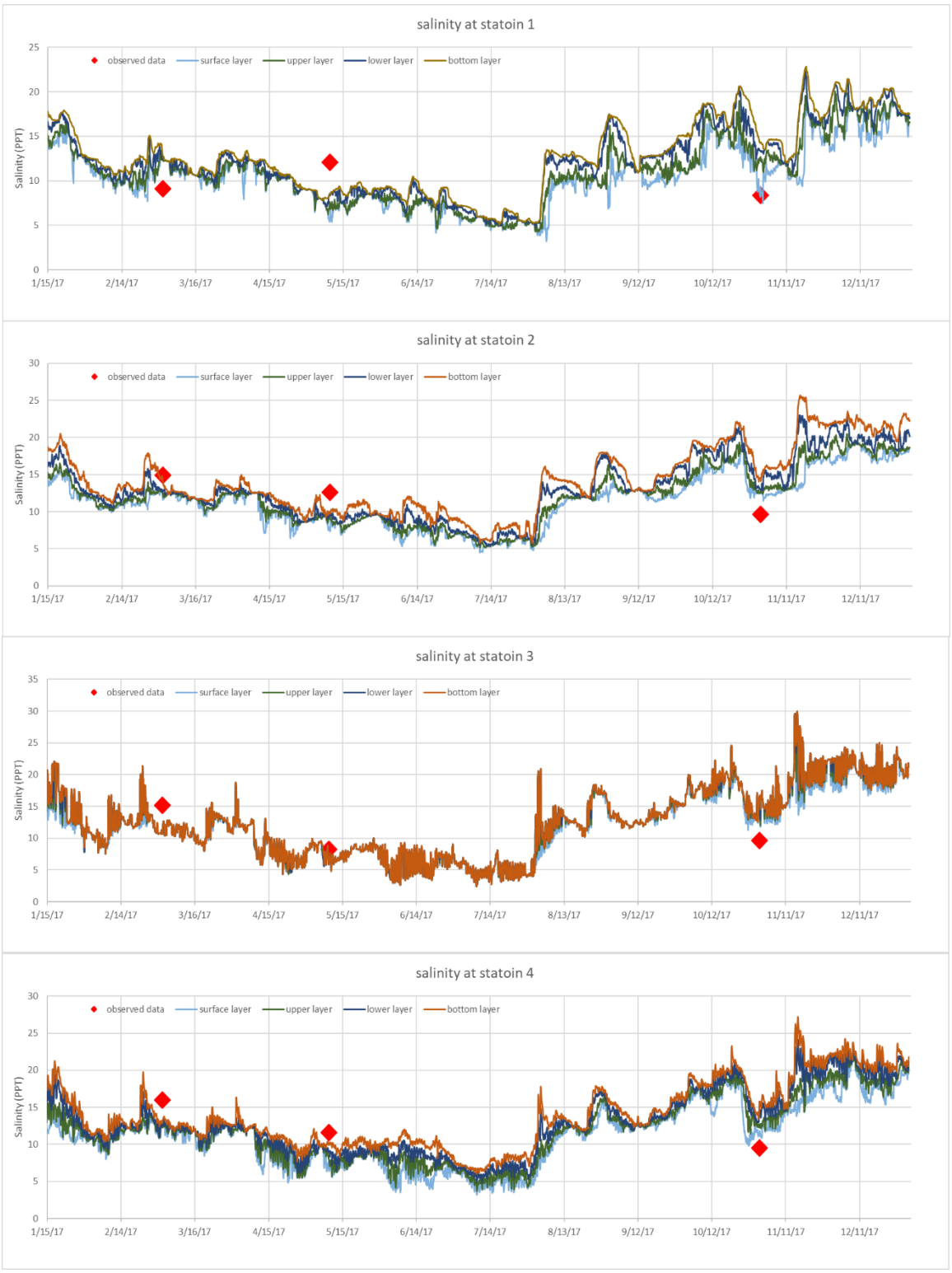

Figure 4-16 Salinity validation at stations 1, 2, 3, and 4 (Wolf Bay) in 2017

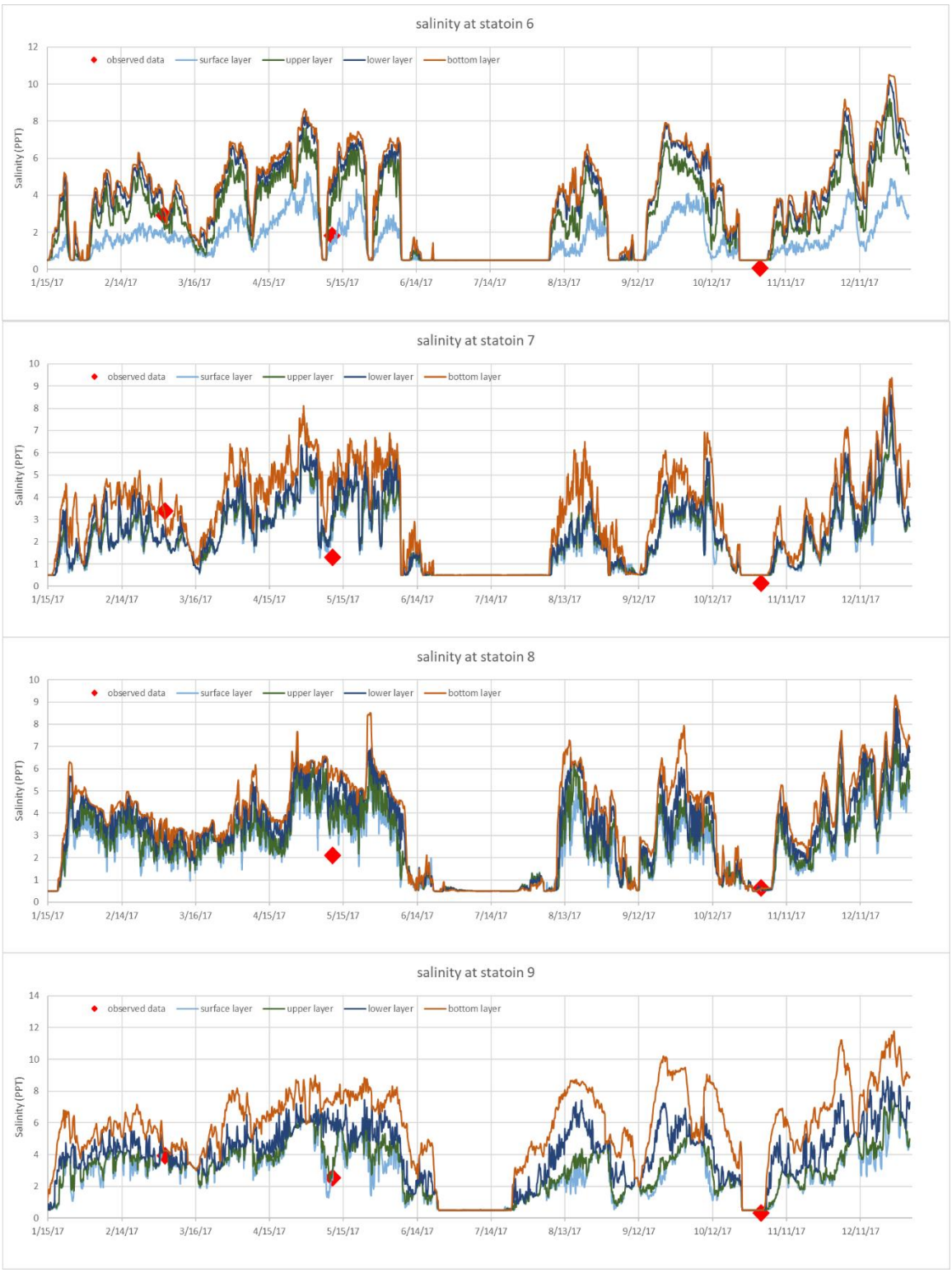

Figure 4-17 Salinity validation at stations 6, 7, 8 and 9 (the upper Perdido Bay) in 2017

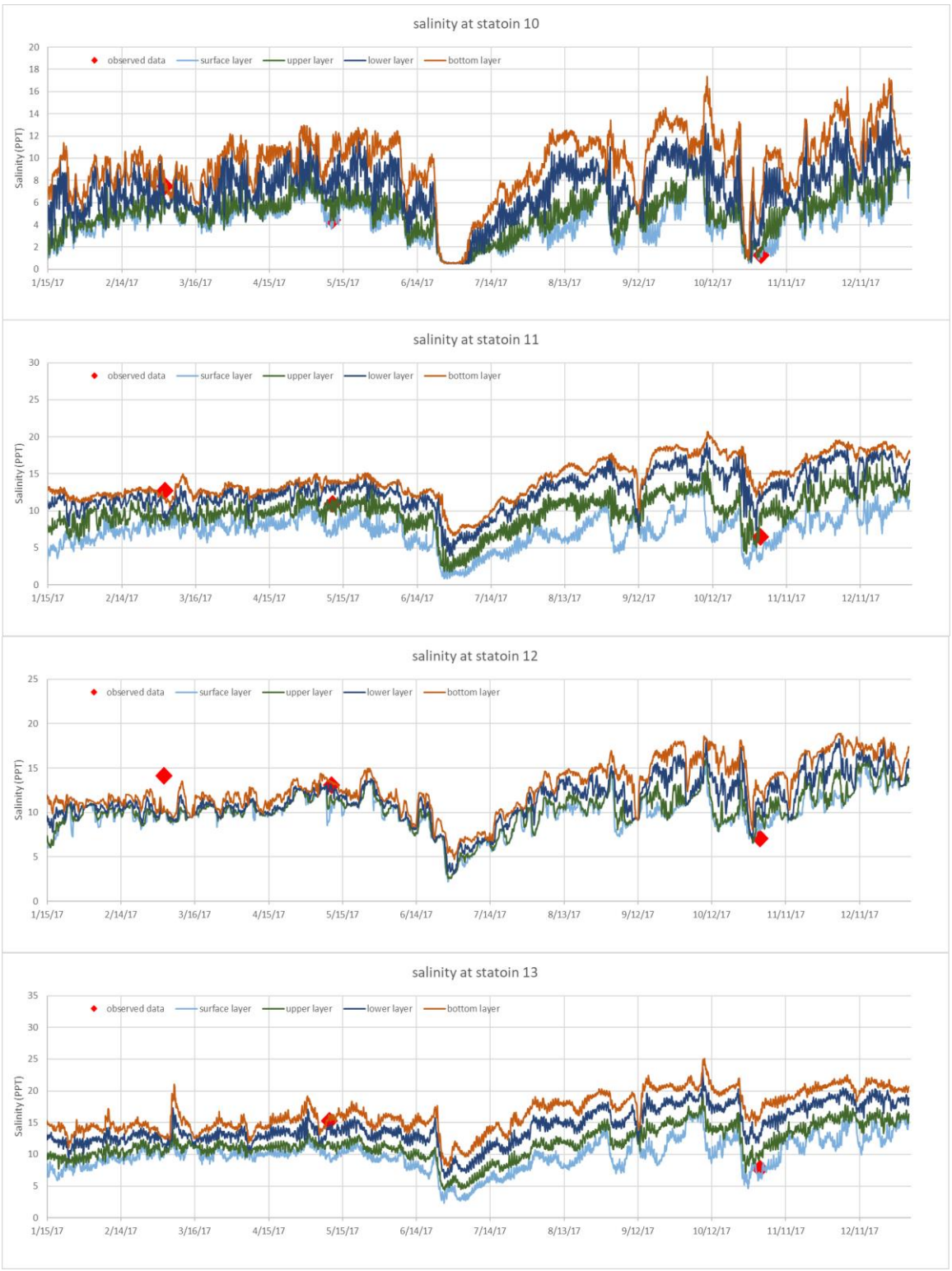

Figure 4-18 Salinity validation at stations 10, 11, 12, and 13 (the middle Perdido Bay) in 2017

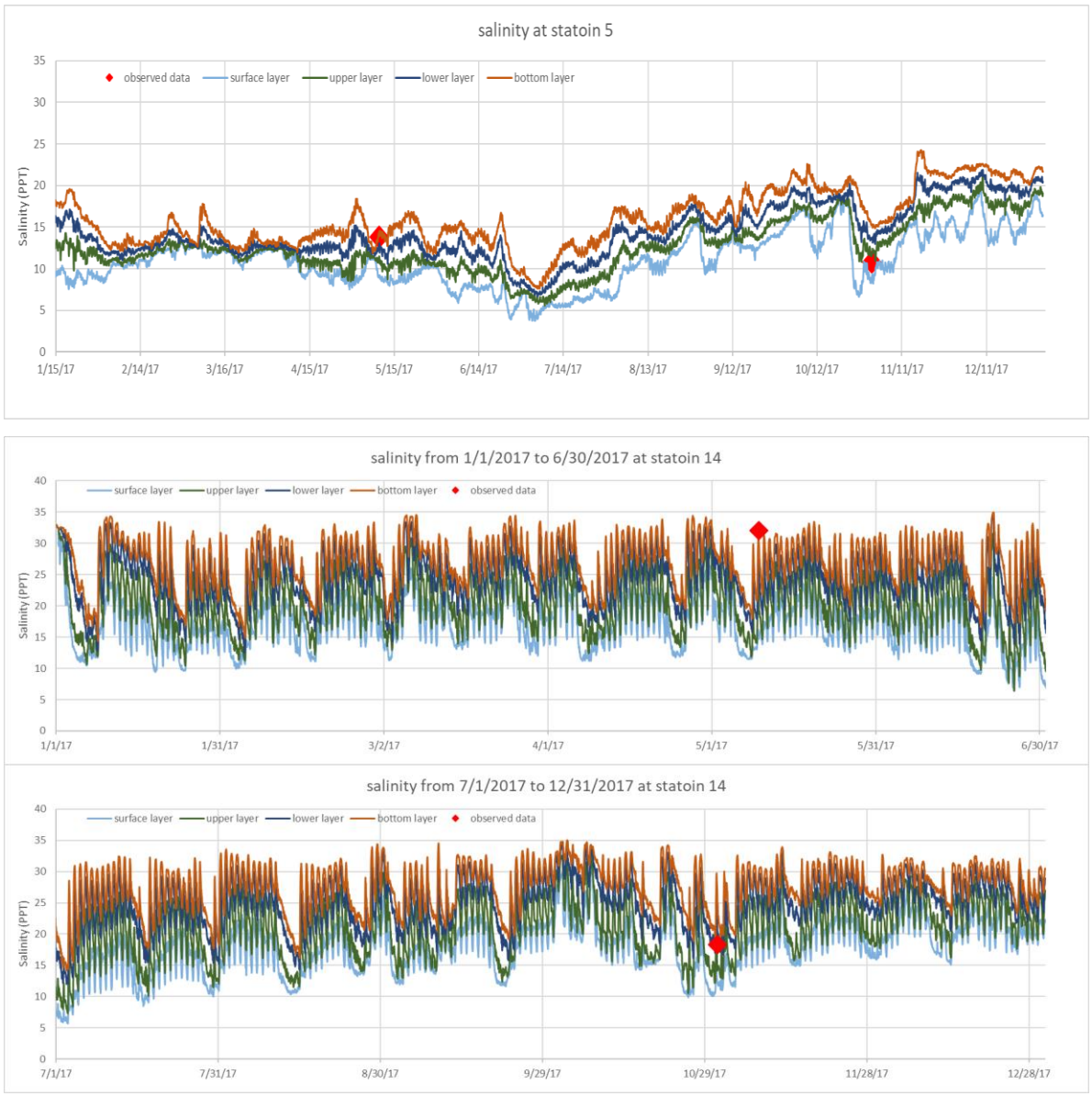

Figure 4-19 Salinity validation at stations 5 (upper panel) (Wolf Bay) and 14 (1/1/2017-6/30/2017 in the middle panel and 7/1/2017 – 12/31/2017 in the bottom panel) (Cotton Bayou) in 2017

4.1.4 Water Temperature Validation in 2015 and 2016

Water temperature is a physical property expressing how hot or cold water is. It plays a key role in the water quality modeling because it affects the water column stratification and has a direct relationship with the phytoplankton biological activity such as algal growth rates, nutrients recycle kinetics, and biological decomposition. In addition, water temperature also can influence several other parameters, such as DO concentration, salinity, water density and so on.

Comparing with salinity validation, there were only eight available stations in Table 4-1 providing observed water temperature and no data from Kee Avenue, Spanish Cove, and Bear Point stations (Figure 4-1). The statistical error parameters *NSE*, R^2, and *RMSE* were calculated between the recorded data and the simulated water temperature at the surface layer from the EFDC (Table 4-4). Figure 4-20 to Figure 4-27 show the time series plots of the simulated temperatures at four layers in 2015 (top frame) and 2016 (middle frame) with recorded data. The simulated water temperatures from the upper layer in 2015 and 2016 were compared directly in the lower frame of each figure (Figure 4-20—Figure 4-27). Water temperature is strongly correlated and linked with seasonal climate pattern, e.g., increase in spring and summer and decrease in fall and winter, but less affected by daily oceanic wave or water level variations.

Figure 4-20 and Figure 4-21 show that the simulated water temperatures matched well with the observed data for stations 04012039 and 33010G10 in the upper Perdido Bay region with $R^2 >$ 0.97 (Table 4-4). Water temperature at 04012039 (~1.6 m depth) had a certain vertical stratification but much less stratification at the station 33010G10 (~0.6 m).

In the Wolf Bay region, Figure 4-22 and Figure 4-23 show that the EFDC model can accurately simulate the water temperature at station 04012020 and 04012032. However, Figure 4-24 shows that the observed data are around 2° C lower than the observed water temperature at 04012041 and Figure 4-25 shows that there are around 1° C difference at 04012042.

Statistical error parameters in Table 4-4 show that the simulated temperatures agreed very well with observations in seven stations (R^2 > 0.92 and *NSE* > 0.77) except for the station 04012050 (R^2 = 0.52, *NSE* = -0.37, and *RMSE* = 2.85) (Figure 4-2, near a boat docking area) in the Cotton Bayou region. Visually the simulated temperatures are a little higher than the observed in 2016 while in 2015 the simulated temperatures are in good agreement with the observed data (Figure 4-26); also only ten observed temperatures were available at the station 04012050. Table 4-5 lists the observed and simulated water temperatures at the station 04012050, and there are around 5° C difference between simulated and observed temperatures on 6/17/2016 and 10/12/2016. If removed these two data points, R^2 and *NSE* increase to 0.83 and 0.54 from 0.51 and -0.37, respectively. Figure 4-27 shows that simulated temperatures matched quite well with observed temperatures at Perdido Pass, ~405 m east of the station 04012050 (Figure 4-2), with R^2 = 0.95 and *NSE* = 0.93 against 16,672 observed temperatures (Table 4-4) when simulated temperatures at the lower layer were compared with observed ones. Observed water levels and water temperatures at Perdido Pass station were collected using YSI 6600 multi-parameter sampling instrument at 0.5 m above the bottom where the water depth is 1.48 m. The *RMSE* is 1.81 ℃ that is the smallest when observed was compared with simulated at all four layers.

Figure 4-28 shows a zoomed-in time series of simulated and observed water temperatures over 10 days (8/30–9/8) in 2015 and 2016. The simulated surface water temperatures had more daily fluctuation, with the highest temperatures around noon and lowest temperatures at around 3:00 am. The differences between simulated daily maximum and minimum water temperatures ranged from 2.02 to 3.87 °C with an average of 3.14 °C in these 10 days in 2015 (Table 4-6). This is because the surface water temperatures were primarily affected by the solar radiation that varies from 0 (night) to 1300 W/m^2. The highest water temperature at the bottom layer occurred at around midnight. Figure 4-28 also clearly shows during night simulated lower-layer water temperatures were higher than simulated surface temperatures. This does not occur in freshwater aquatic systems:

in shallow streams where water temperatures are well mixed and in deep enough lakes/reservoirs where surface (epilimnion) water temperatures are larger than bottom (hypolimnion) water temperatures. This is because the density of freshwater is smaller at higher temperatures when temperatures > 4 °C. In density stratified estuary, surface water temperatures decrease quickly during the night because of no solar radiation and heat loss by evaporation at lower air temperature. Bottom water could receive heat from top layers by diffusion and heat released from bottom sediment.

Comparing with the surface water temperatures, the water temperatures at the other three layers had smaller fluctuations. The differences of simulated daily maximum and minimum water temperatures at the lower layer ranged from 0.94 to 2.03 °C with an average of 1.5 °C in these 10 days in 2015. The observed water temperatures were measured at 0.5 m above the bottom, which was located at the lower layer and had small daily fluctuations. The differences between observed daily maximum and minimum water temperatures ranged from 0.99 to 2.38 °C with an average of 1.54 °C in those 10 days (Figure 4-28) in 2015. Statistical results of differences of simulated daily maximum and minimum water temperatures are summarized in (Table 4-6) for both 2015 and 2016.

Table 4-4 Statistical results of water temperature validation in 2015-2016 in different stations

Perdido Bay	Station	04012039	33010G10		
	# of observed data	19	48		
	R^2	0.98	0.97		
	NSE	0.98	0.96		
	RMSE	0.96	1.65		
Wolf Bay	Station	04012020	04012042	04012041	04012032
	# of observed data	23	14	15	21
	R^2	0.94	0.99	0.99	0.95
	NSE	0.91	0.82	0.77	0.95
	RMSE	1.87	2.75	3.01	1.46
Cotton Bayou	Station	04012050	Perdido Pass		
	# of observed data	10	16672		
	R^2	0.51	0.95 [1]		
	NSE	-0.37	0.93 [1]		
	RMSE	2.85	1.81 [1]		

Note: [1] — these were developed between simulated at the lower layer and observed water temperatures

Table 4-5 Observed and simulated water temperature at 04012050

	Observed	Simulated
5/8/15 12:00 PM	26.5	25.2
8/16/15 10:00 AM	29.5	29.4
9/10/15 10:30 AM	28.0	30.3
10/14/15 8:30 AM	23.0	22.6
5/10/16 10:45 AM	24.0	24.3
6/17/16 3:05 PM	27.0	33.2
7/13/16 5:44 PM	29.0	29.7
8/15/16 9:57 AM	27.0	29.0
9/11/16 1:59 PM	28.0	30.3
10/12/16 2:25 PM	22.0	27.1

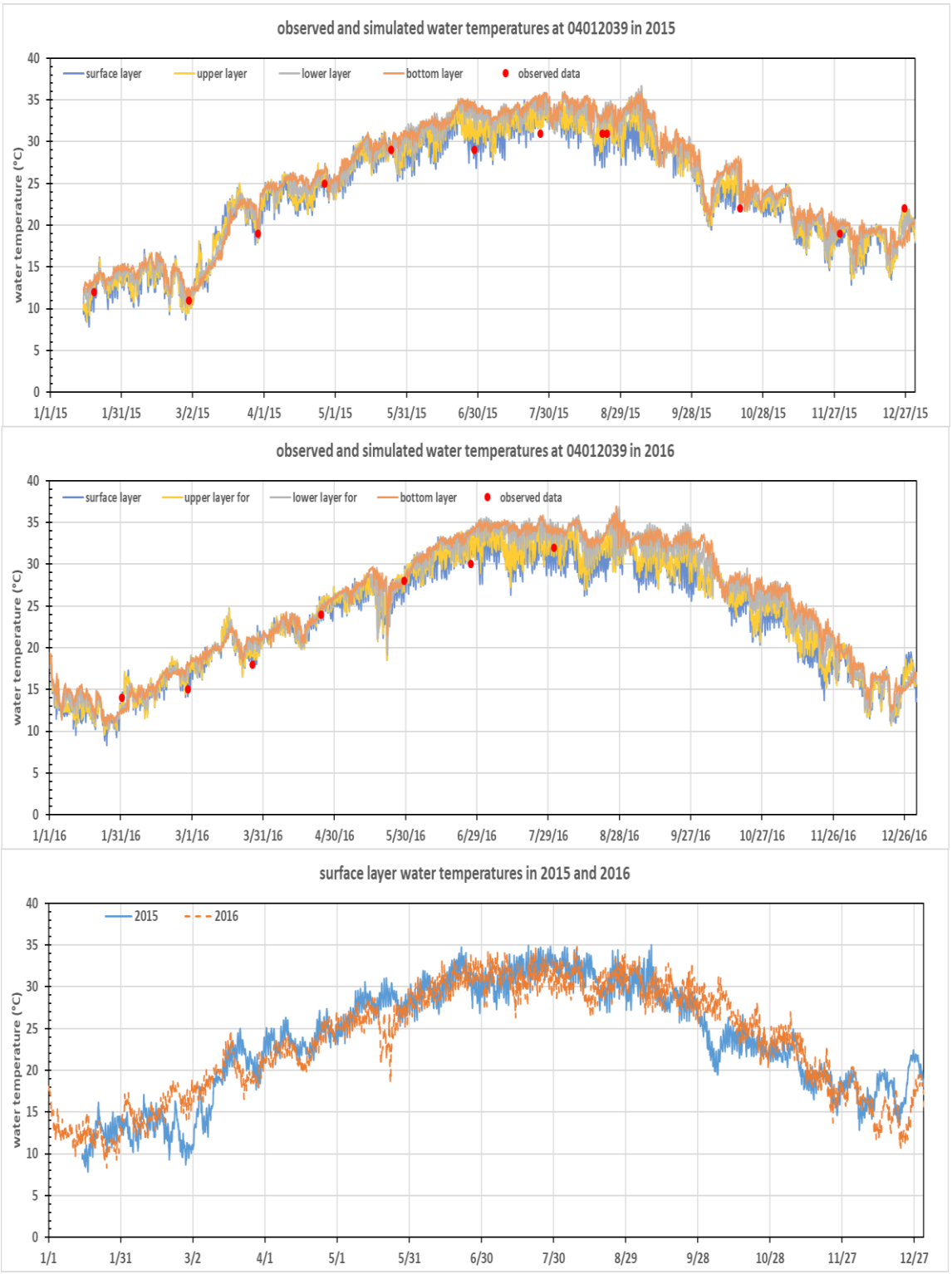

Figure 4-20 Water temperature comparison among 2015–2016 simulated results at four layers and observed data at 04012039 (Perdido Bay)

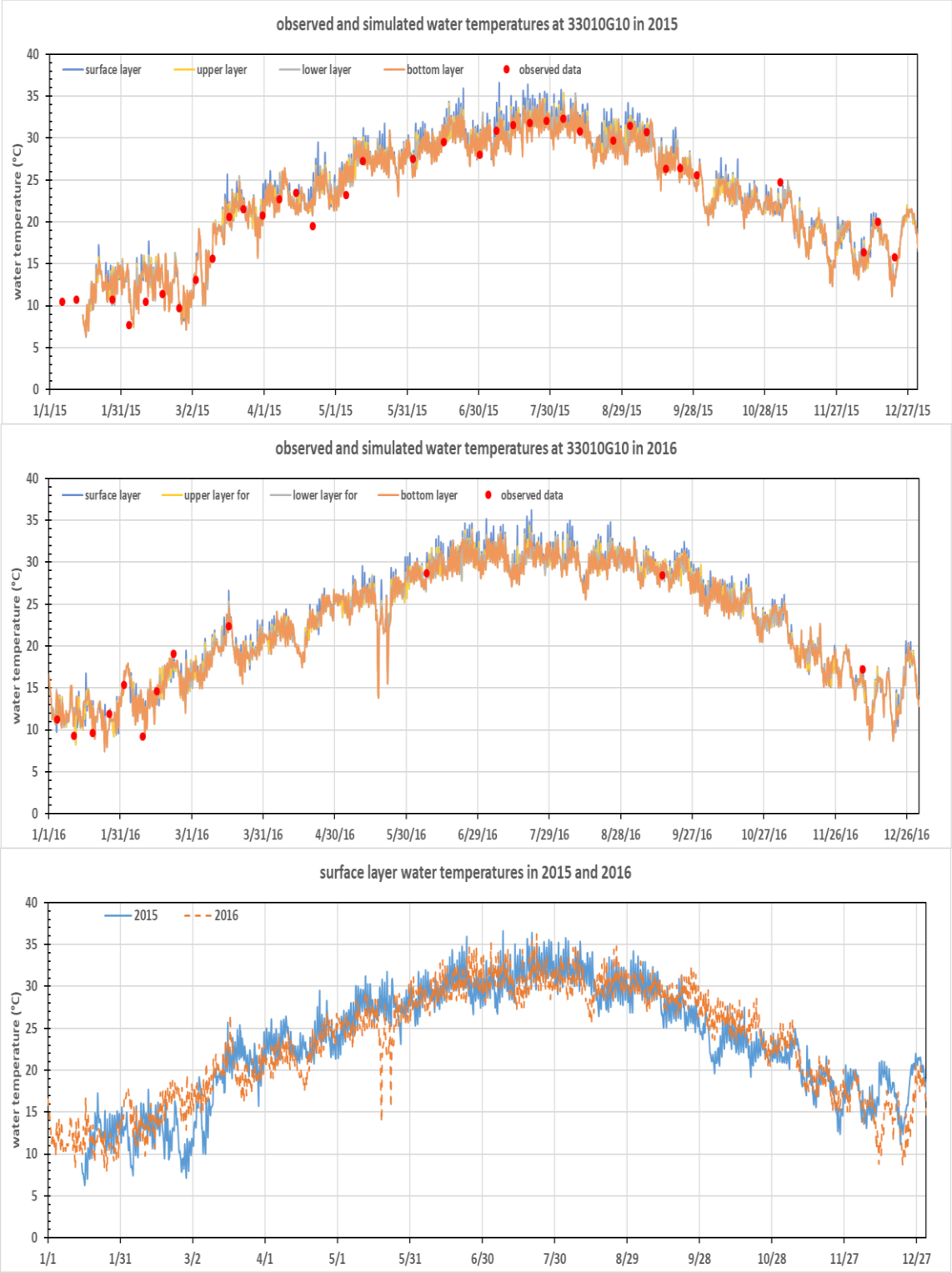

Figure 4-21 Water temperature comparison among 2015–2016 simulated results at four layers and observed data at 33010G10 (Perdido Bay)

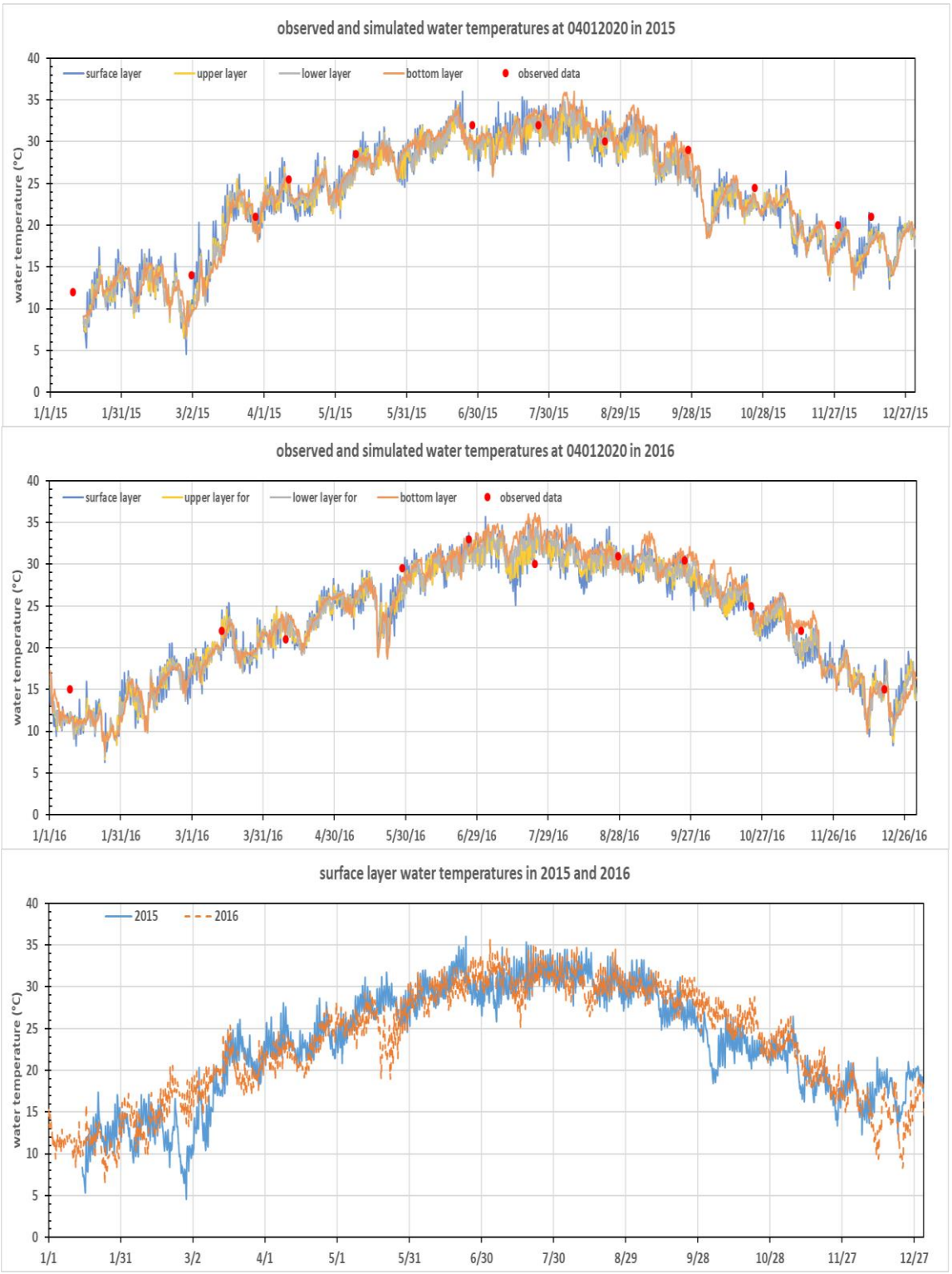

Figure 4-22 Water temperature comparison among 2015–2016 simulated results at four layers and observed data at 04012020 (Wolf Bay)

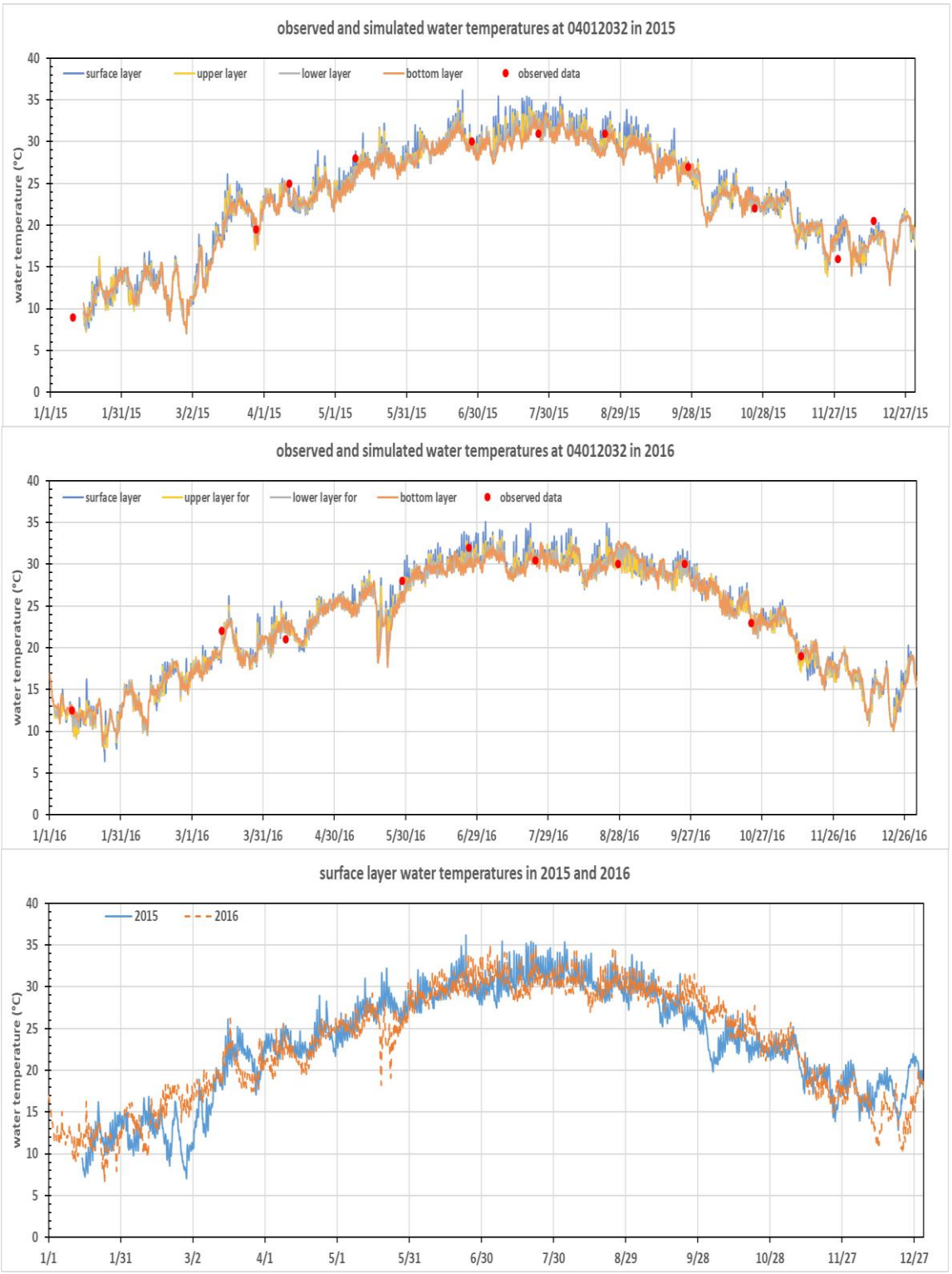

Figure 4-23 Water temperature comparison among 2015–2016 simulated results at four layers and observed data at 04012032 (Wolf Bay)

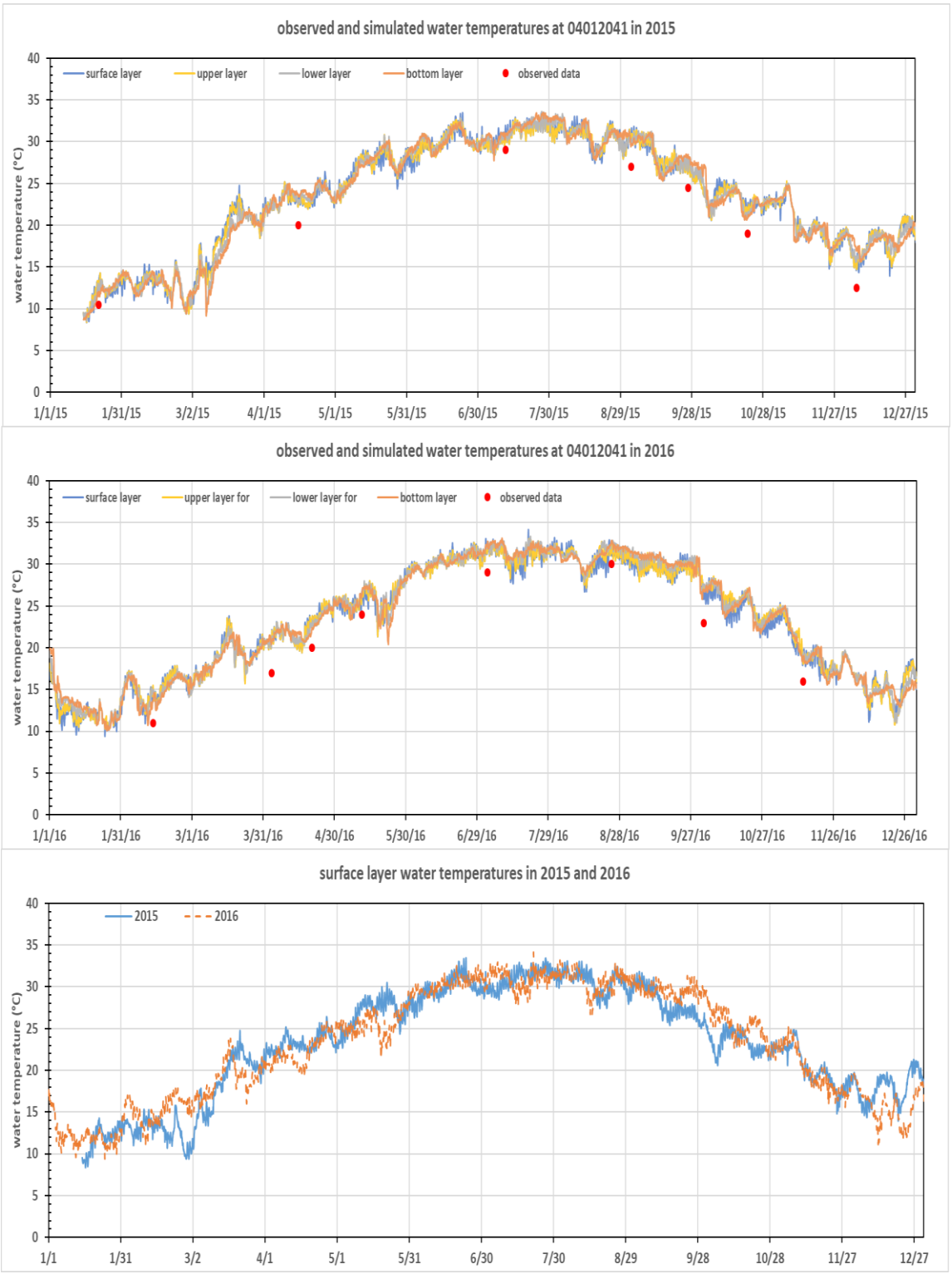

Figure 4-24 Water temperature comparison among 2015–2016 simulated results at four layers and observed data at 04012041 (Wolf Bay)

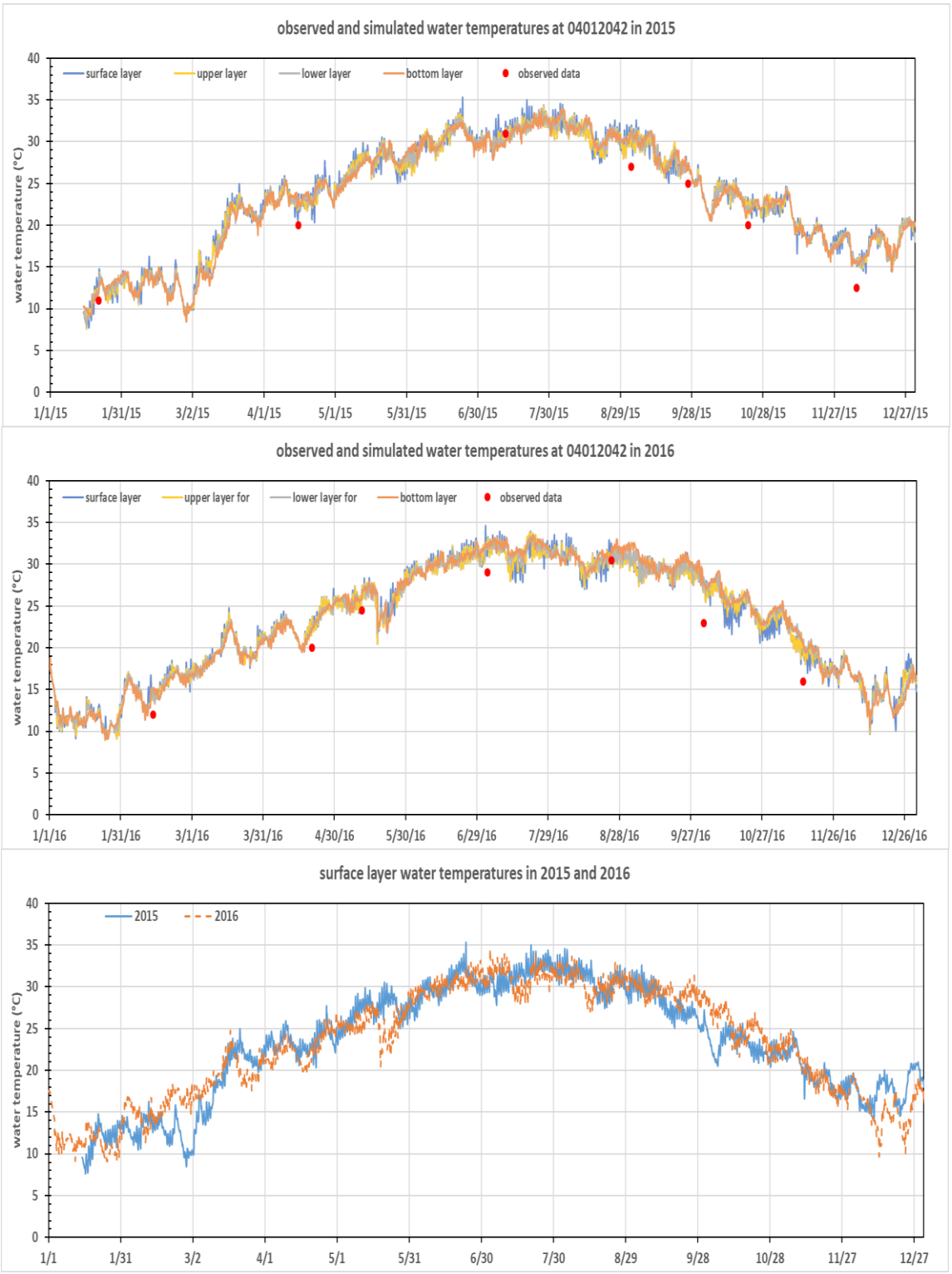

Figure 4-25 Water temperature comparison among 2015–2016 simulated results at four layers and observed data at 04012042 (Wolf Bay)

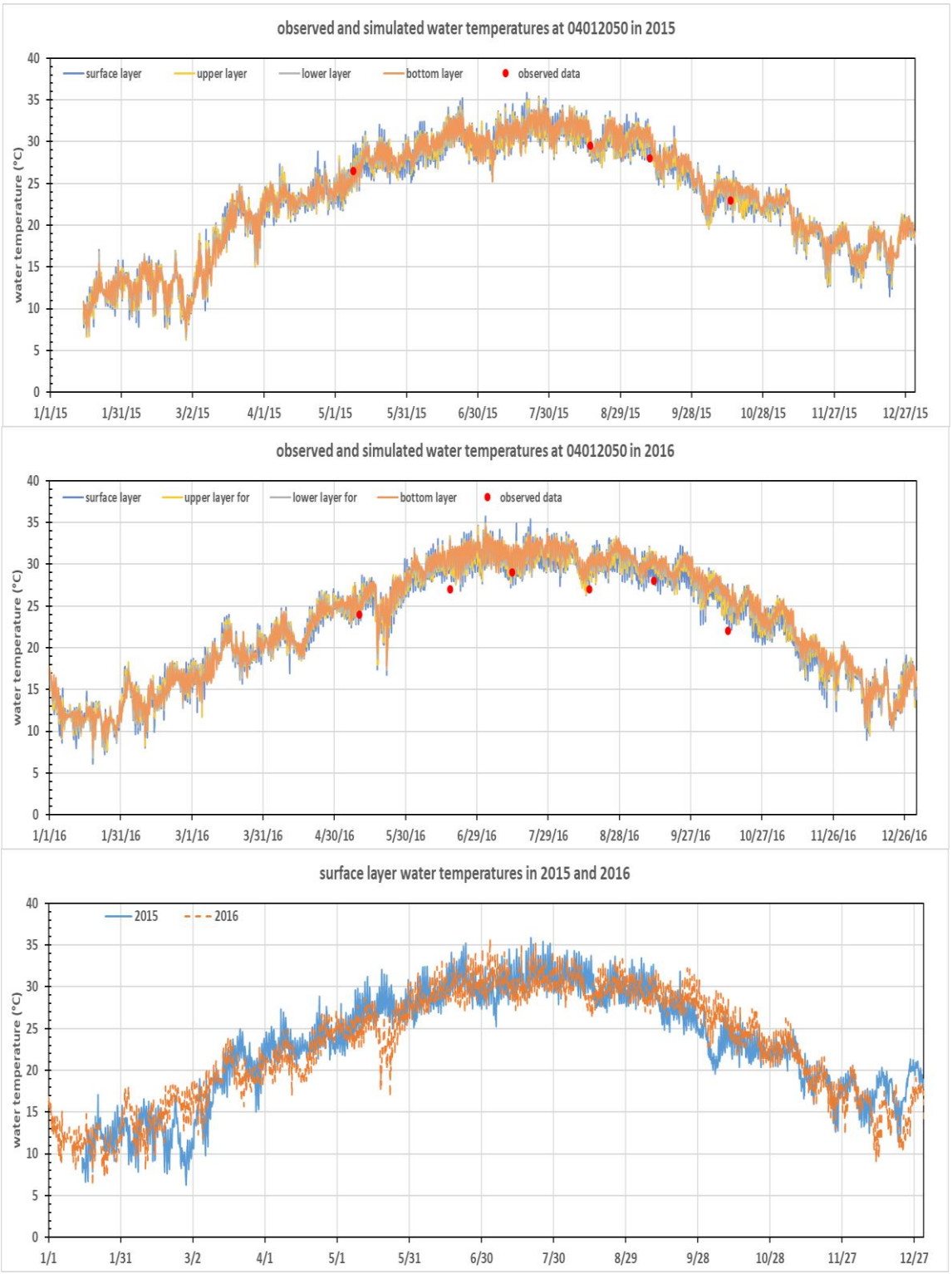

Figure 4-26 Water temperature comparison among 2015–2016 simulated results at four layers and observed data at 04012050 (Cotton Bayou)

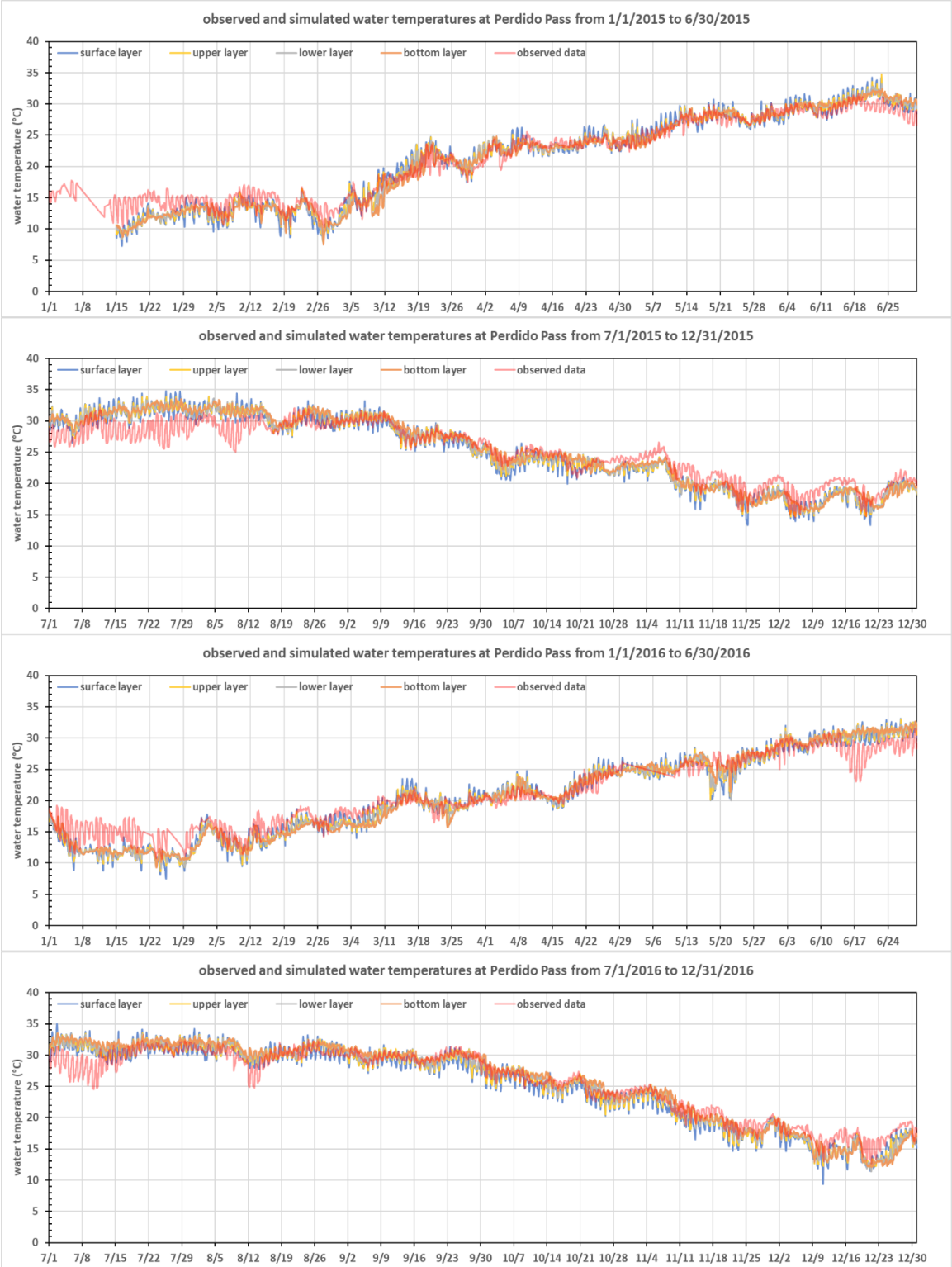

Figure 4-27 Water temperature comparison among 2015–2016 simulated results at four layers and observed data at Perdido Pass

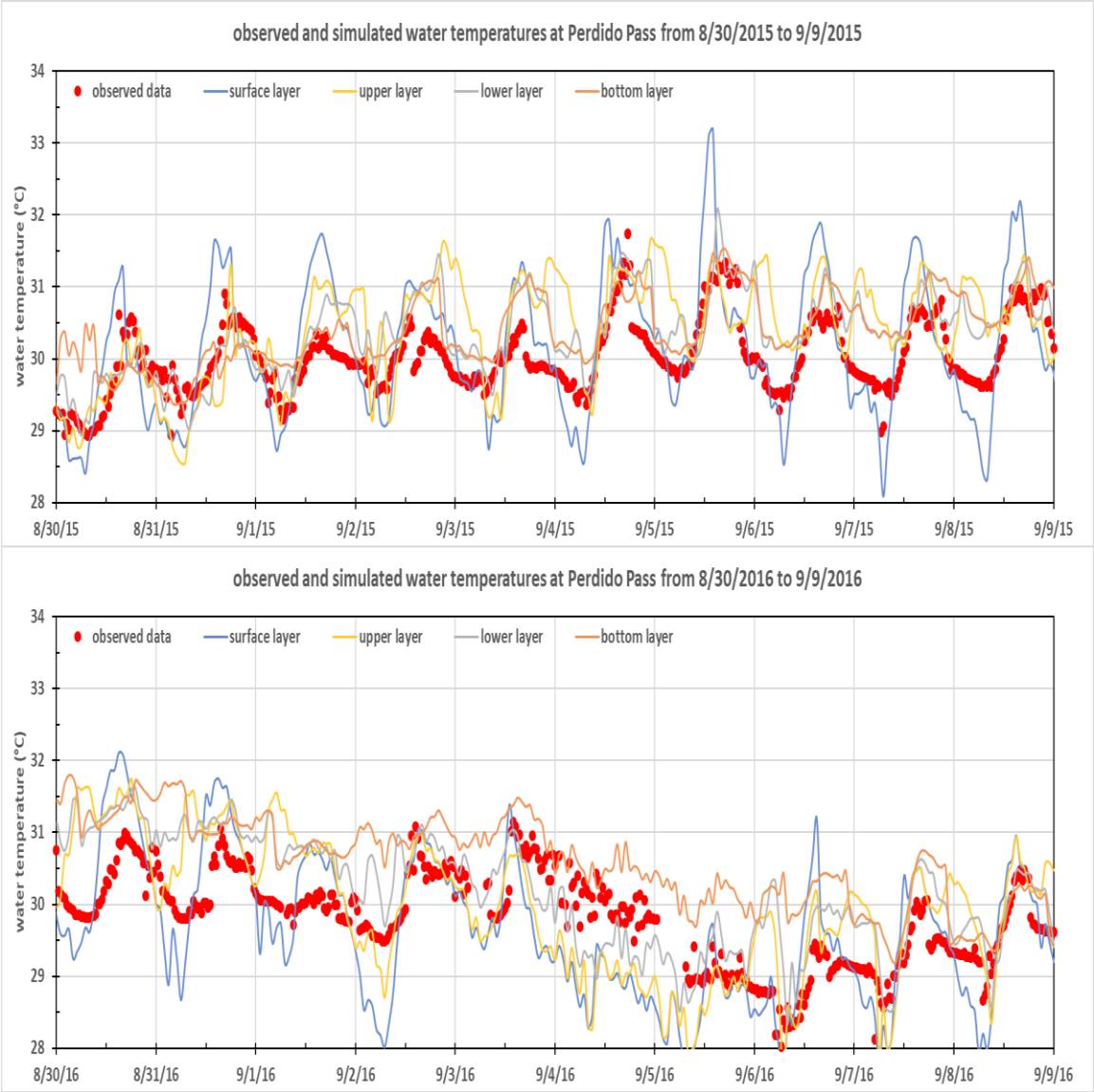

Figure 4-28 Time series of simulated and observed water temperatures on 8/30—9/9 in 2015 and 2016.

Table 4-6 The statistical results for the daily max, min, difference, and the average values for the four layers simulated water temperatures from 8/30 to 9/9 in 2015

	surface layer			upper layer		
	Daily max	Daily min	Diff.	Daily max	Daily min	Diff.
8/30/15	31.27	28.41	2.86	30.42	28.78	1.64
8/31/15	31.64	28.78	2.86	31.31	28.55	2.76
9/1/15	31.73	28.72	3.01	31.14	29.08	2.06
9/2/15	31.08	29.06	2.02	31.63	29.13	2.49
9/3/15	31.35	28.74	2.60	31.40	29.16	2.24
9/4/15	31.93	28.55	3.38	31.67	29.23	2.44
9/5/15	33.19	29.36	3.83	31.61	29.97	1.63
9/6/15	31.88	28.53	3.35	31.43	30.02	1.41
9/7/15	31.69	28.09	3.61	31.32	29.96	1.36
9/8/15	32.19	28.32	3.87	31.43	29.93	1.49
Average	31.80	28.66	3.14	31.34	29.38	1.95
	lower layer			bottom layer		
	Daily max	Daily min	Diff.	Daily max	Daily min	Diff.
8/30/15	30.21	28.93	1.28	30.48	29.57	0.91
8/31/15	30.71	29.02	1.69	30.22	29.36	0.86
9/1/15	30.89	29.48	1.42	30.55	29.89	0.66
9/2/15	31.46	29.73	1.72	31.11	29.93	1.18
9/3/15	31.19	29.50	1.69	31.16	29.96	1.21
9/4/15	31.47	29.52	1.95	31.22	29.94	1.28
9/5/15	32.07	30.03	2.03	31.52	30.07	1.46
9/6/15	31.36	30.14	1.22	31.17	30.15	1.02
9/7/15	31.24	30.29	0.94	31.19	30.28	0.90
9/8/15	31.36	30.28	1.07	31.41	30.44	0.97
Average	31.19	29.69	1.50	31.00	29.96	1.04

	observed data		
	Daily max	Daily min	Diff.
8/30/15	30.61	28.93	1.68
8/31/15	30.90	28.95	1.95
9/1/15	30.33	29.16	1.17
9/2/15	30.56	29.52	1.04
9/3/15	30.49	29.50	0.99
9/4/15	31.74	29.36	2.38
9/5/15	31.33	29.74	1.59
9/6/15	30.72	29.29	1.43
9/7/15	30.81	28.98	1.83
9/8/15	30.98	29.62	1.36
Average	30.85	29.31	1.54

4.1.5 Water Temperature Validation in 2017

Figure 4-29 — Figure 4-32 show water temperature validation in 2017 at 14 water sample collection stations for the study area. They show that the observed water temperatures matched well with the observed data. Since the depths of collected data were ranging from 0.45 to 2.13 m, they can be roughly regarded to measure in the upper layers of the water body. Table 4-7 lists the statistical results for all four layers of water temperatures versus observed data (combined all observed temperatures at all stations). For the upper layer, the statistical results (R^2 = 0.9, *NSE* = 0.83, and *RMSE* = 1.86°C) show that the simulated water temperatures are in good agreement with observed data. The time series plots show that most of the time simulated water temperatures in the surface layer are higher than ones in other lower layers; but in some short periods, e.g., at station 6, 9, and 11, simulated water temperatures at surface layer are lower than ones in the other three layers, which is impossible in freshwater lake. This is possible in estuaries because both salinity and temperature affect water density in an estuary. The interaction between the fresh-water from upstream rivers and the tide from the south developed these complex situations.

Figure 4-32 shows the time series of simulated and observed water temperatures at station 14 in the Cotton Bayou. The simulated values matched well with the observed water temperatures. Like the water temperatures at Perdido Pass, 04012050, and 04012049 in 2015 and 2016 discussed before, the simulated surface water temperatures also show larger fluctuation in 2017, which were lower than the water temperatures at the other layers, especially in spring and winter. It shows that obvious stratification occurred in 2017 since the surface water temperatures would not be lower than the bottom water temperatures in the well-mixed water body.

Table 4-7 Statistical results of water temperature validation in 2015-2016 in different stations

	R^2	*NSE*	*RMSE*
Bottom Layer	0.79	0.68	2.58
Lower Layer	0.84	0.77	2.17
Upper Layer	0.9	0.83	1.86
Surface Layer	0.92	0.85	1.64

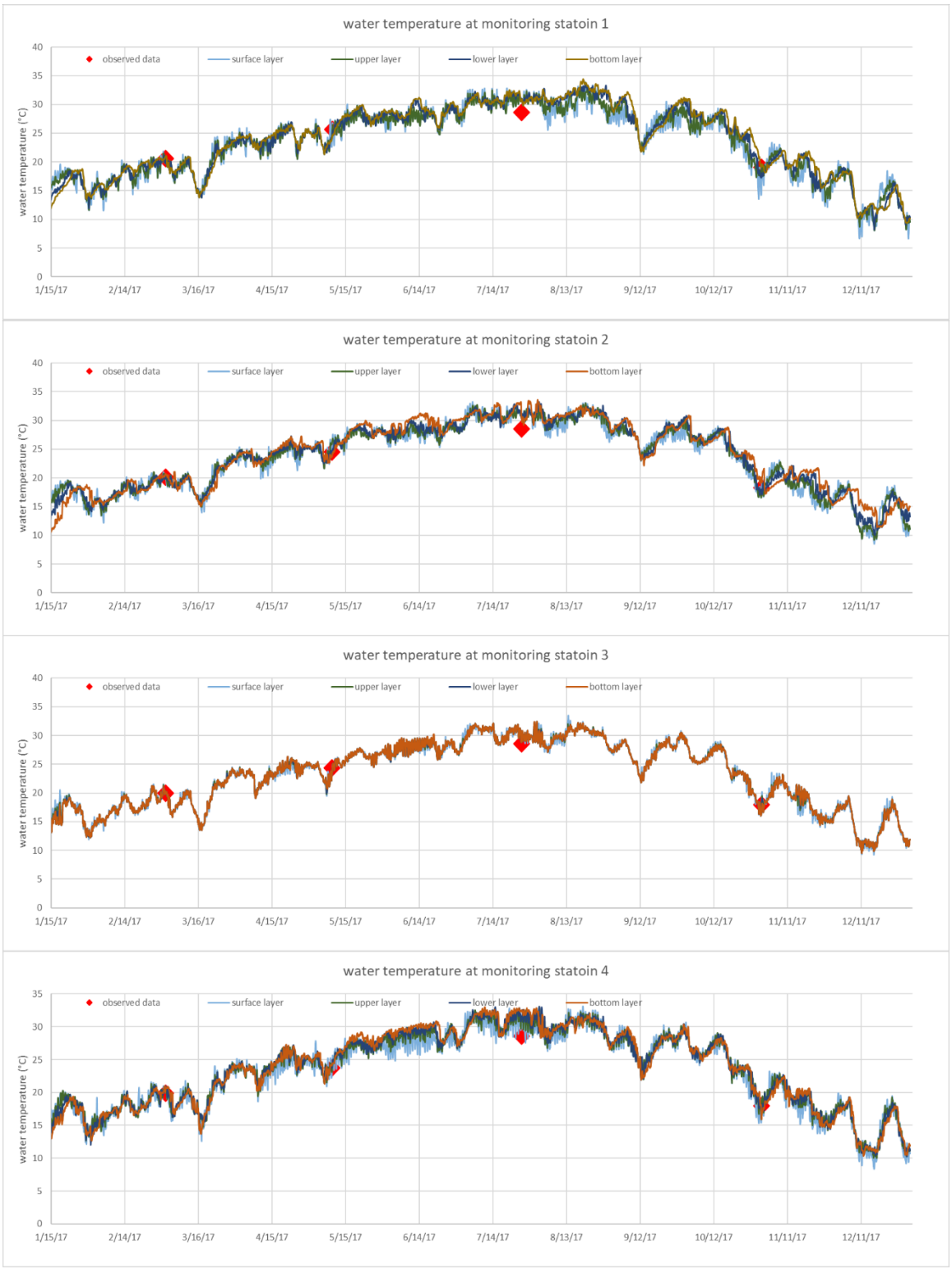

Figure 4-29 Water temperature validation at stations 1, 2, 3, and 4 (Wolf Bay) in 2017

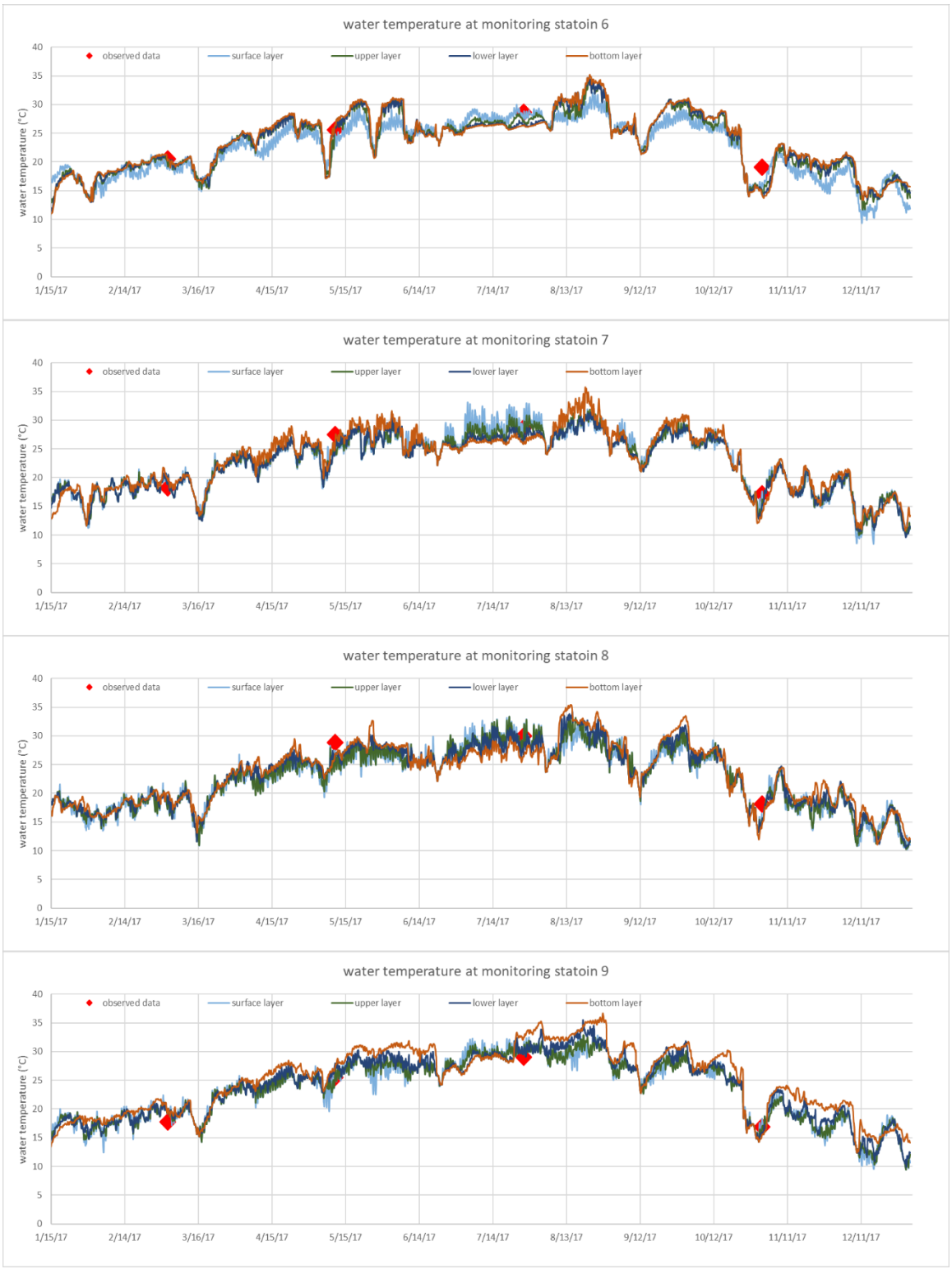

Figure 4-30 Water temperature validation at stations 6, 7, 8, and 9 (Perdido Bay) in 2017

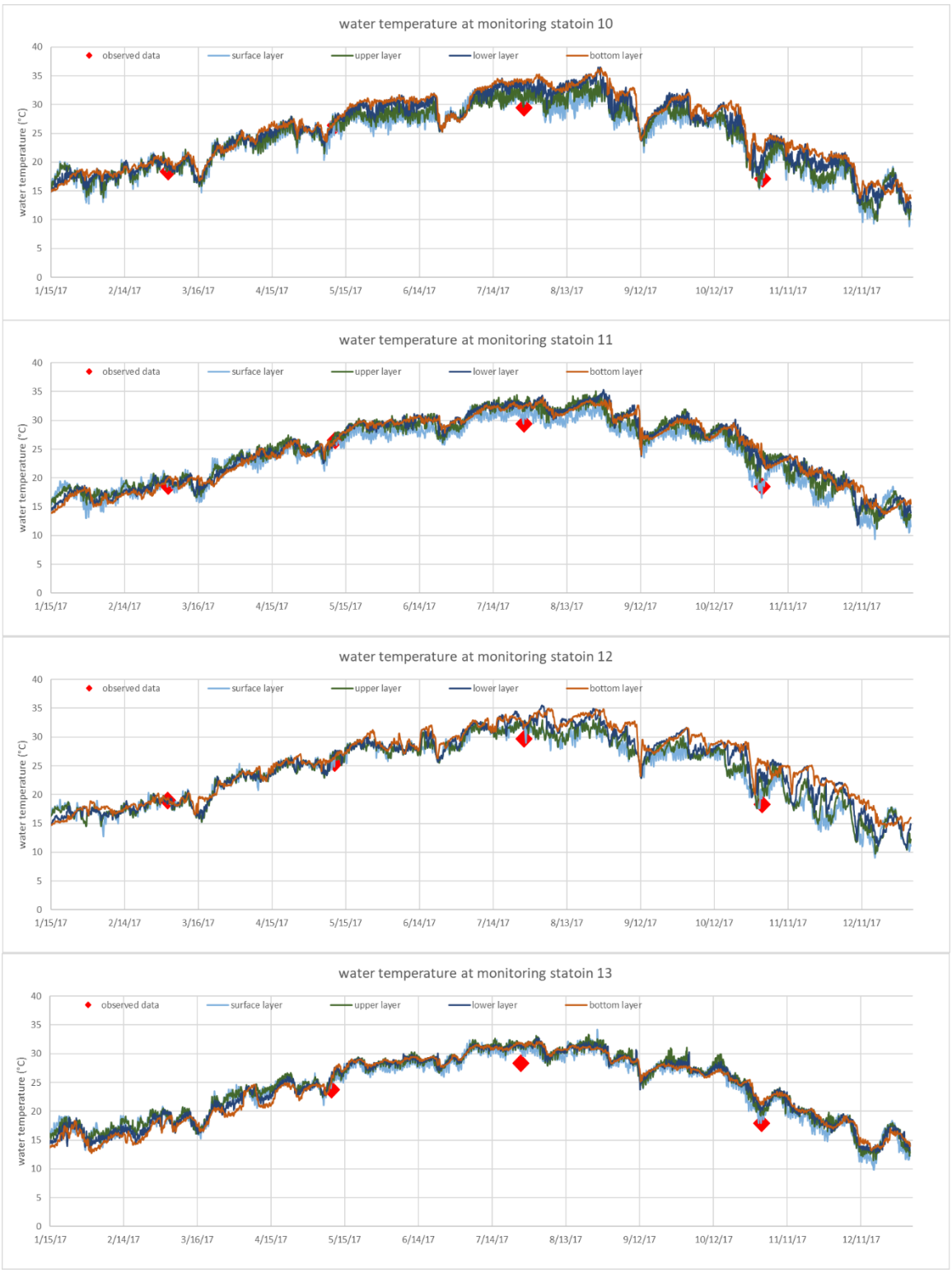

Figure 4-31 Water temperature validation at stations 10, 11, 12, and 13 (Perdido Bay) in 2017

Figure 4-32 Water temperature validation at stations 5 (upper panel) (Wolf Bay) and 14 (1/1/2017- 6/30/2017 in the middle panel and 7/1/2017 – 12/31/2017 in the bottom panel) (Cotton Bayou) in 2017

4.1.6 Dissolved Oxygen Concentration Validation in 2015-2016

Previous acceptable validations of hydrodynamic parameters (salinity and water temperature) show the current model configurations are reasonable. Therefore, based on this model,

the water quality sub-model was activated to simulate the dissolved oxygen (DO) change in 2015–2016. The DO is oxygen that is dissolved in water. In the aquatic systems, DO is often regarded as one of the most important parameters. This parameter is directly linked with the health of the aquatic ecosystem. If DO is too low to support the fish and aquatic insects, large mortalities may occur. In consideration of the fish kill in the Cotton Bayou, low DO in the summer can be supposed to be an important reason.

Figure 4-33–Figure 4-40 plot the time series of simulated DO at the surface and bottom layers versus observed data at seven stations. Comparing with the salinity and water temperature simulation, DO modeling involves more complex processes. The DO change can be regarded as a combination of the source (photosynthesis, reaeration, and external loads) and sink (respiration, nitrification, sediment oxygen demand, chemical oxygen demand, and carbon decomposition) terms, which link with algae, nitrogen, phosphorus, carbon, and other water quality variables simulated by EFDC.

For the monitoring station 04012039 located in the upper Perdido Bay (Figure 4-1), simulated surface DO are in good agreement with the observed data (Figure 4-33). The minimum DO occurred in summer when the water temperature was high and saturated DO was low, and the maximum DO occurred in winter under low water temperature. Simulated surface DO also agree reasonably well with observed DO at 04012042 in 2016 (Figure 4-35), 04012032 in 2015 and 2016 (Figure 4-37), and 04012050 (near Cotton Bayou) station in 2016 (Figure 4-39). For 04012020 station (Figure 4-44) in Wolf Bay near the freshwater streams, observed DO in both summers were much higher than simulated DO. Saturated DO concentrations were calculated based on surface temperature and salinity, and it was found that these high observed surface DO concentrations were oversaturated, which indicates possible errors of observed DO measured by the citizen volunteer. For other stations in other years, the agreement between simulated and observed DO was not good

in some days when observed DO was much lower than simulated DO. These low DO could be due to DO sink terms such as COD or larger SOD that were not accounted by EFDC input data of the current EFDC model. For Perdido Bay station 04012050 near the Cotton Bayou (Figure 4-2), observed DO in later summer in 2015 was much lower than simulated surface DO (Figure 4-39).

Figure 4-38–Figure 4-40 show the time-series plots and observed DO at 04012049, 04012050, and Perdido Pass in the Cotton Bayou (Figure 4-2). The observed DO concentrations at 04012039 and 04012050 were very similar in 2015 since their locations are very close, but they were much lower than simulated surface DO in later summer 2015 (Figure 4-38 and Figure 4-39). It could be due to the larger COD and SOD consumptions during the summer that were set to the constant in the current model. Besides, there were only four observed DO concentrations in 2015 that affected the validation results (*NSE* = -3.72 for 04012049, and *NSE* = -1.39 for 04012050). In 2016, the observed DO at 04012050 visually matched well with the simulated surface DO. However, the observed DO concentrations at 04012049 show large fluctuation comparing with ones at the station 04012050. The station 04012049 (Figure 4-2) is located in the inner part of a small channel surrounded by boating docks. The current EFDC model did not consider these docks. Figure 4-40 shows simulated DO at the lower layer and observed DO at Perdido Pass monitoring station where 1-minute observed water temperature (Figure 4-27), salinity (Figure 4-13), and DO were measured using YSI (what equipment). Many of the observed DO in the summer were higher than the simulated DO at the lower layer, whereas the simulated DO at the lower layer matched well with observed data in other periods. After calculating the saturated DO concentrations based on measured water temperature and salinity, it was found that the oversaturated (more than 100%) DO took up 21.5% of all the observed data (7088 out of 32992 DO readings). After removing the oversaturated observed DO data, the simulated DO at the lower layer agree reasonably well with the observed DO (Figure 4-41). The R^2 and *NSE* improved from 0.53 and 0.27 to 0.63 and 0.51 in 2015, and from 0.53 and 0.37 to 0.63 and 0.47 in 2016, respectively (Table 4-9).

Certain DO stratification between the surface and the bottom layer was simulated by EFDC model. The DO at different depths often had a large difference. The DO at the surface layer should have the smaller fluctuations (Table 4-10) because surface reaeration can add oxygen from the atmosphere into water or release oxygen from water into the atmosphere where it is saturated (e.g., oxygen over-production by photosynthesis). Figure 4-42 shows simulated daily maximum and minimum DO concentrations in the surface layer at station 04012039 in 2015 and 2016 as an example to show small surface DO daily variations. Table 4-10 summarizes statistical results (maximum, minimum, average, and standard deviation) for daily minimum surface DO and difference of daily maximum and minimum surface DO in 2015–2016 in seven stations with observed DO in the study area. Average of daily minimum surface DO concentrations ranged from 6.37 to 7.06 mg/L with standard deviations of 1.35–1.42 mg/L. Average difference of daily maximum and minimum surface DO concentrations ranged from 0.68 to 1.19 mg/L with standard deviations of 0.33–0.71 mg/L. The maximum difference of daily maximum and minimum simulated surface DO concentrations was 4.74 mg/L at the station 04012049 (near Cotton Bayou). In the open estuary, surface waves often create turbulence and DO at the surface layer is usually near ~80% saturation. DO in lower layers had relatively large fluctuations (e.g., Figure 4-34 for station 04012020). Sometimes bottom DO increased rapidly and became close to surface DO; which is believed due to short-period strong wind/tidal mixing. After the mixing, bottom DO often started to decrease, which is because SOD and other chemical oxygen demand would directly consume DO at lower layers. DO from the photosynthesis process would decrease due to lack of sufficient sunlight. The wind/tidal mixing can pass/diffuse the DO at the surface layer to the lower layers.

Table 4-8 Statistical results for DO validation at surface layer in 2015–2016 in six stations

Year	2015				2016			
Station	Obs [1]	R^2	NSE	RMSE	Obs [1]	R^2	NSE	RMSE
04012020	12	0.04	-3.89	3.04	11	0.00	-1.38	2.35
04012042	7	0.51	-0.18	2.57	7	0.51	0.10	1.66
04012041	7	0.03	-4.10	3.30	8	0.43	-0.20	2.12
04012032	**11**	**0.83**	**0.81**	**0.53**	10	0.51	-0.08	1.24
04012039	**12**	**0.92**	**0.68**	**0.91**	7	0.95	0.49	1.19
04012049	4	0.73	-3.72	2.23	6	0.00	-0.72	1.97
04012050	4	0.76	-1.39	1.91	6	0.17	-0.19	0.71

Note: Obs [1] — it represents the number of observed DO

Table 4-9 Statistical results for simulated DO at four layers compared with observed DO in 2015–2016 at Perdido Pass stations

Year	2015			2016		
Parameters	R^2	NSE	RMSE	R^2	NSE	RMSE
Surface	0.59(0.72)[1]	0.47(0.5)	0.86(0.82)	0.57(0.66)	0.40(0.38)	1.01(0.92)
Upper	0.51(0.61)	0.37(0.52)	0.94(0.80)	0.51(0.59)	0.40(0.45)	1.02(0.86)
Lower	0.53(0.63)	0.27(0.51)	1.01(0.82)	0.53(0.63)	0.37(0.47)	1.04(0.84)
Bottom	0.60(0.70)	-0.44(-0.08)	1.42(1.20)	0.58(0.67)	-0.17(-0.15)	1.42(1.25)

Note: [1] – Numbers inside brackets were developed after removing observed data that were more than 100% saturation.

Table 4-10 Statistical results for minimum surface DO and difference of maximum and minimum surface DO in 2015–2016 in seven stations

Year	Minimum DO				Difference			
Station	Max	Mini	Average	STD	Max	Mini	Average	STD
04012020	10.05	3.11	6.54	1.76	2.54	0.12	0.91	0.50
04012042	9.90	3.56	7.06	1.41	2.66	0.12	0.68	0.37
04012041	9.86	4.48	7.04	1.14	2.06	0.13	0.78	0.33
04012032	10.31	1.80	6.37	1.82	3.88	0.11	1.12	0.64
04012039	10.18	3.00	6.75	1.74	3.39	0.22	1.14	0.53
04012049	9.90	1.57	6.48	1.43	4.73	0.18	1.19	0.71
04012050	9.58	3.22	6.72	1.35	2.75	0.19	0.92	0.42

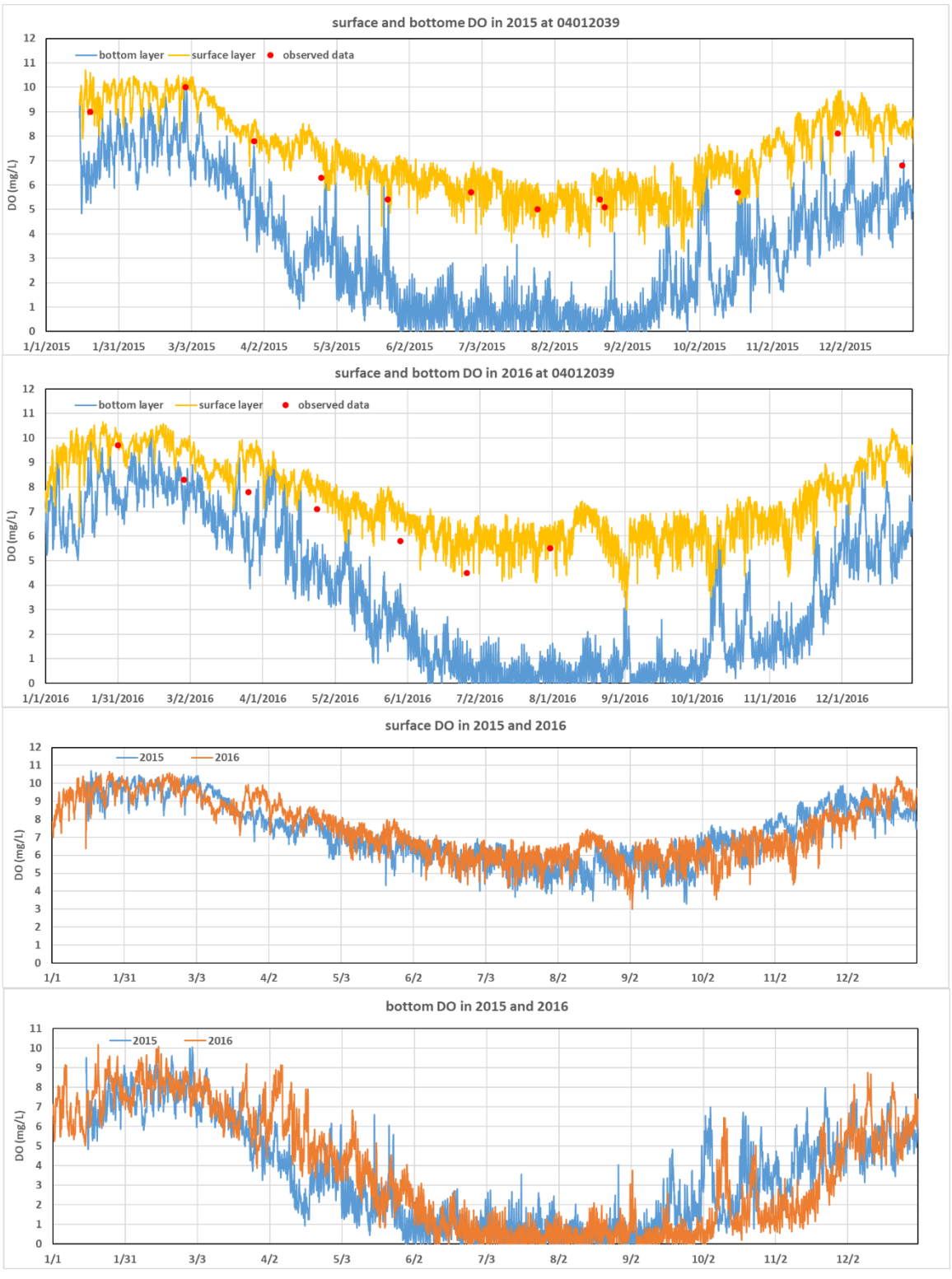

Figure 4-33 Simulated DO at surface and bottom layers versus observed DO at 04012039 station (Perdido Bay).

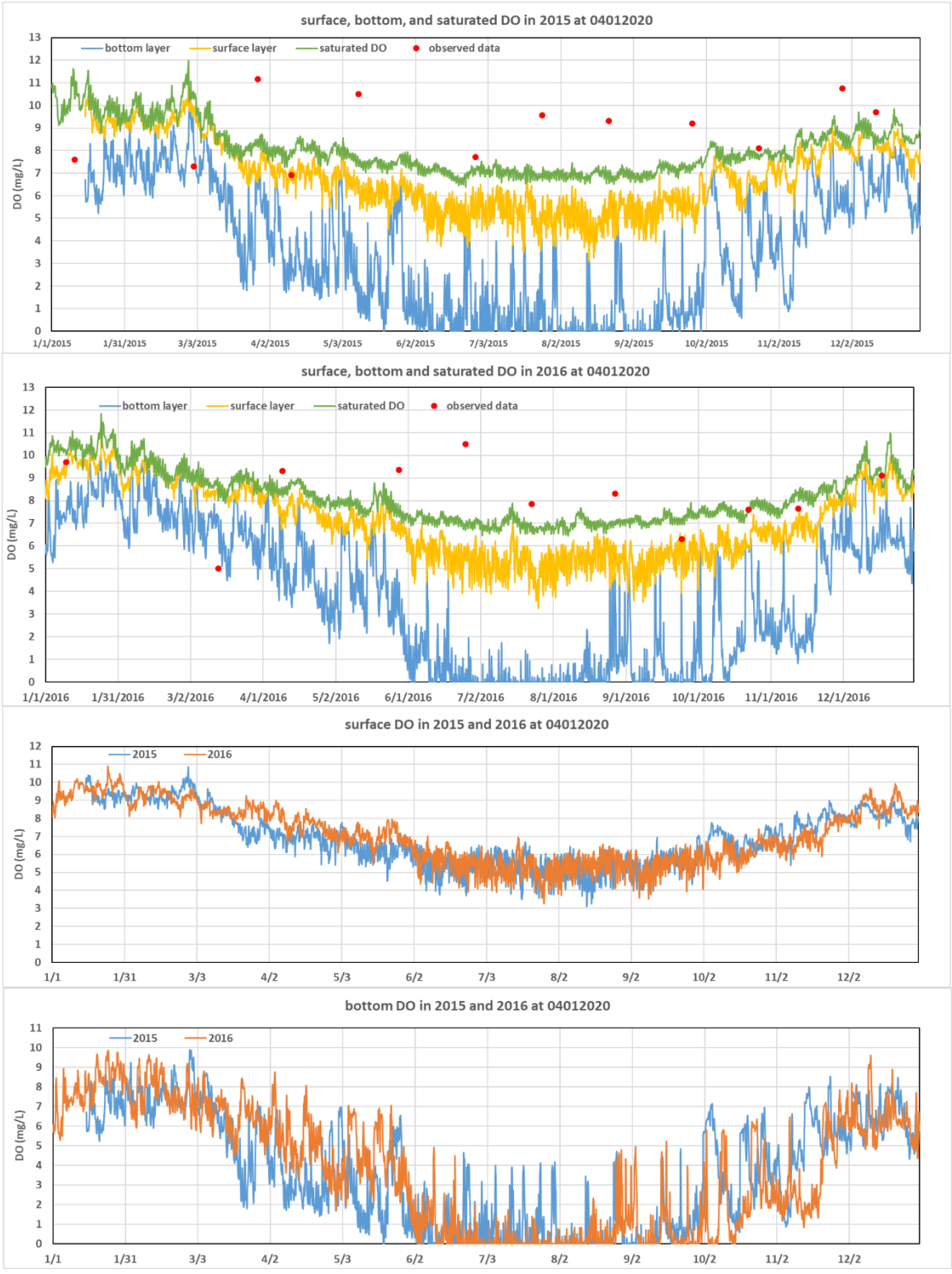

Figure 4-34 Simulated DO concentrations at the surface and bottom layers, saturated DO calculated for the surface layer, and observed DO at 04012032 station (Wolf Bay).

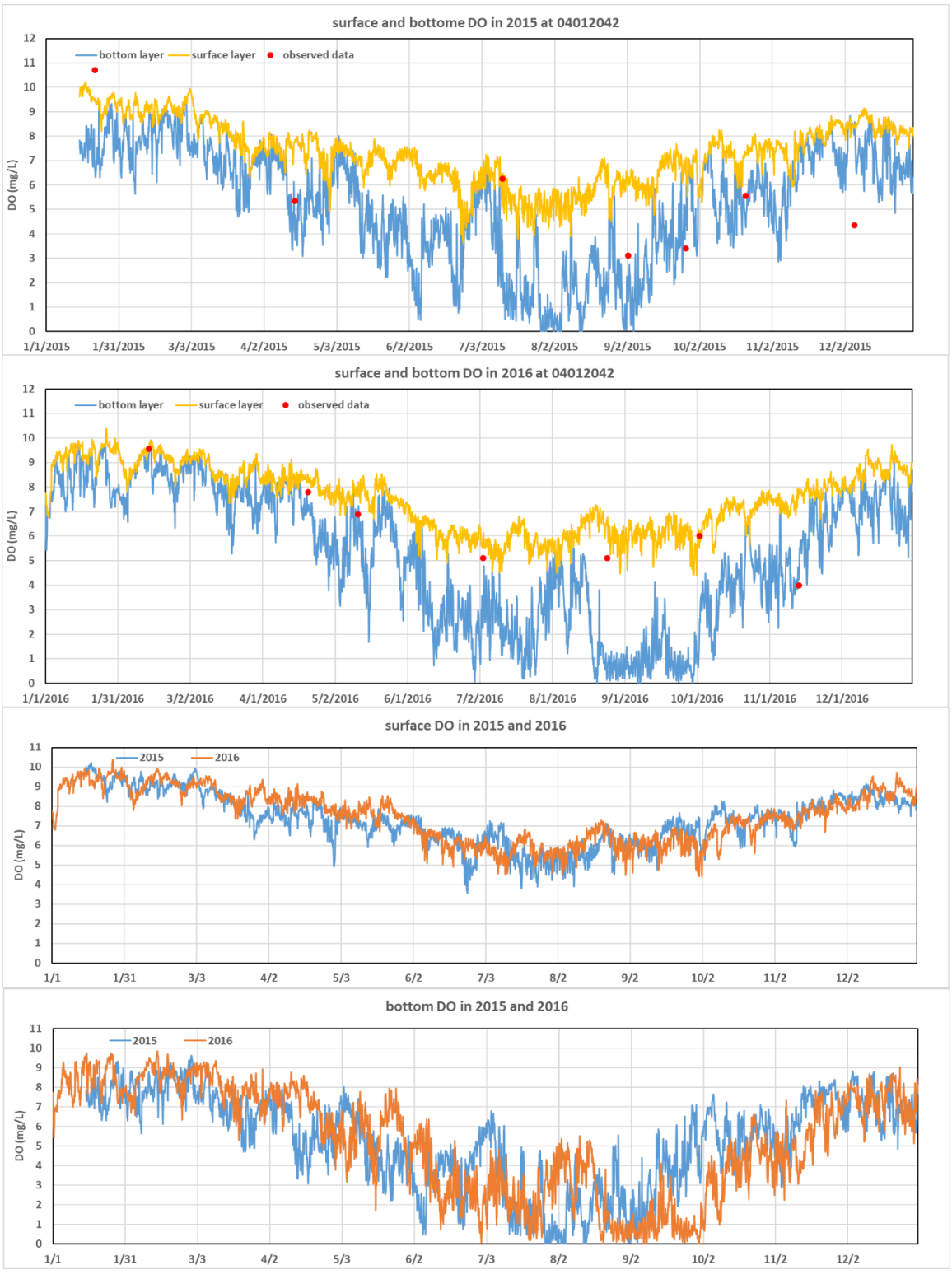

Figure 4-35 DO at the surface and bottom layers versus observed DO at 04012042 station (Wolf Bay).

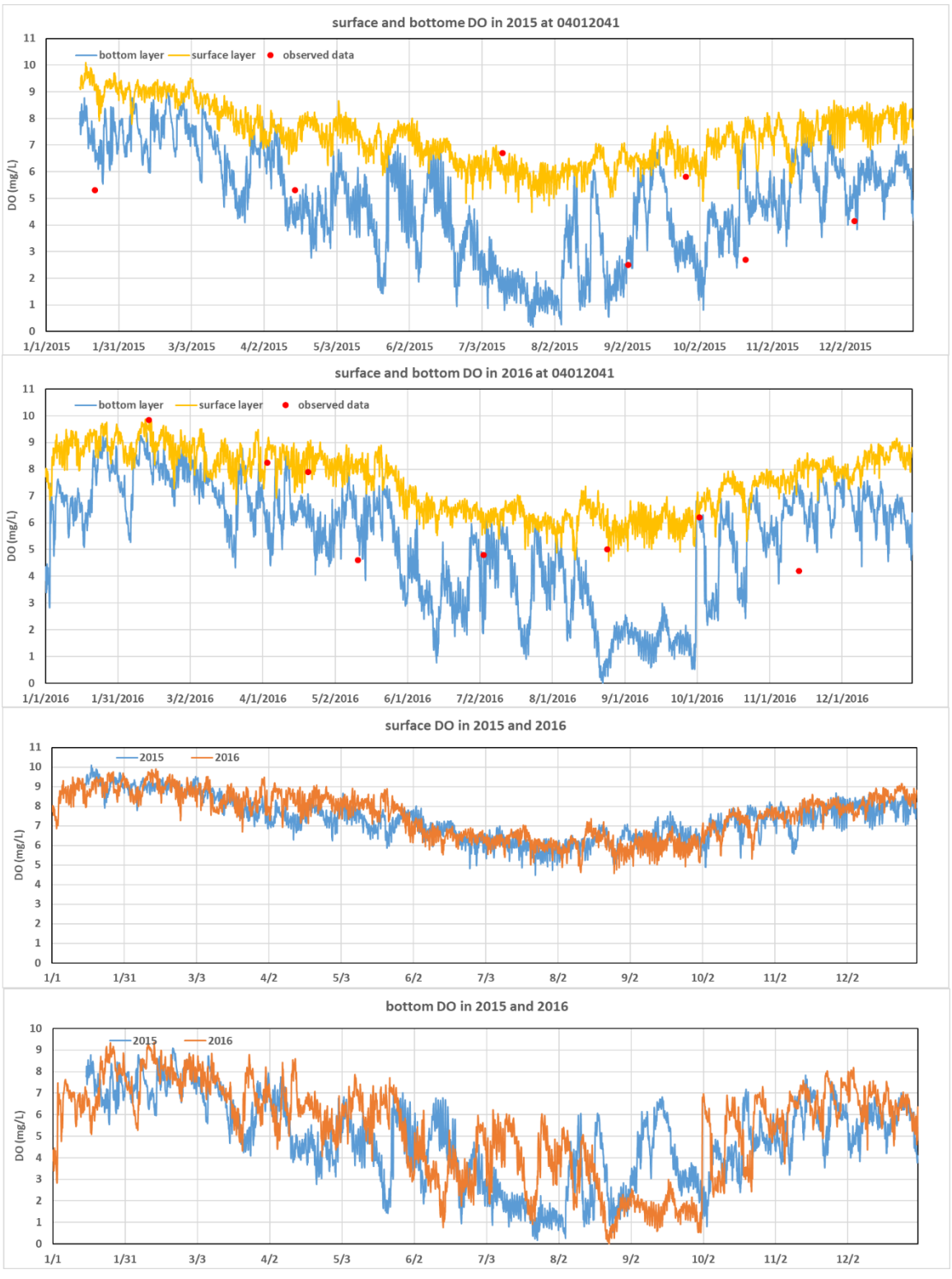

Figure 4-36 Simulated DO at the surface and bottom layers versus observed DO at 04012041 station (Wolf Bay).

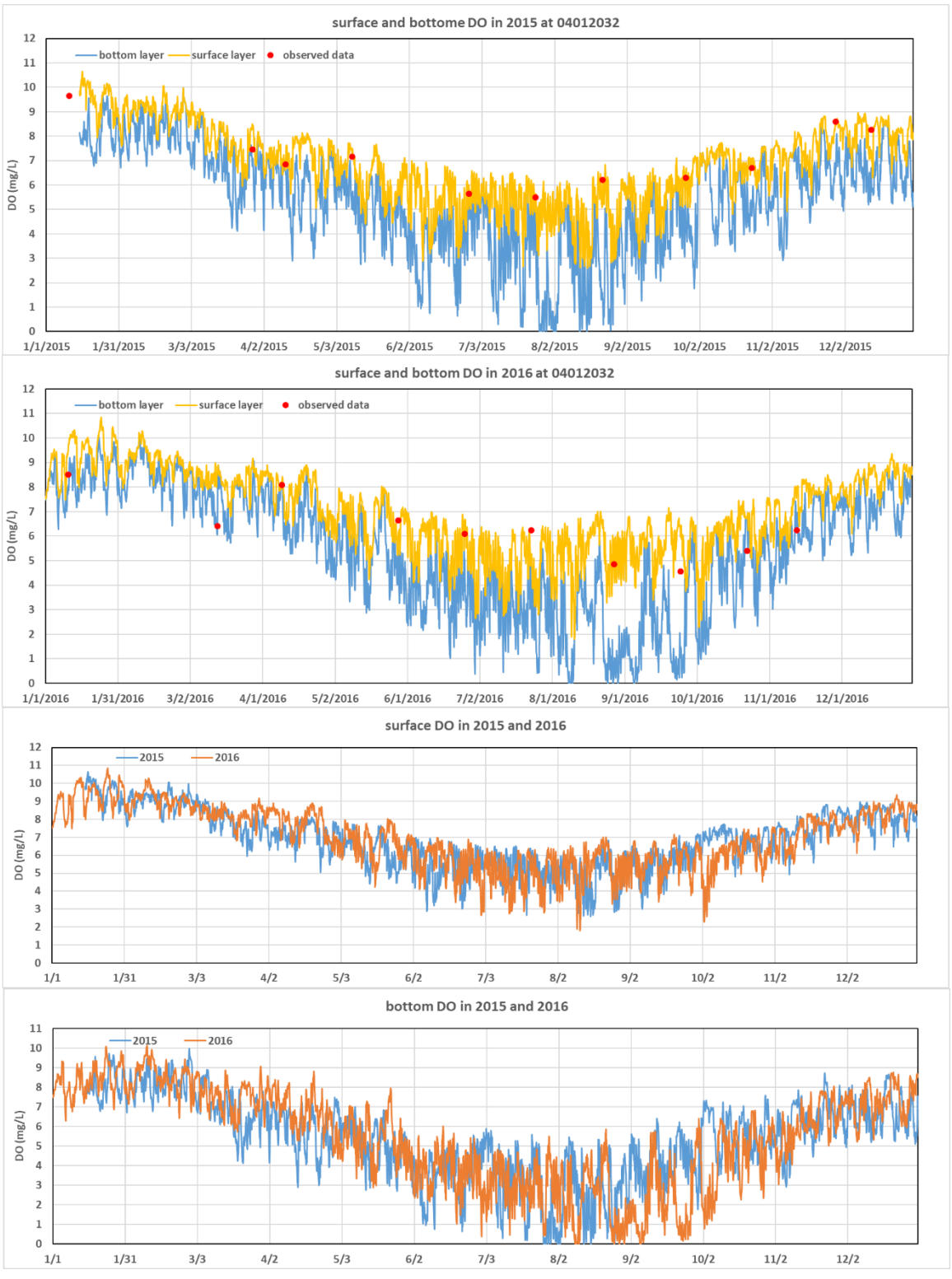

Figure 4-37 Simulated DO at the surface and bottom layers versus observed DO at 04012032 station (Wolf Bay).

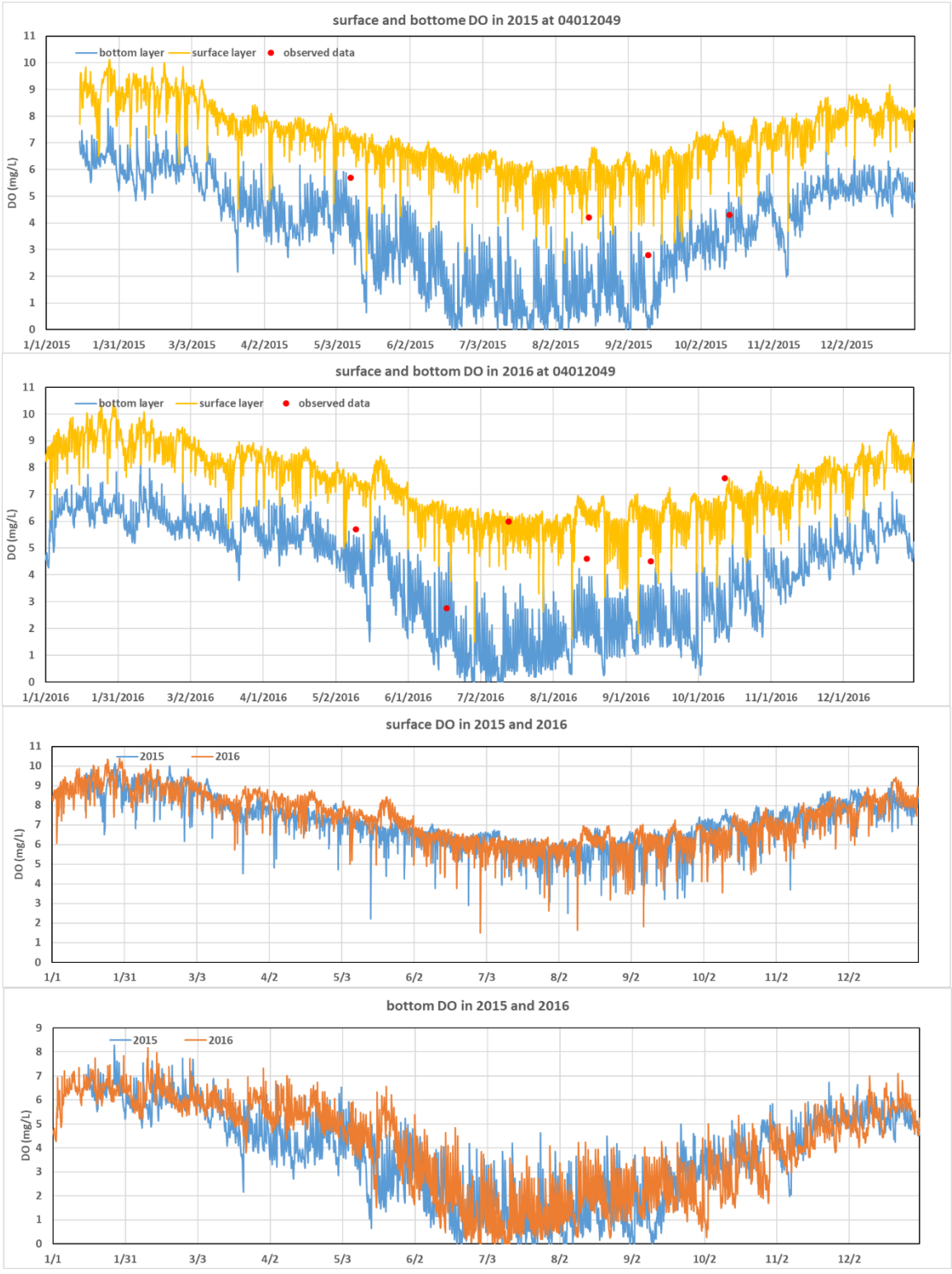

Figure 4-38 Simulated DO at the surface and bottom layers versus observed DO at 04012049 station (Cotton Bayou).

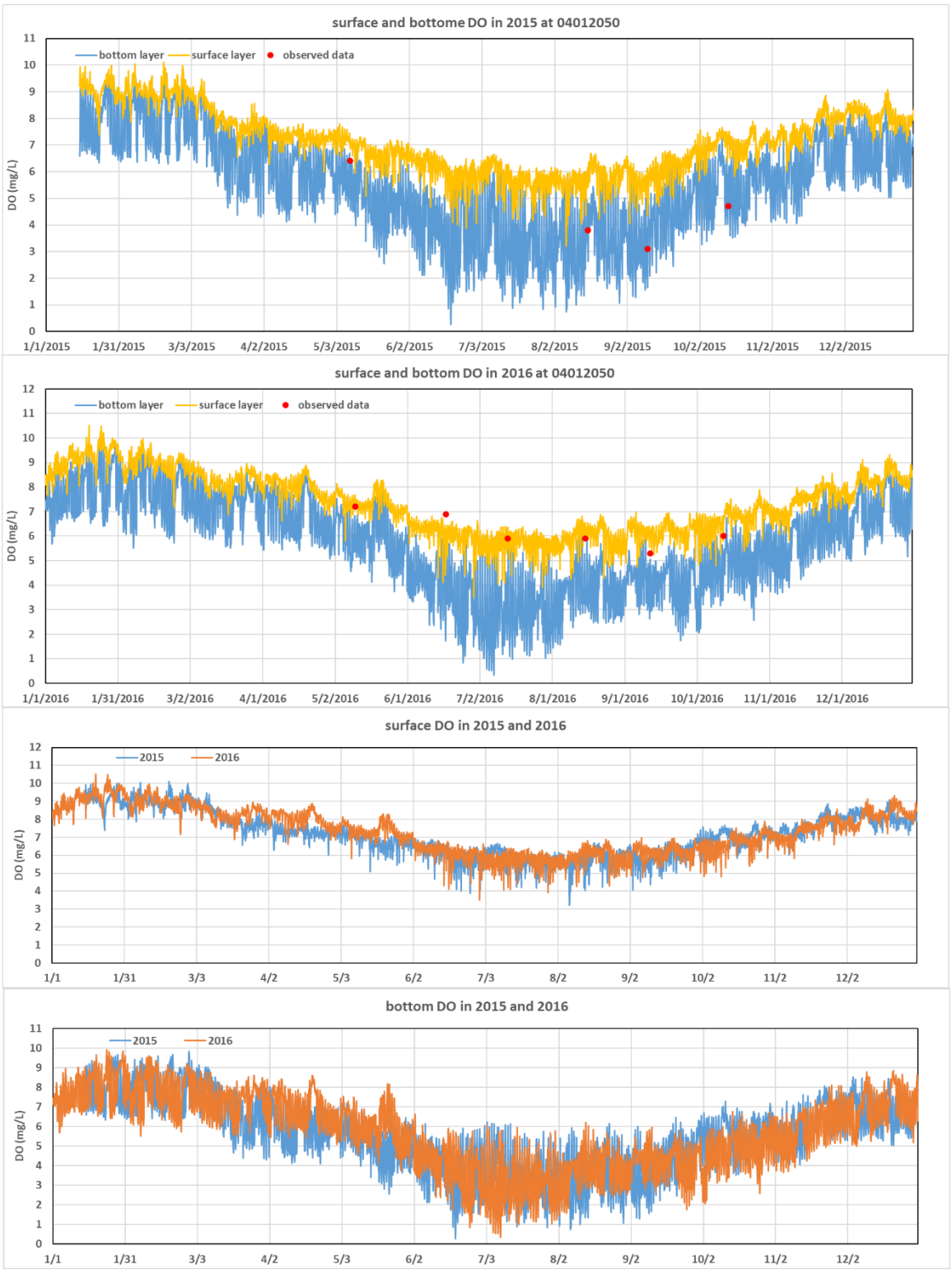

Figure 4-39 Simulated DO at the surface and bottom layers versus observed DO at 04012050 station (Cotton Bayou).

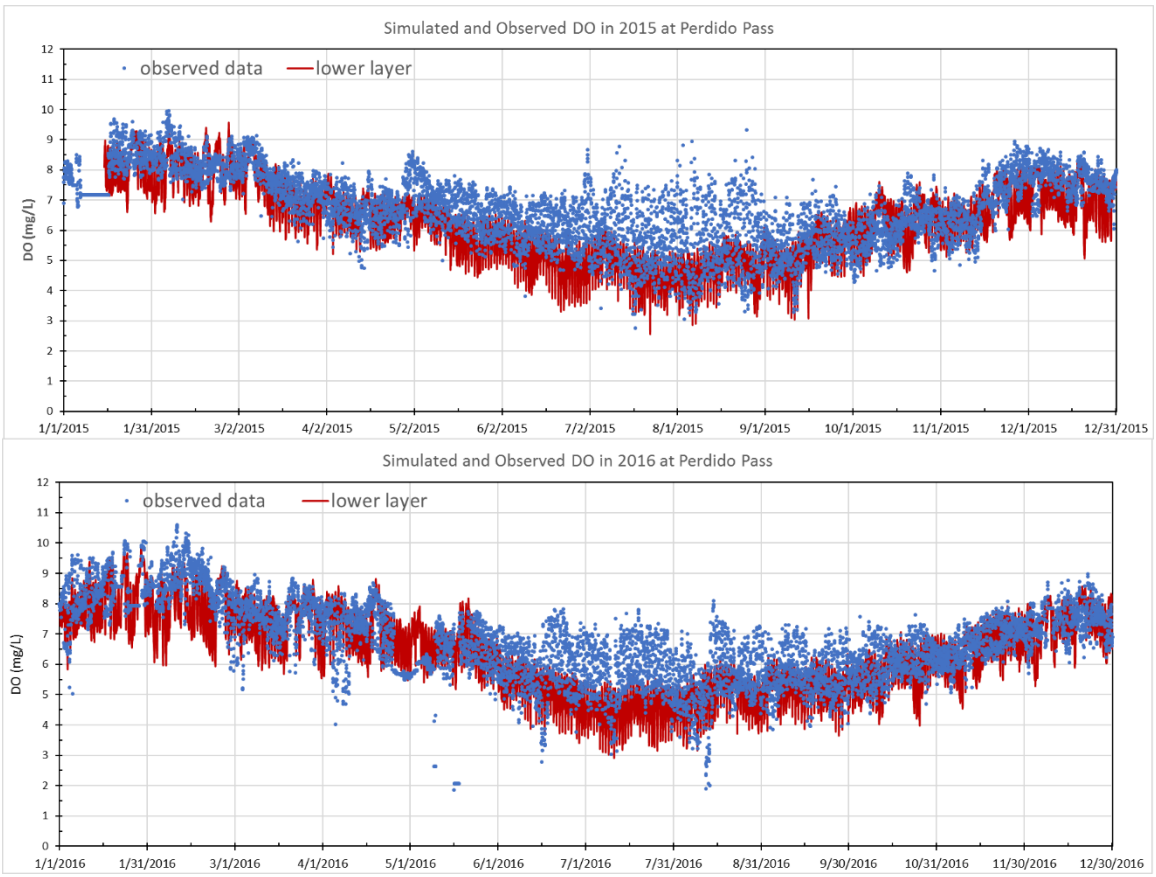

Figure 4-40 Simulated DO at the lower layer and observed DO at Perdido Pass station.

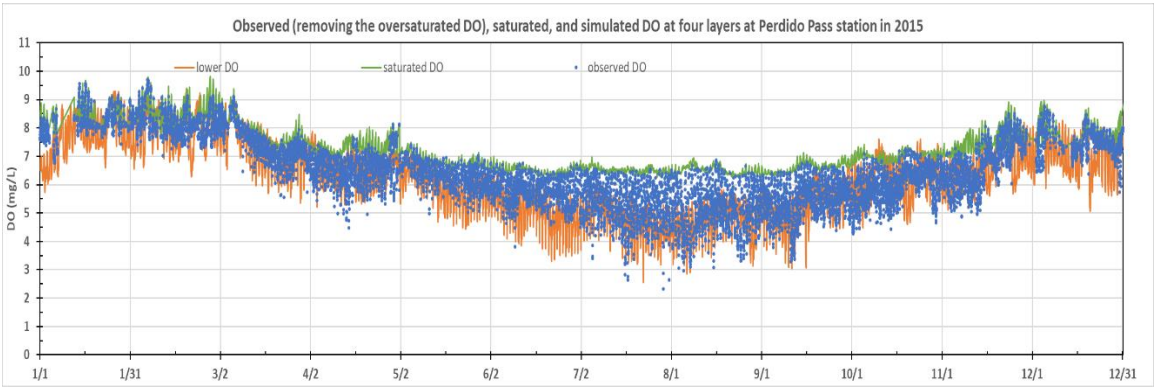

Figure 4-41 Simulated DO at the lower layer and observed DO (after removing the oversaturated DO) at Perdido Pass station including saturated DO calculated as a function of temperature and salinity.

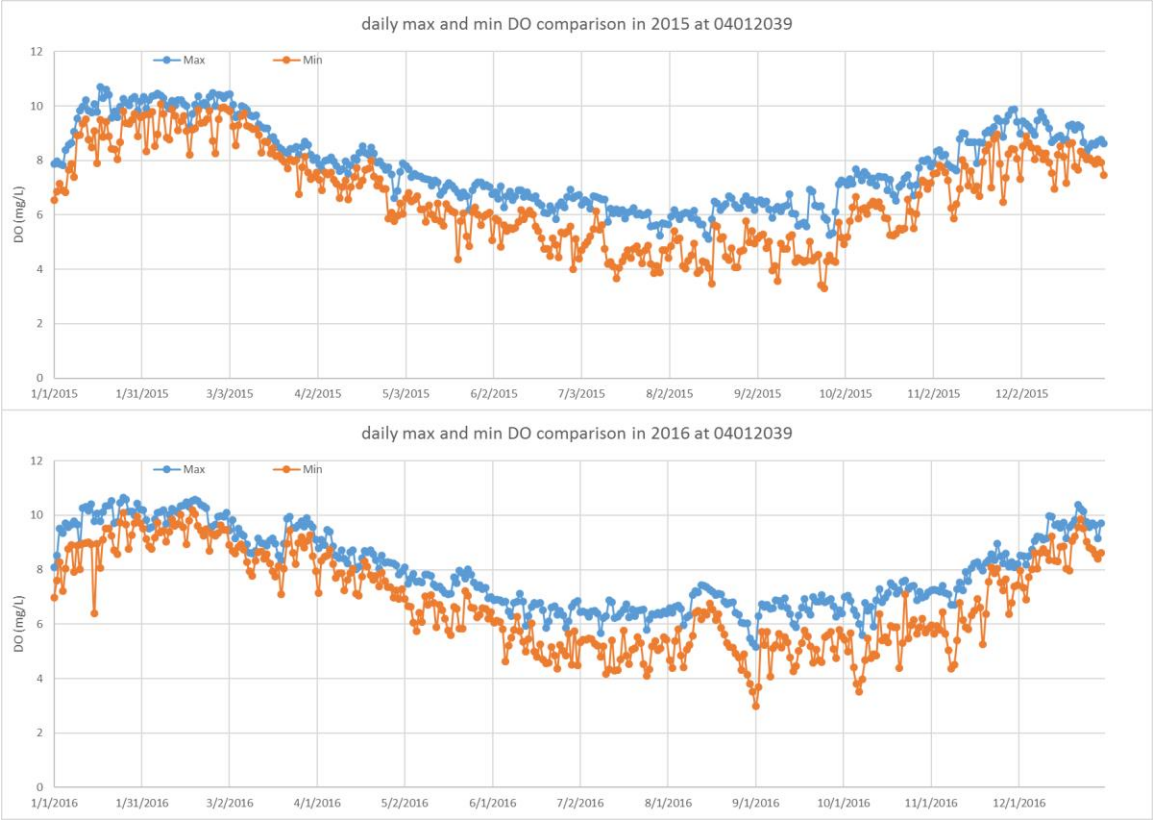

Figure 4-42 Simulated daily maximum and minimum DO in the surface layer at station 04012039 in 2015 and 2016.

4.2 Water Temperature and DO Analysis in the Perdido Bay

4.2.1 Analysis of Simulation Results from 7/1/2015 to 8/1/2015

Stratification is an important character in waterbodies (lakes, reservoirs, and estuaries). In freshwater lakes, water temperature stratification is primarily controlled by heat input by solar radiation and wind mixing. In estuary, salinity can play a very important role on stratification and salinity distribution is primarily determined by interactions or dynamics of oceanic tides, freshwater inflow, and wind. The study area (Perdido and Wolf Bay system) is wide and shallow estuary system. To further analyze the mixing of fresh and saline water, three girds or stations were selected

as the representations of three typical regions in the estuary from north to south, freshwater-dominated, transitional, and tide-dominated regions (Figure 4-43). Besides, the three stations are deepest in their own adjacent areas, with the depth 2.1, 3.6, 6.3 m, respectively from north to south.

Figure 4-44–Figure 4-46 show time-series of simulated water temperature, salinity, and density in the four layers at these three locations from 7/1/2015 to 8/1/2015. Simulated surface temperatures fluctuated in each day as a function of variable solar radiations and air temperatures. At station 1, all (100%) simulated bottom temperatures were higher than surface water temperatures, which is physically impossible for freshwater water bodies. At stations 2 and 3, 59% and 33% simulated bottom temperatures were higher than surface water temperatures. The higher bottom water temperature would bring a negative effect to the local ecosystem because the higher temperature means the lower DO due to higher chemical and biological oxygen demand. Besides, in the region where the stratification is strong, the tides leading vertical mixing would propagate upward, which inhabit the DO transportation from the surface layer with sufficient DO to the hypoxia bottom layers when the wind impact is weak.

Figure 4-44–Figure 4-46 clearly show there was salinity stratification from surface to bottom layers: lower salinity near the surface. Time-series plots of density at four layers also clearly approve that despite unusual temperature stratification, these four layers have density stable stratification. Therefore, simulated water temperatures at four layers were physically feasible and stable stratification.

At station 1 (maximum water depth of 2.1 m), in July 2015, surface salinity was 9.5±1.24 ppt and bottom salinity was 15.4±0.57. The difference between surface and bottom temperatures ranged from -0.13 to -7.08 °C (average of -3.43 °C). The maximum difference occurred late afternoon when the surface temperature was highest and the minimum difference occurred in early morning. Figure 4-44 shows simulated bottom temperature gradually increased up to 36.8 °C due

to continuous solar heating but no complete mixing along the water column. At station 2 (maximum water depth of 3.6 m), in July 2015, surface salinity was 14.8±1.00 ppt and bottom salinity was 20.6±0.60. The difference of surface and bottom temperatures ranged from -3.58 to 1.59 °C (average of -0.32 °C), and during the daytime, some surface temperatures were higher than bottom temperatures. At station 3 (maximum water depth of 6.3 m), 67% surface temperatures were higher than bottom temperatures in July 2015. The difference between surface and bottom temperatures ranged from -2.23 to 2.29 °C (average of 0.39 °C). Simulated surface temperatures were 30.9±1.06 °C (from 27.5 to 33.0 °C). Simulated bottom temperatures were 30.5±0.50 °C (from 29.0 to 31.8 °C). Figure 4-44–Figure 4-46 indicate very complex water temperature stratification dynamics in the Wolf and Perdido Bay estuary. In the early afternoon, the surface water temperature reached to the highest with the maximum solar radiation and air temperature. At night, the lack of solar radiation and lower air temperature caused lower water temperatures. For the surface DO, its maximum simulated values were found around 4:00 pm and the minimum data occurred around 6:00 am. This change rule complies with the activity of algae that produced most DO when the water temperatures are high and radiation are strong and do not produce DO without solar radiation.

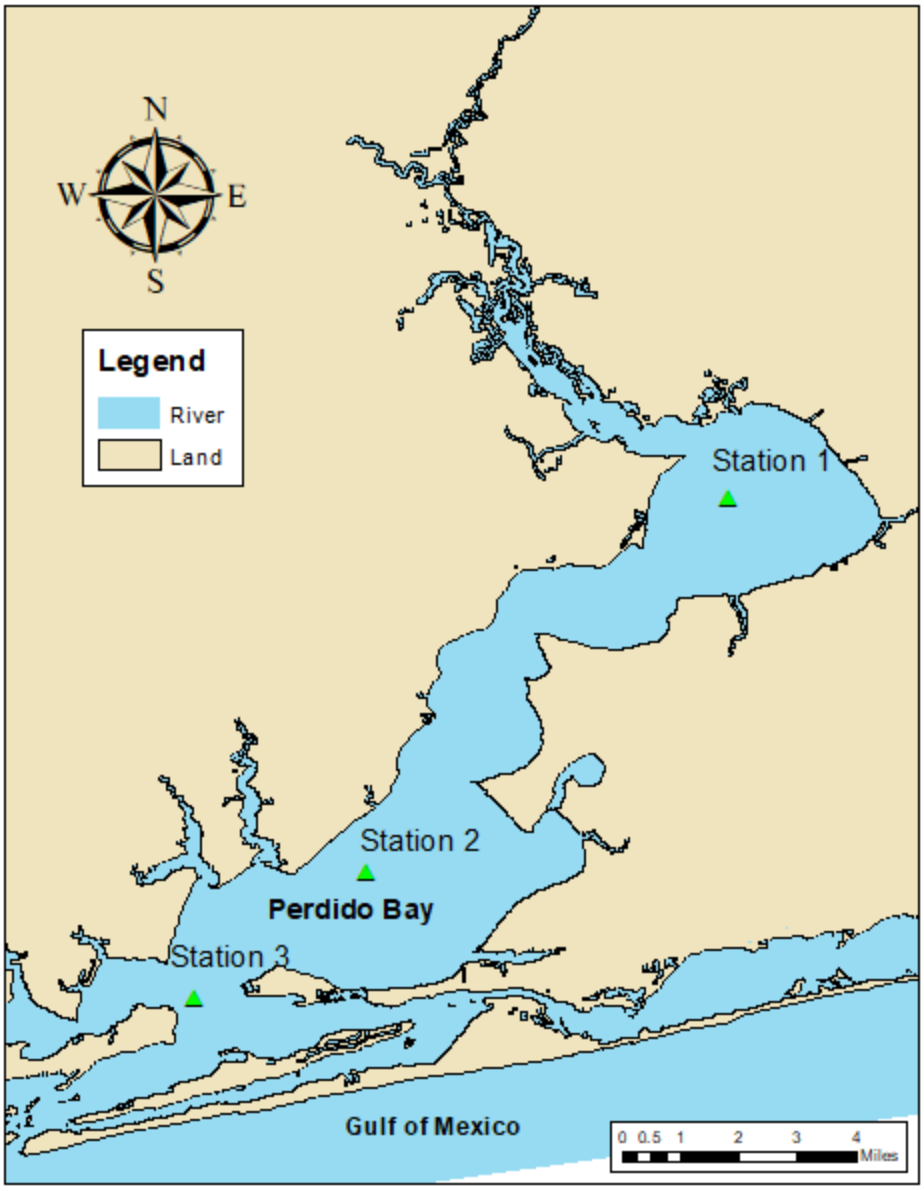

Figure 4-43 Bathymetry in Perdido Bay and the locations of three typical stations

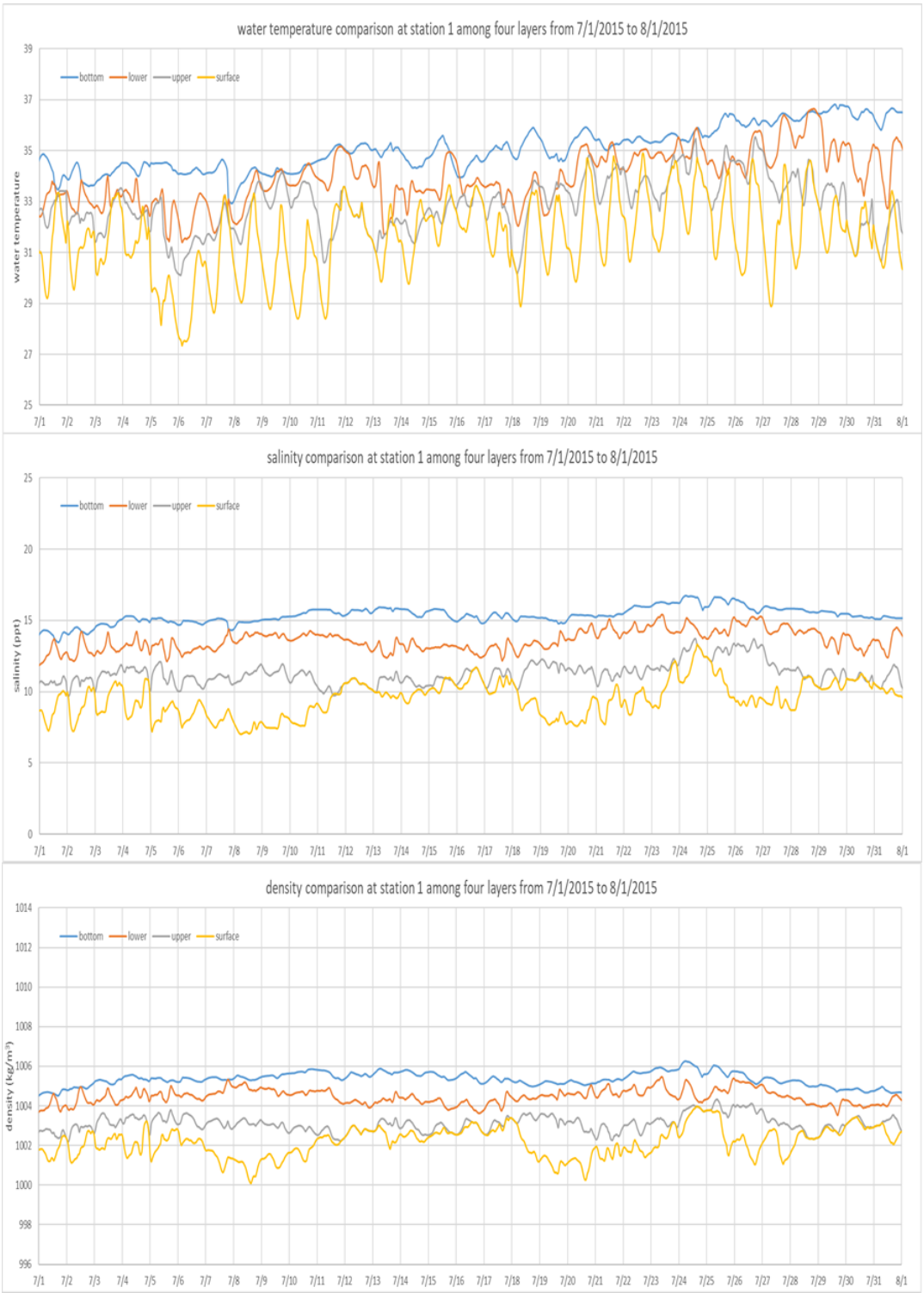

Figure 4-44 Simulated water temperature, salinity, and density comparison among four layers at station 1 (2.1 m deep) from 7/1/2015 to 8/1/2015

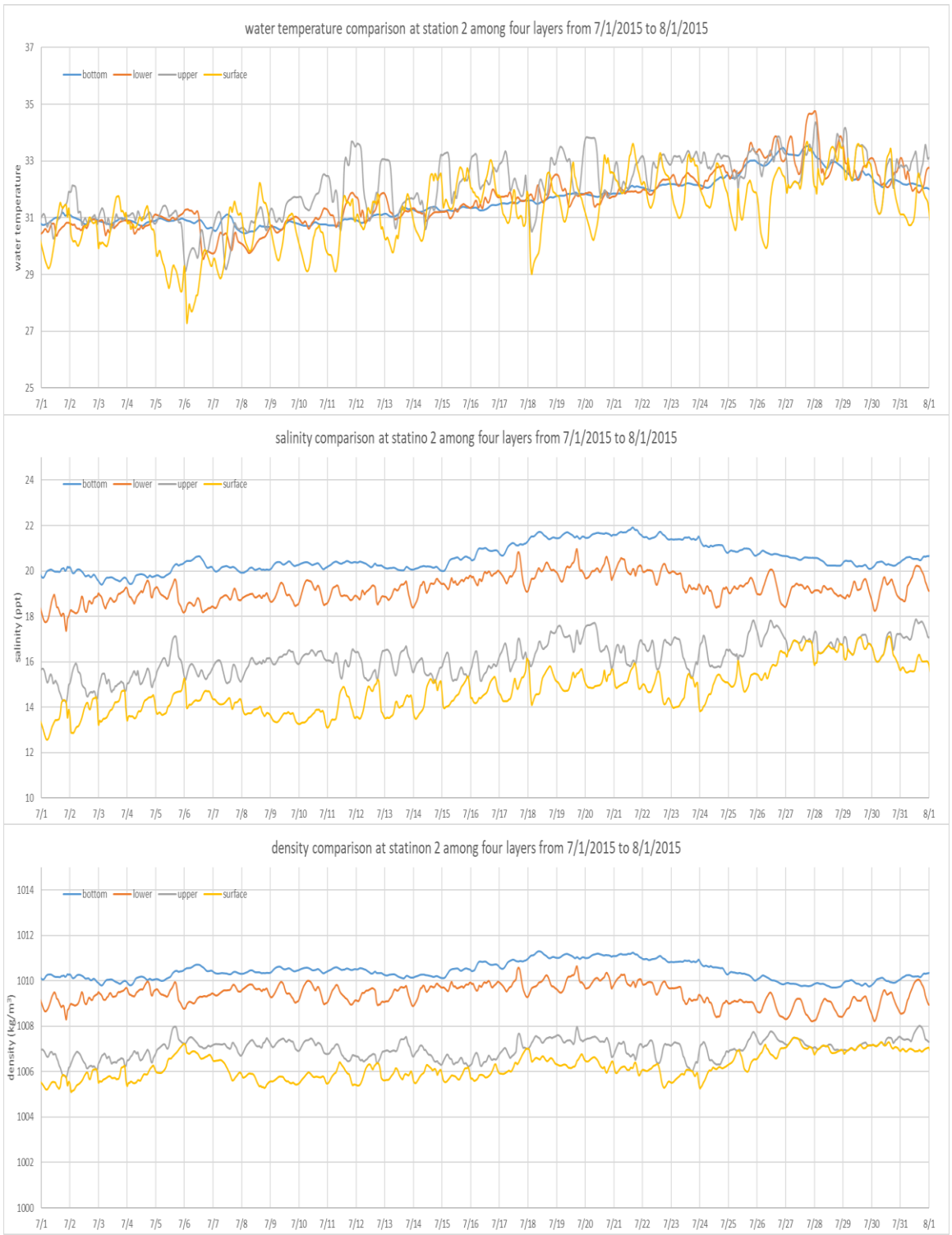

Figure 4-45 Simulated water temperature, salinity, and density comparison among four layers at station 2 (3.6 m deep) from 7/1/2015 to 8/1/2015

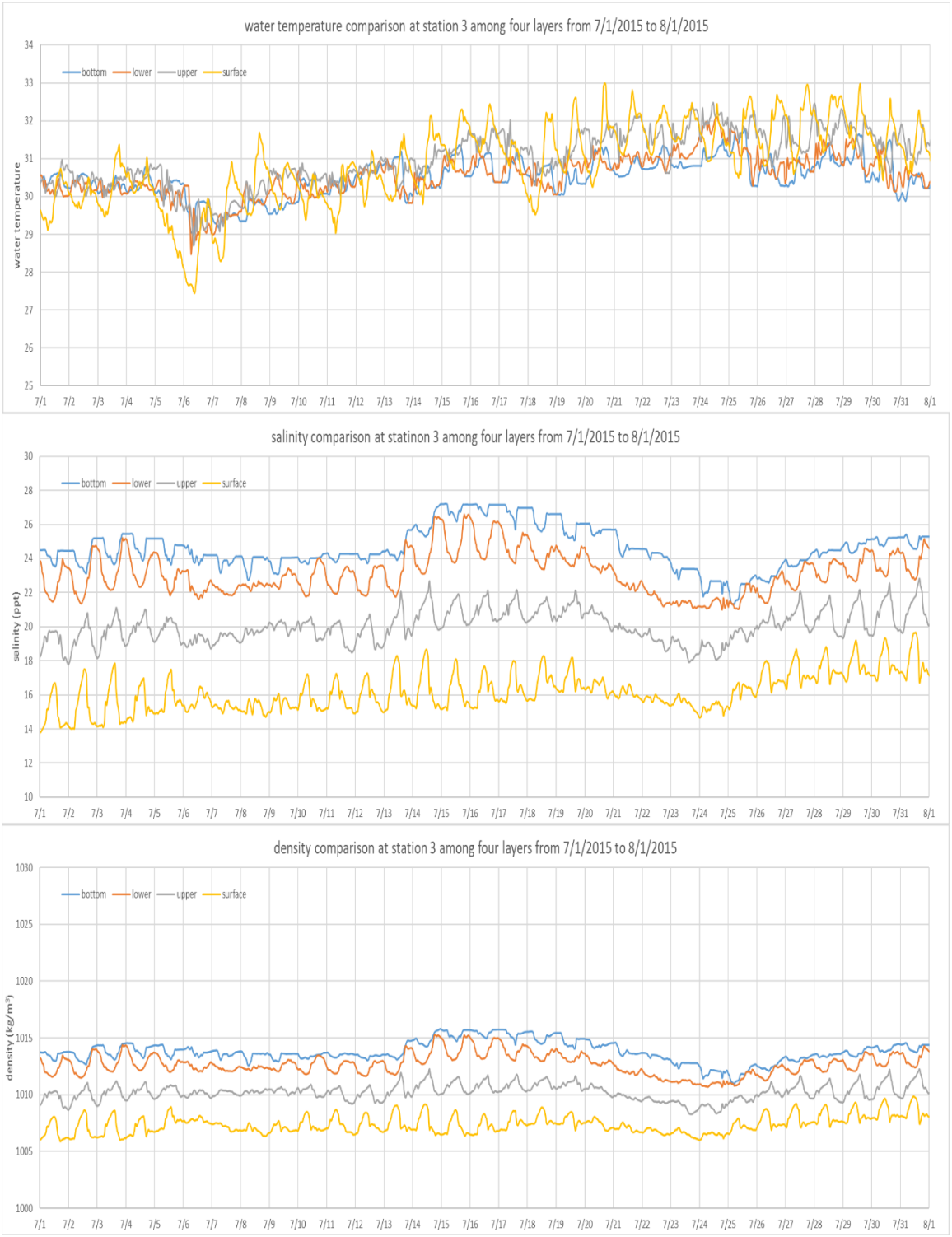

Figure 4-46 Simulated water temperature, salinity, and density comparison among four layers at station 3 (6.3 m deep) from 7/1/2015 to 8/1/2015

4.2.2 Analysis of Daily Simulation Results in 2015 and 2016

Figure 4-47 plots the daily maximum and minimum simulated water temperatures at the surface and the bottom layer at station 2 in 2015 and 2016. Statistical results for all three stations are given in Table 4-11. For the bottom layer, the simulated daily maximum and minimum water temperatures were relatively small with the average difference of 0.46 °C, whereas for the surface layer, the differences between daily maximum and minimum temperatures were much larger except for station 3 (Table 4-11), for example, the average difference for the surface layer was 1.84 ^{o}C for station 2 (4 times of 0.46 °C for the bottom layer). This is because the water in the surface layer received more heat input and was affected more by air temperature and solar radiation. Both daily maximum and minimum surface and bottom water temperatures followed the same trend with the season, the highest in summer and lowest in winter. For stations 1 and 2, the bottom average water temperatures are slightly higher the average surface water temperatures due to the density stratification as discussed before.

The bottom daily maximum and minimum DO show the large fluctuation comparing with the maximum and minimum DO at the surface layer (Figure 4-48). As discussed before, this is because the surface DO are primarily affected by the reaeration and photosynthesis processes, which maintain the surface DO at a level close to the 80% saturation, and the bottom DO are resulted by the DO diffusion from the upper layer, the SOD and COD consumption, and short-period tidal/wind mixing, which causes the large fluctuation. Besides, the surface DO are always higher than the bottom DO. Among the three stations, station 1 has the maximum surface average DO, since the surface layer were primarily affected by the upstream freshwater with higher DO

concentration at this station. However, its average bottom DO were the smallest among the three stations because significant stratification occurs in this region.

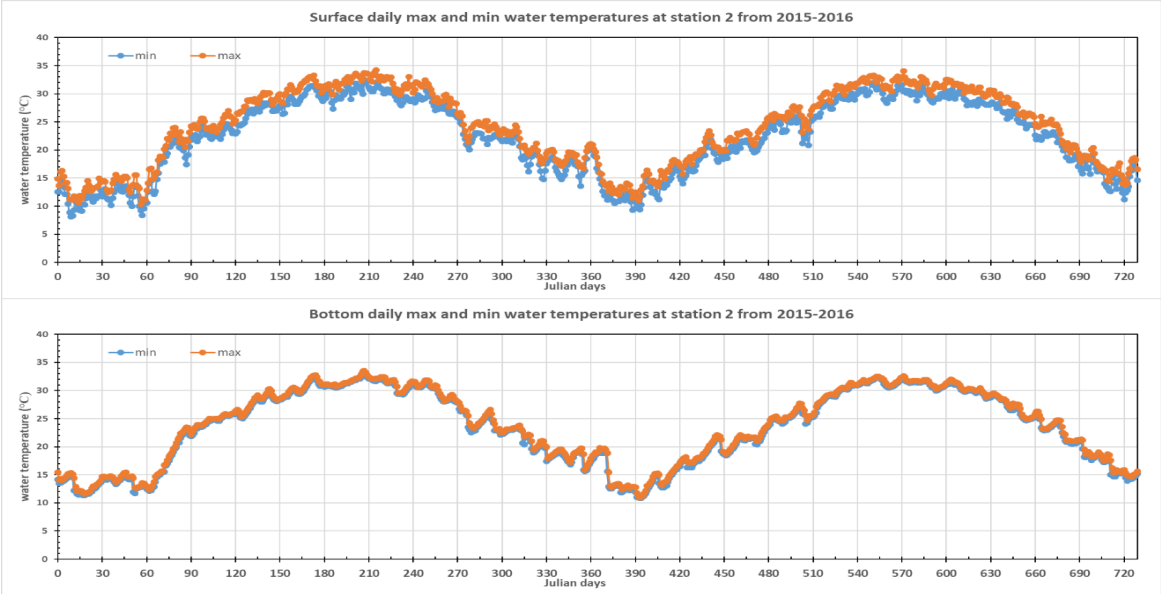

Figure 4-47 Simulated daily maximum and minimum water temperatures at the surface and bottom layers at station 2 in 2015 and 2016

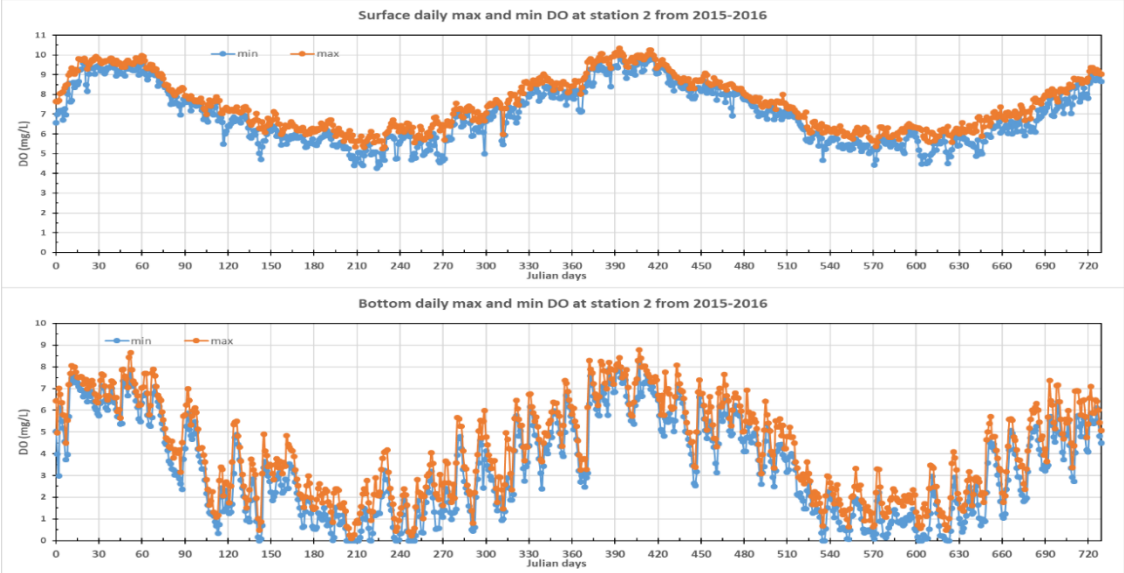

Figure 4-48 Simulated daily maximum and minimum DO concentrations at the surface and bottom layers at station 2 in 2015 and 2016

Table 4-11 Statistical results for average daily simulated water temperatures and DO at the surface and bottom layers at three stations in Perdido Bay in 2015–2016

Variable	Average Daily Water temperatures (ºC)					
Layer	Surface layer			Bottom layer		
Parameter	Max [1]	Min [1]	Diff. [1]	Max	Min	Diff.
Station 1	24.22	21.81	2.41	26.08	25.23	0.84
Station 2	24.10	22.26	1.84	23.81	23.35	0.46
Station 3	23.17	22.35	0.82	23.69	22.21	1.49
Variable	Average Daily DO Concentrations (mg/L)					
Layer	Surface layer			Bottom layer		
Parameter	Max	Min	Diff.	Max	Min	Diff.
Station 1	8.07	7.32	0.76	2.92	2.21	0.71
Station 2	7.57	6.95	0.61	4.24	3.34	0.90
Station 3	7.68	7.04	0.65	6.05	5.15	0.90

Note: [1] – standard for average daily maximum, minimum, and difference between daily maximum and minimum values.

4.3 Analysis of Simulation Results in Cotton Bayou

Based on the previous DO validation results (especially in the Cotton Bayou), the detail discussions of the hydrodynamic and water quality parameters in the Cotton Bayou were done in where the fish kills occurred on 7/31–8/4/2015. The section comprises of three sectors, time-series plots of water temperature, DO, salinity, and density from 7/15 to 8/15, three hours average DO from 7/15 to 8/15, and surface and bottom DO contour from 7/30 to 8/5 in 2015 for some selected locations/stations in Cotton Bayou (Figure 4-49).

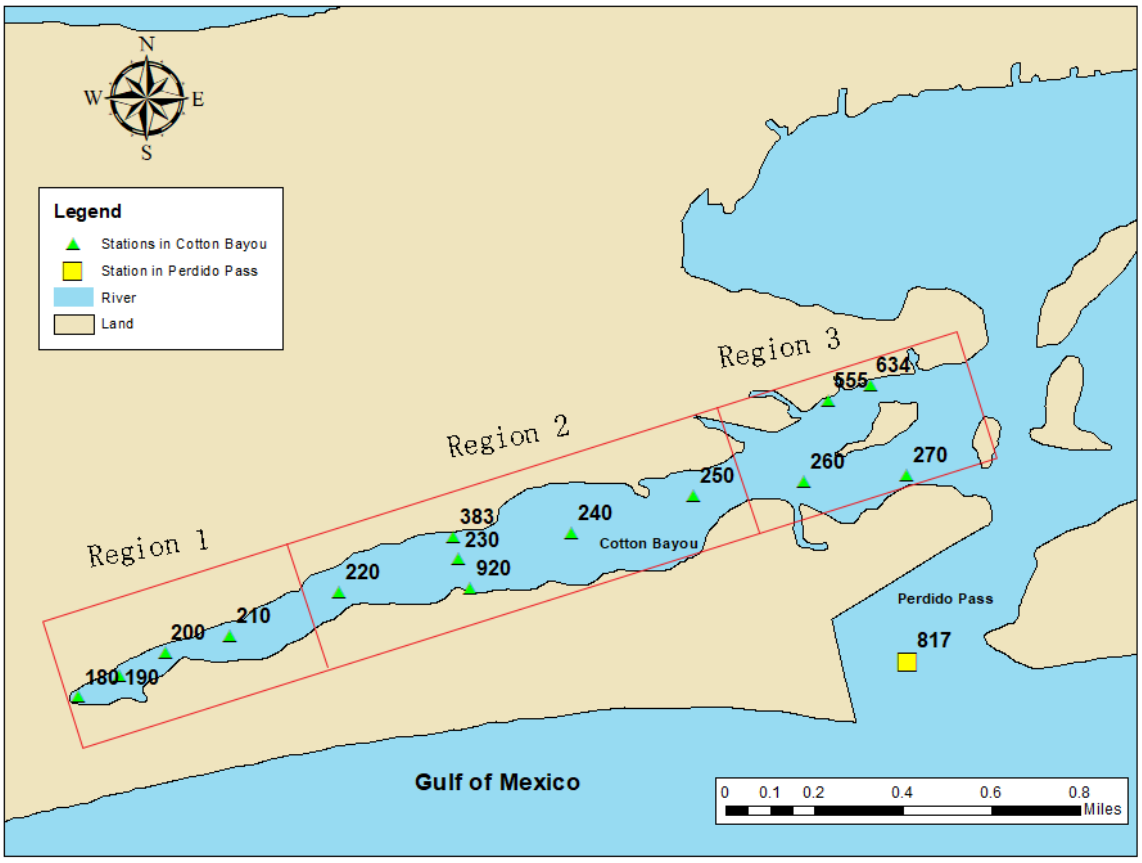

Figure 4-49 Location of stations in Cotton Bayou where time-series plots were developed.

4.3.1 Flow Dynamics in Cotton Bayou

Hydrodynamic characteristics in the Cotton Bayou are dynamic and complex because of the complex bathymetry of the Perdido Pass Complex (Figure 3-2) that contains several islands surrounding by deeps channels. Figure 4-50 shows the observed water levels in the Gulf of Mexico and the simulated water levels from 7/28 to 7/29 in 2015 at four stations 190, 240, 270, and 817 (Figure 4-49). The station 817 is located in the Perdido Pass, and its water level variation (-0.04–0.38 m) is almost the same as the variation (-0.1–0.4 m) at the model boundary (Gulf of Mexico). The water levels at stations 190, 240, and 270 in Cotton Bayou had similar variations with time as

the water levels at the Gulf of Mexico but smaller amplitudes (0.07–0.36 m = 0.25 m) and some delay. The average minimum water level in the Gulf of Mexico on 7/28 and 7/29 was -0.10 m while the corresponding value at station 270 was 0.07 m.

Figure 4-51 plots the surface- and bottom-layer flow horizontal vector velocities at the above four stations. The positive velocities represent the water flowing out of the Cotton Bayou (from west to east) at stations 190, 240, and 270, respectively, and flowing into the Perdido Bay (from south to north) at station 817. At station 817, the surface- and bottom-layer flow had the same direction variation following the water level change at the Gulf: primarily flowing into the Perdido Bay during the morning and flowing out of the Perdido Bay in the afternoon. The magnitudes of bottom-layer velocity (-0.5–0.3 m/s) were slightly smaller than the values in the surface layer (-0.64–0.74 m/s). Horizontal velocities in Cotton Bayou stations were much smaller so that a smaller scale (-0.2–0.2 m/s) was used for the velocity axis for station 190, 240, and 270. Station 270 near Perdido Pass had horizontal velocity from -0.07 to 0.10 m/s and station 190 near the end of Cotton Bayou had horizontal velocity from -0.02 to 0.03 m/s. The horizontal flow directions at three stations in the Cotton Bayou had more complex variations which were different from station 817 in the Perdido Pass. For the stations 190 and 240, the bottom-layer water primarily flowed into the Cotton Bayou with very smaller magnitudes. At station 270, the bottom-layer flow had a similar change pattern with the flow in the Perdido Pass but smaller magnitudes. At three stations in Cotton Bayou, the flow directions at the surface and bottom layers were frequently different, especially at station 240.

Figure 4-52 plots the surface- and bottom-layer vertical vector velocities at the four stations. It seems like there were no obvious relationships between the vertical velocities in surface and bottom layers with the water level change, in the aspect of flow directions and speeds. At four stations, the vertical velocity magnitudes at bottom layers were all higher than the surface values.

However, the vertical velocity speeds were very small, up to ~±0.0006 m/s at station 817 and < ±0.0001 m/s at station 190.

Two selected times: 6:00 am before the maximum tide arrived on 7/28 and 12:00 pm after the maximum tide on 7/29, were chosen to display the flow dynamics in the surface and bottom layers in the Cotton Bayou and its neighbor Perdido Pass and Terry Cove (Figure 4-53 to Figure 4-56). The flow directions were basically the same in the Terry Cove, Bayou Saint John, and Perdido Pass that were directly affected by the tides–major flow path to Perdido Bay without much flow blockages. The saline water from the Gulf of Mexico flowed into the Perdido Bay before the maximum tidal level arrived and then flowed out the Perdido Bay. Since the magnitude of flow velocity is shown as the arrow length, Figure 4-53 to Figure 4-56 clearly show flow velocities in Cotton Bayou were significantly smaller than the velocities in the Perdido Pass complex and had complex velocity directions changes. Figure 4-56 also shows some grids in Cotton Bayou had flow velocities almost zero that could not be shown as an arrow. Therefore, flow-induced mixing in Cotton Bayou was typically very small to result in strong stratification of water quality, even water level variation in Cotton Bayou was similar to one in Perdido Pass (Figure 4-50).

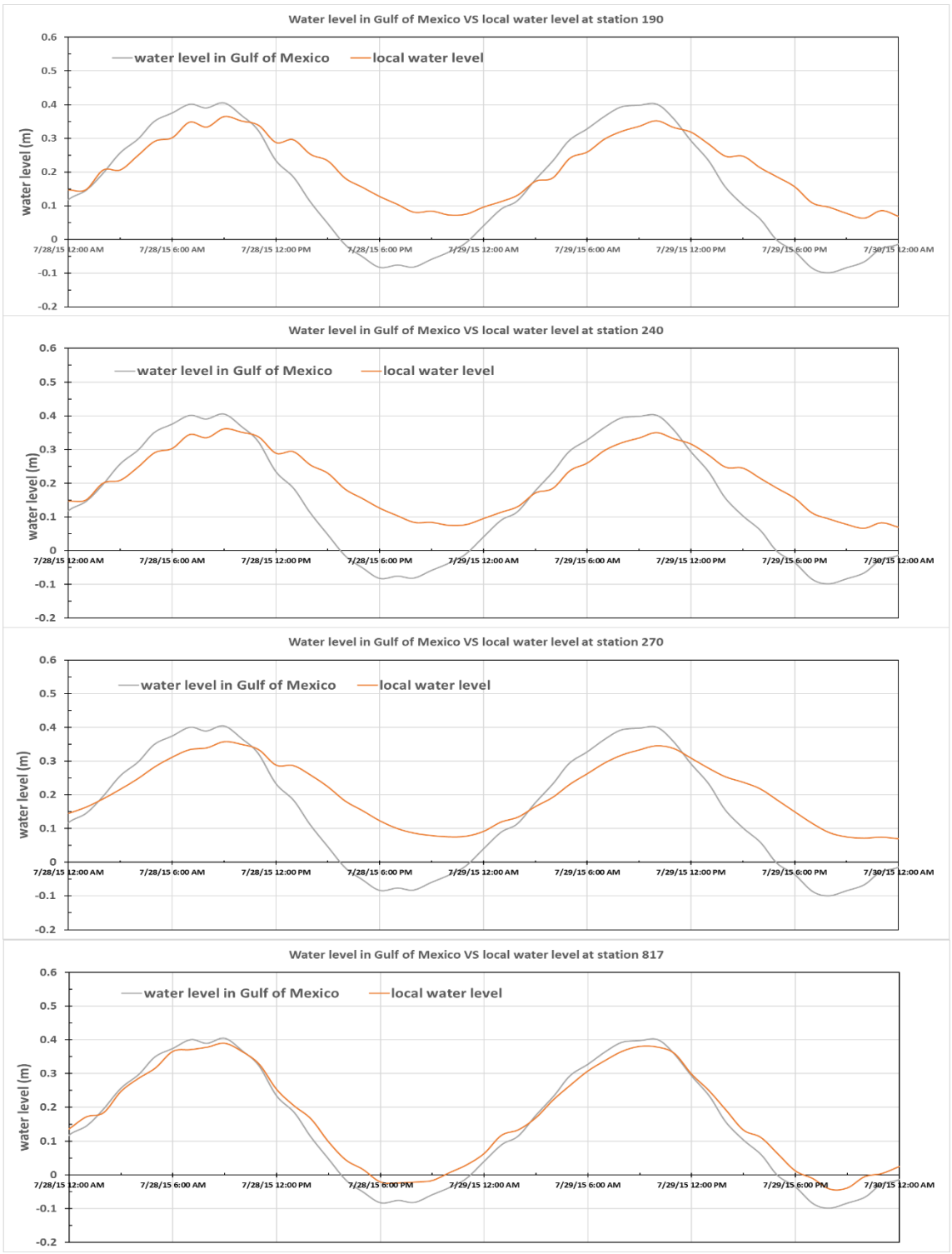

Figure 4-50 Times series of observed water level in the Gulf of Mexico (Dolphin Island) and simulated water levels at the stations 190, 240, 270 and 817 (from top to bottom) (Figure 4-49) in Cotton Bayou.

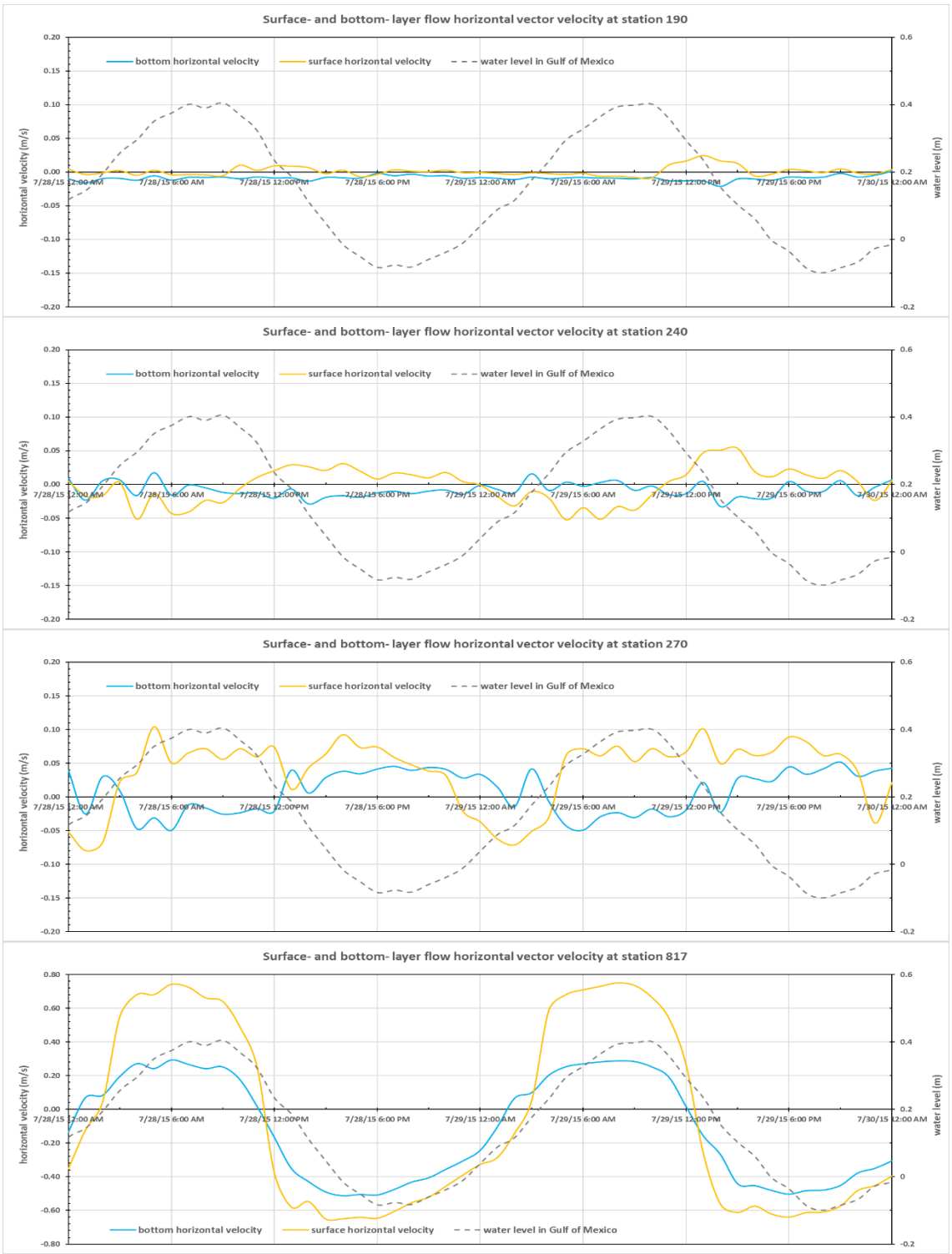

Figure 4-51 Surface- and bottom-layer horizontal velocity at station 190, 240, 270 and 817 (from top to bottom) (positive values meaning water flowing into the Cotton Bayou from west to east at stations 190, 240 and 270 and flowing into Perdido Bay from south to north at station 817).

Figure 4-52 Simulated surface- and bottom-layer vertical velocity at stations 190, 240, 270 and 817 (from top to bottom) (positive velocities meaning water flowing from bottom to surface)

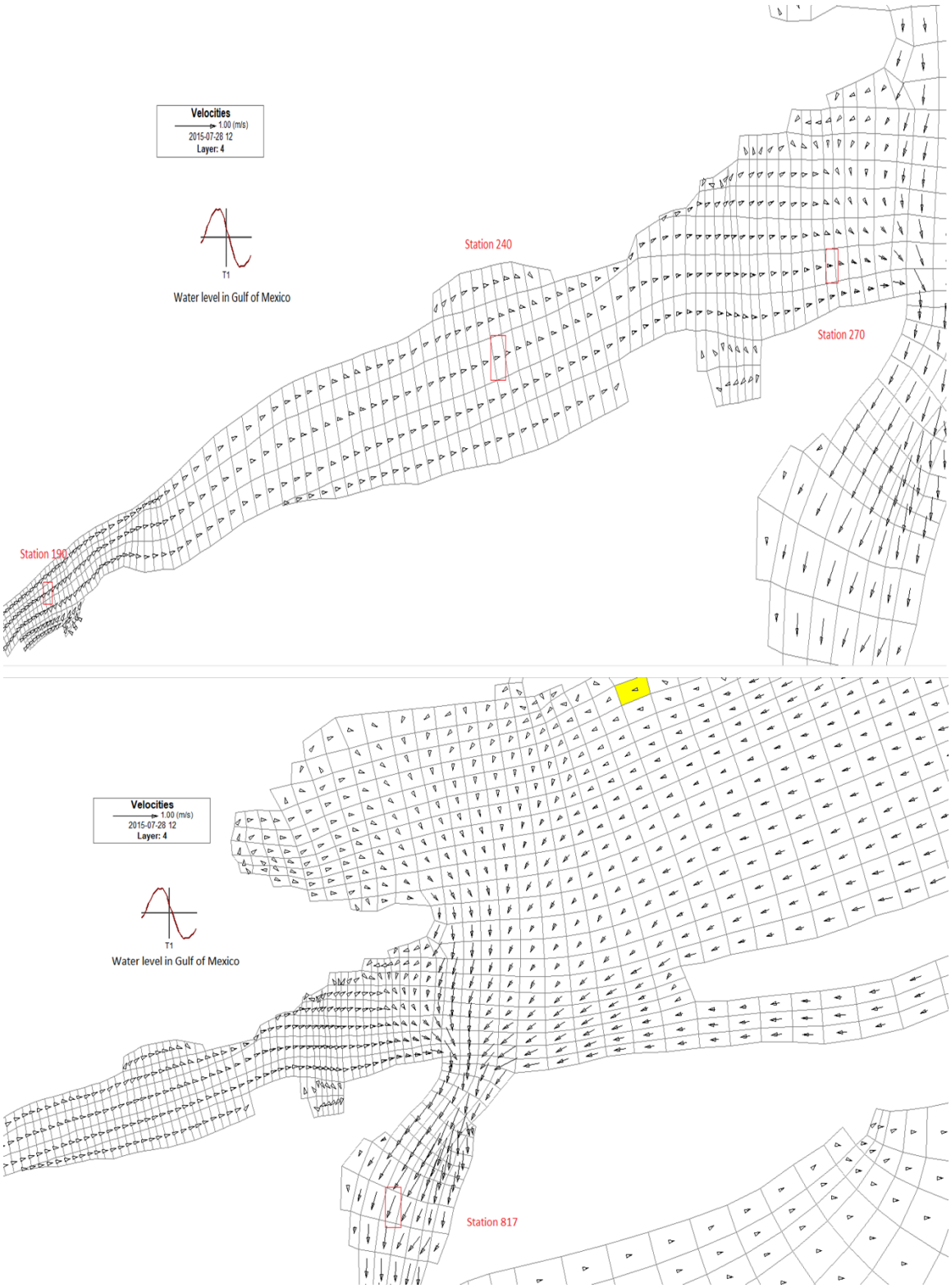

Figure 4-53 Surface-layer flow velocity at 12:00 pm on 7/28 in Cotton Bayou (upper panel) and Perdido Pass and Terry Cove (lower panel)

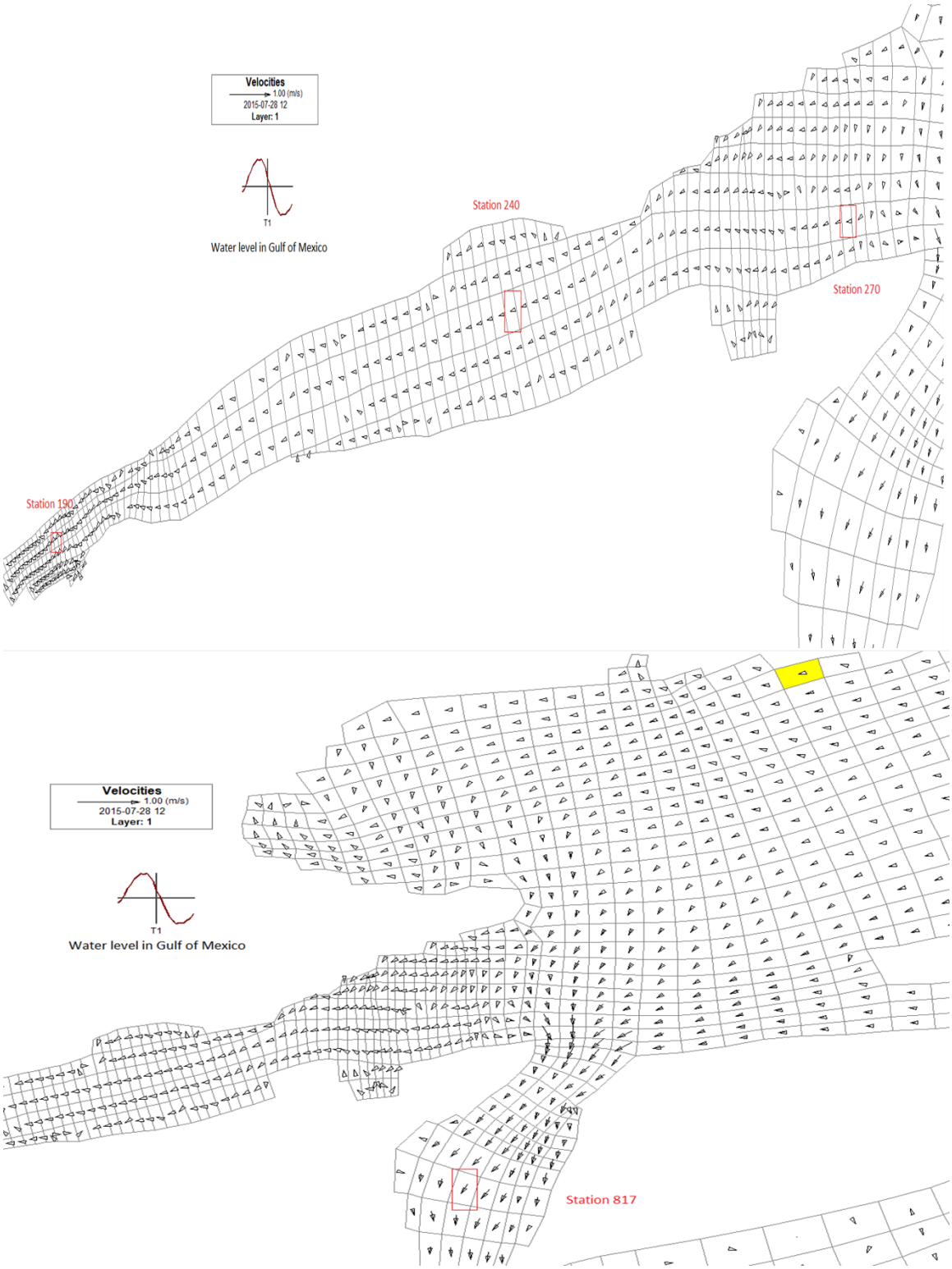

Figure 4-54 Bottom-layer flow velocity at 12:00 pm on 7/28 in Cotton Bayou (upper panel) and Perdido Pass and Terry Cove (lower panel)

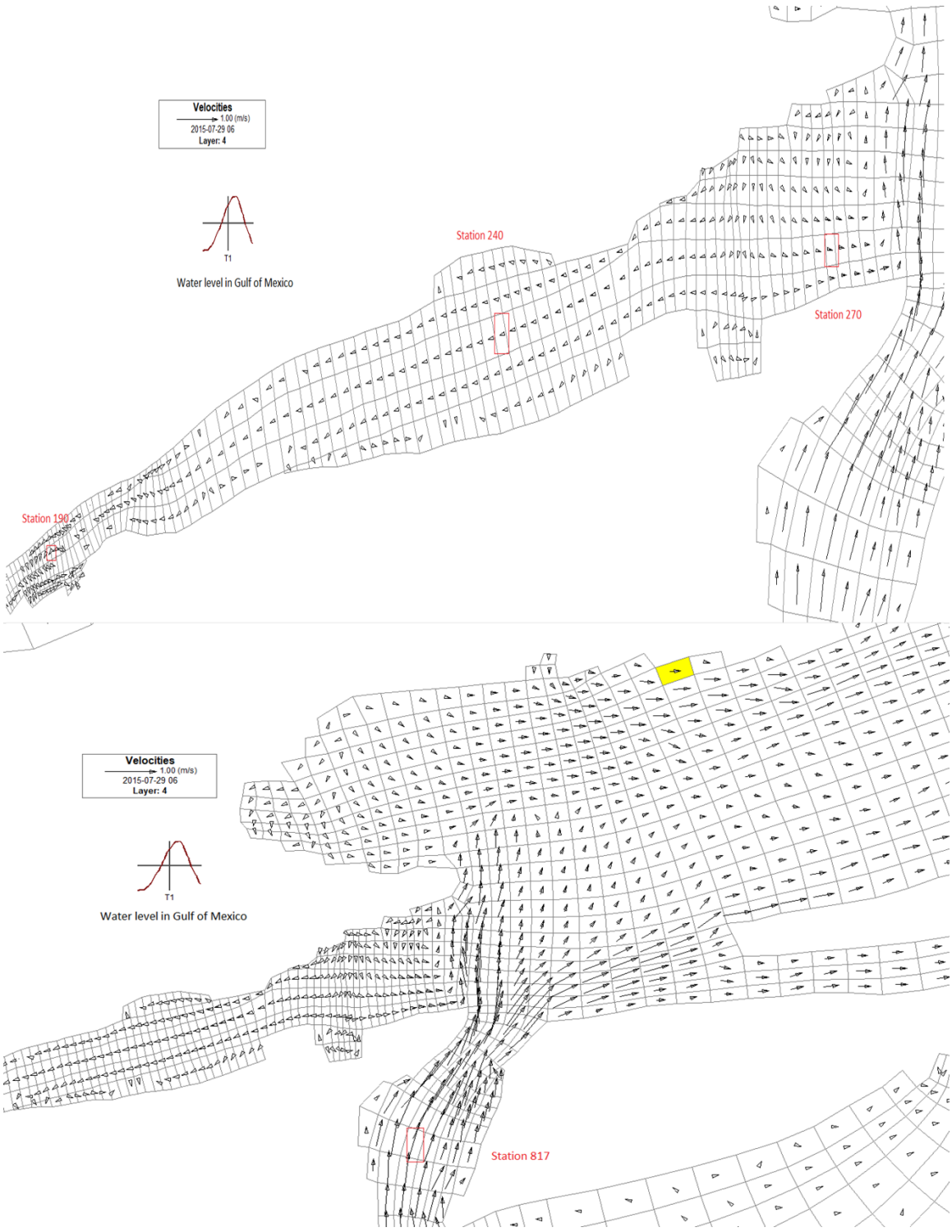

Figure 4-55 Surface-layer flow velocity at 6:00 am on 7/29 in Cotton Bayou (upper panel) and Perdido Pass and Terry Cove (lower panel)

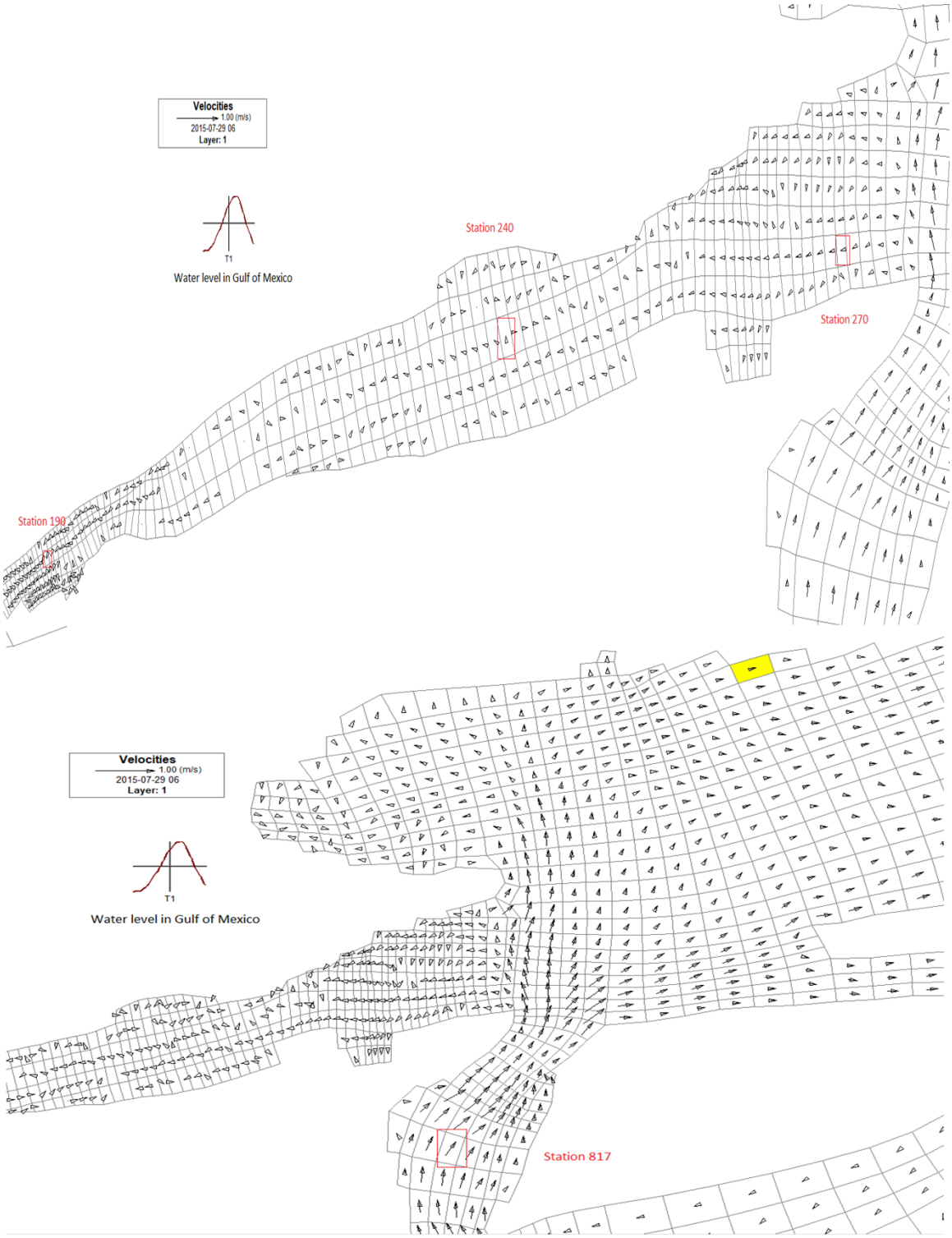

Figure 4-56 Bottom-layer flow velocity at 6:00 am on 7/29 in Cotton Bayou (upper panel) and Perdido Pass and Terry Cove (lower panel)

4.3.2 Time-series Plots of DO and Water Temperature

DO and water temperature are the primary concern in this study because the low DO (< 3 mg/L) is a frequent cause to deteriorate the fish habitat compared with other factors, such as toxic. In addition, high water temperature (>30 °C) is directly linked to thermal stress of Gulf menhaden, which was reported to avoid water temperature above 30 °C (Christmas and Waller 1973), and closely related to low DO distribution along with the depth. Figure 4-49shows location of a number of stations or grids in Cotton Bayou that time-series plots of simulated water temperature and DO (Figure 4-57—Figure 4-64) were created and analyzed further. Table 4-12 lists water depths of these stations (grids), which ranged from 0.72 to 2.7 m, shallower than the stations 2 and 3 in Perdido Bay (Figure 4-43).

Figure 4-57 plots the time series of water temperature, DO, salinity, and density from 7/15 to 8/15 in 2015 for station 180 where is the west end of the Cotton Bayou. Based on the change pattern of salinity and density, Cotton Bayou was roughly divided into three regions (Figure 4-49). Region 1 (stations 180—210) is the area where is typically less affected by the tides from Gulf of Mexico and Figure 4-57 as an example shows salinity and density distribution. The salinity changed smoothly from 18 to 27 ppt over about 10 days and then repeated again. Both salinity and density stratification from the surface to bottom was small but stable (less density in the surface). The density in the surface layer had small fluctuation in each day. There was obvious daily change pattern for the surface water temperature e.g., as a function of solar radiation. In region 1, the low DO (<3 ng/L) occurred from 7/27 to 8/3 in the bottom and lower layers, slight higher DO occurred in upper and surface layers. Most of the temperatures were above 30 ^{o}C, and bottom temperatures were higher than surface temperatures over many hours in many days.

The region 2 is a transitional region between region 1 and region 3. Figure 4-60 shows simulated water temperature, DO, salinity, and density among four layers at station 230 from

7/15/2015 to 8/15/2015, which show stronger stratification for all four variable but still smooth variations in salinity and density. The region 2 was in a wide open area of Cotton Bayou. Most of simulated DO at the bottom and lower layers were less than 3 mg/L, the lethal limit for menhaden, but surface DO were above 3 mg/L in the open water area. Figure 4-61 shows simulated temperature and DO at stations 383 and 920, which was shallower, north and south of station 230; their temperatures and DO concentrations had more fluctuations because they are near the shoreline.

Region 3 is an area that was significantly affected by the tides from the eastern Gulf of Mexico. Figure 4-62 compares simulated temperatures and DO in station 250 (region 2) and 260 (region 3). Figure 4-63 shows that the salinity and density of all layers at station 270 had strong daily variations like the tides. There were smaller variations of surface salinity and larger variations of bottom salinity that were obviously affected by both less saline water from the Perdido Bay and tides from the Gulf of Mexico. Both the maximum and minimum water temperatures nearly all occurred in the surface layer. The largest fluctuations of bottom water temperatures show that the water at different layers had more frequently and strongly mixing, which were also indicated by less DO vertical variations. DO concentrations in region 3 were higher in all four layers. Except for several discrete short time periods, simulated bottom DO were higher than 3 mg/L.

Table 4-12 Water depths (m) of stations for time-series plots

Station	180	190	200	210	220	230	240	250
Depth (m)	1.63	1.42	1.63	2.4	2.5	2.7	1.82	1.52
Station	260	270	383	920	456	930	555	634
Depth (m)	0.99	1.98	1.12	1.08	0.72	2.22	1.8	1.12

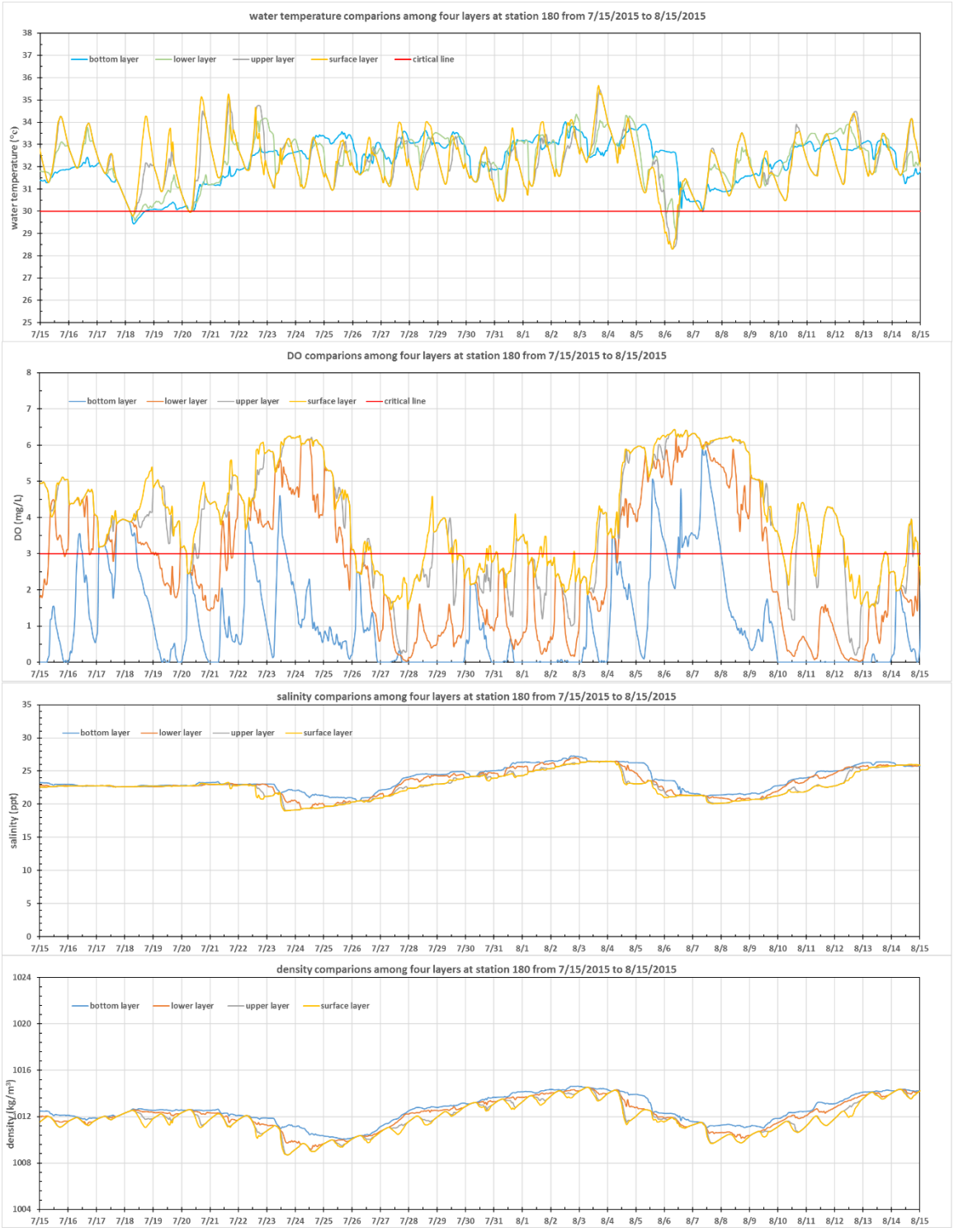

Figure 4-57 Simulated water temperature, salinity, density, and DO among four layers at station 180 from 7/15/2015 to 8/15/2015 (in region 1)

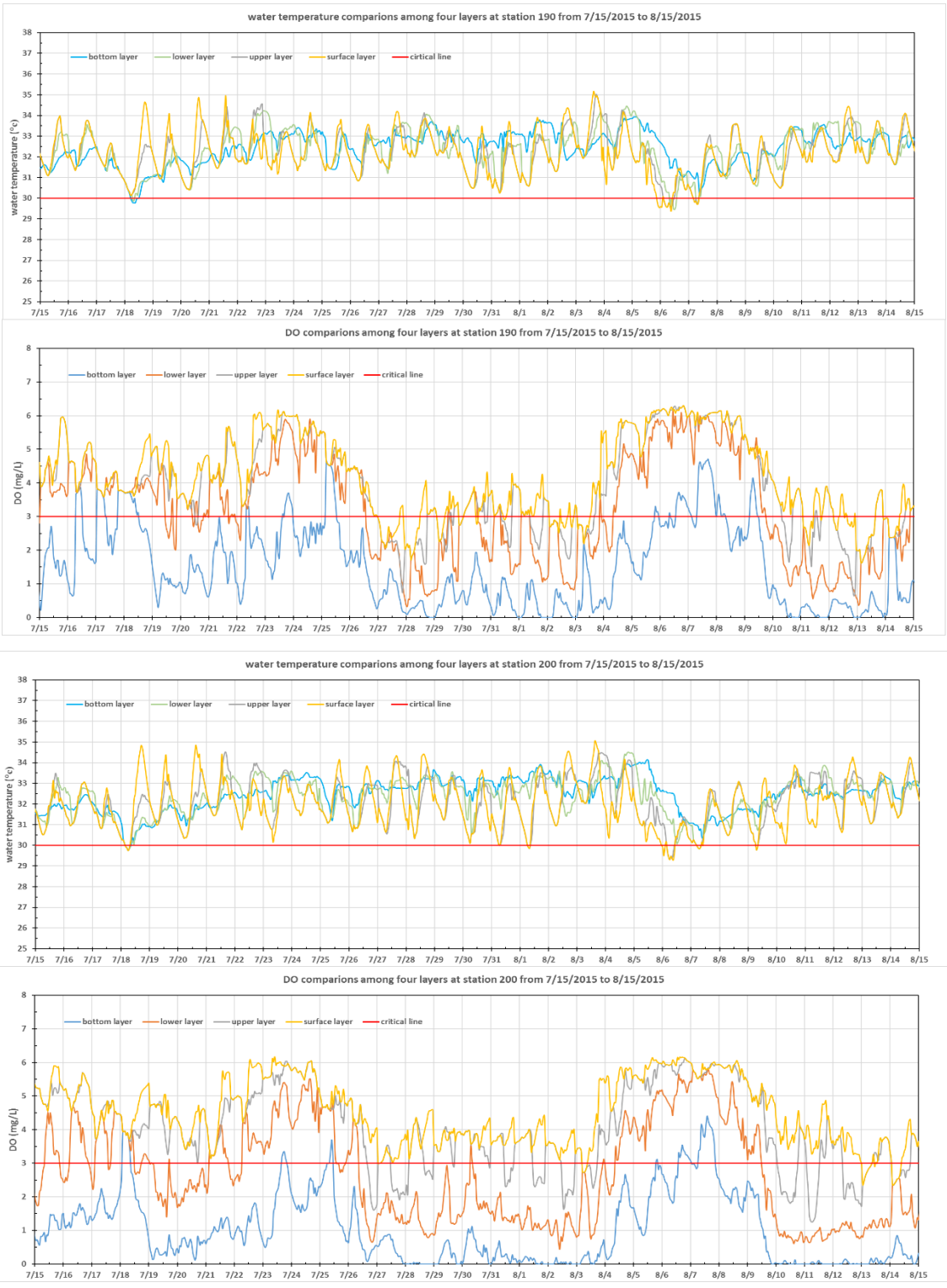

Figure 4-58 Time-series of simulated water temperature and DO among four layers at station 190 and 200 from 7/15/2015 to 8/15/2015 (in region 1)

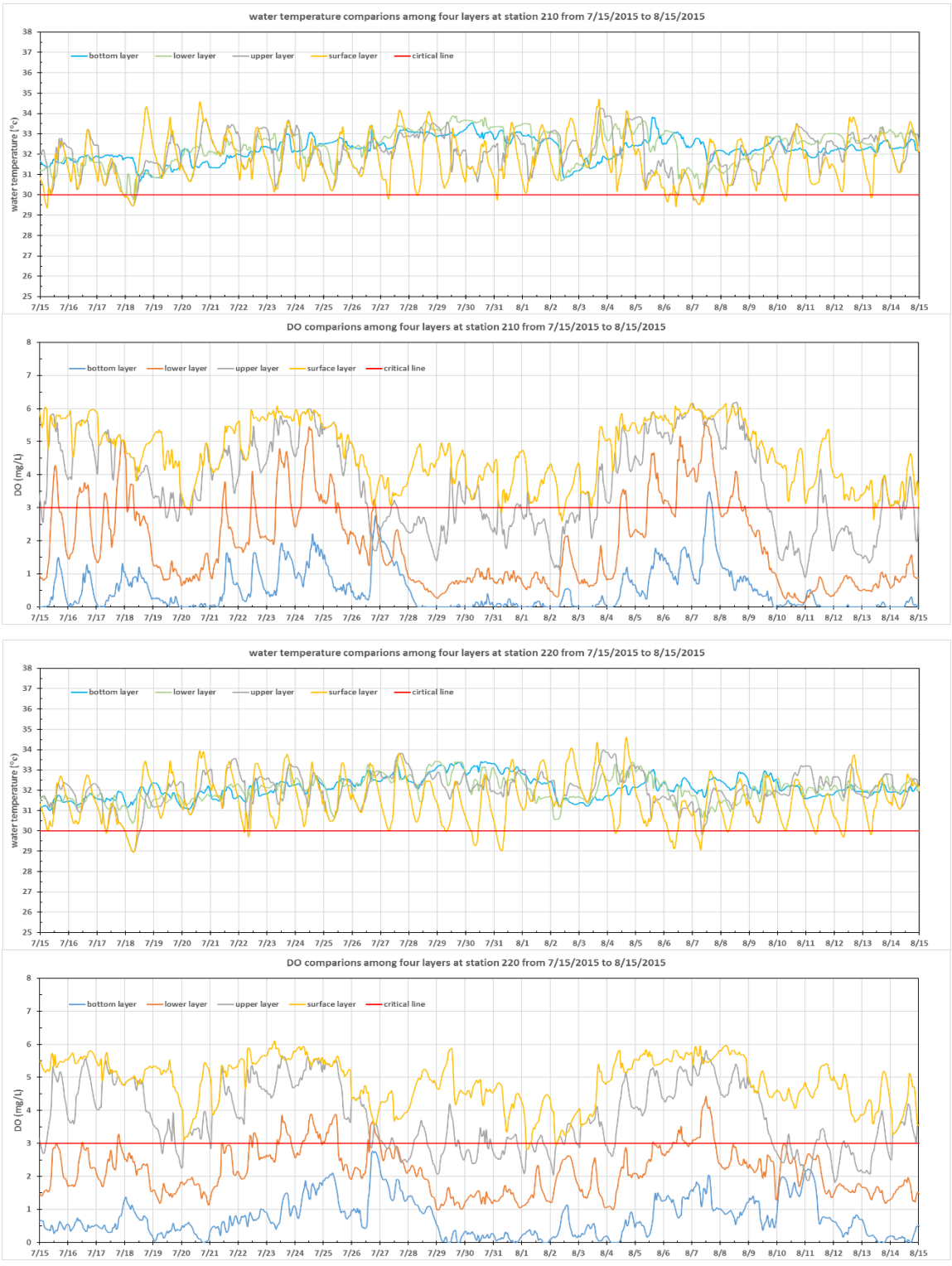

Figure 4-59 Time-series of simulated water temperature and DO among four layers at station 210 (top two frames, region 1) and 220 (region 2) from 7/15/2015 to 8/15/2015 (in region 1)

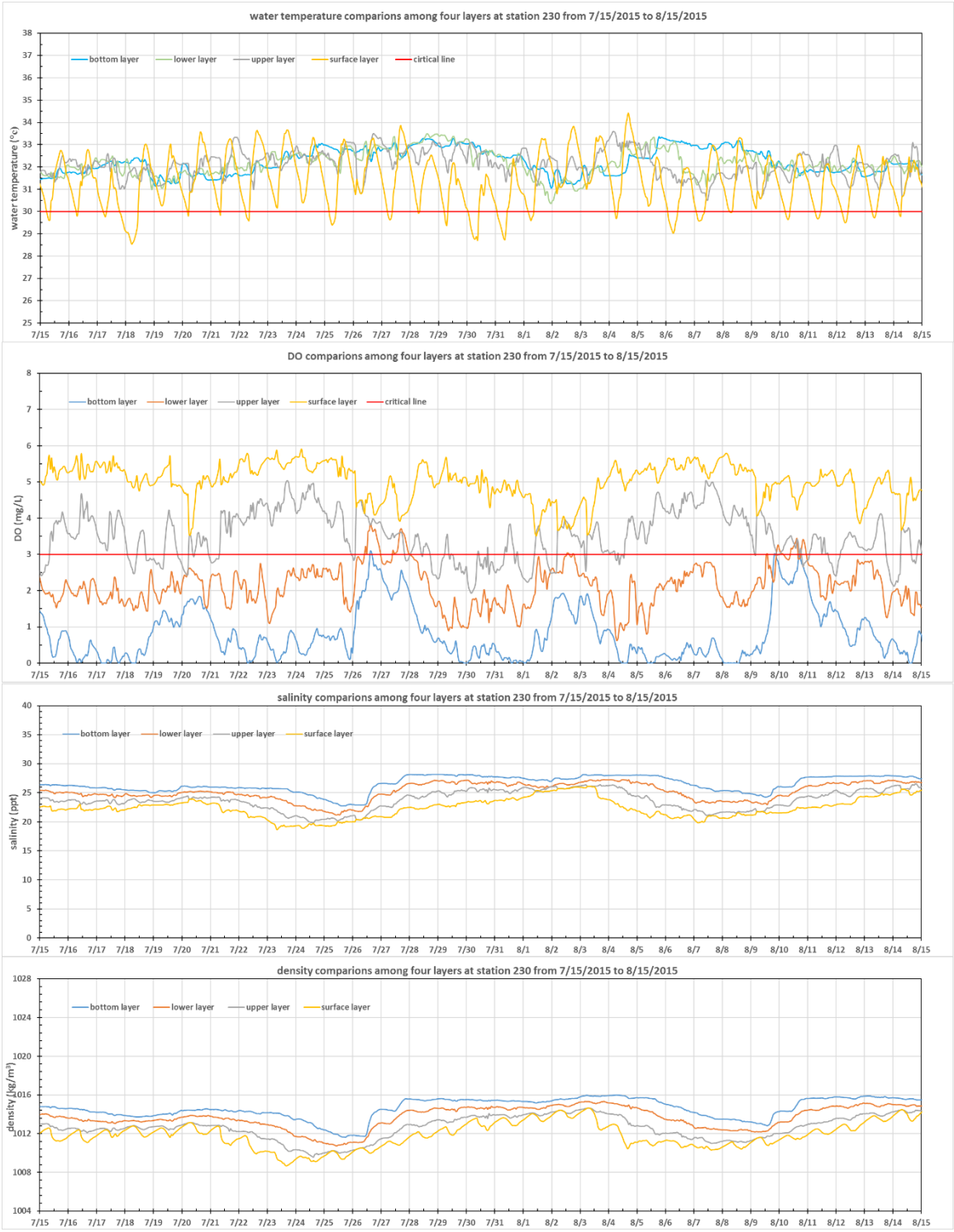

Figure 4-60 Simulated water temperature, salinity, density, and DO among four layers at station 230 (region 2) from 7/15/2015 to 8/15/2015 (in region 1)

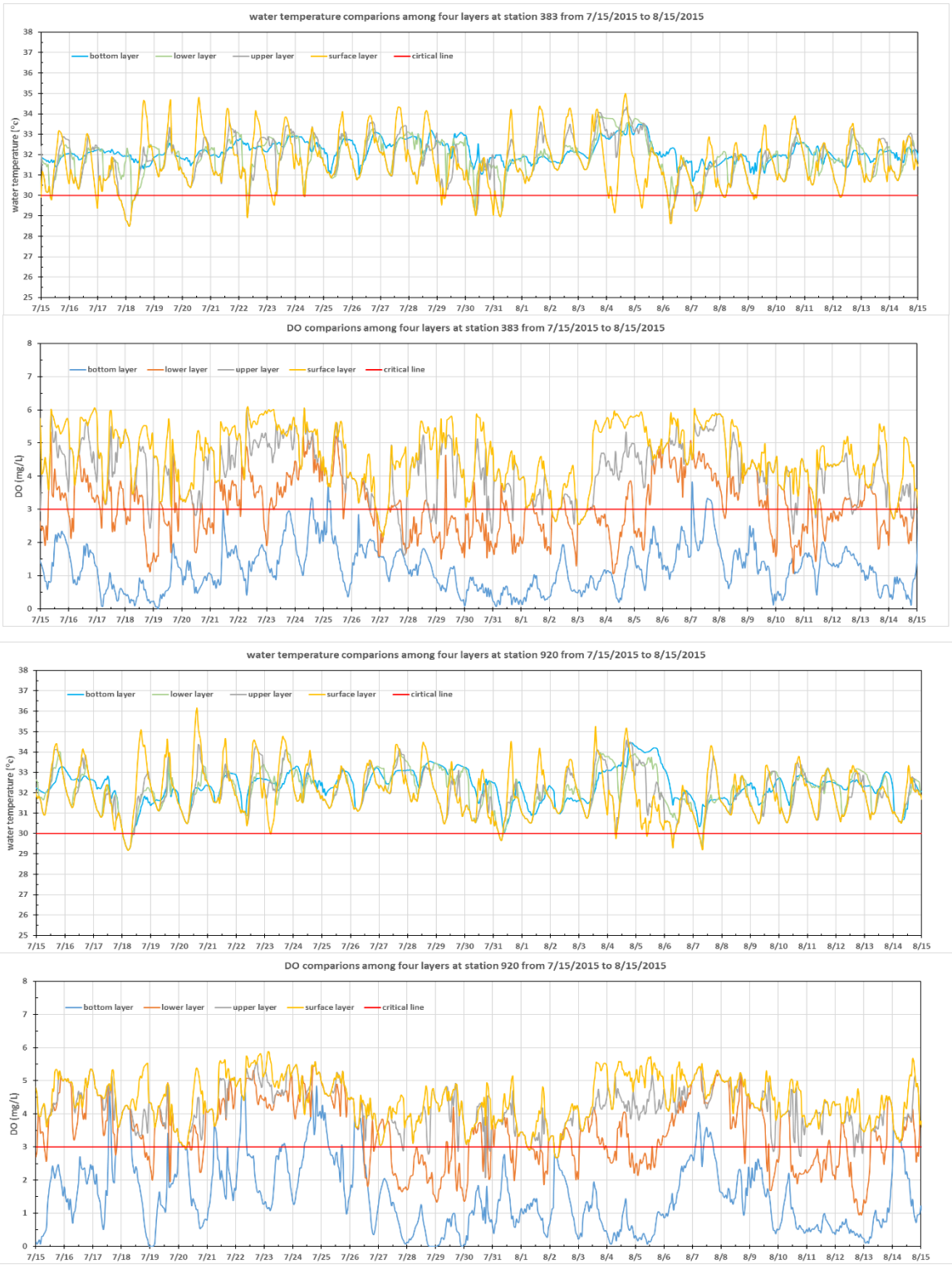

Figure 4-61 Time series of simulated water temperature and DO among four layers at station 383 (top two frames) and 920 from 7/15/2015 to 8/15/2015 (in region 2)

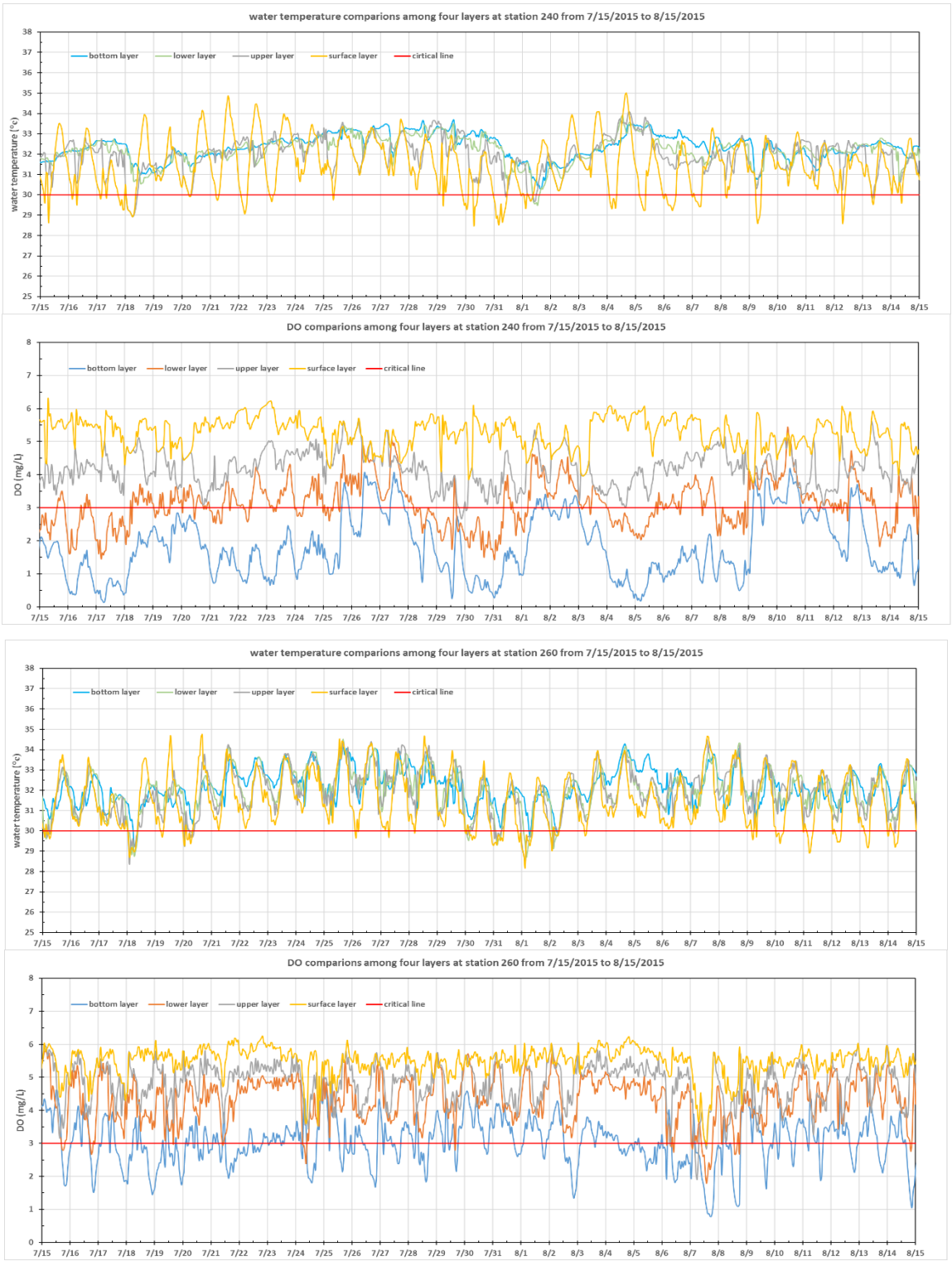

Figure 4-62 Time series of simulated water temperature and DO among four layers at station 250 (two top frames, region 2) and 260 (region 3) from 7/15/2015 to 8/15/2015 (in region 2)

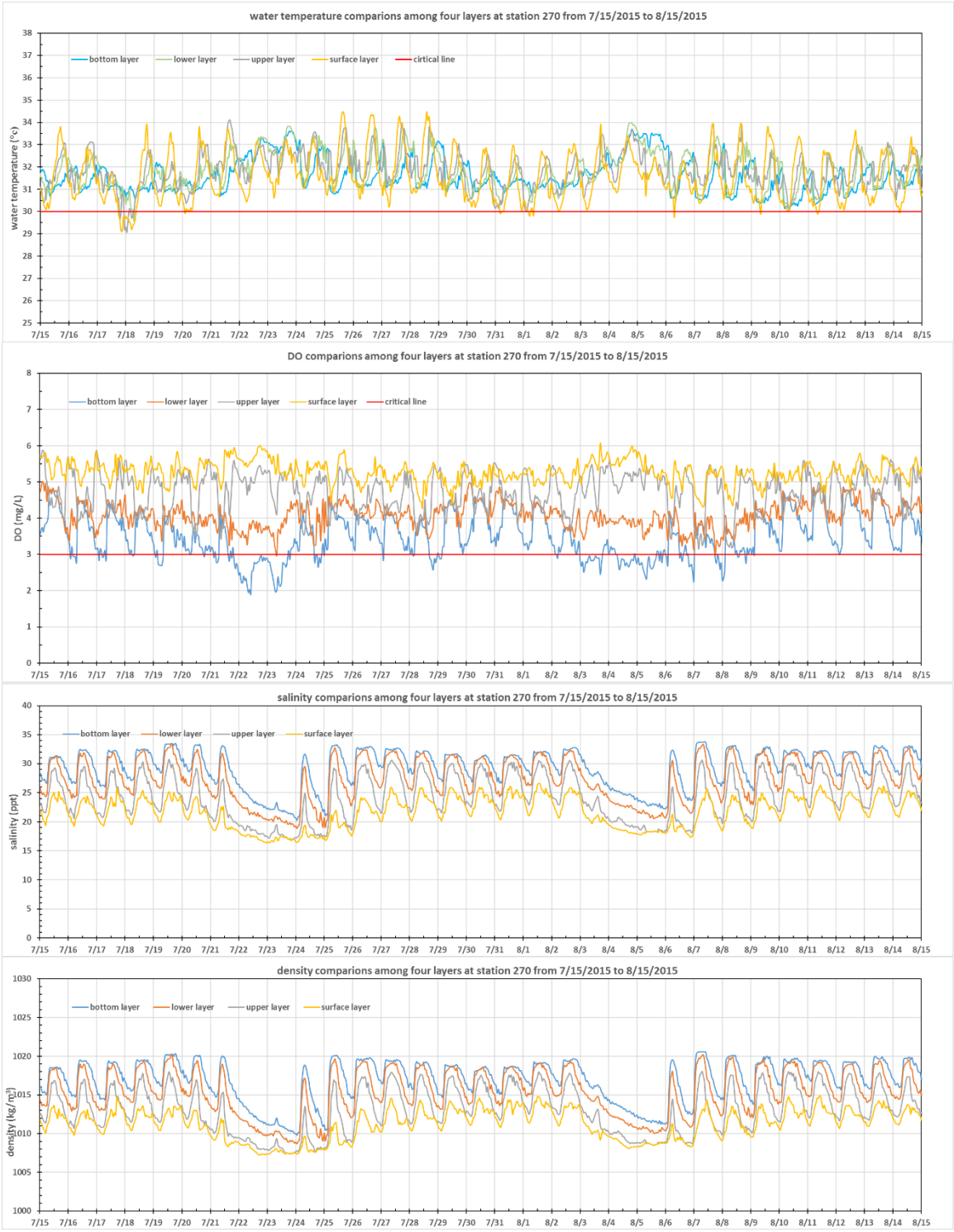

Figure 4-63 Time series of simulated water temperature, salinity, density, and DO among four layers at station 270 (region 3) from 7/15/2015 to 8/15/2015.

Figure 4-64 Time series of simulated water temperature and DO among four layers at station 555 (two top frames) and 634 from 7/15/2015 to 8/15/2015

4.3.3 Three-hour Average DO Analysis from 7/27/2015 to 8/5/2015 in Cotton Bayou

Figure 4-65—Figure 4-66 plot the three-hour average DO at four layers from 7/27 to 8/5 in 2015 for several stations in Cotton Bayou. In region 1 (stations 180—220), the DO stratification was very obvious and DO differences between the surface and bottom layer were large (Figure 4-65). DO concentration in the bottom and lower layers were less than 3 mg/L in the critical period 7/30–8/4/2015 when the fish kill of Gulf menhaden occurred. Most of DO in the upper layer were also less than 3 mg/L but in the surface layer were typically greater than 3 mg/L. DO show some daily variations in the surface and upper layers: maximum DO in the later night and minimum DO near the dawn. DO in the lower and bottom layers at stations 210 and 220 were very low with minimum daily variations and at station 190 had a similar magnitude of daily variations but the maximum and minimum occurred at a different time in comparison to the surface layer. Strong DO stratification was because region 1 was less affected by the tides. The lack of the tidal force furtherly inhabits the water vertical mixing, which caused the significant DO stratification as discussed before.

In region 3 where the region was frequently affected by both the freshwater and tides from Gulf of Mexico (stations 260—270), the DO difference among the layers were the smallest (Figure 4-66), e.g., at 11:00 am, the bottom DO concentrations were close to the upper DO concentrations. The surface and upper DO concentrations generally reached the maximum around 11:00 am. At station 270, when the surface and upper DO were the minimum in one day but it was the maximum at the lower and bottom layers. This is because spring tide primarily occurred at this time point. The upcoming tides will force the surface water with large DO into the bottom layer, which caused the vertical mixing. Due to more frequent mixing, most of DO in station 270 at all layers were higher enough for fish habitat (> 3 mg/L). At station 260, some DO concentrations at the bottom layer were less than 3 mg/L.

In the transitional region 2 (stations 230–250), the DO difference among different layers gradually decreased from west to east, since the bottom DO gradually increased due to the mixing. Besides, the bottom DO show larger and larger fluctuations from west to east, since affection from the tides gradually increased from west to east as discussed before.

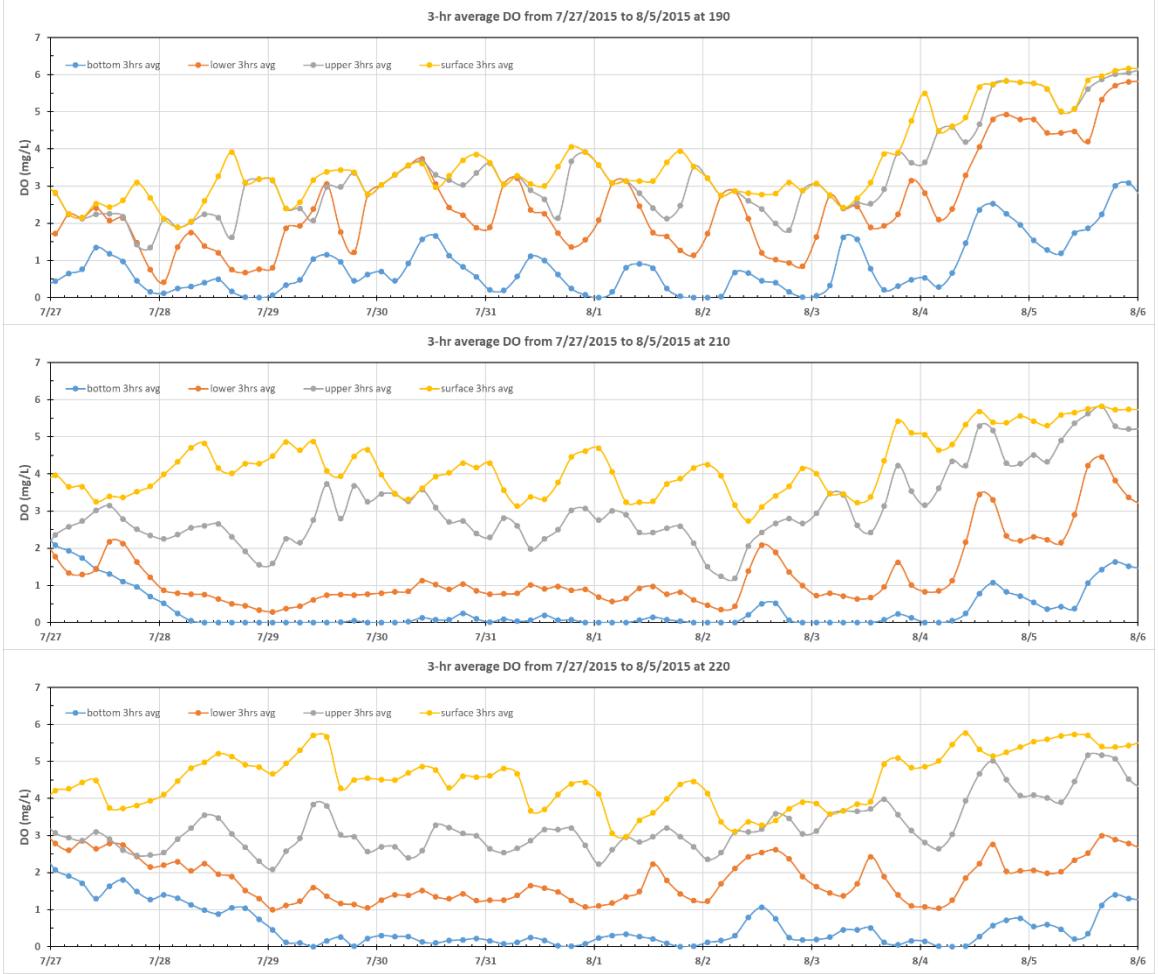

Figure 4-65 Three-hour average of simulated DO at stations 190, 210, 220 (region 1) in Cotton Bayou from 7/27 to 8/5/2015

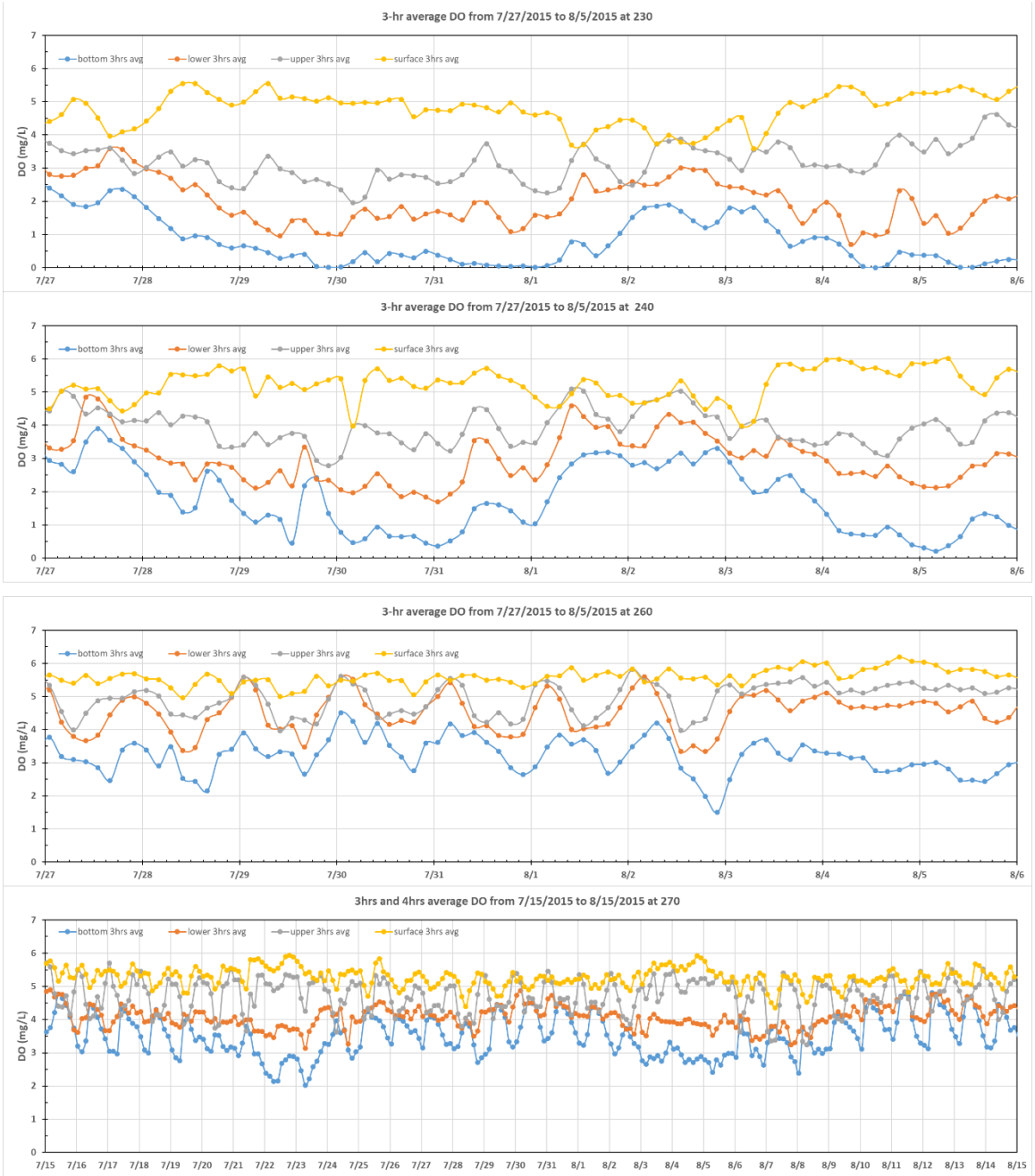

Figure 4-66 Three-hour average of simulated DO at stations 230, 240 (region 2), 260, and 270 (region 3) in Cotton Bayou from 7/27 to 8/5/2015

4.3.4 Contour Map of DO from 7/230/2015 to 8/5/2015

In contrast with the previous time-series plots that only focus on one station, the surface and bottom DO contour map (7/30/2015 to 8/5/2015) in the Cotton Bayou and its adjacent Terry Cove are shown in Figure 4-67—Figure 4-73. The DO contours were divided into ten groups from 0 to 5 mg/L with 0.5 mg/L as an interval. Each group was assigned a distinctive color by the color ramp from red to blue, which red means 0 mg/L and blue means 5 mg/L (the legends cannot be zoomed in the contour map of EFDC). For the DO concentration higher than 5 mg/L were assigned a grey color. The green colors represent the range from 2 to 3.5 mg/L (lower DO has a more yellow color in green).

The bottom DO in the region 1 of Cotton Bayou gradually deteriorated from 7/30 to 8/2 in 2015. Beginning 8/3/2015, the bottom DO increasingly came back. From 7/30 to 8/2, the east part of region 1 continuously suffered the lower DO concentrations (< 1 mg/L). For the west part of region 1, however, they decreased from 2 to < 1 mg/L (color changing from light green to red). On 8/4, the bottom DO in the west part increased to be higher than 3 mg/L, while the bottom DO in the east part was still lower than 3 mg/L. Comparing with the east part of region 1, the west region more easily got rid of the low DO because the shallow water (< 1 m) is more easily mixed by the wind, making the surface DO reach to the bottom. Unlike the region 1, the bottom DO in region 3 kept on decreasing from 7/30 to 8/5. The bottom DO in the west part of region 3 decreased from around 4.5 to 3 mg/L while the DO at east part changed from 5 to 3.5 mg/L The bottom DO in the west part of region 3 were generally slightly lower than DO in the east part. This is because the east part was more heavily affected by the tides which can push the surface DO to the bottom. Although the DO continuously decreased, they were still higher than 3 mg/L in region 3. The bottom DO in region 2 exhibited different change pattern comparing with changes in region 1 and region 2. The bottom DO decreased from 7/30 to 7/31 and then gradually increased to 8/2. Since 8/2, the bottom DO decreased again. In Terry Cove, the bottom DO at the region along the shoreline decreased

from 8/1 to 8/2 (5 to 4.5 mg/L) and the increased from 8/3 to 8/5. For the other parts of Terry Cove, the bottom DO continuously decreased from 5 to 3 mg/L.

For the DO concentrations in the upper layer in the region 1 of Cotton Bayou, they decreased gradually until 8/3 and then increased. The DO in the upper layer at the east part remained around 3.5 mg/L by and large before 8/3 and then increased to higher than 5 mg/L, while the upper DO at the west part continuously increased from 3.5 mg/L to higher than 5 mg/L except for 8/2 with 3 mg/L. Unlike the bottom layer, the DO in the upper layer at the west part was slightly lower than one in the east part. This might be caused by higher surface average salinity in the west part since there was less interaction between tide and still water comparing with the east part. The higher salinity decreased the DO solubility. For the region 3, the DO changed dynamically but the values were generally higher than 4 mg/L. For the upper region of the east part in region 3, the DO in the upper layer were continuously higher than 5 mg/L from 7/30 to 8/5. For the DO in the upper layer in region 2, they generally show a similar change trend with the data in region 1 that decreased gradually until 8/3 and then increased. For the east part, the DO in the upper layer was generally higher than the 4 mg/L while in the west part, the DO in the upper layer remained around 4 mg/L (7/30—8/3) and then increased to higher than 5 mg/L. For the DO in the upper layer in Terry Cove, they were higher than 5 mg/L although there existed a slight decrease on 8/2.

Overall, daily average DO contour maps show that bottom DO concentrations in Cotton Bayou had mortality conditions (< 3 mg/L) in different places (regions) from 7/27 to 8/4/2015 and upper DO concentration had high stress to fish (< 5 mg/L), which was lower than normal water quality standard to sustain aquatic habitat.

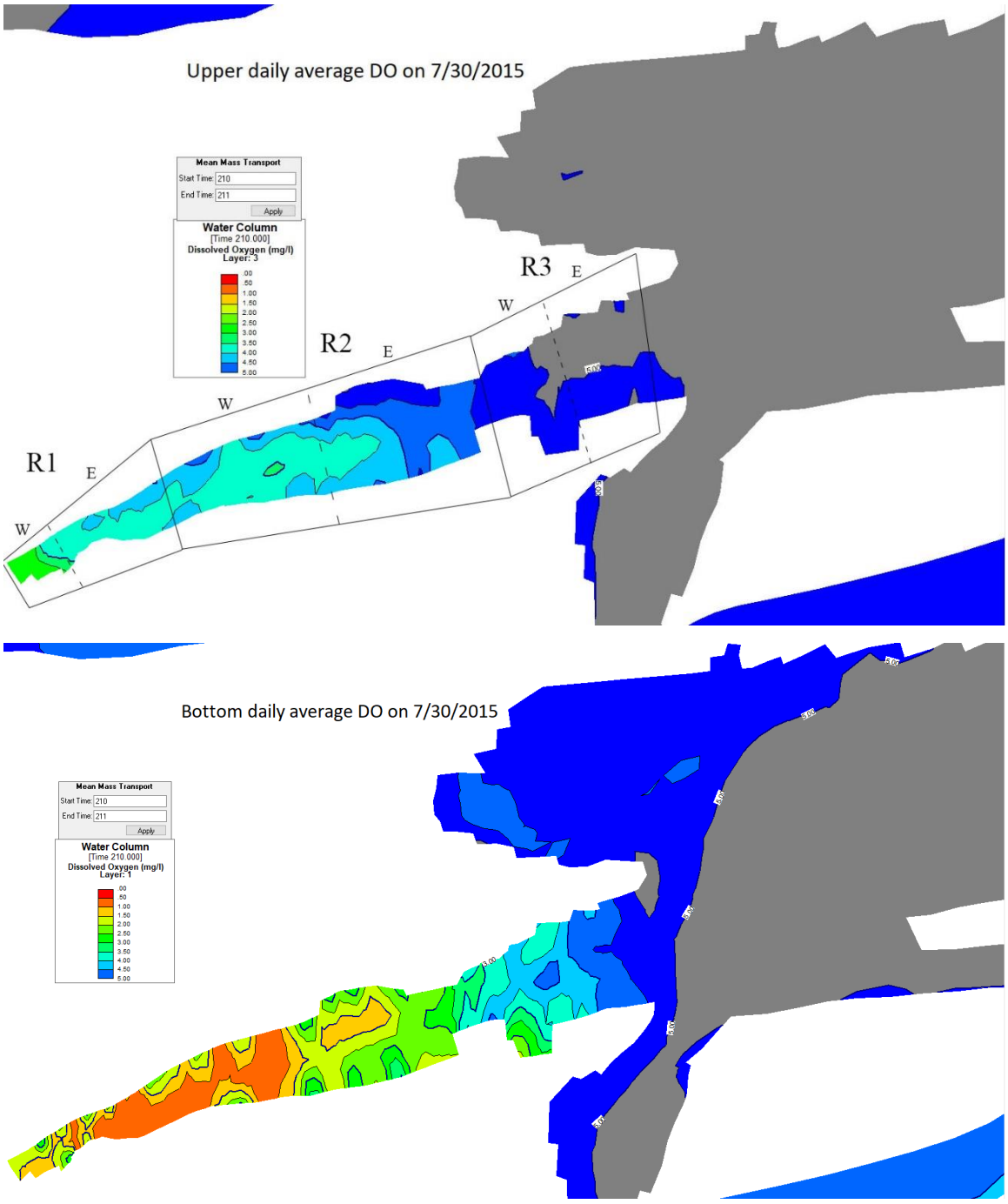

Figure 4-67 Upper- and bottom-layer daily average DO contour maps on 7/30/2015 (W indicates west and E for East part of each sub-region in Cotton Bayou)

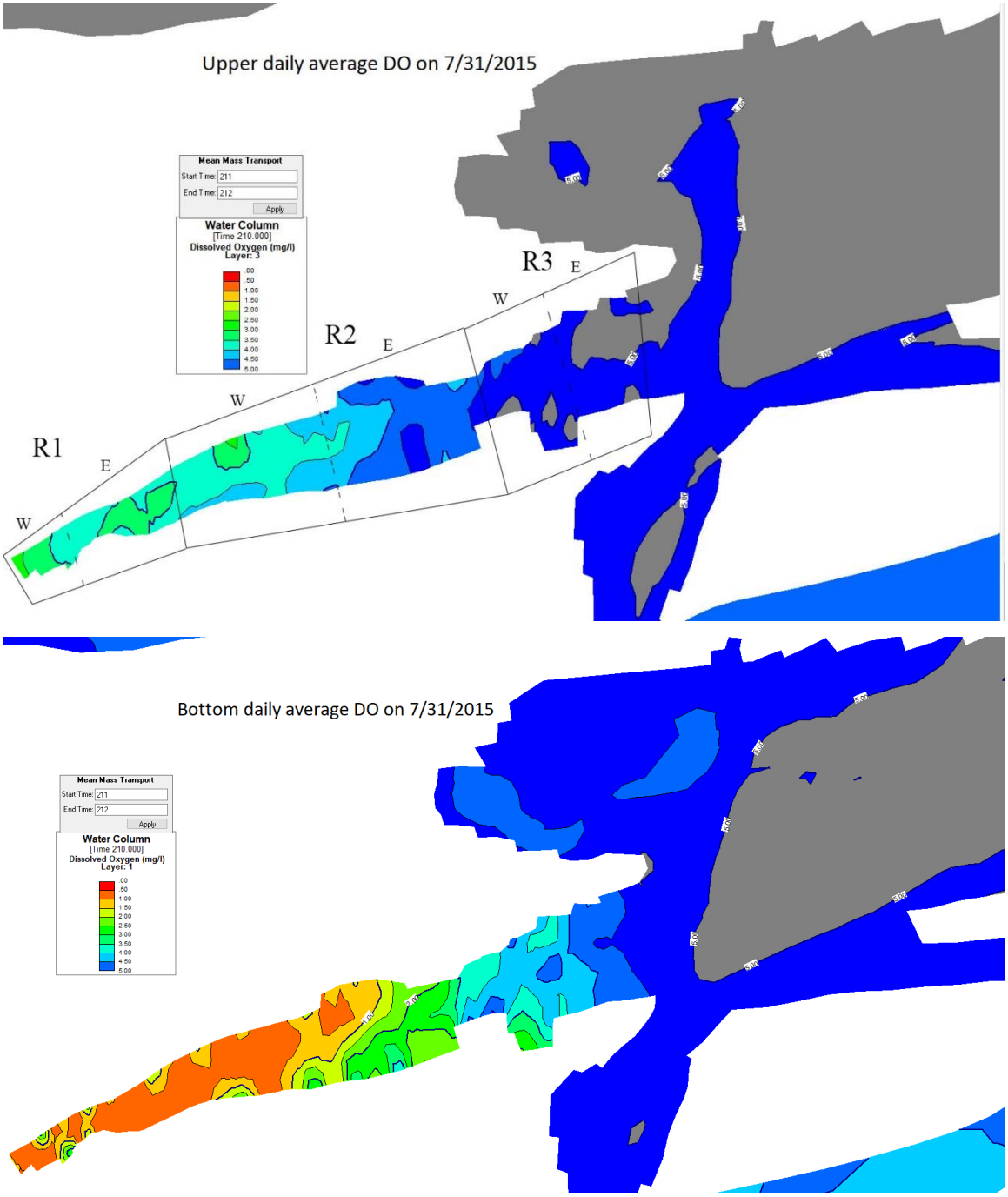

Figure 4-68 Upper- and bottom-layer daily average DO contour maps on 7/31/2015 (gray color for DO > 5 mg/L)

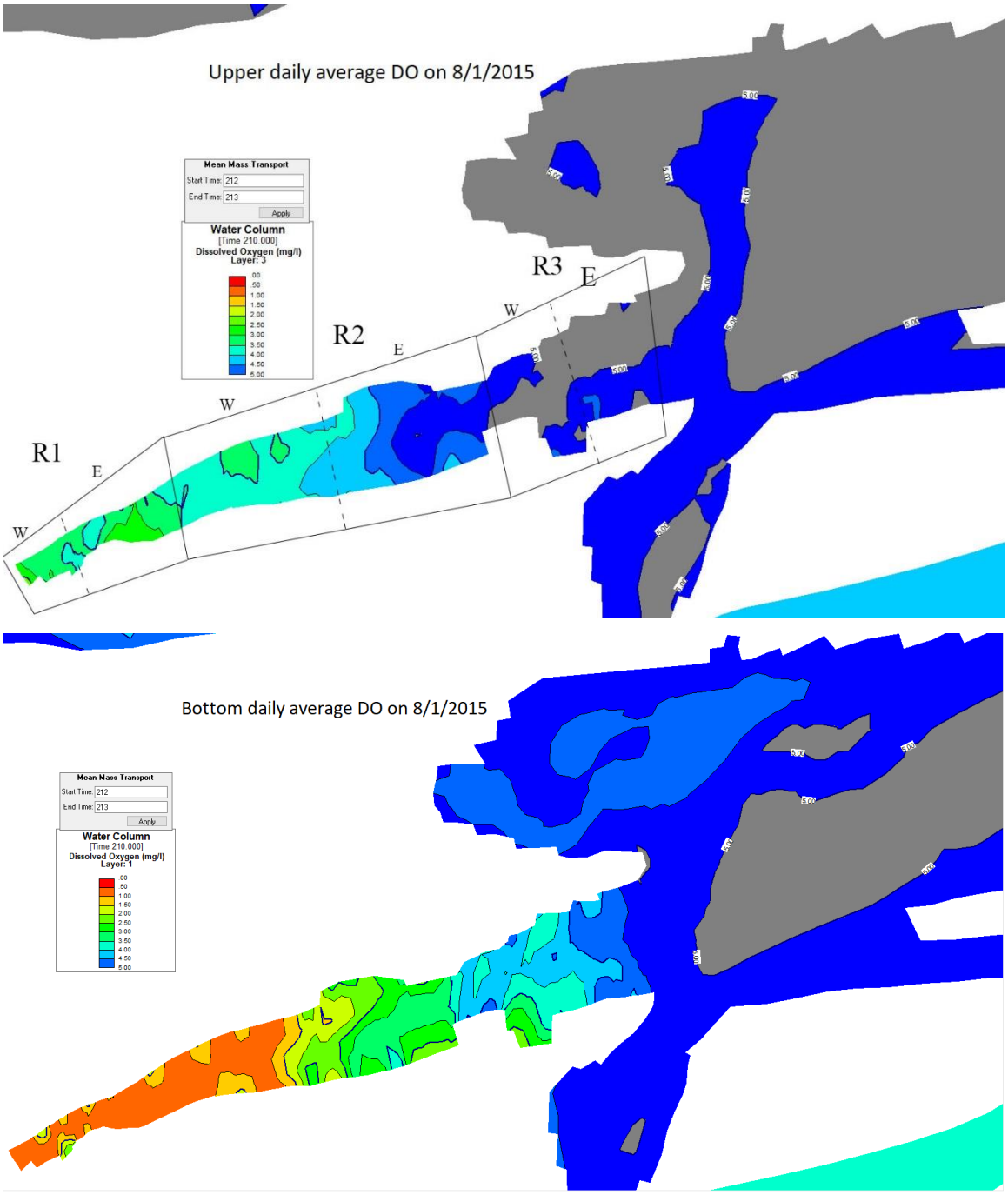

Figure 4-69 Upper- and bottom-layer daily average DO contour maps on 8/1/2015

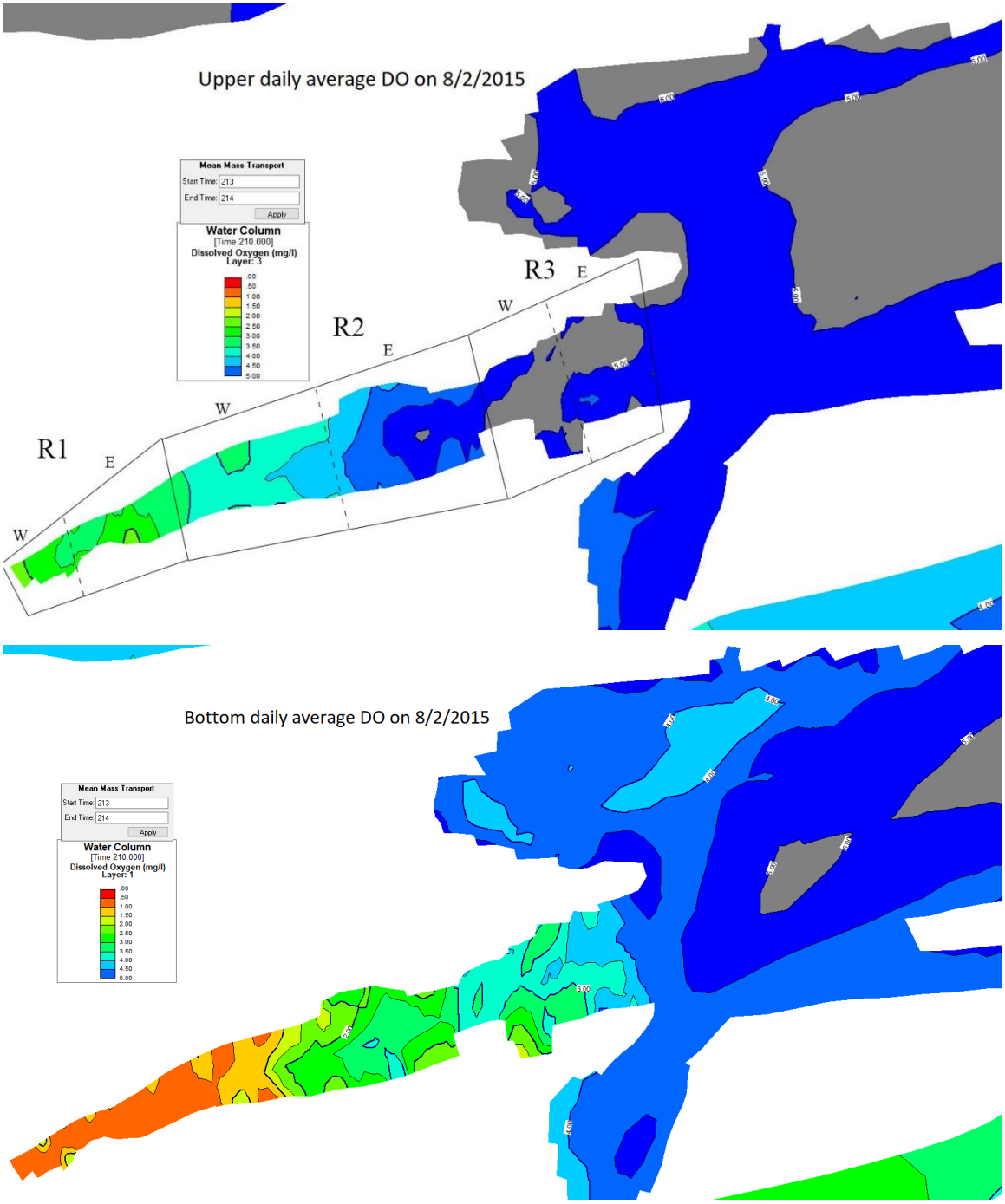

Figure 4-70 Upper- and bottom-layer daily average DO contour maps on 8/2/2015

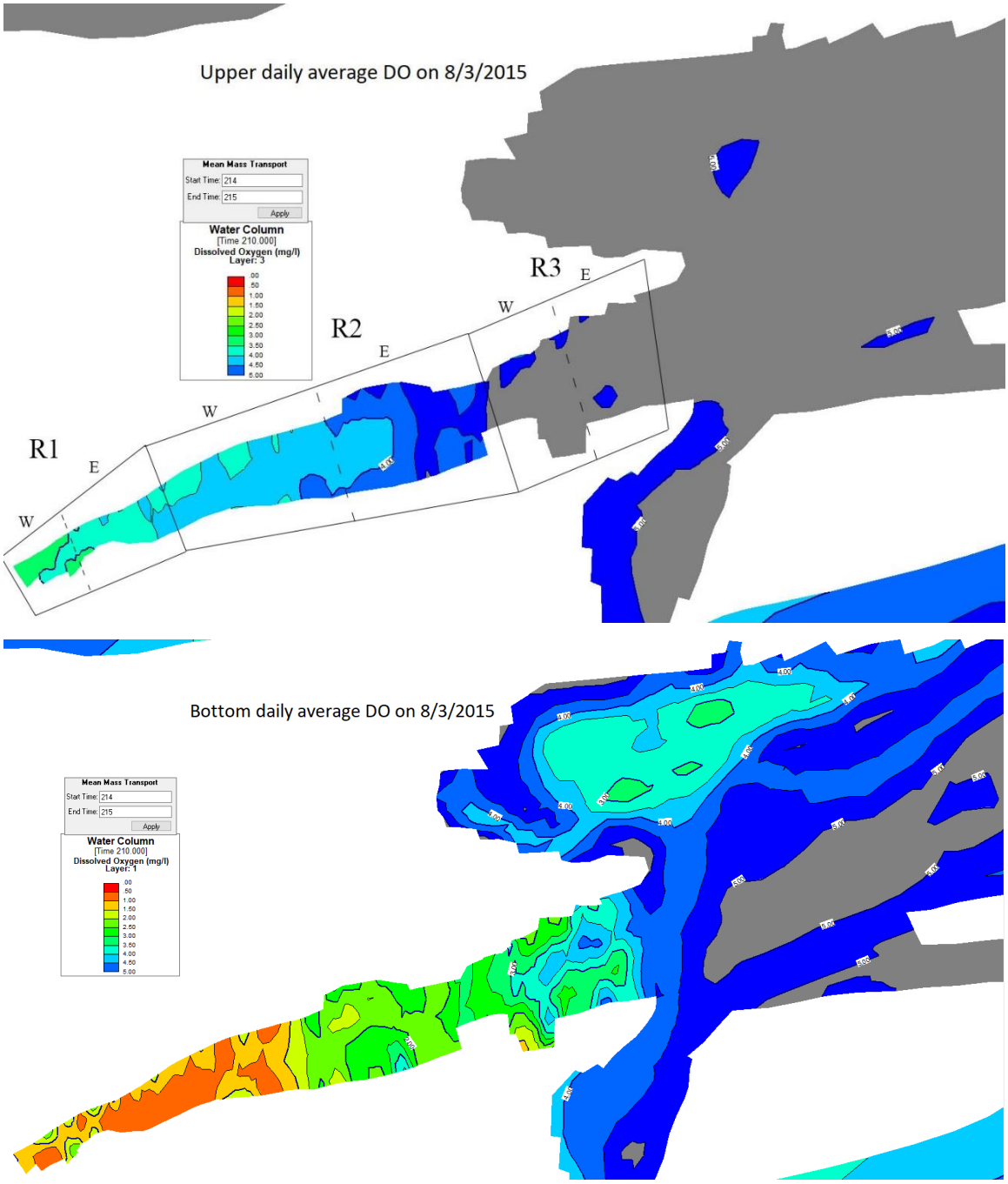

Figure 4-71 Upper- and bottom-layer daily average DO contour maps on 8/3/2015

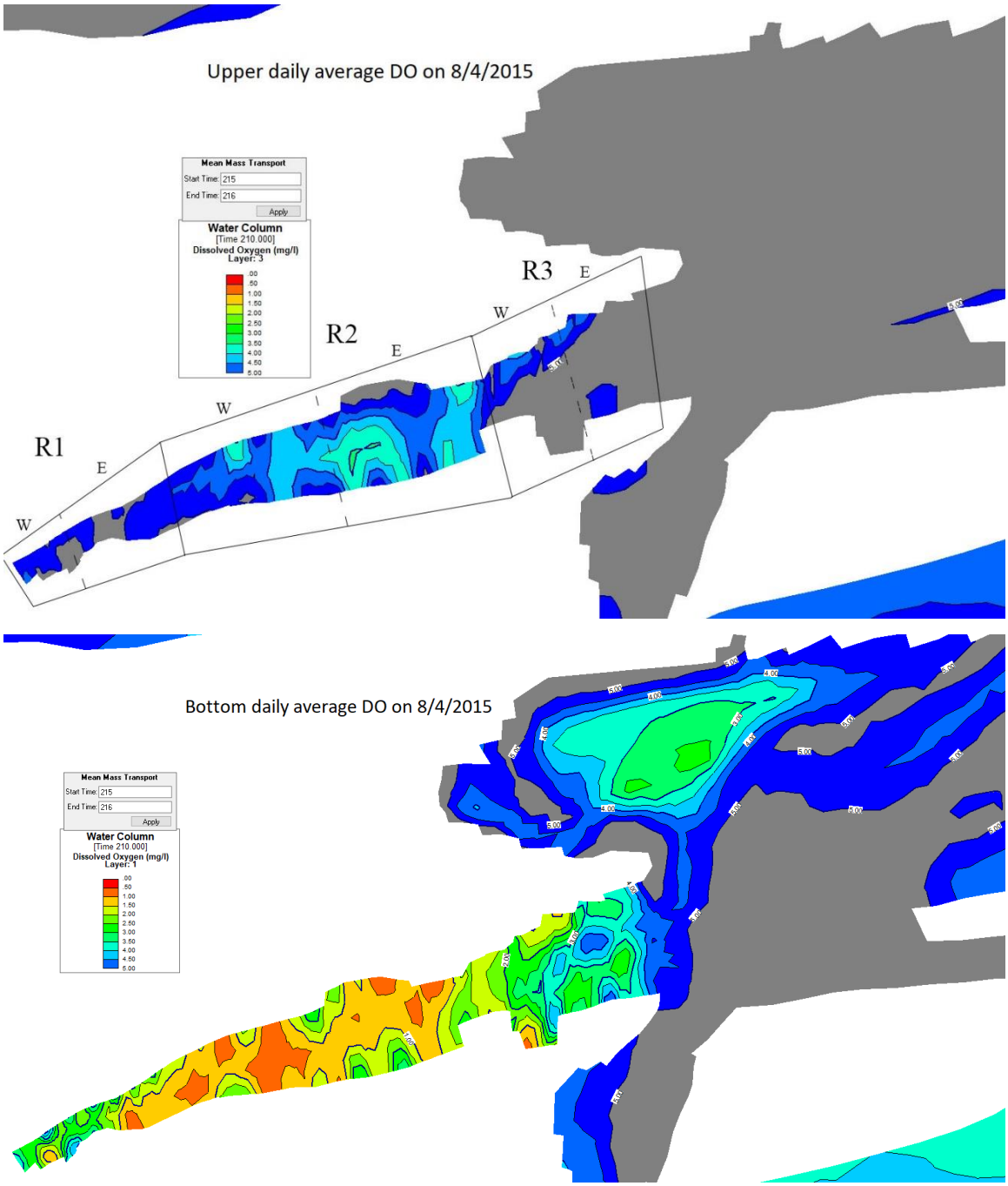

Figure 4-72 Upper- and bottom-layer daily average DO contour maps on 8/4/2015

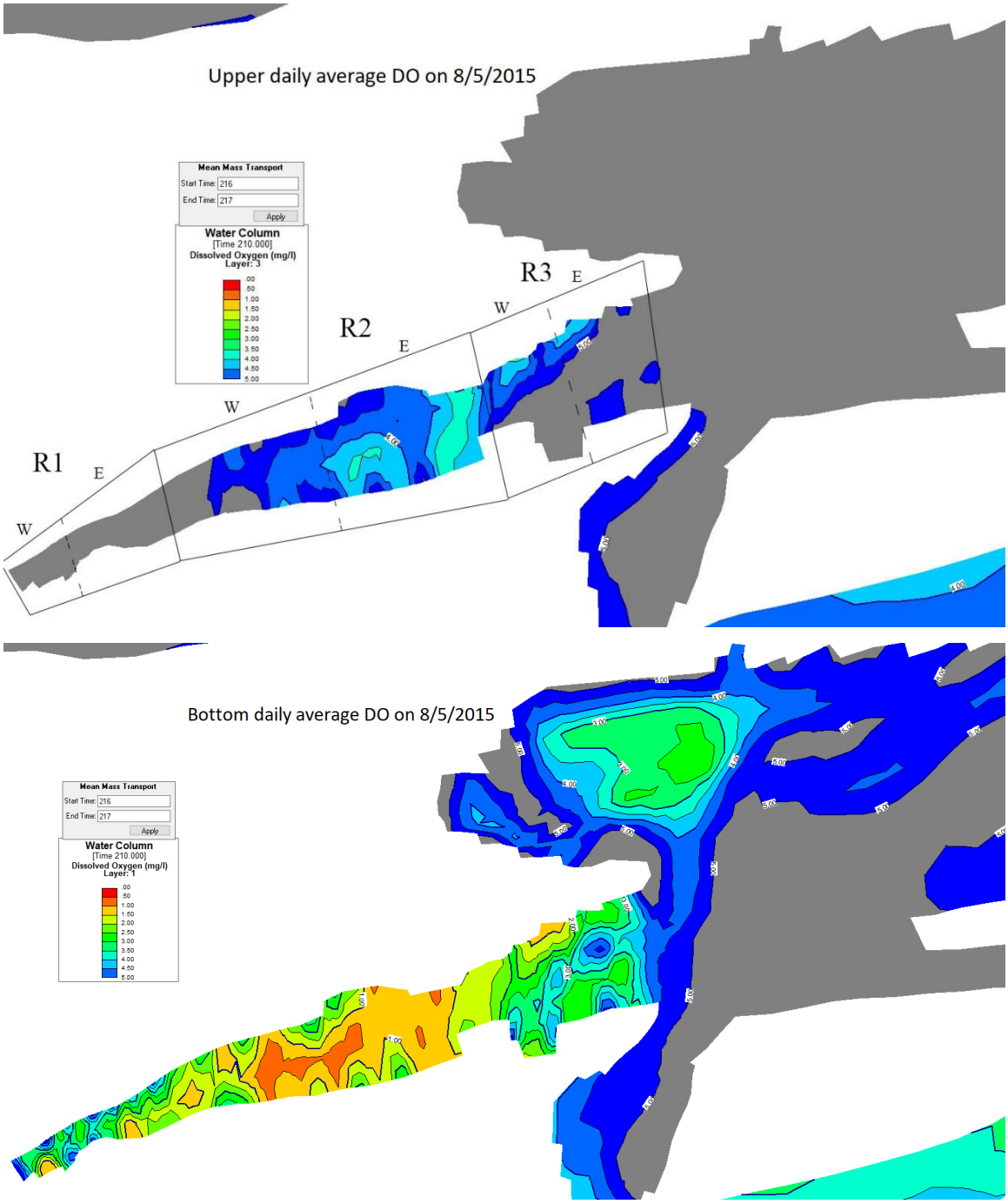

Figure 4-73 Upper- and bottom-layer daily average DO contour maps on 8/5/2015

4.3.5 Gulf Menhaden Habitat Analysis

Figure 4-74 shows the simulated DO and projected lethal DO concentrations based on the water temperature using Eq. 4.4 in the surface- (upper panel) and bottom-layer (middle panel) from 7/15 to 8/15 in 2015 at station 200.

$$DO_{lethal} = 3.0 + 0.000005e^{0.41T_{lethal}} \quad (4.4)$$

where DO_{lethal} and T_{lethal} are the DO concentrations (in mg/L) and the water temperatures (in °C), respectively, which define the hypothetic lethal niche boundary for menhaden. This was based on the lethal niche boundary for cisco (Equation 1.1) by Jacobson et al. (2008). Minimum lethal DO of 3.0 mg/L is used for Gulf menhaden, slightly larger than 2.5 mg/L used in a previous study for warm-water fish species, and much large than 0.4 mg/L for cisco in cold regions (Minnesota, Wisconsin, and Michigan) since many cold-water fish species could survive at very low DO during the winter ice cover period at temperature of 0–4 ^{o}C. For Gulf menhaden, there is no ice cover in the estuary of the study area, and water temperatures are ~ 10 ^{o}C (Figure 4-27) in winter.

Using the hypothetic lethal niche boundary for menhaden, for both surface and bottom layers, the projected lethal DO change dynamically and are higher than 3 mg/L, a suggested minimal DO to support Gulf menhaden (Lassuy 1983). The projected lethal DO in the surface layer have a similar change pattern with the simulated water temperatures (Figure 4-58) since lethal DO are an exponential function of water temperatures (Equation 4.4). When calculated lethal DO is greater than 7 mg/L, it means Gulf menhaden could not survive at that temperature since saturated DO at normal salinity would not higher than 7 mg/L when temperature > 30 ^{o}C. The hypothetical niche boundary curve using Equation 4.4 indicates Gulf menhaden could not live above 33 ^{o}C water, which is slightly lower than 34.9 ^{o}C when menhaden was also found (Lassuy 1983). The surface layer at station 240 had high enough DO at certain periods that were a possible habitat for Gulf menhaden. Overall the surface layer could support Gulf menhaden about 55% of the time from

7/15 to 8/15, while there were only 2% time periods that the simulated DO were higher than lethal DO in the lower-layers (Table 4-13). The percentage of habitat time periods (simulated DO higher than projected lethal DO) at other stations are listed in Table 4-13. The surface-layer oxythermal habitat percentage increases from west (region 1) to east (Perdido Pass Complex). For the other three layers, the percentages at stations 210, 220, and 230 (region 2) were lower than the values at station 180, 190, and 200 (region 1). This is because the average DO in the deeper layers in region 1 were slightly higher than ones in region 2 and the lethal DO are similar due to the similar water temperatures (Table 4-14). The lower panel of Figure 4-74 shows the total number of layers with menhaden habitat, i.e., the simulated DO is higher than the projected lethal DO, from 7/15 to 8/15. The maximum number of the habitat layers was 3 meaning that menhaden could live in top three layers excluding the bottom layer. As long as the number of the habitat layers is 1 or greater, menhaden could live in one or more layers.

When the number of the habitat layers becomes zero, summer kill for Gulf menhaden would occur since there are no places along the water column for menhaden to survive, which was projected to exist in some periods at station 240. Figure 4-75 shows the total number of habitat layers at station 200, 230, 240 and 260 from 7/31 to 8/3/2015 (4 days), where and when the fish kills occurred in Cotton Bayou (Figure 1-2). For the surface- and upper-layer, the percentages of habitat periods are 16% and 9% at station 200 from 7/15 to 8/5/2015, respectively. The lethal DO were higher than simulated DO in the other two layers, which gives 0% habitat at station 200. The surface-layer DO at station 230 were more favorable for the living of Gulf menhaden with 29% habitat periods, but occurred before the noon on 8/1 in 2015; there were fish kills afterward. At stations 240 and 260 (east of station 230), some time periods had fish kills and other time periods had the DO in at least one layer with high enough DO for Gulf menhaden to survive. Only at station 634, near Perdido Pass, it always one layer with menhaden habitat. These results were when COD was not activated.

Table 4-13 Percentage of habitat time periods (simulated DO higher than projected lethal DO) in four layers from 7/15 to 8/15 in 2015

Stations	Bottom layer	Lower layer	Upper layer	Surface layer
180	1% (0%)[1]	12% (0%)	17% (0%)	17% (0%)
190	1% (0%)	9% (0%)	14% (0%)	16% (2%)
200	0% (0%)	0% (0%)	9% (0%)	16% (2%)
210	0% (0%)	3% (0%)	20% (0%)	34% (9%)
220	0% (0%)	0% (0%)	16% (0%)	45% (9%)
230	0% (0%)	0% (0%)	1% (0%)	50% (29%)
240	0% (0%)	2% (5%)	15% (26%)	55% (57%)
250	0% (0%)	3% (11%)	24% (39%)	62% (75%)
260	1% (3%)	17% (35%)	36% (51%)	64% (73%)
270	5% (0%)	7% (6%)	25% (33%)	59% (67%)
555	1% (0%)	3% (0%)	26% (38%)	68% (67%)
634	3% (12%)	31% (37%)	47% (42%)	64% (67%)
383	0% (0%)	6% (0%)	20% (4%)	30% (8%)
920	1% (0%)	5% (0%)	8% (0%)	14% (4%)

Note: [1]—Numbers inside brackets were the statistical percentage from 7/31 to 8/3 in 2015

Table 4-14 Average DO (mg/L) and water temperatures (°C) in four layers from 7/15 to 8/15 at stations in the Cotton Bayou

Stations	Bottom layer	Lower layer	Upper layer	Surface layer
180	1.08 (32.23)[1]	2.72 (32.21)	3.79 (32.12)	3.99 (32.20)
190	1.50 (32.40)	3.26 (32.24)	3.94 (32.14)	4.16 (32.17)
200	0.99 (32.46)	2.66 (32.33)	4.07 (32.04)	4.48 (31.97)
210	0.50 (32.24)	1.88 (32.32)	3.71 (32.02)	4.60 (31.72)
220	0.73 (32.13)	2.15 (32.02)	3.79 (32.00)	4.83 (31.53)
230	0.79 (32.22)	2.13 (32.14)	3.53 (32.09)	4.99 (31.37)
240	1.82 (32.33)	3.15 (32.15)	4.20 (31.88)	5.24 (31.42)
250	2.28 (32.15)	3.47 (32.18)	4.32 (31.91)	5.39 (31.34)
260	3.05 (32.15)	4.30 (32.00)	4.83 (31.88)	5.47 (31.47)
270	3.51 (31.60)	4.10 (31.82)	4.73 (31.83)	5.27 (31.56)
555	2.64 (31.59)	3.63 (31.84)	4.59 (31.73)	5.60 (31.23)
634	3.61 (31.82)	4.81 (31.66)	5.31 (31.64)	5.70 (31.51)
383	1.25 (32.09)	3.10 (31.80)	4.10 (31.61)	4.59 (31.60)
920	1.57 (32.25)	3.48 (32.06)	4.16 (31.90)	4.42 (32.00)

Note: [1]—Numbers outside brackets were average DO with unit mg/L and average water temperature are listed inside the bracket with unit °C from 7/15 to 8/15

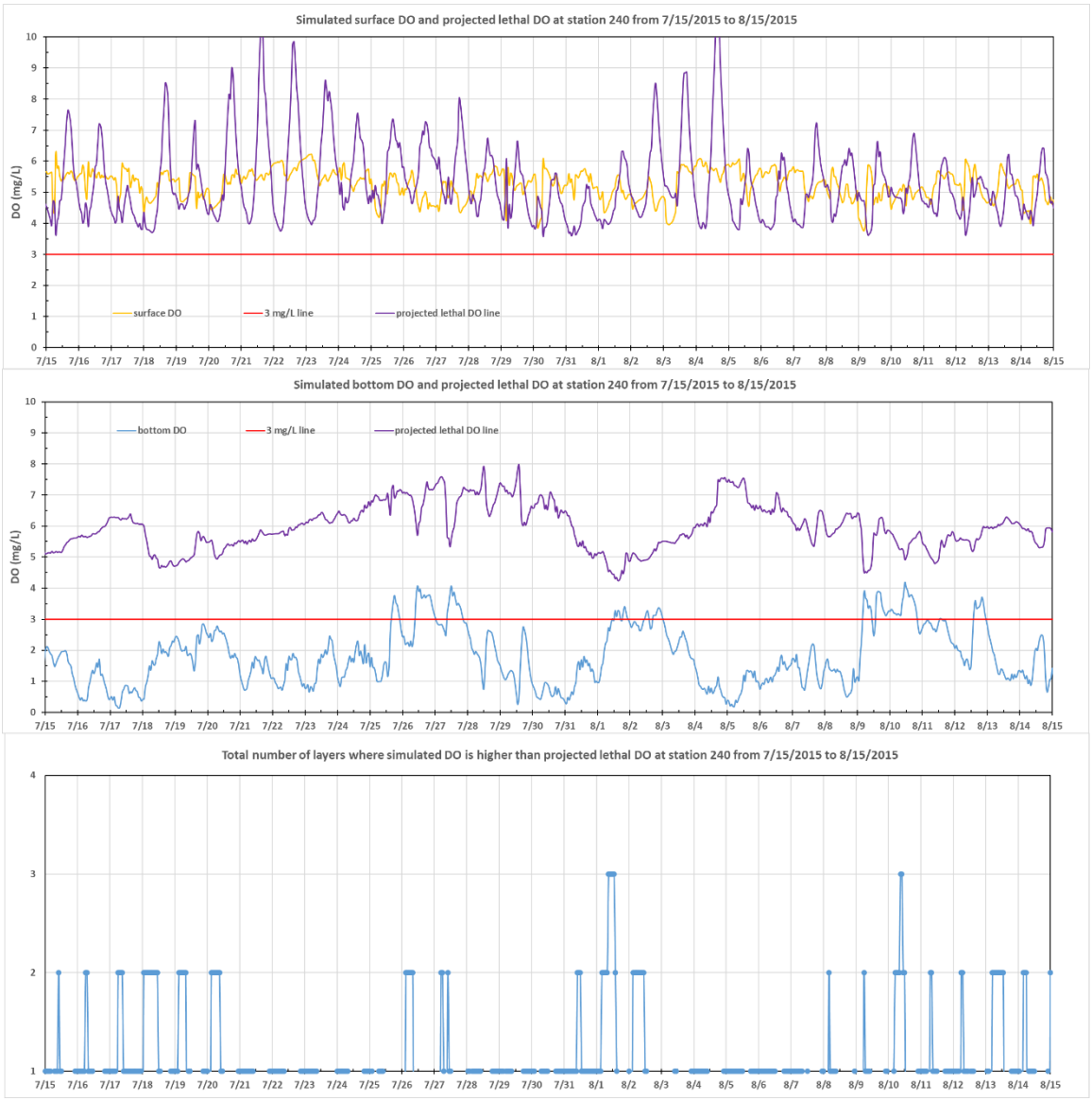

Figure 4-74 Time-series of simulated DO and the projected lethal DO based on simulated water temperatures from 7/15 to 8/15 in 2015 at station 240: surface layer (upper panel) and bottom layer (middle panel). The lower panel is the total number of layers where simulated DO is higher than the projected lethal DO.

Figure 4-75 The total number of habitat layers where simulated DO is higher than the projected lethal DO at stations 200, 230, 240 and 260 from 7/31 to 8/3/2015 (4 days).

4.4 Sensitivity Analysis

Although water temperature, salinity, and DO simulation results in the previous section have shown that the current EFDC model was a trusted hydrodynamic and water quality simulator, there are still rooms to improve the accuracy of the model, especially for DO. The measured DO that was used to validate the model was from the surface water by the citizen volunteers from AWW (Alabama Water Watch), except for the observed data from Perdido Pass station that were collected at 0.5 m off the bottom. The SOD was set to the constant value, 0.9 $g/m^2/day$, and COD was not activated due to the lack of the observed data. Limited by the locations of observed DO and fixed SOD setting for the whole study area, there was room to improve the accuracy of DO simulated results, especially for the Wolf Bay region. The larger fluctuation of observed DO at 04012041 and 04012042 show that the SOD and COD should be different for different regions and changed with time (Figure 4-35 and Figure 4-36). Besides, the wind direction and wind speed also played an important role in the DO simulation at different layers through mixing the water at different layers, especially for the shallow water. The use of fixed wind speed and direction from Jay station may not be suitable to every part in the study area. Thus, the sensitivity analysis was done by changing the COD, SOD, wind direction, and wind speed. Three stations, 190, 240, and 260 from three regions of Cotton Bayou were pick up to look into how these model parameter values would affect the DO at different layers.

4.4.1 DO Analysis using Different COD

COD stands for chemical oxygen demand, which is a sink term in the DO calculation representing the reduction of DO caused by chemical reactions (Eq. 2.23). It is calculated based on the following equation,

$$\frac{\partial COD}{\partial t} = \frac{DO}{KH_{COD} + DO} KCOD \cdot COD + \frac{BFCOD}{\Delta z} + \frac{WCOD}{V} \tag{4.5}$$

where KH_{COD} = half saturation of DO required for oxidation of COD (g O^2/m^3); *KCOD* = oxidation rate of COD (day^{-1}); *BFCOD* = COD sediment flux (g $O^2/m^2/day$); and *WCOD* = external loads of COD (g O^2/day).

In EFDC model, default values for KH_{COD} and *KCOD* are 1.5 mg/L O_2 and 0.1 day^{-1}. The reference temperature for COD decay rate is 20 ^oC and temperature adjustment coefficient θ_{COD} is 0.041. These default values were used in the current EFDC model for the sensitivity analysis in Perdido and Wolf Bay system, but *WCOD* as the external source was not used. Therefore, only *BFCOD* was adjusted since the sediment composition and chemical reaction rates could be different in different regions of the study area. The simulated DO concentrations in the four layers at station 190 (as an example) were plotted in Figure 4-76 using the three selected *BFCOD* values (3, 6, and 12 g $O^2/m^2/day$). Figure 4-77 to Figure 4-79 show the simulated surface and bottom DO using the above three *BFCOD* at stations 190, 240, and 260 in comparison to the simulation without COD modeling. The average DO from 7/27 to 8/5 in 2015 in the four layers using four *BFCOD* are summarized in Table 4-15.

Figure 4-76 shows that the simulated DO concentrations in all four layers decrease with the increase of *BFCOD*. Simulation results from EFDC show that the increase of BFCOD affect the DO concentrations in every layer but does not change the DO vertical structure: the higher DO in the surface layer and lower DO in the bottom layer. Figure 4-77 shows that the upper DO could have a significant decrease after activating COD, even surface DO are also supplied by the photosynthesis and reaeration. By comparing the upper DO concentrations from two *BFCOD* increase scenarios (*BFCOD* = 0 vs *BFCOD* = 3, *BFCOD* = 3 vs *BFCOD* = 6, and *BFCOD* = 6 vs *BFCOD* = 12 g $O^2/m^2/day$) at station 190, one can find that DO decreases are not the same: 1.26 mg/L (from 3.25 to 1.99 mg/L), 0.46 mg/L (from 1.99 to 1.53 mg/L), and 0.98 mg/L (from 1.53 to 0.55 mg/L). The same situation occurs at the bottom DO: 0.58 mg/L (from 0.79 to 0.21 mg/L), 0.15 mg/L (from 0.21 to 0.06 mg/L), and 0.06 mg/L (from 0.06 to 0.00 mg/L). This is because Michaelis-

Mention formula is used for the COD oxidation with KH_{COD} = 1.5 mg/L. When DO becomes smaller, the COD oxidation rate is also smaller and becomes zero at the anoxic condition.

For stations 240 (Figure 4-78) and 260 (Figure 4-79), the upper and bottom DO concentrations using different *BFCOD* show a similar change pattern as the station 190 except for the magnitude. The DO concentrations in all four layers would increase from the west to east in the Cotton Bayou as discussed before. When BFCOD = 12 g O^2/m^2/day, the bottom DO is projected to be anoxic and pretty low (average 0.5 and 0.17 mg/L) at BFCOD = 3 or 6 g O^2/m^2/day at station 240. At BFCOD = 3 g O^2/m^2/day, the upper-layer DO at station 240 and the bottom DO at station 260 are projected to be mostly lower than 3 mg/L. When many Gulf menhaden were crowded in Cotton Bayou at the end of July 2015, especially when some menhaden started to die, chemical oxygen demand in the water column could increase even not initiated from the sediment.

Table 4-15 Average simulated DO (mg/L) at four layers from 7/27 to 8/5 in 2015 using four BFCOD at stations 190, 240, and 260.

	BFCOD [1]	0	3	6	12
Station 190	surface	3.58	2.43	1.72	0.91
	upper	3.25	1.99	1.53	0.55
	lower	2.46	1.27	0.71	0.23
	bottom	0.79	0.21	0.06	0.00
Station 240	surface	5.23	3.90	3.01	1.78
	upper	3.95	2.20	1.34	0.47
	lower	2.97	1.30	0.63	0.16
	bottom	1.77	0.50	0.17	0.00
Station 260	surface	5.59	4.46	3.70	2.36
	upper	4.94	3.55	2.77	1.35
	lower	4.52	3.05	2.33	0.98
	bottom	3.20	1.77	1.20	0.26

Note: [1] – BFCOD in g O^2/m^2/day.

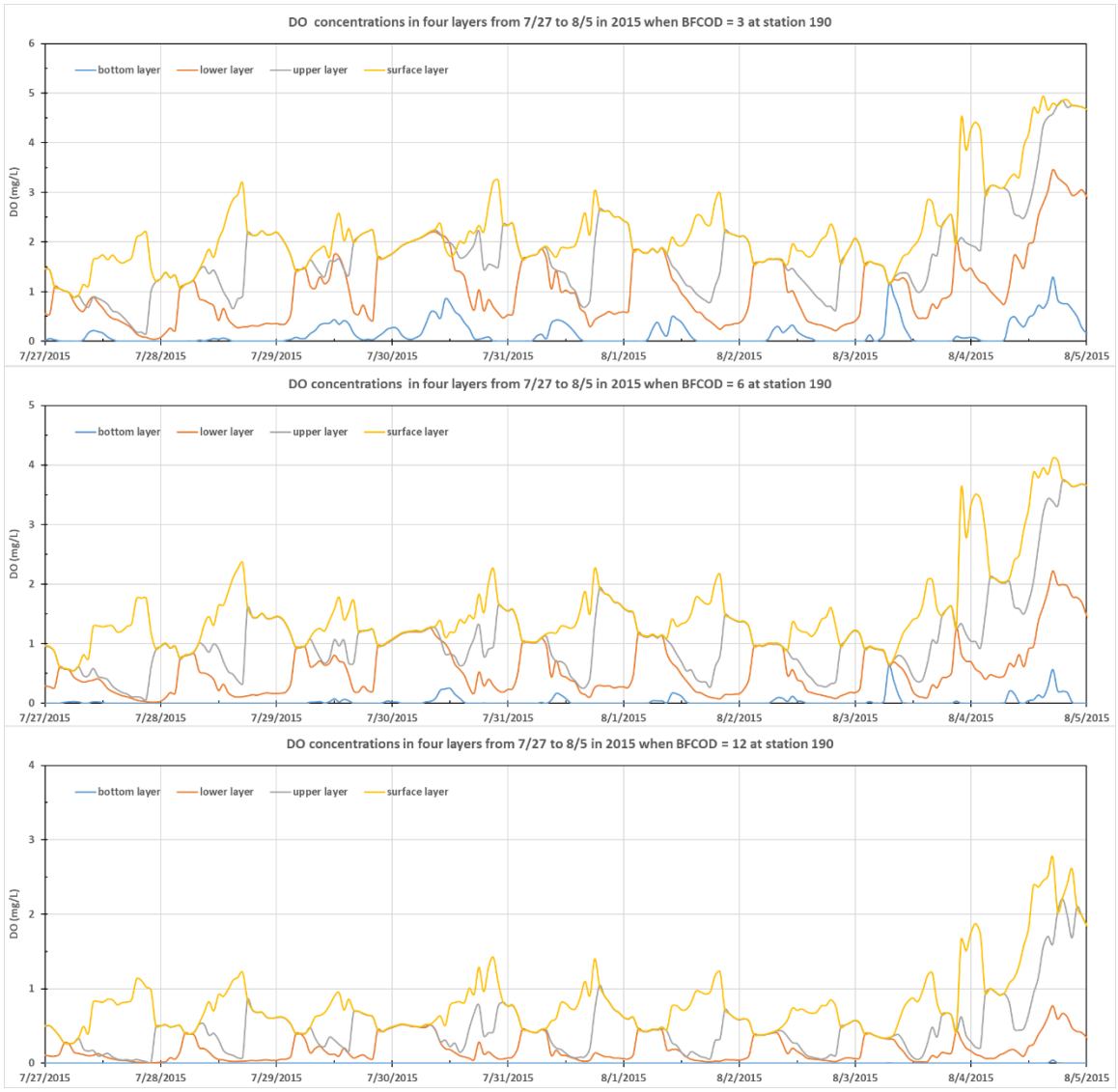

Figure 4-76 Simulated DO in the four layers at station 190 from 7/27 to 8/5 in 2015 using three BFCOD at station 190: BFCOD = 3 (upper panel), 6 (middle), and 12 (lower).

Table 4-16 Percentage of habitat time periods (simulated DO higher than projected lethal DO) in four layers from 7/31 to 8/3 in 2015 with BFCOD = 3 g O_2/m^2/day.

Stations	Bottom layer	Lower layer	Upper layer	Surface layer
180	1% (0%)	4% (0%)	8% (0%)	9% (0%)
190	0% (0%)	2% (0%)	6% (0%)	7% (0%)
200	0% (0%)	1% (0%)	4% (0%)	8% (0%)
210	0% (0%)	0% (0%)	4% (0%)	12% (0%)
220	0% (0%)	0% (0%)	0% (0%)	10% (0%)
230	0% (0%)	0% (0%)	0% (0%)	10% (1%)
240	0% (0%)	0% (0%)	0% (0%)	19% (13%)
250	0% (0%)	0% (0%)	5% (10%)	31% (36%)
260	0% (0%)	3% (12%)	6% (20%)	30% (47%)
270	0% (0%)	0% (0%)	2% (6%)	5% (5%)
555	0% (0%)	0% (0%)	9% (19%)	42% (51%)
634	0% (0%)	13% (29%)	24% (35%)	41% (46%)
383	0% (0%)	0% (0%)	3% (0%)	13% (2%)
920	0% (0%)	1% (0%)	1% (0%)	3% (0%)

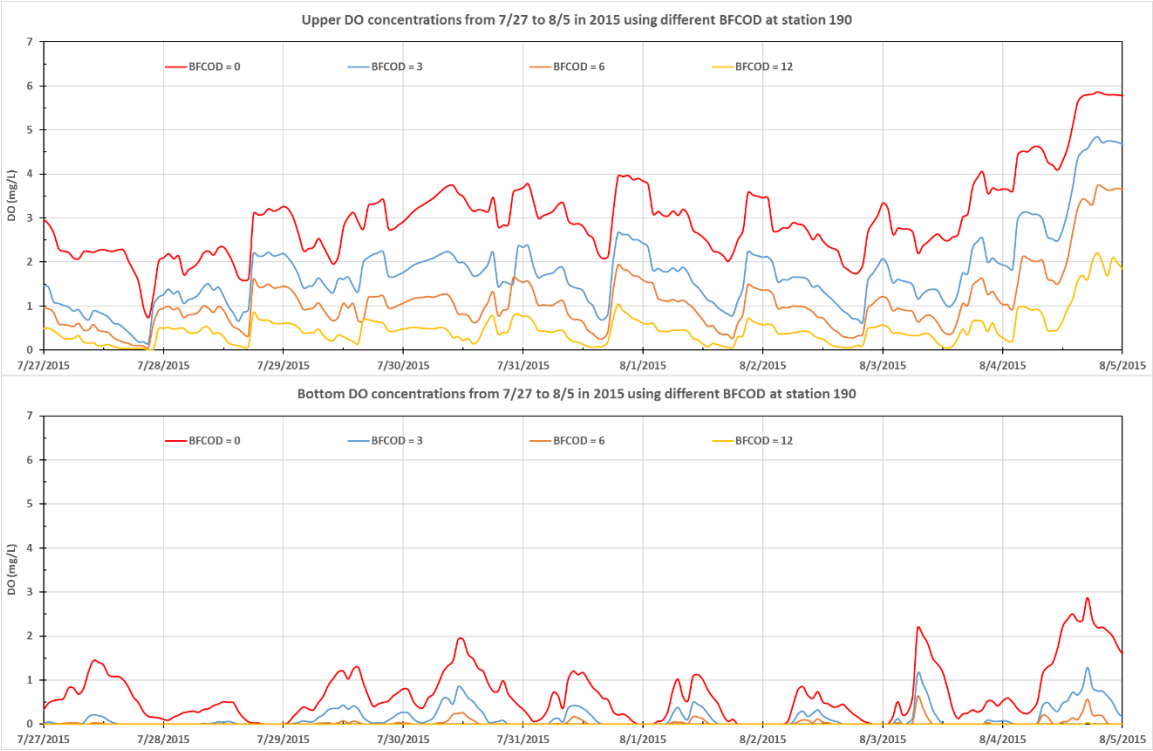

Figure 4-77 Simulated DO at station 190 from 7/27 to 8/5 in 2015 using four BFCOD in the upper layer (upper panel) and bottom layer (lower panel)

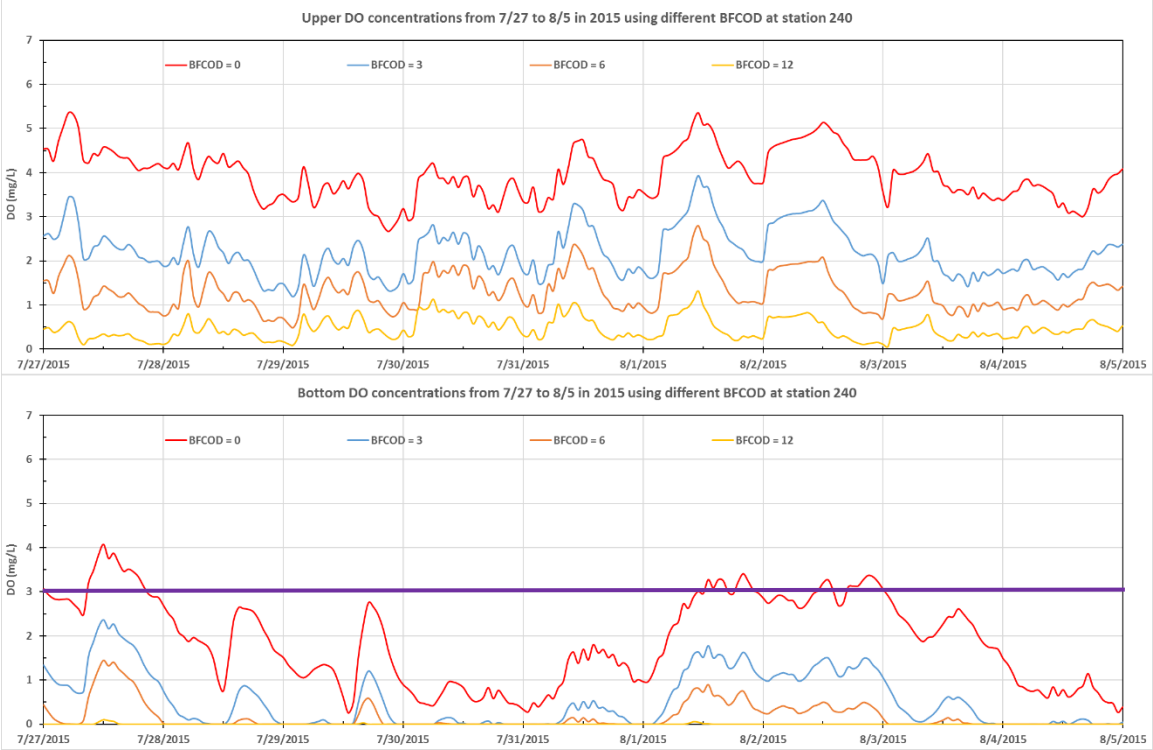

Figure 4-78 Simulated DO at station 240 from 7/27 to 8/5 in 2015 using four BFCOD in the upper layer (upper panel) and bottom layer (lower panel)

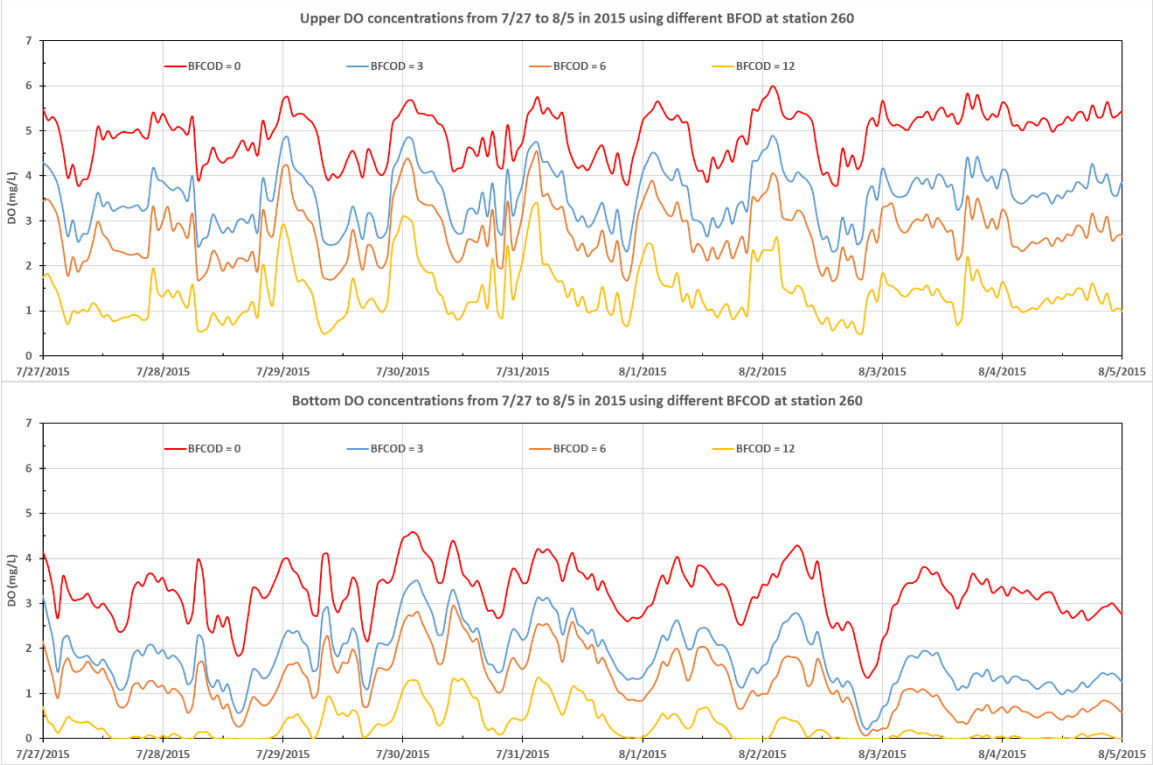

Figure 4-79 Simulated DO at station 260 from 7/27 to 8/5 in 2015 using four BFCOD in the surface layer (upper panel) and bottom layer (lower panel).

4.4.2 DO Analysis using Different SOD

SOD stands for the sediment oxygen demand that is consumption of DO by the organic matter decomposition in benthic sediments. Unlike the COD affecting all DO concentrations from the surface to bottom in the water, SOD only applies to the bottom DO in the EFDC model. For the current model, the SOD was set to 0.9 g O_2/m^2/day, which is an average value from other water quality models (Ji et al. 2002). Given that the study area is the estuary that easily piles up the sediment, 1.2, 1.5, and 2 g O_2/m^2/day SOD were chosen to do the sensitivity analysis. Figure 4-80 shows the time-series plots of DO in the four layers from 7/27/2015 to 8/5/2015 at stations 190 (as an example) using different SOD values (1.2, 1.5, and 2 g O_2/m^2/day). Figure 4-81—Figure 4-83

plot the simulated surface and bottom DO using difference SOD. Table 4-17 lists the average DO in the four layers using different SOD at the selected three stations from 7/27/2015 to 8/5/2015.

Figure 4-80 shows that the DO change patterns along with depth and with time were very similar even the SOD was different. At station 190, in some time periods, the simulated DO in the surface and upper layers or all three top layers were basically the same or very close to each other for all the scenarios with different SOD. These more or less well mixed over 2 to 3 layers were most likely created by wind/current mixing and not controlled/affected by the change of SOD. It should point out that the mechanism that DO decreased with the increase of SOD is different from the previous COD sensitivity analysis. SOD can only consume the bottom DO. The vertical diffusion caused a decrease of DO above the bottom layer. However, COD as a model variable is modeled in all layers and can directly affect DO at every layer by COD oxidation, even the source of COD (i.e., BFCOD) only applies to the bottom layer (Equation 4.1), which is the same as SOD source. At station 190, the upper DO difference from scenarios using two SOD increases (SOD = 0.9 vs SOD =1.2, SOD = 1.2 vs SOD = 1.5, and SOD = 1.5 vs SOD = 2) values were 0.2, 0.13, and 0.13 mg/L with an average 0.15 mg/L change, calculated using average surface DO in Table 4-17. However, the bottom DO differences were 0.31, 0.15, and 0.14 mg/L, respectively, with an average 0.2 mg/L change. The bottom DO changes were larger than the surface DO when the SOD changed. The surface and bottom DO changes with respect to the change of SOD at stations 240 and 260 also show the same trend: the changes in surface DO were about a half of the changes in bottom DO. From west to east in Cotton Bayou (station 190 to 260), the average DO decrease in the upper layer when SOD increased 0.3, 0.6 and 1.1 g O_2/m^2/day (comparing with the base model with 0.9 g O_2/m^2/day) was 0.12, 0.23, and 0.32 mg/L, while for the bottom layer, the average DO decrease was 0.2, 0.52, and 0.7 mg/L, respectively. At station 260, the average bottom DO were lower than 3 mg/L when SOD was larger than 0.9 g O_2/m^2/day.

Table 4-17 Average DO (mg/L) in four layers from 7/27 to 8/5 in 2015 using different SOD at stations 190, 240, and 260

	Layers	SOD = 0.9 [1]	SOD = 1.2	SOD =1.5	SOD = 2
Station 190	surface	3.58	3.41	3.31	3.22
	upper	3.25	3.05	2.92	2.79
	lower	2.46	2.17	2.01	1.87
	bottom	0.79	0.48	0.33	0.19
Station 240	surface	5.23	4.95	4.75	4.55
	upper	3.95	3.50	3.19	2.91
	lower	2.97	2.33	1.89	1.52
	bottom	1.77	1.06	0.57	0.20
Station 260	surface	5.59	5.29	5.01	4.62
	upper	4.94	4.53	4.12	3.61
	lower	4.52	4.07	3.58	2.97
	bottom	3.20	2.54	1.86	1.11

Note: [1] – for original and validated model.

Table 4-18 Percentage of habitat time periods (simulated DO higher than projected lethal DO) in four layers from 7/15 to 8/15 in 2015 with SOD = 1.2 g O_2/m^2/day.

Stations	Bottom layer	Lower layer	Upper layer	Surface layer
180	1% (0%)[1]	8% (0%)	14% (0%)	14% (0%)
190	0% (0%)	7% (0%)	11% (0%)	13% (1%)
200	0% (0%)	4% (0%)	13% (0%)	17% (3%)
210	0% (0%)	2% (0%)	16% (0%)	29% (7%)
220	0% (0%)	0% (0%)	12% (0%)	35% (9%)
230	0% (0%)	0% (0%)	0% (0%)	41% (23%)
240	0% (0%)	1% (3%)	6% (19%)	43% (51%)
250	0% (0%)	1% (4%)	18% (33%)	54% (67%)
260	0% (0%)	9% (23%)	24% (42%)	59% (69%)
270	2% (0%)	2% (1%)	11% (20%)	46% (59%)
555	0% (0%)	1% (0%)	20% (36%)	62% (65%)
634	0% (2%)	25% (36%)	40% (39%)	60% (64%)
383	0% (0%)	2% (0%)	10% (0%)	21% (4%)
920	0% (0%)	1% (0%)	2% (0%)	7% (3%)

Note: [1]—Numbers inside brackets were the statistical percentage from 7/31 to 8/3 in 2015

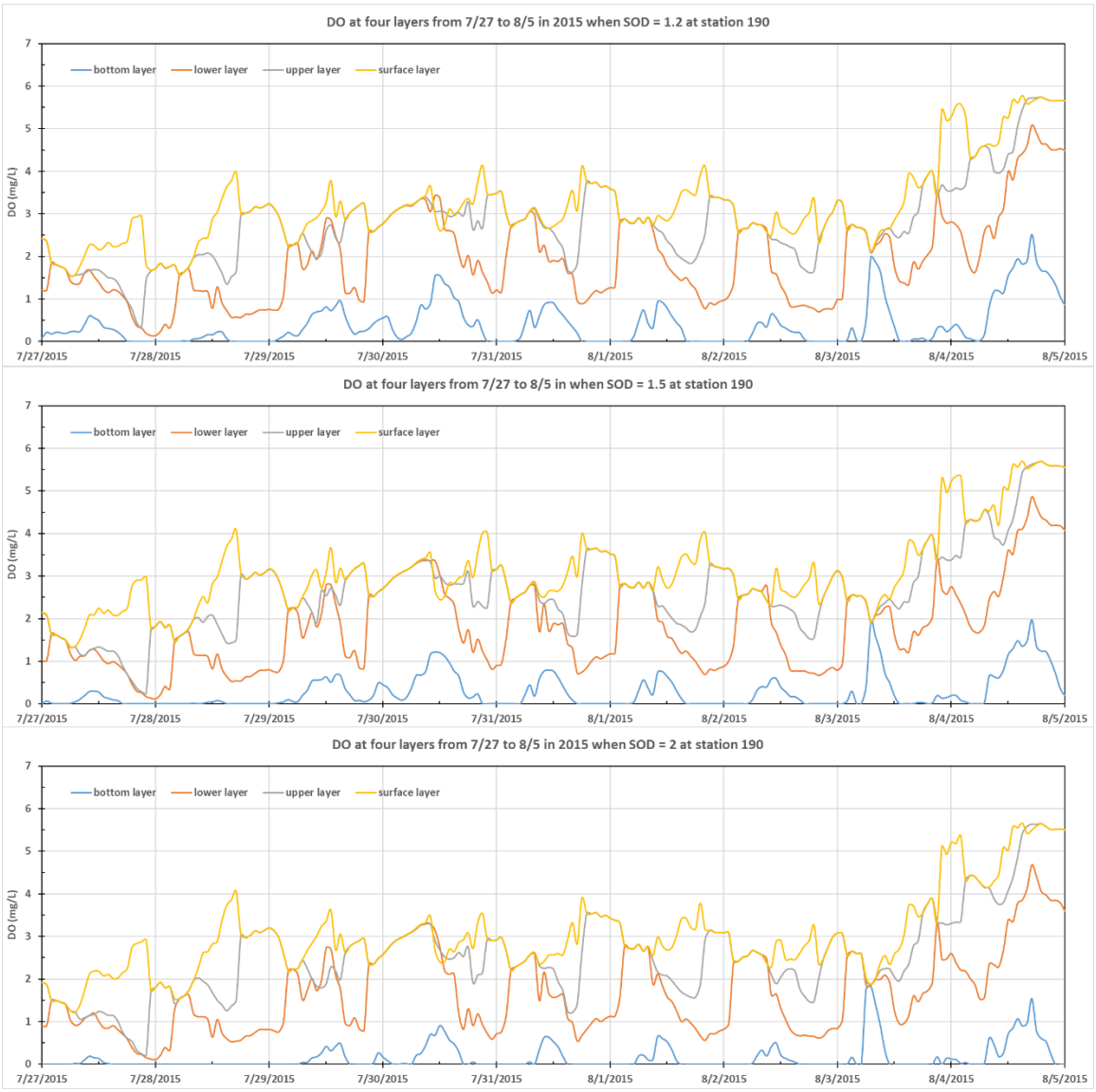

Figure 4-80 Simulated DO in the four layers at station 190 from 7/27 to 8/5 in 2015 using three SOD (g O_2/m^2/day): 1.2 (upper panel), 1.5 (middle panel), and 2 (lower panel).

Table 4-18 summarizes the percentage of habitat time periods (simulated DO higher than projected lethal DO) in four layers from 7/15 to 8/15 in 2015 with SOD = 1.2 g O_2/m^2/day. In comparison to habitat results (Table 4-13) with SOD = 0.9 g O_2/m^2/day, the percentage of habitat periods almost would decrease in all the four layers except for the station 200. This means there would be more layers that could not support menhaden's habitat. Comparing with the habitat results

with SOD = 0.91.2 g O_2/m^2/day, the differences between percentage of habitat time periods increase from west to east (~5% in region 1 and ~10 in region 2) from 7/15 to 8/15. During the fish kills periods (7/31—8/3), the difference decrease with 1% difference in region 1 and ~5% difference in region 2 and region 3 except for the station 270. Simialr to the percentage change pattern when SOD was 0.9, the west region of Cotton Bayou were also suitable for the living of Gulf menhaden (the percentage of habitat time periods increase from west to east). At station 180, the Gulf menhaden can not survive since the DO in all four layers were smaller than the lethal DO. In the regions east of station 240 , there existed averagely more than 12 hrs one day that water maintained more DO concentrations than Gulf menhaden need with more than 50% habitat time periods.

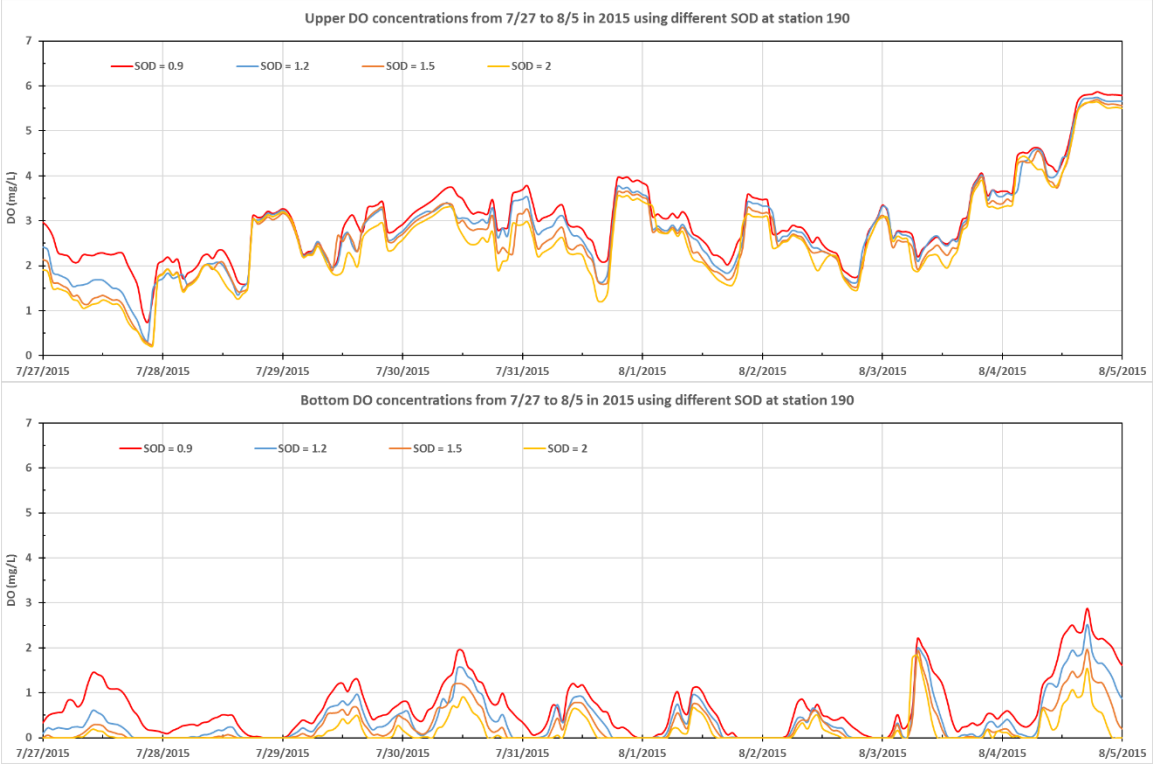

Figure 4-81 Simulated DO at station 190 from 7/27 to 8/5 in 2015 using four SOD (g O_2/m^2/day) in the upper layer (upper panel) and bottom layer (lower panel).

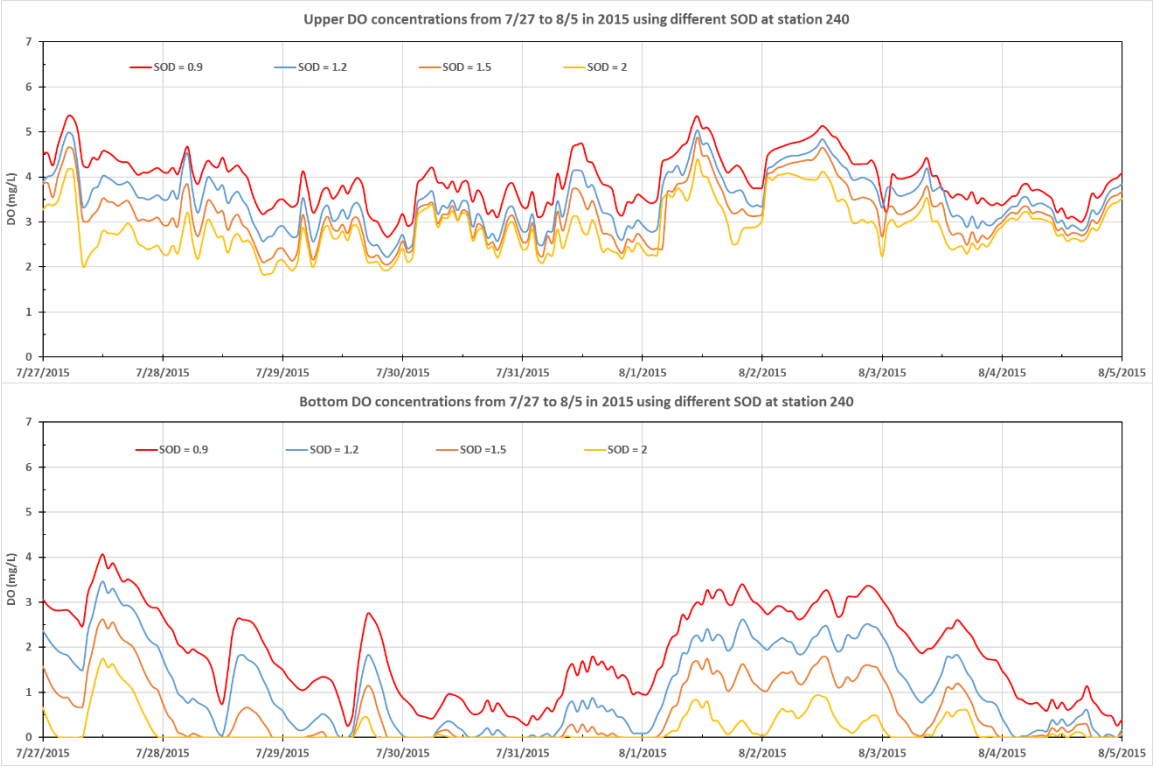

Figure 4-82 Simulated DO at station 240 from 7/27 to 8/5 in 2015 using four SOD (g O_2/m^2/day) in the upper layer (upper panel) and bottom layer (lower panel).

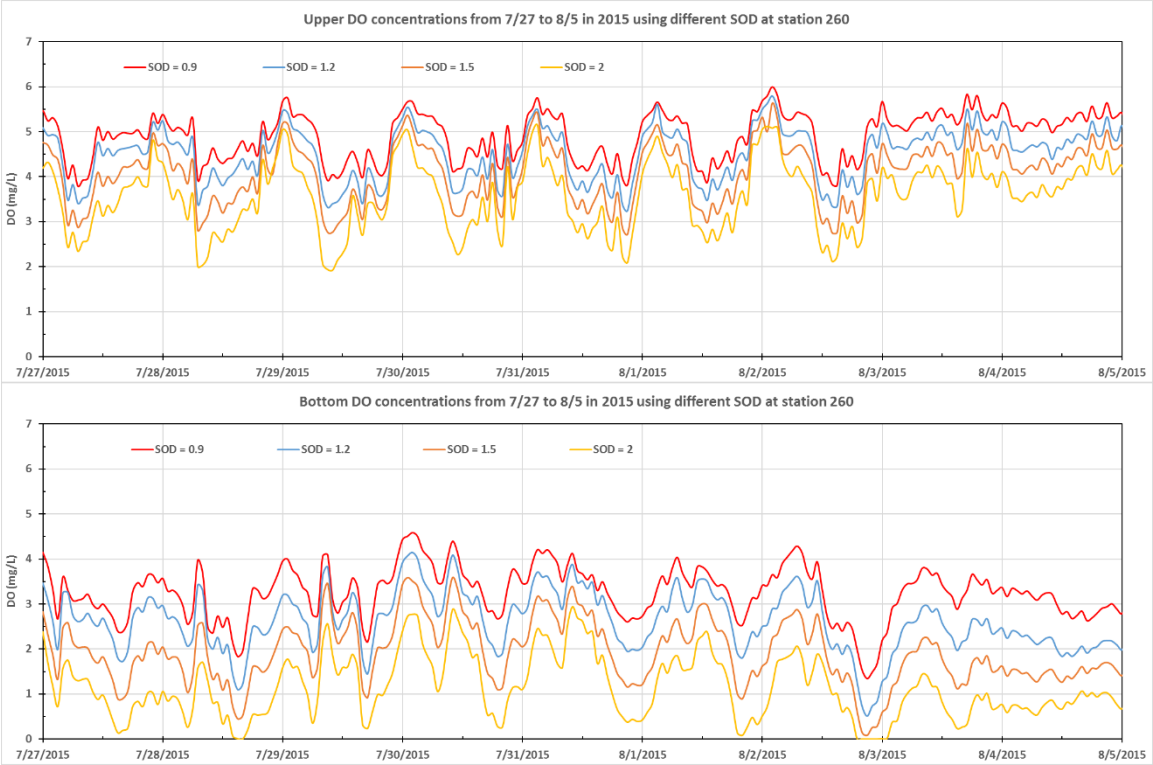

Figure 4-83 Simulated DO at station 260 from 7/27 to 8/5 in 2015 using four SOD (g O_2/m^2/day) in the upper layer (upper panel) and bottom layer (lower panel).

4.4.3 DO Analysis using Different Wind Speeds

The wind speed would affect DO in the water in both direct and indirect ways. The strong wind would directly enhance the vertical mixing of shallow water, which can transmit the surface DO to the bottom. Indirectly, the wind speed would affect the DO by affecting the water temperature since wind speed determines the latent heat of evaporation and convection, sink terms of water temperature model. The water temperature furtherly affects the DO saturation, together with salinity. Generally, lower water temperature leads to higher saturated DO concentration. In this study, water temperature and DO under 0.25, 0.5, 1.25, 1.5, and 2 times of observed wind speeds were simulated to find how wind speed would affect the DO concentrations.

Figure 4-84 plots the simulated DO in the four layers at station 190 (as an example) using five hypothetic wind speeds. The DO magnitude and variations with time using 0.25 and 0.5 times of observed wind speed are very similar. With the increase of wind speed, projected DO in the four layers also increase, especially for the bottom DO. Besides, Figure 4-84 shows that the DO difference among the top three layers would firstly reduce, and then the DO difference between the bottom and top three layers gradually decrease. This is because Cotton Bayou is small and typically well stratified, only when wind speed reaches to a certain magnitude, it can mix all the water in the vertical direction. When observed wind speeds were doubled, the DO in the four layers were the same or very close from 7/29 to 7/31.

Figure 4-85—Figure 4-87 show that the DO would increase with the increase of wind speed. However, the increase rate is projected to be different at different locations and different change ranges of wind speed. Table 4-19 lists projected average DO concentrations in the four layers with five wind speeds and the DO decrease/increase percentages in comparison to simulated DO under the original wind speed. When wind speed is assumed to be a half or one-quarter of the original wind speed, simulated DO in the upper and bottom layer had some small decrease in stations 190 and 260, but large decreases are projected in station 240 between 7/31 and 8/2 in 2015. They show that the DO in the four layers increases from west to east in the Cotton Bayou. Figure 4-88—Figure 4-90 show the contour maps of projected DO in the upper and bottom layers under half of original wind speeds from 7/31 to 8/2 in 2015. In contrast to the DO in upper layers using observed wind speed (Figure 4-68—Figure 4-70), the DO decrease primarily occurred in region 2. The DO in the upper layer simulated using 0.5 times of wind speeds were around 3 mg/L in the west part and 4 mg/L in the east part of region 2, while the DO using observed wind speed in the same layer were around 1 mg/L higher, 4 mg/L, and 5 mg/L, respectively, in the west and east part of region 2. For the bottom DO using 0.5 times of wind speeds, they were around 1 mg/L continuously in the region 1 and west part of region 2

Table 4-19 Average DO (mg/L) and percent decrease or increase in four layers from 7/27 to 8/5 in 2015 using different wind speeds at stations 190, 240, and 260 (WS stands for wind speed)

	0.25 WS	0.5 WS	1.0 WS	1.25 WS	1.5 WS	2 WS
			Station 190			
surface	3.16 (-12%) [1]	3.37 (-6%)	3.58	4.50 (25%)	4.98 (39%)	5.64 (57%)
upper	2.60 (-20%)	2.84 (-13%)	3.25	4.39 (35%)	4.89 (51%)	5.60 (72%)
lower	1.99 (-19%)	2.09 (-15%)	2.46	3.81 (55%)	4.55 (82%)	5.47 (123%)
bottom	0.45 (-44%)	0.48 (-40%)	0.79	2.12 (167%)	3.11 (292%)	4.65 (486%)
			Station 240			
surface	4.91 (-6%)	5.15 (-2%)	5.23	5.44 (4%)	5.62 (7%)	5.99 (14%)
upper	2.86 (-27%)	3.32 (-16%)	3.95	4.79 (21%)	5.24 (33%)	5.85 (48%)
lower	1.66 (-44%)	2.20 (-26%)	2.97	4.00 (35%)	4.50 (51%)	5.33 (79%)
bottom	0.75 (-58%)	1.15 (-35%)	1.77	2.80 (58%)	3.30 (86%)	4.31 (143%)
			Station 260			
surface	5.34 (-4%)	5.49 (-2%)	5.59	5.75 (3%)	5.86 (5%)	6.08 (9%)
upper	4.43 (-10%)	4.67 (-5%)	4.94	5.36 (9%)	5.56 (13%)	5.89 (19%)
lower	4.04 (-11%)	4.25 (-6%)	4.52	4.93 (9%)	5.13 (13%)	5.53 (22%)
bottom	2.70 (-16%)	2.92 (-9%)	3.20	3.77 (18%)	4.05 (27%)	4.67 (46%)

Note: [1] – Numbers inside brackets are simulated DO percent decrease or increase from the DO under the original wind speeds

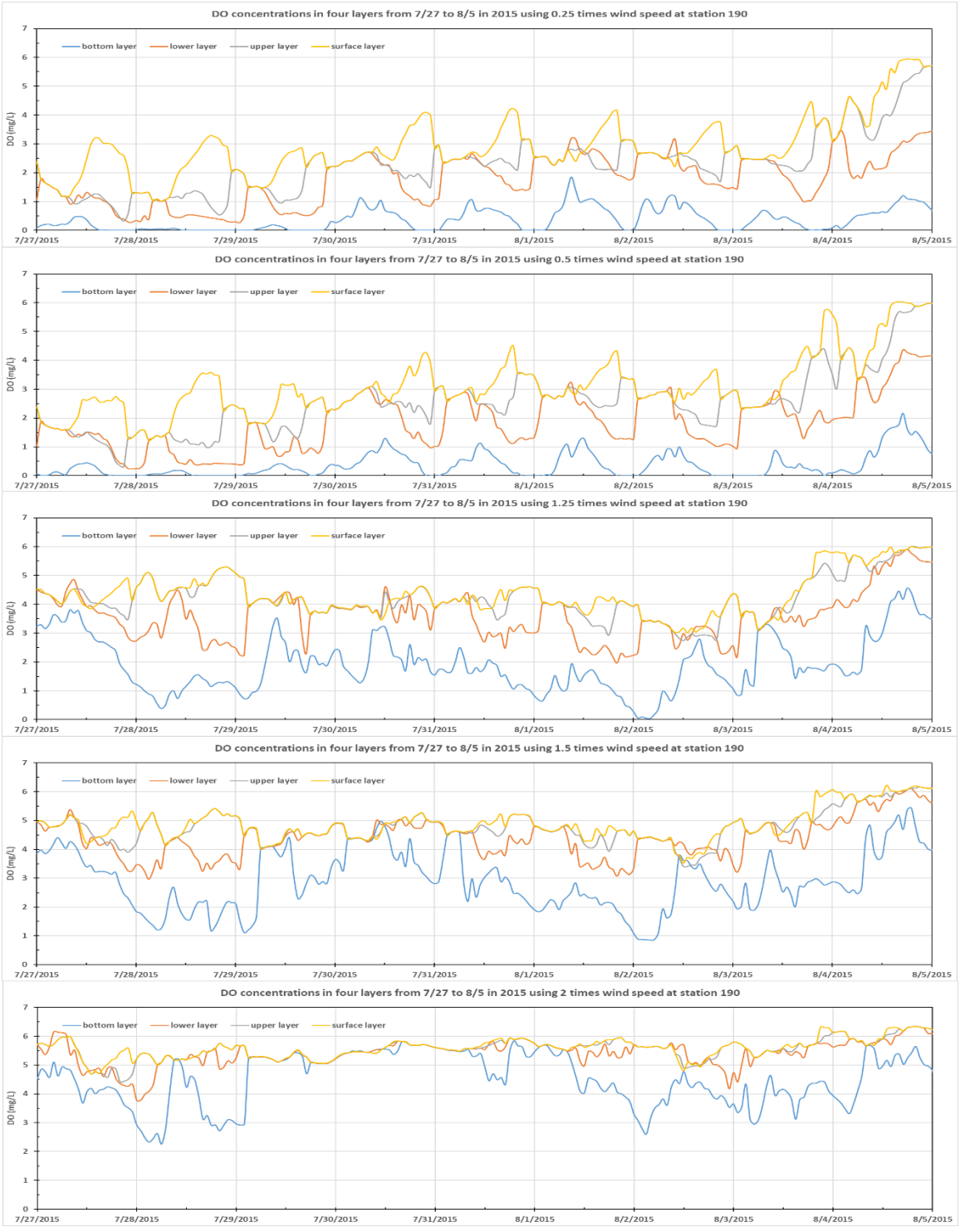

Figure 4-84 Simulated DO in the four layers at station 190 from 7/27 to 8/5 in 2015 using different wind speeds: 0.25, 0.5, 1.25, 1.5, and 2 times of observed wind speed from top to bottom.

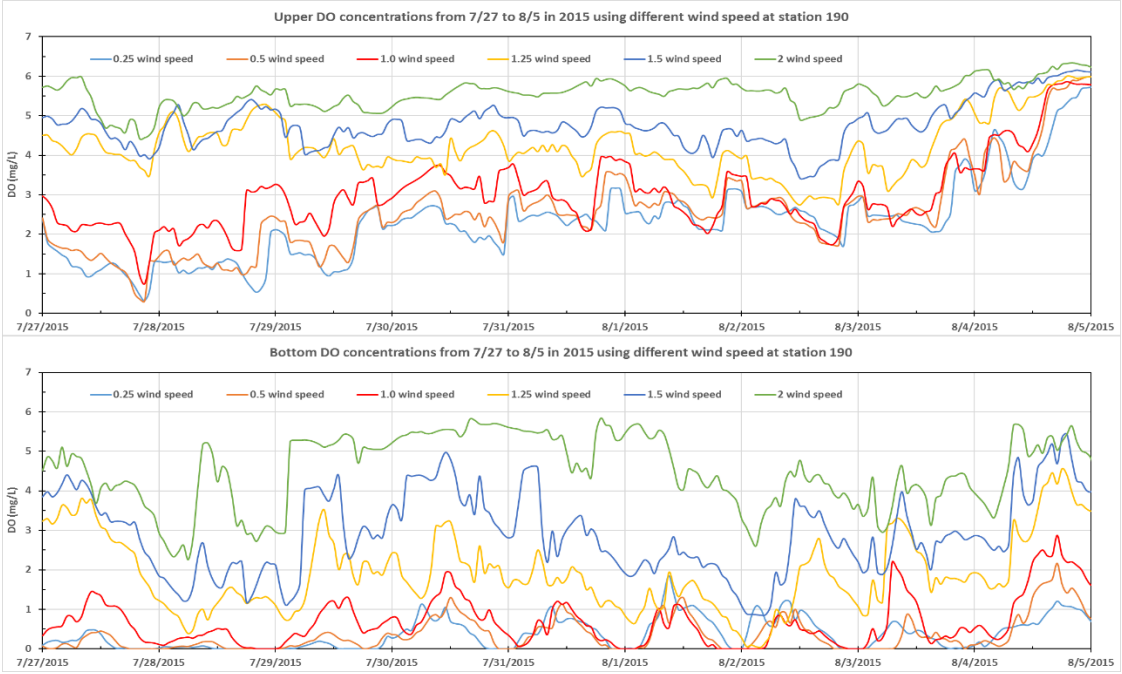

Figure 4-85 Simulated DO at station 190 from 7/27 to 8/5 in 2015 using different wind speed in the upper layer (upper panel) and bottom layer (lower panel).

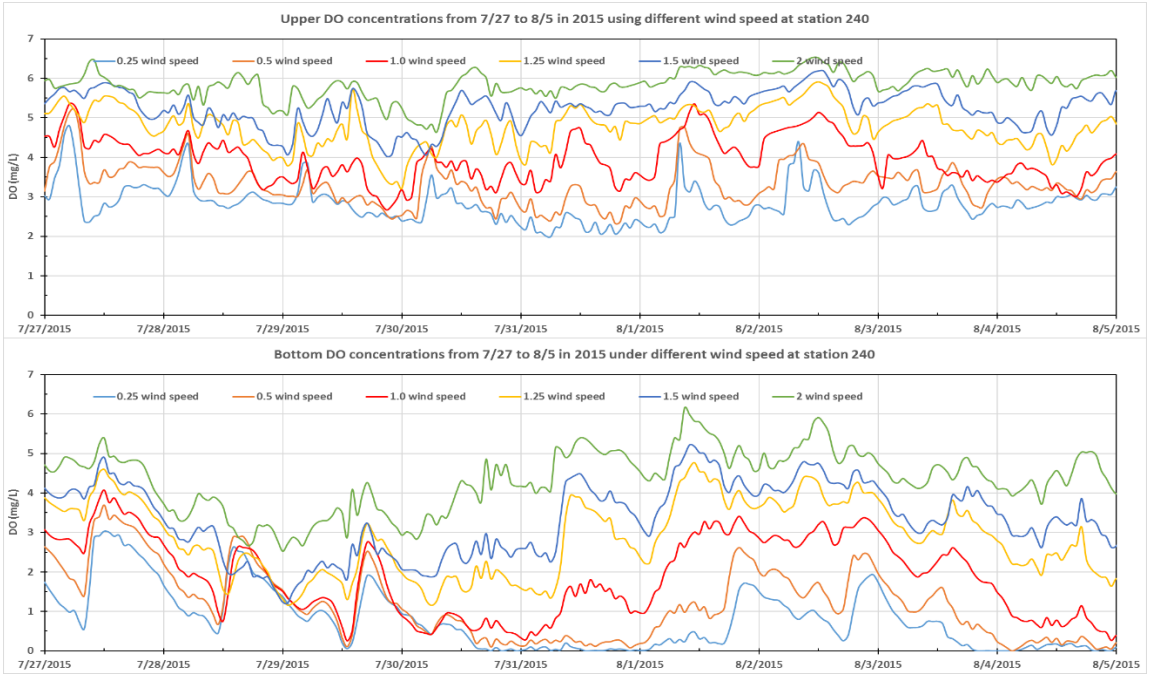

Figure 4-86 Simulated DO at station 240 from 7/27 to 8/5 in 2015 using different wind speed in the surface layer (upper panel) and bottom layer (lower panel).

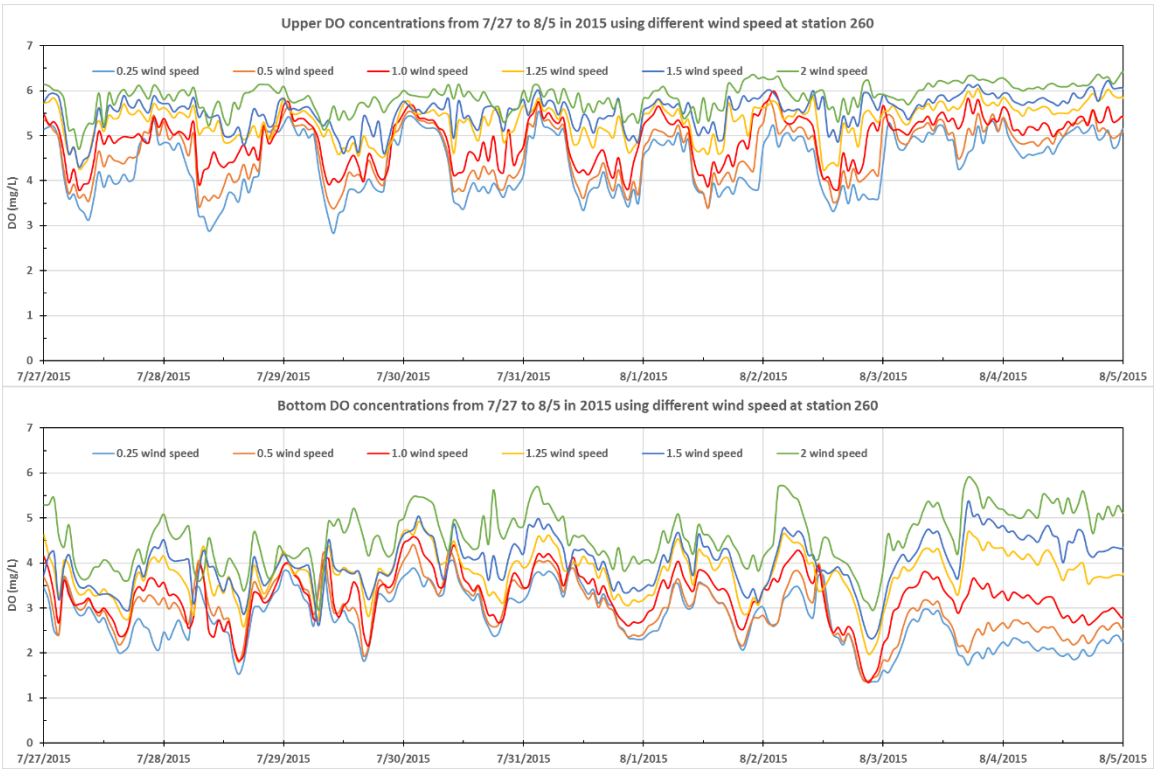

Figure 4-87 Simulated DO at station 260 from 7/27 to 8/5 in 2015 using different wind speed in the upper layer (upper panel) and bottom layer (lower panel).

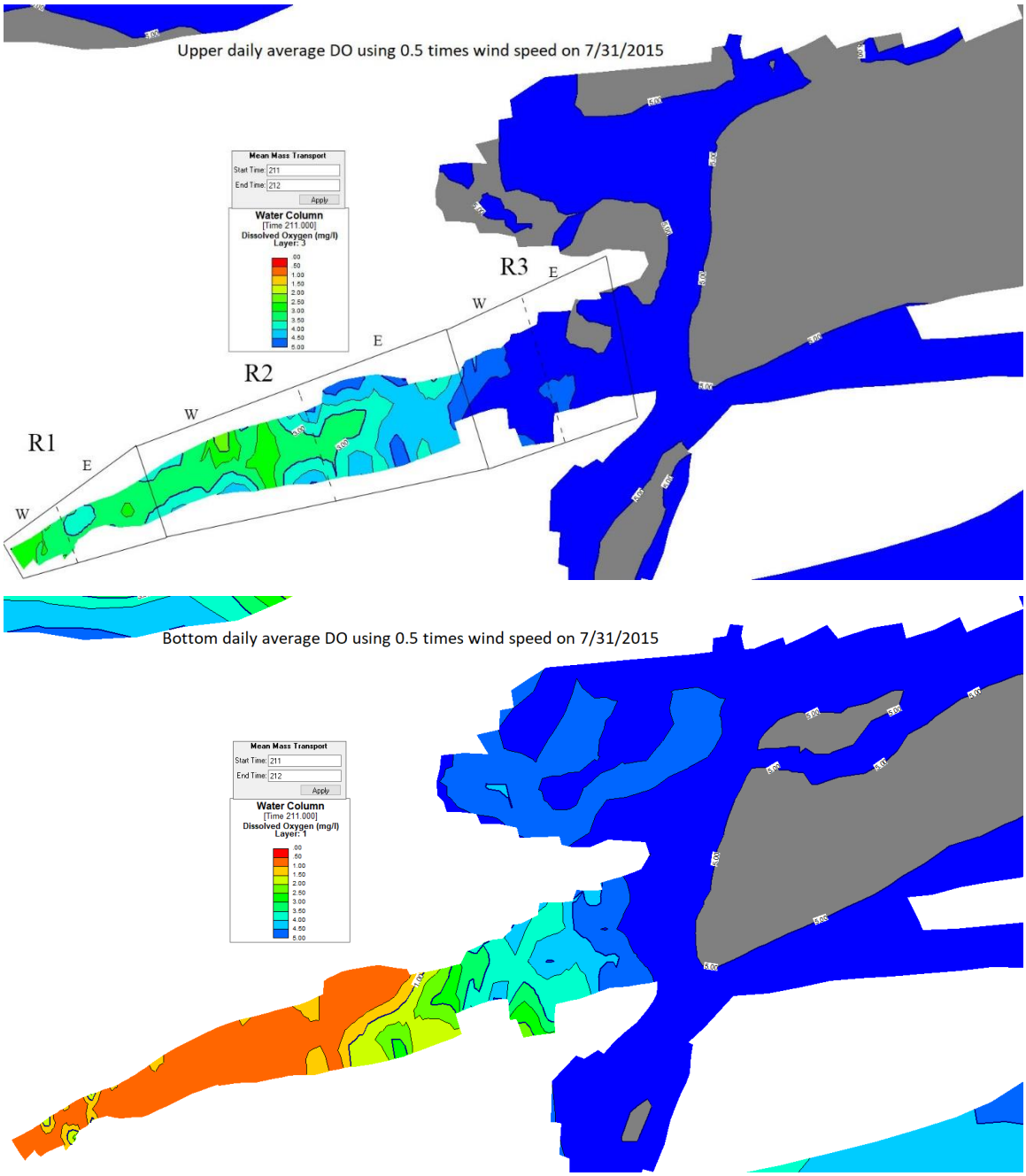

Figure 4-88 Upper- and bottom-layer daily average DO using 0.5 times wind speed contour maps on 7/31/2015

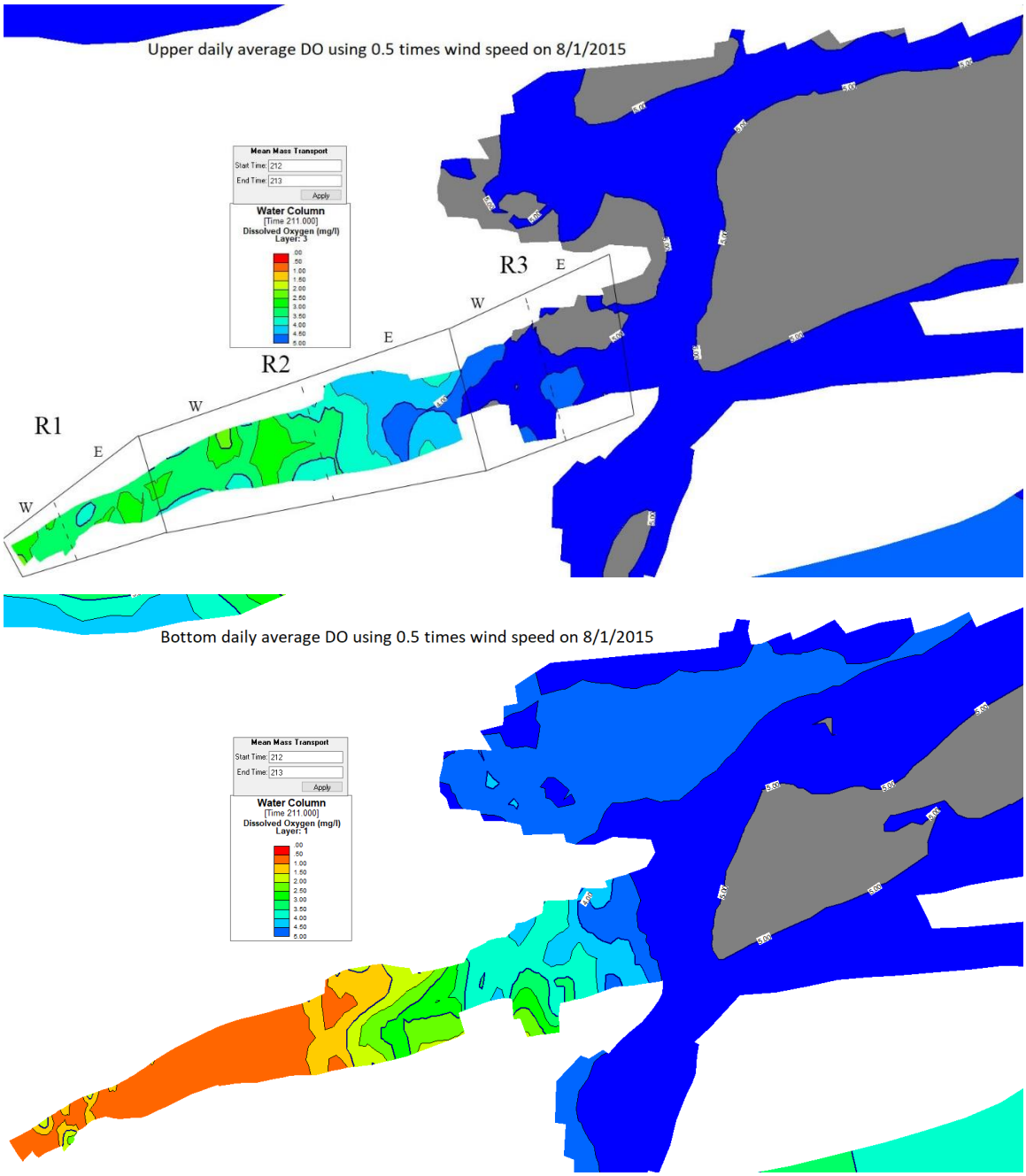

Figure 4-89 Upper- and bottom-layer daily average DO using 0.5 times wind speed contour maps on 8/1/2015

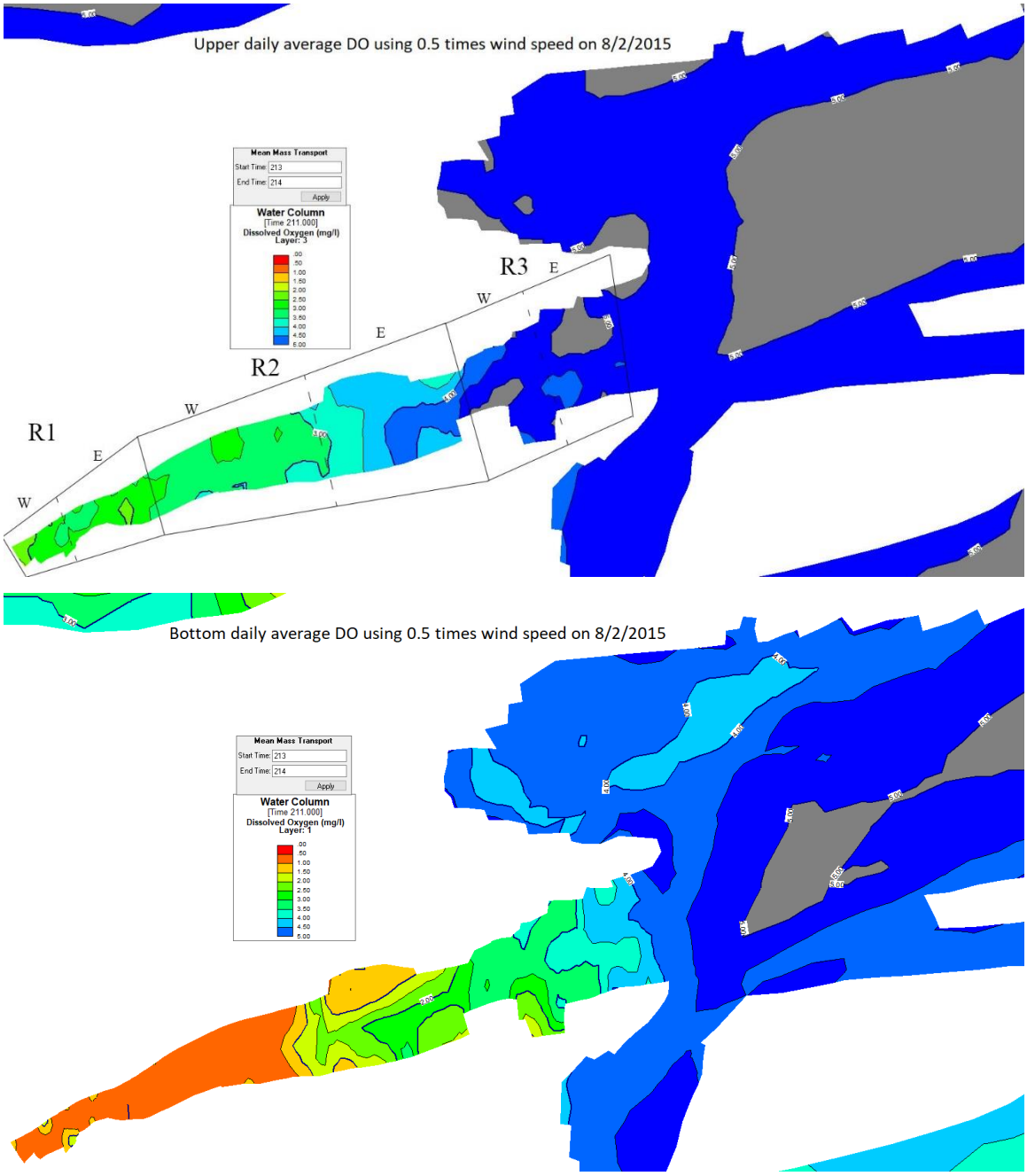

Figure 4-90 Upper- and bottom-layer daily average DO using 0.5 times wind speed contour maps on 8/2/2015

4.4.4 DO Analysis using Different Wind Directions

Wind direction is usually used in the sediment sub model to simulate the wind wave. In the current model, nutrients flux to sediment was represented by constant values instead of using the full sediment diagenesis model. Thus, the wind direction played a limited role in the current model by changing the surface waves, but the wind direction does affect hydrodynamics or velocity field in estuary, therefore, affect the vertical and horizontal mixing. The fixed north and south wind were applied to the model to look into how wind direction affects the DO concentrations. The change of wind direction usually accompanies with the air temperature change in reality. The north wind means the wind blowing from north to south and usually blows the cold air temperature and the south wind frequently comes together with warm air temperature from the ocean. However, in the current sensitive analysis, no changes in air temperature were used (the same as the observed data).

Figure 4-91 Simulated DO in the four layers at station 190 from 7/27 to 8/5 in 2015 using north wind (upper panel) and south wind (lower panel). Figure 4-91 shows that the north wind would create more mixing events than the south wind does at station 190, therefore the bottom DO concentrations could have large fluctuations with the north wind. The average surface DO concentration using the south wind (4.03 mg/L) is slightly higher than DO using the north wind (3.86 mg/L). Figure 4-92—Figure 4-94 show the upper-layer and bottom DO using different wind directions at three stations. For the upper-layer DO, there are no obvious difference using different wind directions at all the three stations. Average surface DO increases from west to east in Cotton Bayou. Both the upper-layer and bottom DO concentrations at station 260 are projected to have small changes using different wind directions. At station 190, both the north and south wind could create higher DO while at station 240 the north wind led to lower bottom DO between 7/31 and 8/4 in 2015 (Figure 4-93) and also lower in the lower and upper layers (Table 4-20). The contour maps were developed under the north wind scenario in Cotton Bayou on 8/1/2015 (Figure 4-95). It shows that the bottom DO in the east part of region 2 would decrease from around 3 mg/L using observed

wind direction to 2.5 mg/L using north wind. Besides, some regions of the west part of region 2 have the ultra-low DO concentrations, 1 mg/L. However, in the other parts of Cotton Bayou, the DO would increase in both upper and bottom layers, especially for the west part of region 1.

Table 4-20 Average DO (mg/L) in four layers from 7/27 to 8/5 in 2015 using different wind directions simulated at stations 190, 240, and 260

	original	north wind	south wind
		Station 190	
surface	3.58	3.86	4.03
upper	3.25	3.72	3.87
lower	2.46	3.02	2.92
bottom	0.79	1.34	1.10
		Station 240	
surface	5.23	5.35	5.27
upper	3.95	**3.77**	3.88
lower	2.97	**2.35**	2.99
bottom	1.77	**1.28**	1.95
		Station 260	
surface	5.59	5.65	5.62
upper	4.94	5.04	5.07
lower	4.52	4.63	4.52
bottom	3.20	3.29	3.15

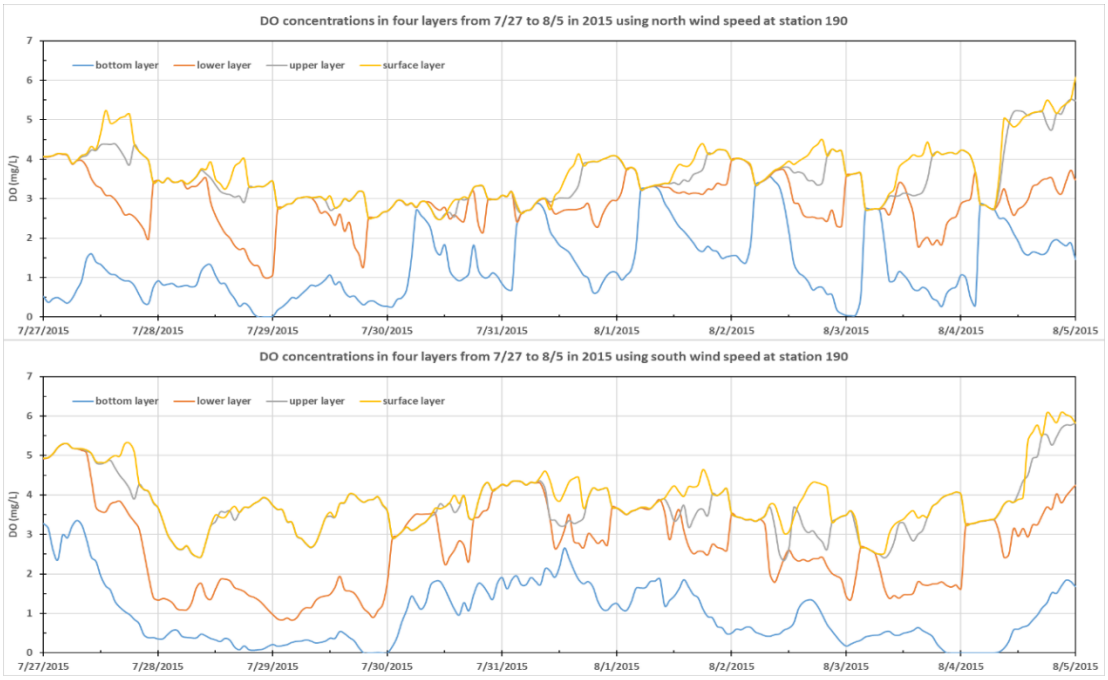

Figure 4-91 Simulated DO in the four layers at station 190 from 7/27 to 8/5 in 2015 using north wind (upper panel) and south wind (lower panel).

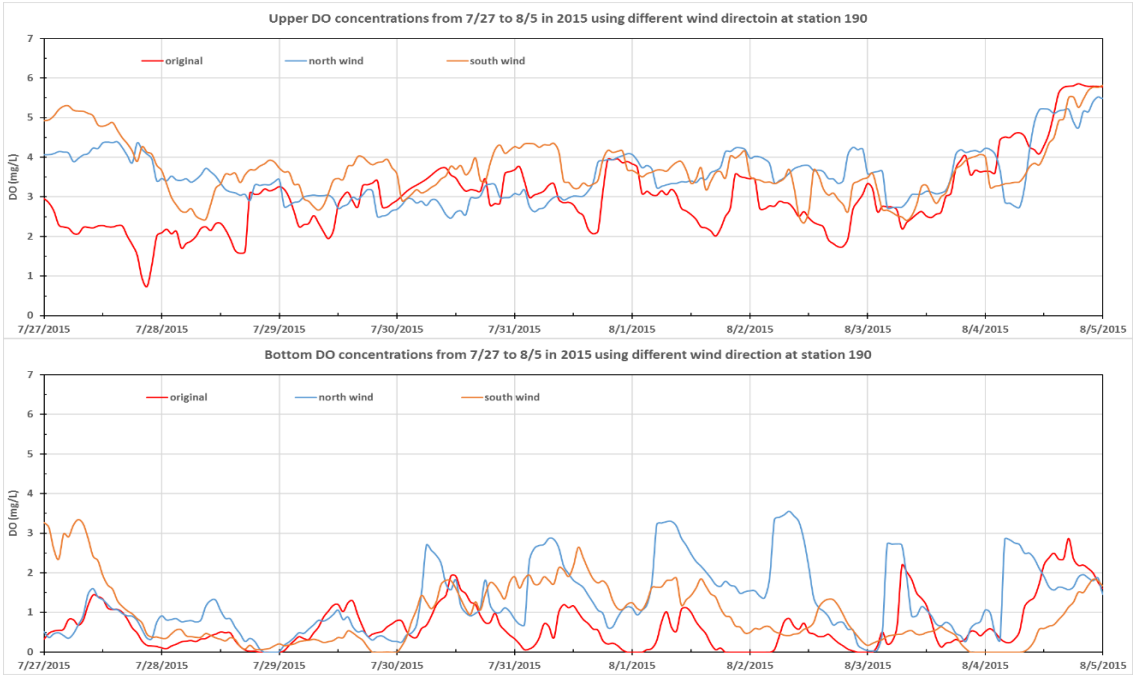

Figure 4-92 Simulated DO at station 190 from 7/27 to 8/5 in 2015 using different wind direction in the upper layer (upper panel) and bottom layer (lower panel).

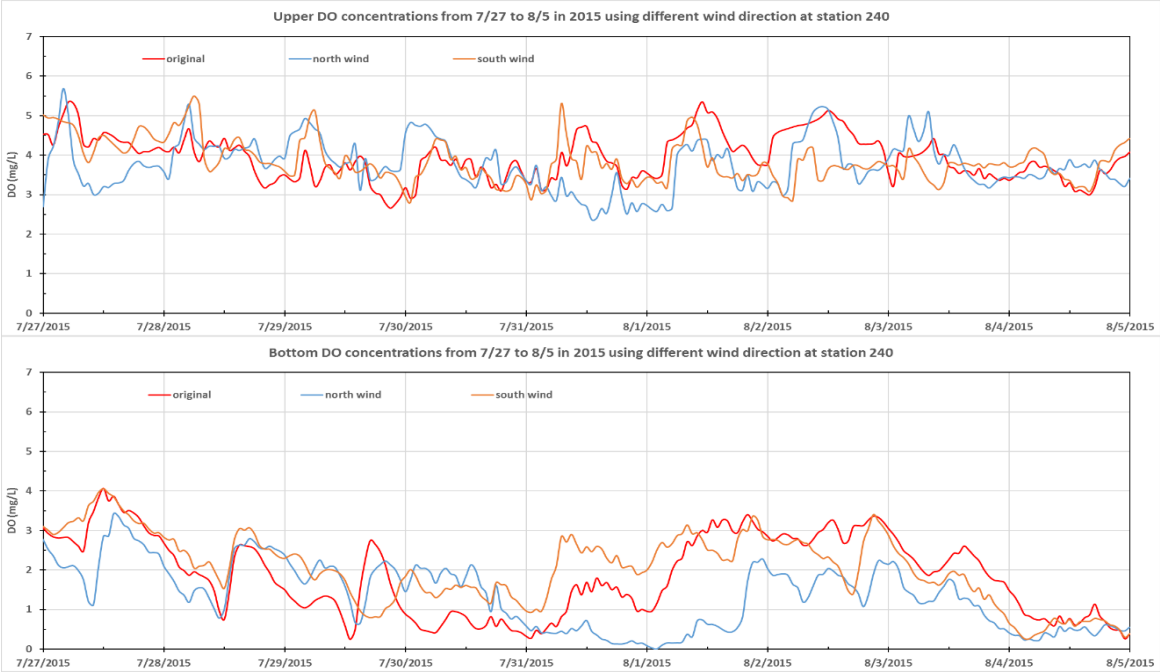

Figure 4-93 Simulated DO at station 240 from 7/27 to 8/5 in 2015 using different wind direction in the upper layer (upper panel) and bottom layer (lower panel).

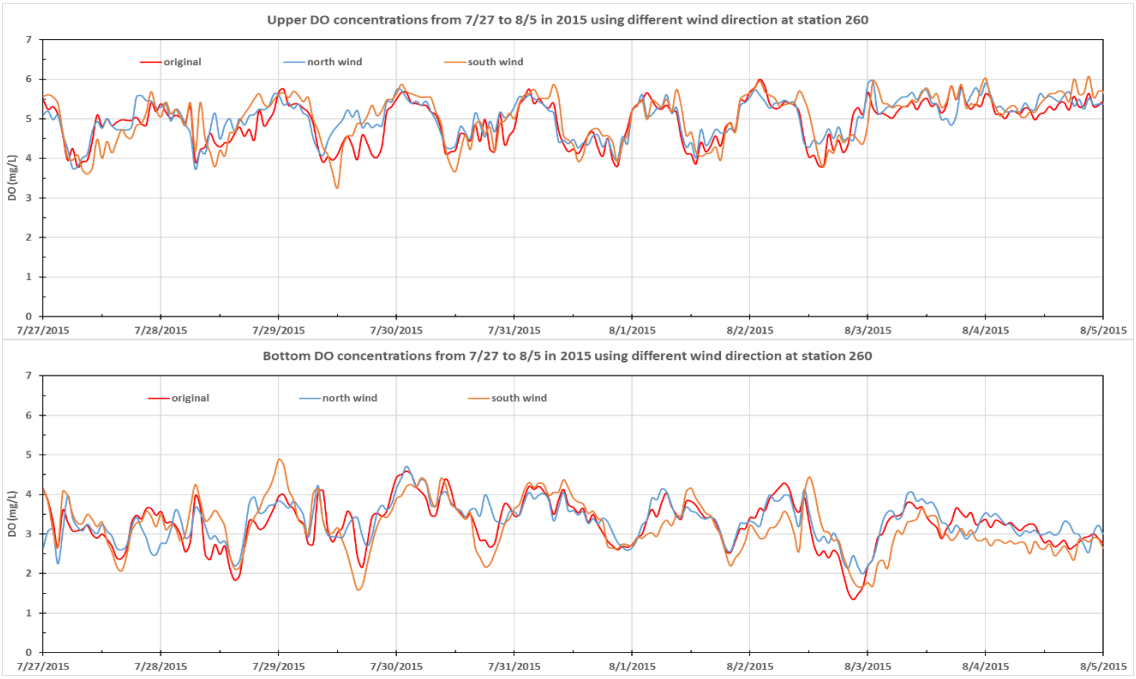

Figure 4-94 Simulated DO at station 260 from 7/27 to 8/5 in 2015 using different wind direction in the upper layer (upper panel) and bottom layer (lower panel).

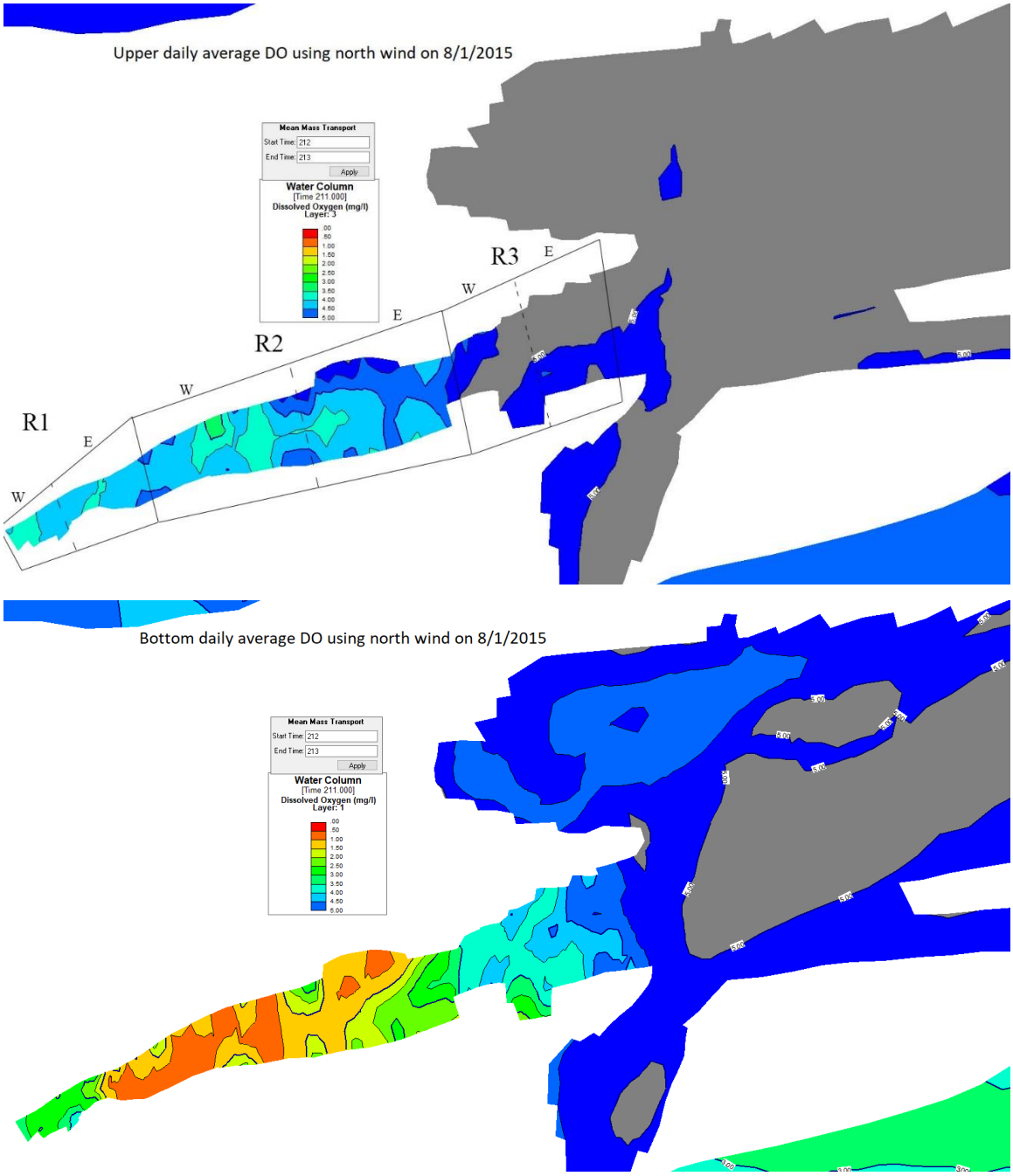

Figure 4-95 Upper- and bottom-layer daily average DO contour maps on 8/1/2015 simulated using north wind

4.4.5 Projected Water Temperatures and DO under the Future Climate Scenarios

If one examines long-term weather data, air temperatures seem increasing year by year due to the emissions of lots of greenhouse gases. The increasing air temperature speeds up the melts of icebergs in the North Pole and the South Pole, which furtherly lead to the sea level rises. Since the hydrodynamic and water quality parameters are significantly affected by the tides and freshwater flow into the estuary, the increasing sea level would affect these parameters. This section presents how the projected air temperature and sea level rises in 2075 would affect water temperatures and DO concentrations in the Cotton Bayou.

For the sea level rise, the following equation proposed by Titus and Narayanan (reference) was used,

$$Local(t) = Normalized(t) + (t - 1990) * Trend \tag{4.3}$$

where *t* is the year after 1990, *Normalized(t)* is the normalized projection of the sea level rise at the year t, and Trend is the historical rate of sea level rise. The value 1990 represented the beginning year that is used to calculate the sea level rises in the future. It was replaced to 2015 since it is the year when the observed water level was collected to set up the current model. The trend was set to 2.4 mm/year that is measured at Pensacola, Florida, the closest station to the study area that provides the sea level rise rate. The median and 1% high normalized projections are 0.18 and 0.57 m in 2075, respectively (Titus and Narayanan 1995). Then, the 0.324 and 0.714 m were calculated as projected mean and maximum (1% chance) sea level rises, respectively, in the study area.

The projected air temperature increase in 2075 was obtained from the output of MIROC (Model Interdisciplinary Research on Climate), which is a climate model aiming to simulating the Earth's atmosphere or oceans. The MIRCO model with a high spatial resolution with 1.12 degrees spatial resolution was chosen for this study. The SRES A1B (special report on emissions scenarios A1B) output has a grid center point in the Mobile, AL (with latitude 30.68° and longitude 268.25°)

which is close to the study area. The model output can be found at http://www.ipcc-data.org/. From the report, an increase of 4.73 and 5.16 °C for July and August in 2075 were reported, respectively. Constant monthly air temperature increases were used for the model runs under future climate scenarios.

Three model scenario runs were developed for the study area: (1) under projected warm air temperatures in 2075 (without any sea level rise), (2) under projected warm air temperatures and mean sea level rise in 2075, and (3) under projected warm air temperatures and maximum sea level rise in 2075. Under projected air temperature scenario without changing the sea level, projected water temperatures would be higher, but time and depth variations should be very similar to the results from the base model run (Figure 4-96 top frame). However, for the other two scenarios including mean and maximum sea level rises, simulated water depths and velocities (hydrodynamics) and then salinity and other water quality variables could be affected due to higher water levels at the Gulf of Mexico (south boundary). This is also because the increase in water level would increase the vertical mixing of the waterbody. Table 4-21 summarizes average simulated water temperatures and DO concentrations in the four layers from 7/27 to 8/5 at station 240 (as an example results) under above three projected air temperature and sea level rise scenarios in 2075.

Figure 4-96 shows that projected water temperatures increase from the bottom layer to lower layer then the upper layer, nearly similar water temperature pattern in the freshwater, but surface-layer temperatures have large variations with the change of air temperature. Figure 4-97 and Table 4-21 shows that the upper-layer water temperatures would increase with the increase of air temperatures, and water temperatures are projected to have less increase with the increase of sea levels. When air temperatures increase and sea level rises, the increase rate of water temperatures in the different layers is different, with the maximum increase rate in the surface layer (Table 4-22). There is an exception: under the maximum sea level rise, projected average bottom

water temperature is 2% smaller than one from the base model. Figure 4-97 shows that the bottom water temperature from the model using projected water level rises in 2075 are even smaller than the corresponding data from the original model from 7/27 to 8/3 except for 8/1. For all three future climate scenarios, water temperatures are greater than 30 °C that Gulf menhaden tried to avoid (too warm). Although the surface water temperatures increase under the three projected scenarios, they are almost lower than 34.9 °C, that is the critical point Gulf menhaden could live free of stress.

Figure 4-98 shows that the lower- and bottom-layer DO would show obvious daily change with the increase of the water level in the Gulf, while the surface DO change pattern are close under the three scenarios (Figure 4-99). Projected bottom DO would increase with the increase of water levels under the same air temperature (Table 4-21) and have large daily variations with standard deviations of ~1.0 mg/L. Standard deviations from mean DO decrease from the bottom to surface layer, which is 0.35–0.49 mg/L at the surface layer. Figure 4-99 shows that projected maximum bottom-layer DO could be higher than 3 mg/L under two sea level rises scenarios. The upper-layer DO concentrations are projected mostly higher than 3 mg/L under all the scenarios. However, the DO under the base model shows the maximum surface DO because the lower water temperature due to the lower air temperature would have higher surface DO saturated concentration.

Table 4-21 Average water temperature (°C) and DO (mg/L) in four layers from 7/27 to 8/5 at station 240 under projected air temperature and sea level rise scenarios in 2075

	base	projected air temperatures	projected air temperatures and mean sea level	projected air temperatures and max sea level
		Water Temperature (°C)		
surface	31.38 ± 1.34	34.34 ± 1.39	33.84 ± 1.33	33.53 ± 1.24
upper	32.10 ± 1.01	34.58 ± 1.07	33.94 ± 1.01	33.42 ± 0.98
lower	32.31 ± 0.92	34.17 ± 1.06	33.33 ± 0.97	32.52 ± 1.00
bottom	32.49 ± 0.80	33.70 ± 0.96	32.66 ± 0.98	31.77 ± 0.95
		DO Concentration (mg/L)		
surface	5.23 ± 0.51	4.94 ± 0.42	5.11 ± 0.35	5.22 ± 0.39
upper	3.95 ±0.55	3.68 ± 0.59	3.55 ± 0.56	3.91 ± 0.56
lower	2.97 ± 0.75	2.80 ± 0.75	2.77 ± 0.60	3.15 ± 0.57
bottom	1.77 ± 1.01	1.68 ± 1.01	1.77 ± 1.05	2.22 ± 1.00

Table 4-22 Simulated mean water temperature and DO percent decrease or increase at station 240 from the mean water temperature and DO of the validated model

	projected air temperature	projected air temperature and mean sea level	projected air temperature and max sea level
		Water Temperature (°C)	
surface	9% [1]	8%	7%
upper	8%	6%	4%
lower	6%	3%	1%
bottom	4%	1%	-2%
		DO Concentration (mg/L)	
surface	-6%	-2%	0%
upper	-7%	-10%	-1%
lower	-6%	-7%	6%
bottom	-5%	0%	25%

Note: [1] – Percents were computed based on average water temperatures and DO in Table 4-21.

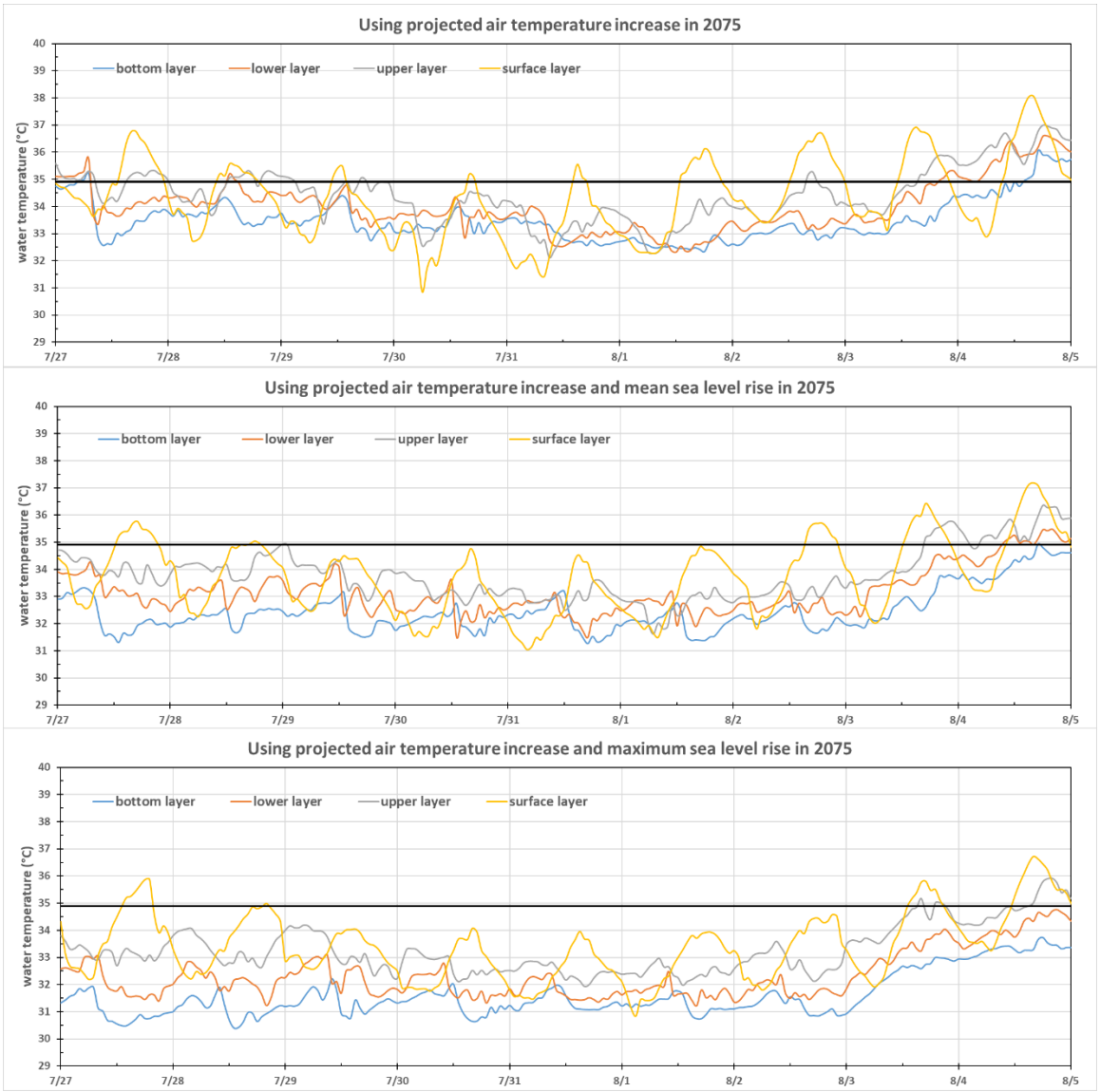

Figure 4-96 Simulated water temperature in the four layers at station 240 from 7/27 to 8/5 using three projected air temperature and sea level rise scenarios in 2075.

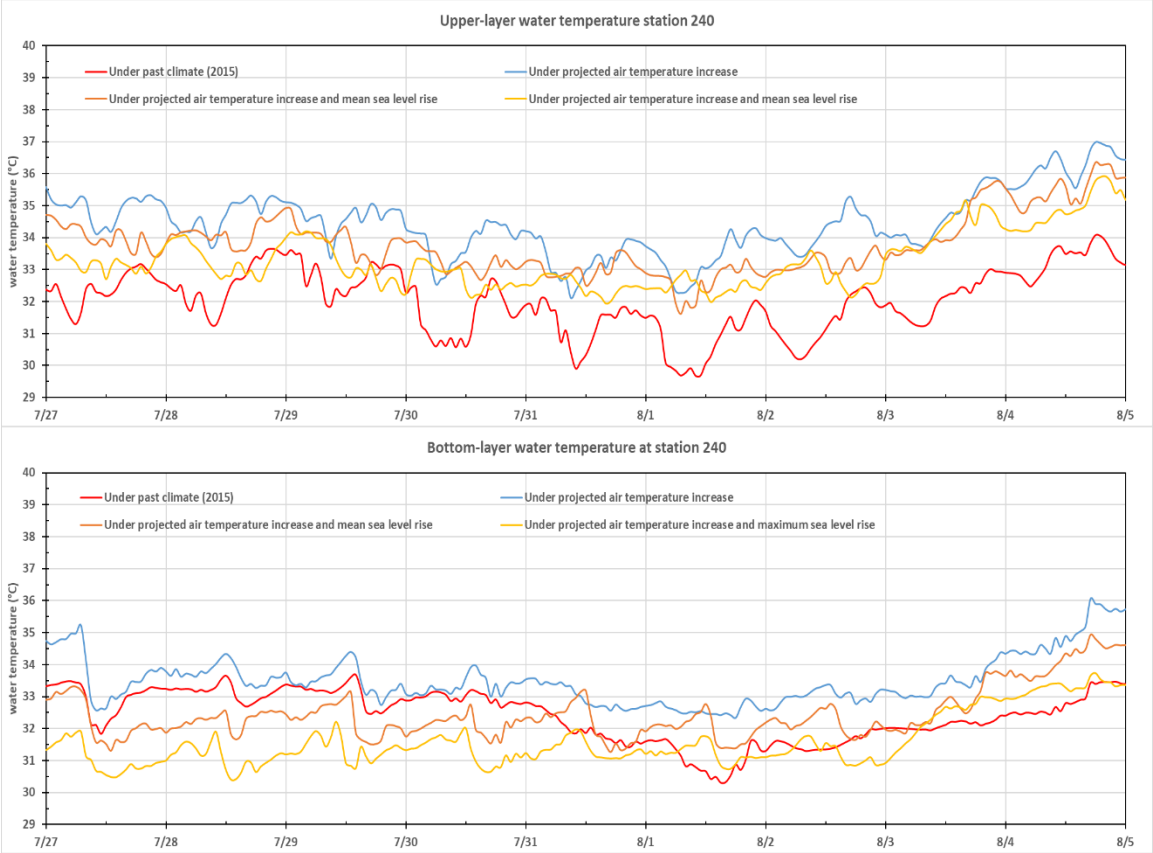

Figure 4-97 Simulated water temperature at station 240 from 7/27 to 8/5 using three projected air temperature and sea level scenarios in the upper- (upper panel) and bottom-layer (lower panel).

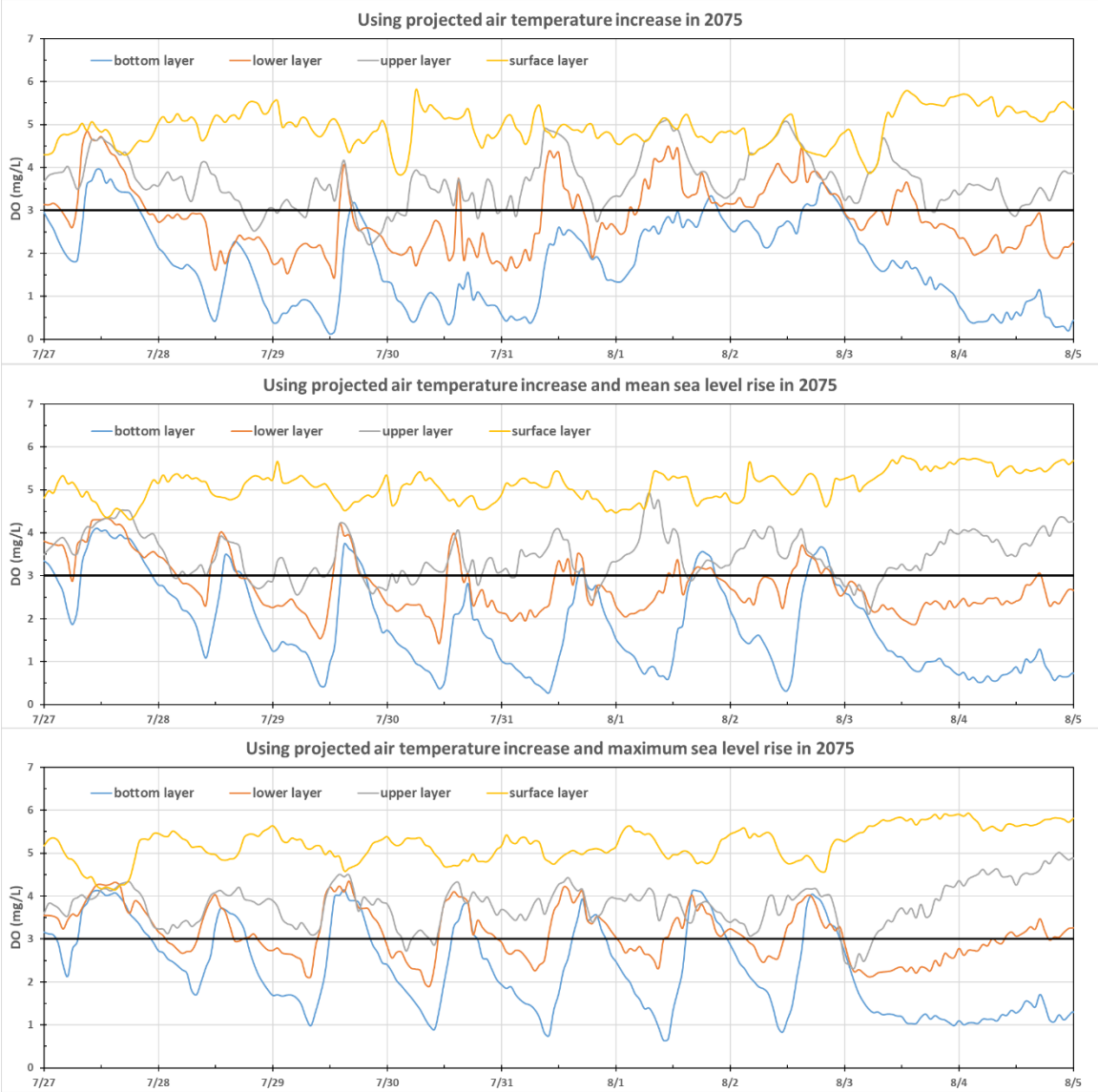

Figure 4-98 Simulated DO in the four layers at station 240 from 7/27 to 8/5 using three projected air temperature and sea level rise scenarios in 2075.

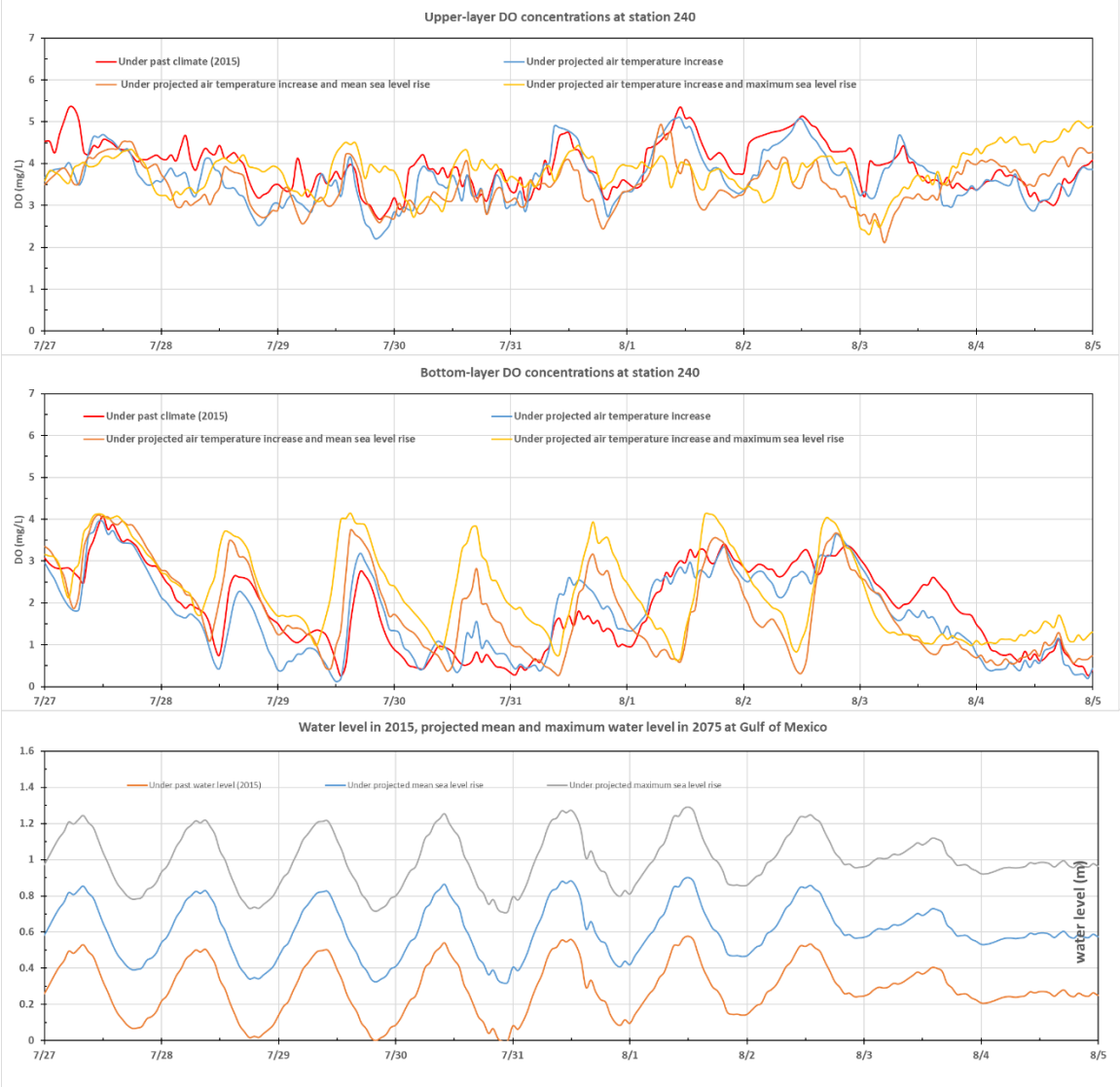

Figure 4-99 Simulated DO at station 240 from 7/27 to 8/5 using three projected air temperature and sea level rise scenarios in the upper- (upper panel) and bottom-layer (middle panel) and the projected water level in 2075 (bottom panel).

CHAPTER 5 Summary and Conclusions

5.1 Summary

The large fish kills in the 2015 summer (7/31—8/3) around Perdido Pass and other areas of Orange Beach, AL, hit the local tourism and raised concern over the health status of the local water quality. A detailed analysis of the possible reasons why large fish kills occurred could benefit the local government and residents in order to avoid the tragedy occurring again in the future. This study is aimed at developing a reliable water quality model to simulate the water temperature, salinity, and DO in the Perdido and Wolf Bay system with the focus area of Cotton Bayou. Given that the Cotton Bayou is located in the estuary close to the Gulf of Mexico, which is affected by both tides and freshwater flow from upstream, a three-dimensional EFDC hydrodynamic and water quality model was developed to simulate the water temperature, salinity and DO in the study area.

Although Cotton Bayou is the focus area, a model to simulate the whole Perdido and Wolf Bay system, where Cotton Bayou is located, was developed since the required boundary inputs were only available for the Perdido and Wolf Bay. The EFDC software was used to develop the simulation model since it has proved its reliability in many previous studies. EFDC is a comprehensive model framework including hydrodynamic, water quality, sediment, waves, and dye model. Only the hydrodynamic and water quality model was used in the current study. The water quality model is dependent on the results of the hydrodynamic model. The current EFDC model cover 300.8 km^2 of the simulation domain (43.86 km^2 in the upper Perdido Bay, 50.56 km^2 in the middle Perdido Bay, 0.37 km^2 in the Perdido Pass, 0.73 km^2 in the Cotton Bayou, 20.6 km^2

in the Wolf Bay, 184.7 km^2 in the Gulf of Mexico) with 5303 curvilinear horizontal grids and 4 layers in the vertical direction, a total of 21,212 3D cells.

The current Perdido and Wolf Bay simulation model has total twelve boundaries, nine of them representing the freshwater streams/creeks flowing into the study area from upper Perdido Bay and Wolf Bay, and the remaining three representing the west (GIWW), east (Dolphin Pass), and south (Gulf of Mexico) open boundaries, respectively, which are used to represent the flow exchanges between the study area and the sea water (Section 3.3.2). Among the nine freshwater flows, four of them are in the upper Perdido Bay and five of them are in the Wolf Bay. For the four freshwater flows in the Perdido Bay, discharge data were obtained from the closest US Geological Survey (USGS) monitoring stations. For the Wolf Bay region, only flow data in Wolf Creek were available from the USGS station and other flow data were estimated based on contributing watershed areas and the flow data in the Wolf Creek. The water levels instead of flow data were assigned to the three open boundaries to represent tidal influences. The measured water levels from the Dauphin Island and Pensacola station were available for open boundaries.

For the freshwater inflows and the Gulf of Mexico, the constant salinity of 0.5 and 34 ppt were used. For the GIWW and Dolphin Pass, their input salinity data were obtained from ADEM and FDEP 33010H24 monitoring stations, respectively. For the water temperature input for the boundaries, only GIWW and Dolphin Pass have the measured data from Dauphin Island and Pensacola monitoring stations. For the Gulf of Mexico, we used the measured data from Dolphin Island. For all the nine boundaries representing freshwater inflows, river water temperatures were calculated from observed air temperatures based on the method proposed by (Chen and Fang 2015).

The atmospheric boundary data: atmospheric pressure (millibars), solar radiation (W/m^2), rainfall (m/day), relative humidity (fraction), cloud cover (fraction), air temperature (°C), wind speed (m/s), and wind direction, were combined data from the closest weather stations–Mobile

Regional Climate Center and Jay station in Florida. The Jay station recorded all the above meteorological parameters except for the atmospheric pressure and cloud cover, which were measured by the Mobile Regional Climate Center.

The hydrodynamic EFDC model was run from 2015–2017 based on the above input data. Since the simulated water temperature and salinity matched reasonably well with the observed data, the water quality EFDC model was subsequently used to simulate DO in 2015–2016 since there were few observed DO in 2017 for validation. For the water quality model, total twenty-one different types of inputs are needed (Section 3.3.1). They are generally categorized in the six groups: algae, nitrogen, phosphorus, carbon, COD, and DO. Measured water quality data in the study area were very limited and downloaded from the Water Quality Portal (STORET). The water quality input data were combined from observed data at several monitoring stations in the nearby region of each boundary since each station only recorded very limited data in 2015–2016 (Section 3.3.6). Since only total organic nitrogen, phosphorus, and carbon were recorded, the ratios 3:3.5:3.5, 1:3.7:5.7, and 1:1:8 were used to divide the total organic nutrients into the refractory, labile, and dissolved organic forms for organic N, P, and C, respectively, which are the required organic forms for EFDC modeling (Section 3.3.6). A numerical conversion was used to determine the algal biomass concentration in mg C/L from measured chlorophyll-a (Chl) concentration in mg Chl/L. For the validated base EFDC model, the COD function was disabled due to the lack of input data. The default values provided by EFDC were used for most of the internal coefficients in the water quality modeling. For the oxygen reaeration terms, O'Connor-Dobbins formula was chosen since the water depths was ranged from 0.5 to 5 m in the study area. The background light or solar radiation extinction coefficient were calculated to be 1.1 m^{-1} using limited Secchi-disk depth measurements. Algae growth rate, reference temperature, the half-saturation constant of nitrogen, phosphorus, carbon, respiration rate and reference temperature, settling velocity were chosen from

the normal ranges provided by the EPA report. The constant SOD of 0.9 $gO_2/m^2/day$ (Ji 2017) was used and the sediment genesis model was not activated (Section 3.4).

5.2 Conclusions

(1) EFDC water temperature model for the study area was validated in 2015–2017 with good model performance against observed data (Table 4-3 and Table 4-4). The simulation results show that the vertical distribution (along with depth) of water temperatures in the estuary was different from vertical stratification in freshwater lakes. In the estuary, the bottom-layer water temperatures could be higher than the surface water temperatures at some night or morning hours but it is still a stable density stratification due to higher salinity in deeper layers. The vertical stratification enhanced by the salinity difference inhabits or reduces the mixing of the water column. The surface water temperatures have large daily fluctuations that are affected by solar radiation and air temperature variations.

(2) EFDC hydrodynamic model for the study area was also validated by salinity that reasonably matches with the observed salinity (Table 4-2 and Table 4-3). Both simulated water temperature and salinity at 14 locations in 2017 matched well with measured data when water sample collection stations were inside the waterbody in comparison with other monitoring stations close to the shoreline where bathymetry has large change. At the Perdido Pass monitoring station in Cotton Bayou, simulated salinity can effectively track the observe with R^2 = 0.16 although *NSE* was negative (possibly due to some mismatches of the large fluctuations from 15–35 ppt and time shift).

(3) EFDC water quality model for the study area was only validated using observed DO at 8 monitoring stations. The model accuracies of DO validation had large variations from the high correlation (R^2 = 0.92 and *NSE* = 0.68) to the low correlation (R^2 = 0.04 and *NSE* = -3.89) because some observed DO might not be reliable, e.g., station 04012020 had lots of over-saturated

observed DO, and some constant DO sinks, e.g., SOD, might not be suitable to the whole simulation domain.

(4) Cotton Bayou regions show complex hydrodynamic characteristics (flow directions) comparing with its neighbor Perdido Pass and Terry Cove, especially for the bottom layer. In the Perdido Pass and Terry Cove, the flow directions basically followed the water level variations in the Gulf of Mexico (tides in and out) and the magnitude of bottom-layer velocity were slightly smaller than the values in the surface layer. In the Cotton Bayou, the surface-layer horizontal velocities were much smaller (-0.2—0.2 m/s) comparing with the velocities in the Perdido Pass (-0.64—0.74 m/s). The surface-layer flow directions show slight relationship with the water level change in the Gulf of Mexico, especially in the region 3 that is close to the Perdido Pass.

(5) Time-series plots and contour maps indicate that simulated water temperatures in Cotton Bayou were higher than 30 °C from 7/25 to 8/10, which were in the range of temperatures that Gulf menhaden avoid and have thermal stress. Simulated DO concentrations varied from the west end (region 1) to the east part (region 3) connecting to Perdido Pass with strong tide influences. In region 1, the lower- and bottom-layer DO was less than 3 mg/L. In region 2, the surface- and upper-layer DO was larger than 3 mg/L and lower- and bottom-layer DO was around or less than 3 mg/L. In region 3, simulated DO concentrations in all four layers are around or above 3 mg/L. The strong mixing in the region close to the Gulf of Mexico effectively transmits the surface DO to the bottom layer, which increased the bottom DO (Section 4.3.1). All the stations in Cotton Bay show a strong DO stratification.

(6) The DO concentrations and vertical stratification are significantly affected by including COD and increasing SOD. The larger the COD/SOD are, the lower the average DO are. The DO concentrations show a positive correlation with the wind speed, and lower wind speed leads to the decrease of DO concentrations. The constant north wind would also decrease the

bottom-layer DO from 7/31 to 8/3 in 2015 comparing with simulated DO with the south wind and observed wind direction (Section 4.4.4).

(7) Using a hypothetical lethal-niche boundary for menhaden, fish habitat or fish kill conditions were analyzed in the Cotton Bayou. Lethal DO is above 3 mg/L and increases with temperature, e.g., it requires minimum 4.1 mg/L DO at 30 ^{o}C for menhaden to survive. Based on the projected dynamic lethal DO, the station 240 seems like a demarcation point: in the regions east of the station 240, one or more layer contained the enough DO for Gulf menhaden to survive (7/15–8/15 in 2015), in the region west of station 240, fish kills could happen. When COD or SOD is higher, more areas could not support menhaden habitat due to low DO and high temperature.

5.3 Future Studies

Although the developed model can effectively simulate the water temperature, salinity, and DO in the Perdido and Wolf Bay system, there are still rooms to improve the model performance, especially for the DO simulation. Further studies are needed to determine COD and SOD in Cotton Bayou and other sensitive regions of the study area. The different SOD or COD in the different regions would lead to different DO simulation results. The measured large fluctuations of the surface DO in the Wolf Bay might indicate that the SOD could be a time-series input instead of a constant value. Overall, the lack of time-series of input data at the key boundaries creates uncertainty of water quality modeling.

Fish kills especially for Gulf menhaden were reported many times in the past in Orange Beach backwaters and other areas, unfortunately there are no published accounts of controlled experimental testing of Gulf menhaden response to temperature and/or salinity (or any other environmental parameters such as DO) at any life stage, it is difficult to define causal mechanisms and have defined limits (thresholds) to determine exact habitat or mortality conditions for Gulf

menhaden. Further studies in the laboratory or field are definitely needed to determine Gulf menhaden's water temperature and DO survival requirements. A further study to understand menhaden's living depth range, migration rule, and salinity survival requirement is also useful

More field data should be collected to understand water quality dynamics in the study area. The field data collection of water temperature and DO at different depths at the same location is needed to validate the simulated temperature and DO stratification. Some observed data such as water temperature, salinity, and DO were collected by citizen volunteers at the number of locations or stations near the shoreline in the study area. These data are useful to diagnose/probe water quality conditions and were used for model validation. Due to a sharp change of bathymetry near the shoreline, simulated results near the shoreline are typically less accurate than ones inside the waterbody, therefore, the water quality data collected or monitored at stations inside the waterbody are much more valuable for model studies.

Certain engineering strategy could be implemented to potentially solve/reduce the fish kill of Gulf menhaden in Cotton Bayou. One option is to add oxygen in the west end of Cotton Bayou using aerator during unusual hot summer days. The second option is to add an underground conduit to withdraw water from the west end and discharge to the Gulf of Mexico to increase flow circulation and mixing in Cotton Bayou. The third option is to dredge a deeper channel to allow tidal water flow into Cotton Bayou from the west end or Perdido Pass or Terry Cove to the east end of Cotton Bayou. Above three options and other options can be tested, validated, and revised using EFDC flow and water quality simulation model developed and validated for this study.

APPENDIX A: Delineating the Perdido and Wolf Bay

EFDC supports the grid importation from another hydrodynamic model or a grid generated using a supported third-party grid generator, such as the CVLGrid, Delft RGFGrid, SEAGRID and so on. Although GIS or CAD can be used to generate the shoreline data file, the Google Earth was used to create the active cell polygon of the Perdido and Wolf Bay system. The first step is to use the "add path" tool to delineate the profile of the Perdido and Wolf Bay (Figure A.1). Figure A.2 shows the outline of the study area. The next step is to extract the coordinates from the KML file generated by the Google Earth. Global Mapper was used to do the extraction (Figure A.3). Since the extracted coordinates are in the form of GCS, the conversion from GCS to UTM were done using the Corpscon (Figure A.4). Then, the generated coordinates were used to generate the EFDC grids.

Figure A.1 Interface of the available tools to delineate the outline

Figure A.2 Snapshot of Google Earth showing the outer polygon along the shoreline of the Perdido and Wolf Bay

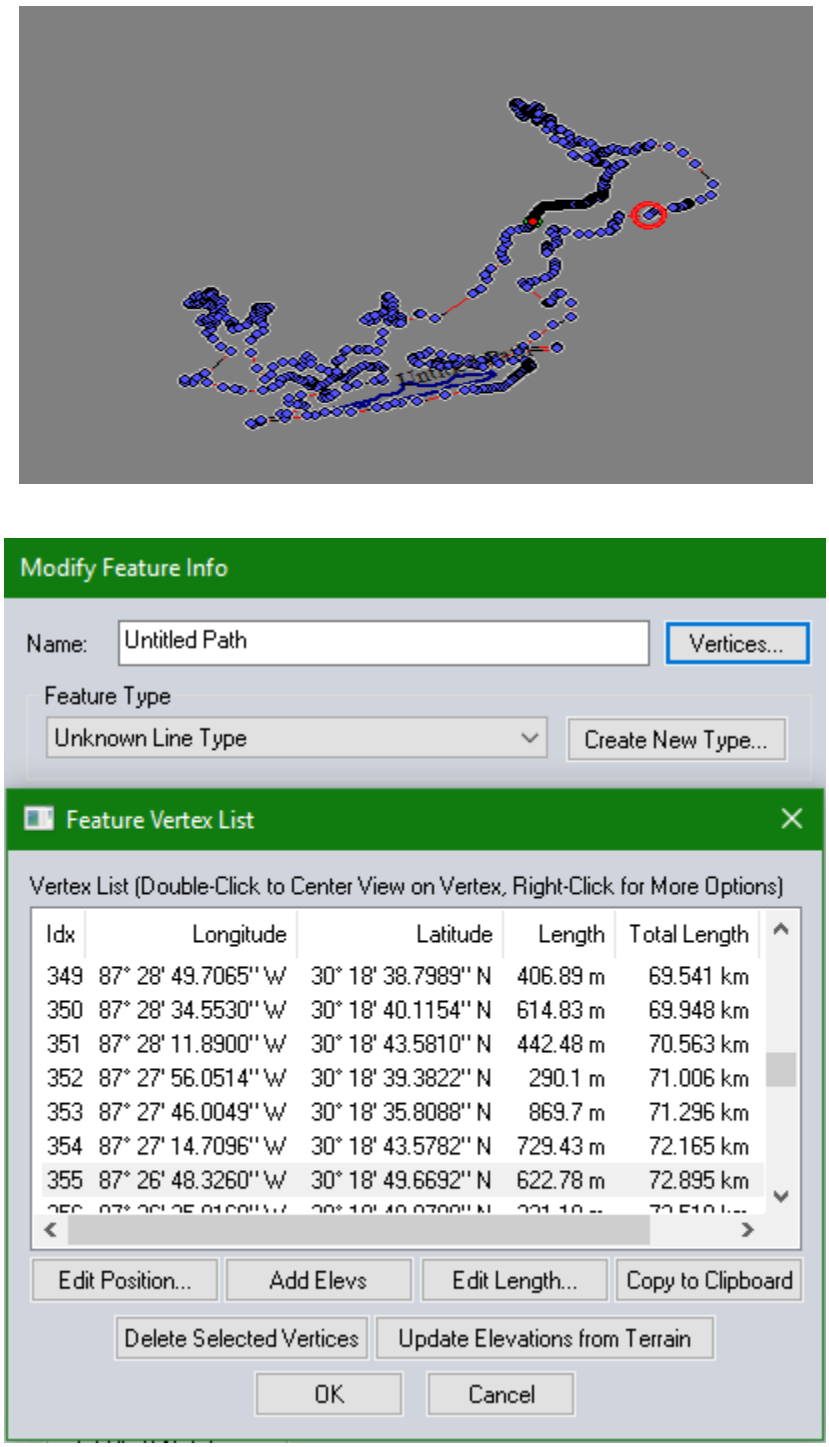

Figure A.3 Outline of Perdido and Wolf Bay shown in Global Mapper (upper panel) and the interface to extract to coordinates (lower panel)

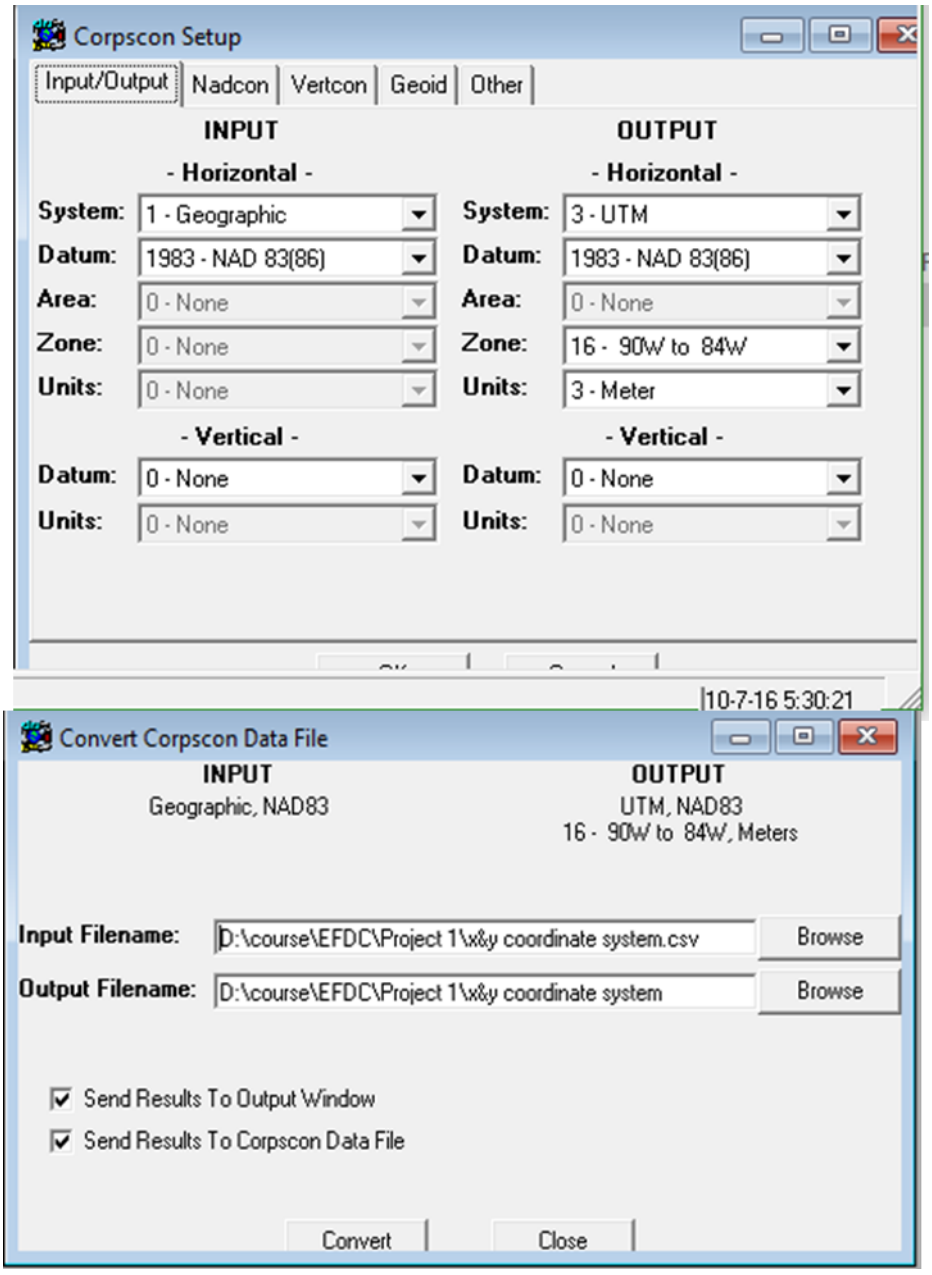

Figure A.4 Interface of Corpscon to convert the GCS to UTM coordinates

References

Ambrose Jr, R. B., Wool, T. A., and Barnwell Jr, T. O. (2009). "Development of Water Quality Modelingin the United States." *Environmental Engineering Research*, 14(4), 200-210.

Benson, N. G. (1982). *Life history requirements of selected finfish and shellfish in Mississippi Sound and adjacent areas*, Fish and Wildlife Service.

Blumberg, A. F., and Mellor, G. L. (1987). "A description of a three-dimensional coastal ocean circulation model." *Three-dimensional coastal ocean models*, 4, 1-16.

Burn, D. H., and McBean, E. A. (1985). "Optimization modeling of water quality in an uncertain environment." *Water Resources Research*, 21(7), 934-940.

Chapman, G. (1986). "Ambient aquatic life criteria for dissolved oxygen." *US Environmental Protection Agency: Washington, DC, USA*.

Chapman, R. S., Chapman, R., Johnson, B. H., and Vemulakonda, S. (1996). "User's Guide for the Sigma Stretched Version of CH3D-WES: A Three-Dimensional Numerical Hydrodynamic, Salinity, and Temperature Model." Army Engineer Waterways Experiment Station Vicksburg MS Hydraulics Lab.

Chen, G., and Fang, X. (2015). "Accuracy of hourly water temperatures in rivers calculated from air temperatures." *Water*, 7(3), 1068-1087.

Chen, L., Yang, Z., and Liu, H. (2016). "Assessing the eutrophication risk of the Danjiangkou Reservoir based on the EFDC model." *Ecological Engineering*, 96, 117-127.

Christmas, J., and Waller, R. S. (1973). "Estuarine vertebrates, Mississippi." *Cooperative Gulf of Mexico Estuarine Inventory and Study p 320-434, 1973. 11 fig, 36 tab, 99 ref*.

Cole, T. M., and Wells, S. A. (1995). "CEQUALW2: A Two-Dimensional, Laterally Averaged, Hydrodynamic and Water Quality Model, Version 3.2." *US Army Crops of Engineers, Vickburg, Miss, USA*.

Devkota, J., Fang, X., and Fang, V. Z. (2013). "Response characteristics of the Perdido and Wolf Bay system to inflows and sea level rise." *British Journal of Environment and Climate Change*, 3(2), 229.

EPA, U. E. P. A. (1976). "Quality Criteria for Water." 256.

Etzold, D. J., and Christmas, J. (1979). "A Mississippi marine finfish management plan."

Fang, X., Jao, M., Zaloom, V., Chu, H. W., Nagrani, N., and Few, J. T. "Design of confined placement areas in sabine-neches waterway, Texas." *Proc., Ports 2004*, ASCE (Conference Proceedings), 29-29.

Fore, P. L., and Baxter, K. N. (1972). "Diel fluctuations in the catch of larval gulf menhaden, Brevoortia patronus, at Galveston entrance, Texas." *Transactions of the American Fisheries Society*, 101(4), 729-732.

Gao, L., and Li, D. (2014). "A review of hydrological/water-quality models." *Frontiers of Agricultural Science and Engineering*, 1(4), 267.

Gough, D. (1969). "Incremental stress under a two-dimensional artificial lake." *Canadian Journal of Earth Sciences*, 6(5), 1067-1075.

GSMFC, G. S. M. F. C. (2015). "The Gulf Menhaden Fishery of the Gulf of Mexico."

Hamrick, J. (1995). "Calibration and verification of the VIMS EFDC model of the James River, Virginia." *The College of William and Mary, Virginia Institute of Marine Science*.

Hamrick, J. M., and Mills, W. B. (2000). "Analysis of water temperatures in Conowingo Pond as influenced by the Peach Bottom atomic power plant thermal discharge." *Environmental Science & Policy*, 3, 197-209.

Hokanson, K. E., Kleiner, C. F., and Thorslund, T. W. (1977). "Effects of constant temperatures and diel temperature fluctuations on specific growth and mortality rates and yield of juvenile rainbow trout, Salmo gairdneri." *Journal of the Fisheries Board of Canada*, 34(5), 639-648.

Hur, Y.-T., and Park, J.-H. (2009). "Assessment of EFDC model for hydrodynamic analysis in the Nakdong river." *Journal of Korea Water Resources Association*, 42(4), 309-317.

Jeong, S., Yeon, K., Hur, Y., and Oh, K. (2010). "Salinity intrusion characteristics analysis using EFDC model in the downstream of Geum River." *Journal of Environmental Sciences*, 22(6), 934-939.

Ji, Z.-G. (2017). *Hydrodynamics and water quality: modeling rivers, lakes, and estuaries*, John Wiley & Sons.

Ji, Z.-G., Hamrick, J. H., and Pagenkopf, J. (2002). "Sediment and metals modeling in shallow river." *Journal of Environmental Engineering*, 128(2), 105-119.

Lassuy, D. (1983). "Gulf menhaden, species profiles: life histories and environmental requirements (Gulf of Mexico). US Department of the Interior, Fish and Wildlife Service." FWS/OBS-82/11.2, US Army Corps of Engineers, TREL-82-4.

Legates, D. R., and McCabe Jr, G. J. (1999). "Evaluating the use of "goodness-of-fit" measures in hydrologic and hydroclimatic model validation." *Water resources research*, 35(1), 233-241.

Livingston, R. J. (2000). *Eutrophication processes in coastal systems: origin and succession of plankton blooms and effects on secondary production in Gulf Coast estuaries*, CRC press.

Lusk, K. (2017). "Modeling of the Wolf Bay and Perdido Bay Watersheds using HSPF."

Moriasi, D. N., Arnold, J. G., Van Liew, M. W., Bingner, R. L., Harmel, R. D., and Veith, T. L. (2007). "Model evaluation guidelines for systematic quantification of accuracy in watershed simulations." *Transactions of the ASABE*, 50(3), 885-900.

Nash, J. E., and Sutcliffe, J. V. (1970). "River flow forecasting through conceptual models part I—A discussion of principles." *Journal of hydrology*, 10(3), 282-290.

Reintjes, J. W., and Pacheco, A. L. (1966). "The relation of menhaden to estuaries." Allen Press, Incorporated.

Roithmayr, C. M., and Waller, R. A. (1963). "Seasonal occurrence of Brevoortia patronus in the northern Gulf of Mexico." *Transactions of the American Fisheries Society*, 92(3), 301-302.

Seo, D.-I., and Kim, M. (2011). "Application of EFDC and WASP7 in series for water quality modeling of the Yongdam Lake, Korea." *Journal of Korea Water Resources Association*, 44(6), 439-447.

Seo, D., Sigdel, R., Kwon, K., and Lee, Y. (2010). "3-D hydrodynamic modeling of Yongdam Lake, Korea using EFDC." *Desalination and water treatment*, 19(1-3), 42-48.

Shipp, R. L. (1986). *Dr. Bob Shipp's guide to fishes of the Gulf of Mexico*, Dauphin Island Sea Lab.

Simmons, E. G. (1957). *An ecological survey of the upper Laguna Madre of Texas*.

Stefan, H. G., Hondzo, M., Fang, X., Eaton, J. G., and McCormick, J. H. (1996). "Simulated long-term temperature and dissolved oxygen characteristics of lakes in the north-central United States and associated fish habitat limits." *Limnol. Oceanogr.*, 41(5), 1124-1135.

Tagatz, M. E., and Wilkens, E. P. (1973). "Seasonal occurrence of young gulf menhaden and other fishes in a northwestern Florida estuary."

Tech, T. (2007). "The environmental fluid dynamics code theory and computation volume 3: Water quality module." *Technical report, Tetra Tech, Inc., Fairfax, VA*.

Titus, J. G., and Narayanan, V. K. (1995). *The probability of sea level rise*, US Environmental Protection Agency, Office of Policy, Planning, and ….

Wang, C., Sun, Y., and Zhang, X. (2008). "Numerical simulation of 3D tidal currents based on the EFDC model in Jiaozhou bay." *Periodical of Ocean University of China*, 38(5), 833-840.

Wang, Q., Li, S., Jia, P., Qi, C., and Ding, F. (2013). "A review of surface water quality models." *The Scientific World Journal*, 2013.

Wilkens, E. P. H., and Lewis, R. M. (1971). "Abundance and distribution of young Atlantic menhaden, Brevoortia tyrannus, in the White Oak River estuary, North Carolina." *FISHERY BULLETIN, VOL 69, NO 4, P 783-789,(1971). 4 FIG, 2 TAB, 15 REF.*

Wlosinski, J. H., and Collins, C. D. (1985). "Evaluation of a water quality model (CE-QUAL-R1) using data from a small Wisconsin reservoir." *Ecological modelling*, 29(1-4), 303-313.

Wu, G., and Xu, Z. (2011). "Prediction of algal blooming using EFDC model: Case study in the Daoxiang Lake." *Ecological Modelling*, 222(6), 1245-1252.

Xia, M., Craig, P. M., Wallen, C. M., Stoddard, A., Mandrup-Poulsen, J., Peng, M., Schaeffer, B., and Liu, Z. (2011). "Numerical simulation of salinity and dissolved oxygen at Perdido Bay and adjacent coastal ocean." *Journal of Coastal Research*, 27(1), 73-86.

Xia, M., and Jiang, L. (2016). "Application of an unstructured grid-based water quality model to Chesapeake Bay and its adjacent coastal ocean." *Journal of Marine Science and Engineering*, 4(3), 52.

Zhao, L., Li, Y., Zou, R., He, B., Zhu, X., Liu, Y., Wang, J., and Zhu, Y. (2013). "A three-dimensional water quality modeling approach for exploring the eutrophication responses to load reduction scenarios in Lake Yilong (China)." *Environmental pollution*, 177, 13-21.

Zou, R., Bai, S., and Parker, A. (2008). "Hydrodynamic and eutrophication modeling for a tidal marsh impacted estuarine system using EFDC." *Estuarine and coastal modeling (2007)*, 561-589.

Zu-xin, X., and Shi-qiang, L. (2003). "Research on hydrodynamic and water quality model for tidal river networks." *Journal of Hydrodynamics Series B-English Edition-*, 15(2), 64-70.